

Proceedings of the
5th Patras Workshop on Axions, WIMPs
and WISPs PATRAS 2009

July 13-17, 2009
Durham, United Kingdom

Editors: Joerg Jaeckel, Axel Lindner and Javier Redondo

Verlag Deutsches Elektronen-Synchrotron

Impressum

Proceedings of the 5th Patras Workshop on Axions, WIMPs and WISPs (PATRAS 2009)

July 13-17, 2009, Durham, United Kingdom

Conference homepage

<http://axion-wimp2009.desy.de/>

Slides at

<http://axion-wimp2009.desy.de/e30/>

Online proceedings at

<http://www-library.desy.de/confprocs.html>

The copyright is governed by the Creative Commons agreement, which allows for free use and distribution of the articles for non-commercial activity, as long as the title, the authors' names and the place of the original are referenced.

Editors:

Joerg Jaeckel, Axel Lindner and Javier Redondo

June 2010

DESY-PROC-2009-5

ISBN 978-3-935702-37-9

ISSN 1435-8077

Published by

Verlag Deutsches Elektronen-Synchrotron

Notkestraße 85

22607 Hamburg

Germany

Organizing Committee

Laura Baudis
*Physik Institut,
University of Zurich
Winterthurerstr. 190
8057 Zurich
Switzerland*

Joerg Jaeckel,
*Institute for Particle Physics Phenomenology (IPPP),
Durham University,
South Road
Durham DH1 3LE
United Kingdom*

Axel Lindner and Andreas Ringwald,
*Deutsches Elektronen Synchrotron (DESY),
Notkestraße 85
D-22607 Hamburg,
Germany*

Konstantin Zioutas,
*Department of Physics,
University of Patras,
26504 Rio,
Greece*

Conference Secretary and Local Organization

Trudy Forster and Linda Wilkinson,
*Institute for Particle Physics Phenomenology (IPPP),
Durham University,
South Road
Durham DH1 3LE
United Kingdom*

Barbara Wittmann,
*Deutsches Elektronen Synchrotron (DESY),
Notkestraße 85
D-22607 Hamburg,
Germany*

Preface

In July 2009 delegates from all around the world gathered in Durham (United Kingdom) for the 5th incarnation of the Patras-Axion-WIMP-WISP workshop. It was organized and supported by CERN, DESY, the University of Patras, the University of Zurich and the IPPP.

Particle physics' most important tools are large colliders exploring the structure of matter at highest energies or searching for rare phenomena with highest intensities. In particular we hope that the latest and most powerful of such colliders, the LHC, will bring us decisive insights into the nature of electroweak symmetry breaking, the existence of supersymmetry, large extra dimension and, perhaps, exciting and unexpected new phenomena. However, the particles lending their name to the conference have one important common feature: their interactions with ordinary matter are weak or even extremely weak. On the one hand this makes it hardly possible to study them in colliders and other experimental approaches have to be investigated. On the other hand, due to their very weak interactions, axions, WIMPs and WISPs are ideal candidates for the constituents of dark matter. They might also be connected to other important questions such as the riddle of dark energy. Different theoretical investigations suggest that the febleness of their interaction is related to fundamental physics at very high energy scales.

In consequence probing these particles may give us exciting new information on the innermost workings of Nature complementary to research at large collider facilities.

With this in mind the aim of this conference series is to bring together both experimentalists and theorists in order to discuss ways to detect these particles and to elucidate what we can learn from their existence or non-observation. Therefore, the success (authors slightly biased) of this conference lies not only in the wide range of topics discussed in excellent talks but maybe even more so in the active discussions and fruitful close collaborations between theorists and experimentalists.

In this spirit the workshop concluded with the 2nd strategy meeting, an open discussion to generate and collect new ideas on promising experimental avenues and to identify theoretically interesting target areas for experimental searches.

From this enjoyable experience we are looking forward to the 6th Patras-Axion-WIMP-WISP workshop (including the 4th strategy meeting) held in Zurich from the 5th to the 9th of July 2010 and we are convinced that it will lead to further progress and perhaps even a discovery in the near future.

Joerg Jaeckel, Axel Lindner and Javier Redondo

Acknowledgements

The organizers would like to thank the IPPP for support and infrastructure and especially Trudy Forster and Linda Wilkinson for their help in ensuring smooth running of the workshop and creating a warm and welcoming atmosphere. Special thanks also to Barbara Wittmann from DESY for invaluable help in creating the online presence of the conference.

The organizing committee

Contents

1 The Physics Case for Axions, WIMPs and WISPs	1
Axions and other (Super-)WISPs	3
Markus Ahlers	
2 Direct Searches for Dark Matter	9
Searching for dark matter with CRESST	11
Hans Kraus for the CRESST collaboration	
CDMS-II to SuperCDMS: WIMP search at a zeptobarn	16
Tobias Bruch for the CDMS Collaboration	
The XENON100 Detector for Dark Matter Searches	20
Alexander Kish for the XENON100 collaboration	
SUSY dark matter and the LHC	24
Howard Baer	
The ArDM - a ton - scale liquid argon experiment for direct Dark Matter Detection	31
Polina Otyugova for the ArDM collaboration	
Particle dark matter in the galactic halo: results from DAMA/LIBRA	35
Pierluigi Belli for the DAMA/LIBRA collaboration	
Dark Matter Search with Germanium Detector at O(100eV) threshold	39
Shin-Ted Lin for the TEXONO Collaboration	
Status of the KIMS experiment	43
SeungCheon Kim for the KIMS collaboration	
3 Indirect Searches for WIMPs	47
Search for Dark matter in the sky in the Fermi era	49
Aldo Morselli	
<i>PATRAS 2009</i>	vii

Dark Matter Searches with Imaging Atmospheric Cherenkov Telescopes and Prospects for Detection of the Milky Way Halo	55
Ullrich Schwanke	
Dark matter and the PAMELA data	59
Julien Lavalle	
Dark Matter Decay and Cosmic Rays	63
Christoph Weniger	
4 Photon Regeneration and Laser Polarization Experiments	67
The CAST experiment: status and perspectives	69
Esther Ferrer-Ribas for the CAST Collaboration	
Search for Solar ALPs in the Low Energy Range at CAST	73
Marin Karuza for the CAST collaboration	
Search for Monoenergetic Solar Axions with CAST	78
Krešimir Jakovčić for the CAST Collaboration	
Prospects of Search for Solar Axions with Mass over 1 eV and Hidden Sector Photons	82
Ryosuke Ohta	
GammeV: results and future plans at Fermilab	86
William Wester for the GammeV collaboration	
The LIPSS search for light neutral bosons	90
Oliver K. Baker for the LIPSS collaboration	
Status of the ALPS Experiment	94
Axel Lindner for the ALPS Collaboration	
Search for Hidden Sector Photons in a Microwave Cavity Experiment	96
Mike Tobar	
Search for 0.1 meV Axions and Hidden Photons Using Cu Resonant Cavities	100
Penny L. Slocum	
Status of the BMV experiment	104
Carlo Rizzo for the BMV collaboration	
The status and prospects of the Q & A experiment with some applications	108
Hsien-Hao Mei for the Q & A Collaboration	
Interferometry in pulsed fields	112
Babette Döbrich	
ADMX's Continuing Search for Dark Matter Axions	116
Gray Rybka for the ADMX collaboration	

Polarization measurements and their perspectives at the Low Energy Frontier Giovanni Cantatore	120
5 Direct Axion Signals	125
Searches for light Higgs/Axions at BABAR Alessandro Gaz for the BABAR collaboration	127
6 Indirect Astrophysical and Cosmological Searches for Axions and WISPs	131
Axion-like Particles and Circular Polarisation of Active Galactic Nuclei Alexandre Payez	133
Solar X-rays from Axions: Rest-Mass Dependent Signatures Konstantin Zioutas	137
Cosmological axion bounds Steen Hannestad	141
7 Tentative Signals for WISPs	145
Searching for Axion-like Particles with Active Galactic Nuclei Clare Burrage	147
Laboratory Tests of Chameleon Models Philippe Brax	151
A Hidden Microwave Background ? - signatures of photon-WISP oscillations in the CMB - Javier Redondo	155
8 WISPs Theoretical Developments	159
Minicharges, Monopoles, and Magnetic Mixing Felix Brümmer	161
Light Hidden $U(1)$s from String Theory Mark Goodsell	165
9 Fifth Forces and Fundamental Symmetries	169
Tests of Lorentz symmetry Ralf Lehnert	171
Constraints on pseudoscalar-photon interaction from CMB polarization observation Wei-Tou Ni	175
10 New Ideas	179
Photon Production From The Scattering of Axions Out of a Solenoidal Magnetic Field Idan Shilon	181

Photon\leftrightarrowAxion conversions in transversely inhomogeneous magnetic fields	185
Javier Redondo	
List of Authors	189
List of Participants	193

Chapter 1

The Physics Case for Axions, WIMPs and WISPs

Axions and other (Super-)WISPs

Markus Ahlers^{1,2}

¹Rudolf Peierls Centre for Theoretical Physics, University of Oxford, Oxford OX1 3NP, UK

²Now at the C.N. Yang Institute for Theoretical Physics, SUNY, Stony Brook, NY 11794-3840, USA

DOI: <http://dx.doi.org/10.3204/DESY-PROC-2009-05/ahlers.markus>

We present some bottom-up motivations of axions and other weakly interacting sub-eV particles (WISPs) coupling to photons. Typically, these light particles are strongly constrained by their production or interaction in astrophysical and cosmological environments. Dedicated laboratory searches can provide complementary probes that are mostly less sensitive but also less model-dependent. We briefly comment on future experiments with the potential to discover photon oscillation effects in kinetic mixing scenarios with massive hidden photons.

1 Motivation

Many extensions of the standard model predict hidden sectors of particles that are only weakly interacting with known matter. Some of these particles may even be extremely light (sub-eV), *e.g.*, if they are (pseudo-)Goldstone bosons of spontaneously broken (anomalous) global symmetries or gauge bosons of exact hidden symmetries. In some cases these light particles can be motivated by short-comings of the standard model, for instance the axion as a dynamical solution to the strong \mathcal{CP} problem. We will give a brief outline of axion models in Sect. 2. Other weakly interacting sub-eV particles¹ (WISPs) can be considered from their phenomenological point of view, having strong influence on early universe physics, astrophysics and even laboratory experiments despite their feeble interactions. In many cases these probes are independent of the particular origin of the light hidden sector and provide very general and simple test scenarios, *e.g.*, if the possible interaction of WISPs with standard model matter can be constrained by gauged and global symmetries. As an example, Sect. 3 discusses mini-charged particles and hidden photons, that may naturally arise in field or string theoretic set-ups with hidden abelian gauge groups and kinetic mixing with the electromagnetic sector. We conclude in Sect. 4.

2 Axions and their Relatives

Non-abelian gauge theories possess non-trivial solutions of the classical equations of motion in 4-dimensional euclidean space-time, so-called *instantons*, that can be classified by an integer

¹Axions can be considered as *super-WISPs* with a coupling inversely proportional to the Peccei-Quinn scale $F_a \gtrsim 10^9$ GeV (see Sect. 2).

number, the Pontryagin index

$$q \equiv \frac{\alpha}{4\pi} \int d^4x \operatorname{tr} G_{\mu\nu} \tilde{G}^{\mu\nu} \in \mathbf{Z}, \quad (1)$$

where $G_{\mu\nu}$ is the field tensor of the non-abelian field with coupling α (see *e.g.* the reviews [1]). Each instanton solution with $q = n$ is associated with a vacuum $|n\rangle$, that is left invariant under infinitesimal gauge transformations. However, there also exist gauge transformations with non-trivial winding number mapping between instanton solutions with different topological index. The true vacuum of non-abelian gauge theories is therefore a superposition of the vacua $|n\rangle$, the θ -vacuum $\sum_{n \in \mathbf{Z}} \exp(in\theta) |n\rangle$. The phase $\exp(in\theta)$ contributes as an effective Lagrangian of the field theory,

$$\mathcal{L}_\theta = \theta \frac{\alpha}{4\pi} \operatorname{tr} G_{\mu\nu} \tilde{G}^{\mu\nu}, \quad (2)$$

which transforms as a pseudo-scalar and hence violates \mathcal{CP} .

The θ -term of strong interaction is in general not invariant under chiral transformations in the presence of weak interactions and massive chiral fermions. The physical parameter is the combination $\bar{\theta} = \theta + \arg \det M$, which contributes to the neutron's electric dipole moment as $d_n \simeq 4.5 \times 10^{-15} \bar{\theta} e \text{ cm}$. The current limit of $|d_n| < 2.9 \times 10^{-26} e \text{ cm}$ translates into a limit of $|\bar{\theta}| \lesssim 10^{-10}$ [2, 1]. The *strong CP problem* can now be formulated as the question why the sum of *a priori* independent phases in $\bar{\theta}$ contributing to strong \mathcal{CP} -violation cancel with such a high accuracy.

An elegant solution to this problem has been proposed by *Peccei and Quinn* [3]. They introduced an anomalous global chiral symmetry $U(1)_{\text{PQ}}$ which is spontaneously broken at the Peccei-Quinn (PQ) scale f_a . The axion corresponds to the pseudo-Goldstone boson of the broken symmetry, that receives a periodic potential at the quantum level [4] due to chiral anomalies²,

$$V(a) = - \left(\bar{\theta} + \mathcal{N} \frac{a}{f_a} \right) \frac{\alpha_s}{4\pi} \operatorname{tr} G_{\mu\nu} \tilde{G}^{\mu\nu} - \mathcal{E} \frac{a}{f_a} \frac{\alpha_{\text{em}}}{8\pi} F_{\mu\nu} \tilde{F}^{\mu\nu}. \quad (3)$$

One can show that the QCD contributions ($\propto \mathcal{N}$) are bounded as $V(0) \leq V(a')$ in terms of a shifted axion field $a' \equiv a - \bar{\theta} F_a$ with effective PQ scale $F_a \equiv f_a / \mathcal{N}$. The strong \mathcal{CP} problem is hence solved dynamically when the axion field settles down at its minimum $a = \bar{\theta} F_a$.

The original PQWW model [3, 4] includes a second Higgs doublet in the breaking of $U(1)_{\text{PQ}}$ which relates the PQ breaking scale to the electroweak scale $F_a \simeq 246 \text{ GeV}$. This model is now ruled out *e.g.* by life-time measurements of mesons [1]. Still viable variants of this model, so-called *invisible* axion models, introduce additional Higgs bosons as electro-weak scalars which decouple the PQ scale from the weak scale. The mass of the axion can be determinant via current algebra techniques and is related to the ratio $z \equiv m_u / m_d \simeq 0.35 \div 0.6$ of up and down quarks together with the pion's mass m_π and decay constant f_π as

$$m_a \simeq \frac{f_\pi m_\pi}{F_a} \frac{\sqrt{z}}{1+z} \simeq 6 \text{ meV} \left(\frac{10^9 \text{ GeV}}{F_a} \right). \quad (4)$$

The QED contribution ($\propto \mathcal{E}$) in Eq. (3) corresponds to a coupling term between axions and photons of the form $\mathcal{L}_{a\gamma\gamma} = -(g_{a\gamma\gamma}/4) a F^{\mu\nu} \tilde{F}_{\mu\nu} = g_{a\gamma\gamma} a \mathbf{E} \cdot \mathbf{B}$ with

$$g_{a\gamma\gamma} = \frac{\alpha_{\text{em}}}{2\pi F_a} \left[\frac{2}{3} \frac{4+z}{1+z} - \frac{\mathcal{E}}{\mathcal{N}} \right]. \quad (5)$$

²For simplicity, we only consider QCD ($\propto \mathcal{N}$) and QED ($\propto \mathcal{E}$) contributions in Eq. (3).

Note that the first term in the coupling (5) is a contribution from chiral symmetry breaking [1]. The most popular examples are the DFSZ(-type) models [5] with $\mathcal{E}/\mathcal{N} = 8/3$ and KSVZ(-type) models [6] with $\mathcal{E}/\mathcal{N} = 0$.

Invisible axion models are constrained by their (model-dependent) axion coupling to matter and photons. In particular, astrophysical environments provide strong limits on the viable range of axion mass m_a and coupling $1/F_a$ via photon conversion into axions in Compton-like scattering, by the Primakoff process or via hadronic or electromagnetic axion bremsstrahlung (for a review see [7]). Depending on their production mechanism in the early universe, axions may also contribute today as (a part of) cold or warm dark matter and could be detected in tunable microwave cavities [8]. All these probes leave a window of viable axion models in the range $10^9 \lesssim f_a/\text{GeV} \lesssim 10^{12}$ and $10^{-5} \lesssim m_a/\text{eV} \lesssim 10^{-2}$.

Generalizations of the QCD axion are *axion-like particles* (ALPs). This class of particles includes pseudo-scalars ϕ with a photon interaction of type (5) but with masses and couplings kept as independent parameters. Pseudo-scalar ALPs may also originate via PQ-type mechanisms and are generic in many supersymmetric extensions of the standard model (see *e.g.* Ref. [9]). Strong bounds on the coupling $g_{\phi\gamma\gamma}$ arise from the direct search of ALPs produced in the Sun via helioscopes [10]. Laboratory bounds from optical and light-shining-through-a-wall (LSW) experiment are typically three orders of magnitude weaker, but somewhat more model-independent [11]. Scalar ALPs with a coupling $\mathcal{L}_{\phi\gamma\gamma} = -\frac{1}{4}g_{\phi\gamma\gamma}\phi F^{\mu\nu}F_{\mu\nu} = \frac{1}{2}g_{\phi\gamma\gamma}\phi(\mathbf{E}^2 - \mathbf{B}^2)$ can not be motivated by a PQ-type mechanism, but generally share the bounds of pseudo-scalar ALP models. In addition, scalar ALPs are strongly constrained by their contribution to non-newtonian forces [12].

3 WISPs from Kinetic Mixing

Extensions of the standard model, in particular supersymmetric and/or string theories predict a plethora of additional particles, some of which might be extremely light [9]. These hidden sectors may couple to the standard model via renormalizable interactions, *e.g.*, via gauge kinetic mixing, the Higgs portal or Yukawa-type couplings. Hence, these interactions are not expected to be suppressed by the mass scale of messenger sectors. We will briefly discuss the case of weakly interacting sub-eV particles (WISPs) arising from kinetic mixing.

Gauge bosons X_μ of a hidden sector $U(1)_X$, so-called *hidden photons* or *paraphotons*, can couple to photons A_μ via a mixing term [13]

$$\mathcal{L}_{\text{mix}} = -\frac{1}{2}\chi F^{\mu\nu}X_{\mu\nu}, \quad (6)$$

where $F_{\mu\nu}$ and $X_{\mu\nu}$ are the field tensors of $U(1)_{\text{em}}$ and $U(1)_X$, respectively. Kinetic mixing naturally arises in field theoretic extensions of the standard model, where hidden sector particles are simultaneously charged under both $U(1)$ s. If kinetic mixing is absent at the tree level, 1-loop diagrams give contributions of the form [13]

$$\chi \sim \frac{\sqrt{\alpha_{\text{em}}\alpha_X}}{4\pi} \ln\left(\frac{m'}{m}\right), \quad (7)$$

where m and m' are the masses of a (non-degenerate) pair of hidden sector particles in the loop. Typically, field or string theoretical predictions of χ are in the range from 10^{-16} to 10^{-2} [14] (see also Ref. [15] and references therein).

The full kinetic Lagrangian can be diagonalized via a shift $X_\mu \rightarrow X_\mu - \chi A_\mu$ and a re-definition of the fine-structure constant $\alpha_{\text{em}} \rightarrow \alpha_{\text{em}}/(1-\chi^2)$. The shift of the hidden photon field can have several effects. If the hidden $U(1)_X$ is unbroken, hidden sector matter with a hidden charge Q_X receives a electromagnetic charge of the form $Q_{\text{em}} = -\chi\sqrt{\alpha_X/\alpha_{\text{em}}}Q_X$, which can be extremely small for $\chi \ll 1$ and/or $\alpha_X \ll \alpha_{\text{em}}$, resulting in *mini-charged particles* (MCPs) [13]. If the hidden photon is massive via a Higgs or Stückelberg mechanism the diagonalization of the kinetic term results in off-diagonal elements in the mass matrix. These terms are responsible for vacuum oscillations between photons and hidden photons with a probability [16]

$$P_{\gamma \rightarrow \gamma'} = 4\chi^2 \sin^2 \left(\frac{m_{\gamma'}^2 \ell}{4\omega} \right). \quad (8)$$

Similar to the previous case, MCPs and hidden photons have a rich phenomenology with strong bounds coming from astrophysical and cosmological environments [17, 15]. The strongest bounds on the charge of sub-keV MCPs come from energy loss arguments of horizontal branch stars or white dwarves giving $|Q_X| \lesssim 2 \times 10^{-13}$. Massive hidden photons in the sub-eV range receive also strong bounds from solar production and distortions of the CMB. However, due to the mass-dependence $P_{\gamma \rightarrow \gamma'} \propto m_{\gamma'}^4$, in the presence of short baselines, $\ell \ll \omega/m_{\gamma'}^2$, future experiments have the potential to probe previously unconstrained hidden photon models (see *e.g.* Ref. [15]). This includes LSW experiments with optical lasers [18, 19] and microwave cavities [20] or hidden photon helioscopes with extended baselines [21].

4 Summary

We have discussed bottom-up motivations of light hidden sector particles that are weakly interacting with photons, so-called WISPs. Axions are introduced as a solution to the strong \mathcal{CP} problem via the Peccei-Quinn mechanism. Other WISPs, in particular axion-like particles, mini-charged particles or hidden photons may arise in field or string theoretic extensions of the standard model. These light hidden sectors interacting with photons have a rich phenomenology, testable by early universe, astrophysical environments and laboratory experiments.

Acknowledgments

The author would like to thank the organizers of the *5th Patras Workshop on Axions, WIMPs and WISPs* for a stimulating conference. He also wishes to thank H. Gies, J. Jaeckel, J. Redondo and A. Ringwald for the fruitful collaboration and acknowledges support by STFC UK (PP/D00036X/1) and the EU Marie Curie Network “UniverseNet” (HPRN-CT-2006-035863).

References

- [1] J. E. Kim, Phys. Rept. **150** (1987) 1; M. S. Turner, Phys. Rept. **197** (1990) 67; R. D. Peccei, Lect. Notes Phys. **741** (2008) 3 [arXiv:hep-ph/0607268]; J. E. Kim and G. Carosi, [arXiv:0807.3125 [hep-ph]].
- [2] C. A. Baker *et al.*, Phys. Rev. Lett. **97** (2006) 131801 [arXiv:hep-ex/0602020].
- [3] R. D. Peccei and H. R. Quinn, Phys. Rev. D **16** (1977) 1791; R. D. Peccei and H. R. Quinn, Phys. Rev. Lett. **38** (1977) 1440.
- [4] S. Weinberg, Phys. Rev. Lett. **40** (1978) 223; F. Wilczek, Phys. Rev. Lett. **40** (1978) 279.

AXIONS AND OTHER (SUPER-)WISPS

- [5] M. Dine, W. Fischler and M. Srednicki, Phys. Lett. B **104** (1981) 199; A. R. Zhitnitsky, Sov. J. Nucl. Phys. **31** (1980) 260 [Yad. Fiz. **31** (1980) 497].
- [6] J. E. Kim, Phys. Rev. Lett. **43** (1979) 103; M. A. Shifman, A. I. Vainshtein and V. I. Zakharov, Nucl. Phys. B **166** (1980) 493.
- [7] G. G. Raffelt, “Stars As Laboratories For Fundamental Physics,” *Chicago, USA: Univ. Pr. (1996) 664 p*
- [8] P. Sikivie, Phys. Rev. Lett. **51** (1983) 1415 [Erratum-ibid. **52** (1984) 695]; L. D. Duffy *et al.*, Phys. Rev. D **74** (2006) 012006 [arXiv:astro-ph/0603108].
- [9] J. Conlon, *Talk at the 5th Patras Workshop, Durham, UK, 13-17 July 2009*
- [10] E. Arik *et al.* [CAST Collaboration], JCAP **0902** (2009) 008 [arXiv:0810.4482 [hep-ex]]; Y. Inoue *et al.* [Tokyo Helioscope Collaboration], Phys. Lett. B **668** (2008) 93 [arXiv:0806.2230 [astro-ph]].
- [11] J. Jaeckel *et al.*, Phys. Rev. D **75** (2007) 013004 [arXiv:hep-ph/0610203].
- [12] A. Dupays, E. Masso, J. Redondo and C. Rizzo, Phys. Rev. Lett. **98** (2007) 131802 [arXiv:hep-ph/0610286].
- [13] B. Holdom, Phys. Lett. B **166**, 196 (1986).
- [14] K. R. Dienes, C. F. Kolda and J. March-Russell, Nucl. Phys. B **492** (1997) 104 [arXiv:hep-ph/9610479].
- [15] M. Goodsell *et al.*, [arXiv:0909.0515 [hep-ph]].
- [16] L. B. Okun, Sov. Phys. JETP **56** (1982) 502 [Zh. Eksp. Teor. Fiz. **83** (1982) 892]; M. Ahlers *et al.*, Phys. Rev. D **76** (2007) 115005 [arXiv:0706.2836 [hep-ph]].
- [17] S. Davidson, S. Hannestad and G. Raffelt, JHEP **0005**, 003 (2000) [arXiv:hep-ph/0001179].
- [18] M. Ahlers *et al.*, Phys. Rev. D **77** (2008) 095001 [arXiv:0711.4991 [hep-ph]].
- [19] K. Ehret *et al.* [ALPS Collaboration], [arXiv:0905.4159 [physics]].
- [20] J. Jaeckel and A. Ringwald, Phys. Lett. B **659** (2008) 509 [arXiv:0707.2063 [hep-ph]]; F. Caspers, J. Jaeckel and A. Ringwald, [arXiv:0908.0759 [hep-ex]].
- [21] S. N. Gninenko and J. Redondo, Phys. Lett. B **664** (2008) 180 [arXiv:0804.3736 [hep-ex]].

Chapter 2

Direct Searches for Dark Matter

Searching for dark matter with CRESST

H. Kraus¹, G. Angloher², M. Bauer³, I. Bavykina², A. Bento^{2,4}, A. Brown¹, C. Bucci⁵, C. Ciemniak⁶, C. Coppi⁶, G. Deuter³, F. von Feilitzsch⁶, D. Hauff², S. Henry¹, P. Huff², J. Imber¹, S. Ingleby¹, C. Isaila⁶, J. Jochum³, M. Kiefer², M. Kimmerle³, J.-C. Lanfranchi⁶, R. F. Lang², B. Majorovits^{1,7}, M. Malek¹, R. McGowan¹, V. B. Mikhailik¹, E. Pantic², F. Petricca², S. Pfister⁶, W. Potzel⁶, F. Pröbst², S. Roth⁶, K. Rottler³, C. Sailer³, K. Schäffner², J. Schmalzer², S. Scholl³, W. Seidel², M. von Sivers⁶, L. Stodolsky², Ch. Strandhagen³, R. Strauss⁶, A. J. B. Tolhurst¹, I. Usherov³ and W. Westphal^{6,†}

¹Department of Physics, University of Oxford, Oxford OX1 3RH, United Kingdom

²Max-Planck-Institut für Physik, Föhringer Ring 6, D-80805 München, Germany

³Eberhard-Karls-Universität Tübingen, D-72076 Tübingen, Germany

⁴on leave from: Departamento de Fisica, Universidade de Coimbra, P3004 516 Coimbra, Portugal

⁵INFN, Laboratori Nazionali del Gran Sasso, I-67010 Assergi, Italy

⁶Physik-Department E15, Technische Universität München, D-85747 Garching, Germany

⁷now at: Max-Planck-Institut für Physik, Föhringer Ring 6, D-80805 München, Germany

[†] Deceased

DOI: http://dx.doi.org/10.3204/DESY-PROC-2009-05/kraus_hans

The CRESST II experiment is a dark matter search using cryogenic phonon-scintillation detectors, aiming to detect WIMP dark matter particle interactions. The detector consists of individual, modular and scintillating (CaWO₄ or ZnWO₄) target crystals, each equipped with a phonon sensor for precise determination of the energy deposited in the crystals. Each module is further equipped with a separate cryogenic scintillation light detector, allowing event-by-event background discrimination. An extended commissioning run during 2007 has set an upper limit on the WIMP-nucleon scattering cross section. Attention is currently focussed on the interpretation of a few remaining nuclear recoils candidate events.

1 Introduction

CRESST (Cryogenic Rare Event Search with Superconducting Thermometers) is a dark matter search experiment located in the Gran Sasso underground laboratory, Italy. The collaboration has developed sensitive cryogenic phonon-scintillation detectors. A particle interaction in the absorber will deposit most of its energy as phonons; these thermalise in a superconducting phase transition (SPT) sensor on the crystal surface, creating a large change in sensor resistance, which is measured using a SQUID. This technique of using SPT sensors to measure the phonon signal can achieve a very low energy threshold and excellent near-threshold energy resolution (~ 300 eV). The low threshold is especially useful for a dark matter search as the expected event rate from WIMP interactions is highest at low energies. A small improvement in the energy threshold can lead to a significant improvement in the sensitivity of the experiment. The energy resolution is less important as the dark matter spectrum is featureless; however it allows

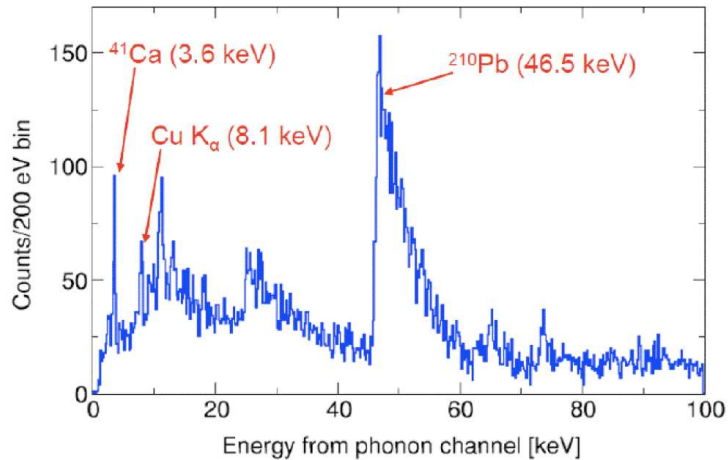


Figure 1: A background spectrum recorded by a CRESST detector.

the accurate identification of impurities in the absorber crystals from spectral lines. This is illustrated in Figure 1; further detail about backgrounds in CRESST is published elsewhere [1]. We expect that this information will be very valuable to allow sourcing radiopure scintillator crystals for EURECA.

The scintillation light produced by a particle interaction is detected by a second cryodetector consisting of a separate silicon absorber, equipped with a tungsten SPT sensor. Comparing the scintillation signal with the phonon signal allows us to identify each event as either being caused by a nuclear recoil or an electron recoil. The scintillating crystals are surrounded by a reflecting foil, which also acts as a scintillator, so any alpha decays on the surface of the dark matter target crystal (where the alpha particle recoils away from the target crystal) also produce a scintillation signal.

This combination of excellent energy resolution and threshold, with powerful event-by-event background discrimination make these detectors ideal for a dark matter search experiment.

2 Setup at Gran Sasso

The CRESST II upgrade was designed to allow us to run up to 33 detector modules [2]. The detector modules are cooled to $\sim 10\text{mK}$ temperature using a dilution refrigerator. The detector support structure is surrounded by shielding made from radiopure copper and lead. As shown in Fig. 2, this volume immediately around the coldbox of the cryostat (containing the detectors modules) and copper and lead shielding is enclosed, and continuously flushed with nitrogen gas to remove radon. Outside this volume, a muon-veto composed of individual scintillator panels is installed. Further, a polyethylene shield is used to moderate the energies of neutrons to below detection threshold.

The detector signals are read out using a 66-channel SQUID system [3]. The SQUID sensors are installed at the bottom of the main helium cryostat (see Fig. 2), and connected to the detectors, and to the room temperature electronics using specially designed woven cables. The

SEARCHING FOR DARK MATTER WITH CRESST

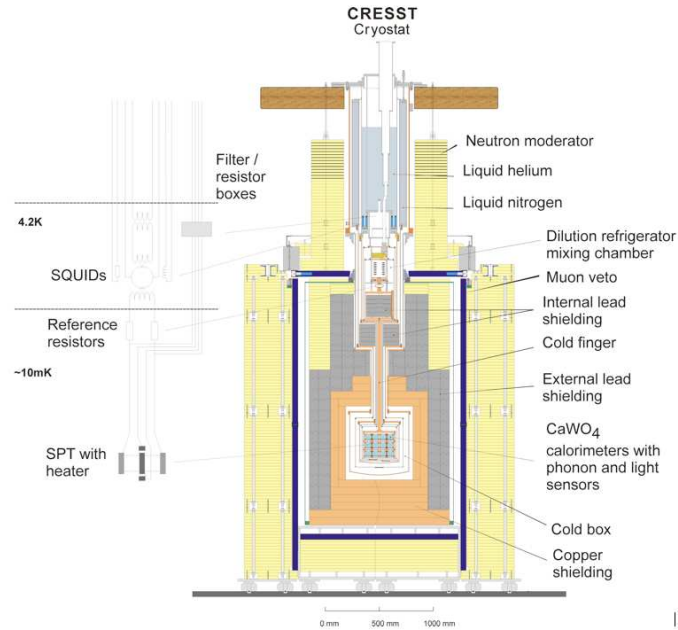


Figure 2: The CRESST cryostat at the Gran Sasso laboratory and the detector readout circuit connecting to an SPT of a detector and a heater on the same detector, used for operation and calibration.

electronics is designed to minimise electromagnetic noise, which could be picked-up by the detectors; and can be controlled remotely from outside the laboratory.

3 Results

An extended commissioning run of the upgraded CRESST II setup was undertaken in 2007. This demonstrated that the detectors could run in a stable fashion for an extended period. Two detector modules produced ~ 48 kg days of data, which was used to set an improved upper limit on WIMP-nucleon elastic scattering [1]. The background discrimination worked well; however, three events were present in the tungsten nuclear recoil band.

The most likely cause of these events was then believed to be either neutrons, or recoiling nuclei from an alpha decay on the surface of the crystal; although any alpha particles hitting the foil surrounding the crystal produced a scintillation signal, the clamps supporting the crystal were not completely covered with this foil. With the aim of reducing the number of these events, the neutron shielding around the cryostat was improved, and the clamps were covered with a scintillating epoxy.

A background run with these improvements, and a total of 9 modules was undertaken between August and December 2008. Some modules saw a small number of events in which no scintillation light signal was recorded. These were believed to be not due to particles, but due to a phonon signal produced by cracks in crystals which were clamped to hard.

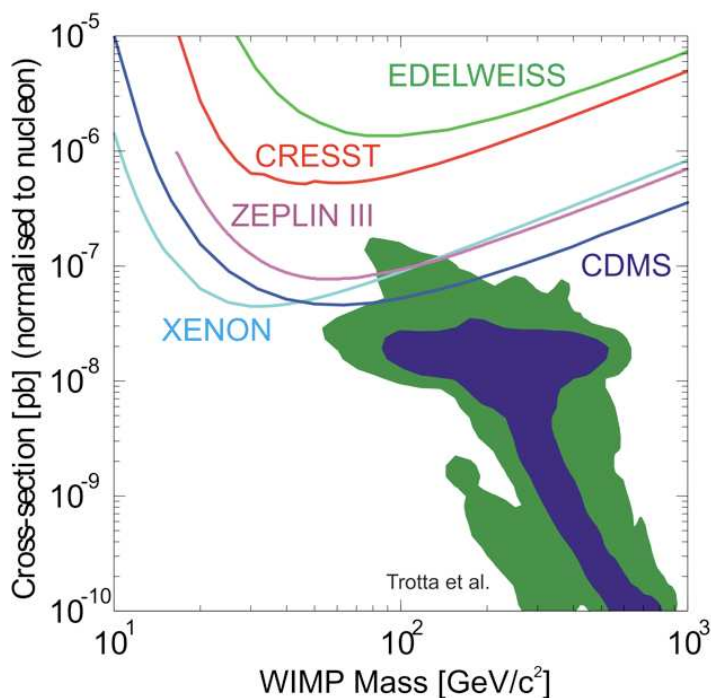


Figure 3: Dark matter limits set by CRESST and selected other experiments [4], and the region predicted by SUSY models [5].

In 2009 all the crystal holders were replaced with new clamps to hold the detectors with less pressure. The cryostat is currently cold and taking data is in progress with this setup; further results are expected shortly.

4 Scintillator research

Until 2008, all CRESST-II detector modules used CaWO_4 absorber crystals. We have an ongoing research programme to develop further scintillator materials [6]. This has led to the installation of ZnWO_4 crystals into the CRESST cryostat. ZnWO_4 is a very promising material with a lower intrinsic radioactivity and potentially higher light yield than CaWO_4 . We are currently investigating further materials including CaMoO_4 and $\text{Al}_2\text{O}_3\text{-Ti}$. A wide range of detector materials will be particularly useful when we find an indication for a dark matter signal. To claim a discovery of dark matter, verification of the event rate scaling with different target nuclei should be performed. A range of scintillating target materials is especially useful as they can all be operated in the same cryogenic setup, thereby reducing systematic effects.

5 EURECA

CRESST, together with the EDELWEISS experiment [7] and other expert groups, is part of the EURECA [8] (European Underground Rare Event Calorimeter Array) project. This is planned to be a tonne-scale experiment using cryogenic techniques, pioneered by CRESST and EDELWEISS, in order to search for dark matter interactions with a cross section down to 10^{-10} pb. EURECA will be built in the Laboratoire Souterrain de Modane.

References

- [1] R. F. Lang *et al.*, *Astropart. Phys.* **32** (2010) 318 [arXiv:0905.4282 [astro-ph.IM]].
- [2] G. Angloher *et al.*, *Astropart. Phys.* **31** (2009) 270 arXiv:0809.1829 [astro-ph].
- [3] S. Henry *et al.*, *JINST* **2** (2007) P11003.
- [4] <http://dmttools.berkeley.edu>
- [5] R. Trotta, F. Feroz, M. P. Hobson, L. Roszkowski and R. Ruiz de Austri, *JHEP* **0812** (2008) 024 [arXiv:0809.3792 [hep-ph]].
- [6] H. Kraus *et al.*, *Nucl. Instrum. Meth. A* **600** (2009) 594.
- [7] V. Sanglard *et al.* [The EDELWEISS Collaboration], *Phys. Rev. D* **71** (2005) 122002 [arXiv:astro-ph/0503265].
- [8] H. Kraus *et al.*, *PoS IDM2008* (2008) 013.

CDMS-II to SuperCDMS: WIMP search at a zep-tobarn

Tobias Bruch¹ for the CDMS Collaboration

¹University of Zürich, Winterthurerstr 190, 8057 Zürich, Switzerland

DOI: http://dx.doi.org/10.3204/DESY-PROC-2009-05/bruch_tobias

The Cryogenic Dark Matter search experiment (CDMS) employs low-temperature Ge and Si detectors to detect WIMPs via their elastic scattering of target nuclei. The last analysis with an germanium exposure of 397.8 kg-days resulted in zero observed candidate events, setting an upper limit on the spin-independent WIMP-nucleon cross-section of $6.6 \times 10^{-44} \text{ cm}^2$ ($4.6 \times 10^{-44} \text{ cm}^2$, when previous CDMS Soudan data is included) for a WIMP mass of 60 GeV. The improvements in the surface event rejection capability for the current analysis with an germanium exposure about a factor of 2.5 greater than used in the last analysis will be discussed. To increase the sensitivity beyond the $1 \times 10^{-44} \text{ cm}^2$ benchmark new 1 inch thick detectors have been developed. A first tower consisting of six of these detectors has been successfully installed at the Soudan site. These detectors will be used in a 15 kg SuperCDMS stage with an expected sensitivity on the spin-independent WIMP-nucleon elastic scattering cross-section of $5 \times 10^{-45} \text{ cm}^2$. In addition, the CDMS Collaboration has started to look for signatures of non WIMP dark matter particles, which may explain the annual modulation signature observed by DAMA.

1 Introduction

The Cryogenic Dark Matter Search (CDMS) experiment operates 19 Ge ($\sim 250 \text{ g}$ each) and 11 Si ($\sim 100 \text{ g}$ each) detectors at the Soudan underground laboratory (MN, USA) to search for non-luminous, non-baryonic Weakly Interacting Massive Particles (WIMPs), that could form the majority of the matter in the universe [1, 2]. The detectors are designed to read out both ionization and phonon signals of an interaction. The ratio of ionization to phonon energy, the ionization yield, enables discrimination of nuclear recoils from electron recoils. The details of the detector structure and operation can be found in [3]. The ionization yield discriminator provides a rejection factor of $> 10^4$ for electron recoils, leaving surface events as the main background in the search for nuclear recoils.

2 Surface contamination of the crystals

Particle interactions may suffer from a suppressed ionization signal if the interactions occur in the first few microns of the crystal surfaces, this ionization loss is sufficient to misclassify such events as nuclear recoils. These surface events mainly occur due to radioactive contamination on detector surfaces, or as a result of external photon interactions releasing low-energy electrons

from surfaces near the detectors. A correlation analysis between alpha-decay and surface-event rates provides evidence that ^{210}Pb is a major component of the surface event background [4]. The correlation analysis also shows some indication that improved detector handling during production and testing reduced the surface contamination for the later three towers. In table 1 the measured surface event rates are summarized. The third row gives the remaining (non ^{210}Pb related) surface-event rate which is compatible with the rate expected from photon induced events, given in the last row.

To discriminate surface events against nuclear recoils the timing properties of the phonon pulses are used. Two possible parameters are the delay of the slower phonon signal with respect to the ionization signal and the risetime of the leading phonon pulse (which is the one with the highest amplitude), since surface events have smaller delays and faster risetimes than bulk nuclear-recoils. The left panel of figure 1 shows a comparison of the distribution of surface events and nuclear recoils in the simple timing discriminator (sum of delay and risetime). An improvement in the separation of the distributions of surface events and nuclear recoils may yield a high selection efficiency for nuclear recoils in the current analysis. In the current analysis new additional parameters have been defined which may provide an even higher selection efficiency of nuclear recoils while maintaining a high rejection of surface events.

Surface event rate 10^{-3} counts/detector/day	10-100 keV singles
Total observed	371 ± 183
^{210}Pb corr. analysis	240 ± 183
non ^{210}Pb	131 ± 63
exp. photon induced	217 ± 103

Table 1: Surface event rate from ^{210}Pb contamination and photon induced events.

3 Recent results and the road to the zeptobarn sensitivity

The recent result used a germanium exposure of 397.8 kg-days. Surface events present in ^{133}Ba calibration data or naturally present in WIMP search data, were studied to determine the surface event leakage into the signal region after the timing cut is applied. The estimated surface event leakage, based on the observed numbers of single- and multiple- scatter events within and surrounding the 2σ nuclear recoil region in each detector, is $0.6_{-0.3}^{+0.5}(\text{stat.})_{-0.2}^{+0.3}(\text{syst.})$ events [5]. Upon the unblinding of the data no event was observed within the signal region. From this data the 90% CL upper limit on the spin-independent WIMP-nucleon cross section is derived [5]. The inclusion of a reanalysis of previous CDMS data, sets the world's most stringent upper limit on the spin-independent WIMP-nucleon cross section for WIMP masses above $42 \text{ GeV}/c^2$ with a minimum of $4.6 \times 10^{-44} \text{ cm}^2$ for a WIMP mass of $60 \text{ GeV}/c^2$ (shown as the black/solid line in figure 1).

To further increase the sensitivity the total accumulated exposure (runtime times mass) has to be increased and the background has to be kept under control. So far the CDMS-II setup has acquired an additional Ge exposure which is about a factor of 2.5 of the exposure used for the recent result. With this accumulated exposure the CDMS-II setup is expected to reach a sensitivity in the low 10^{-44} cm^2 range (see figure 1). For the SuperCDMS setup new 1 inch thick detectors have been developed and tested, providing an increase of a factor 2.54 in mass with respect to the 1 cm thick detectors used in CDMS-II. The first of 5 SuperTowers being operated at the Soudan site has been successfully installed and its performance in terms of background rejection capability is currently investigated. The redesign of the phonon readout, which maxi-

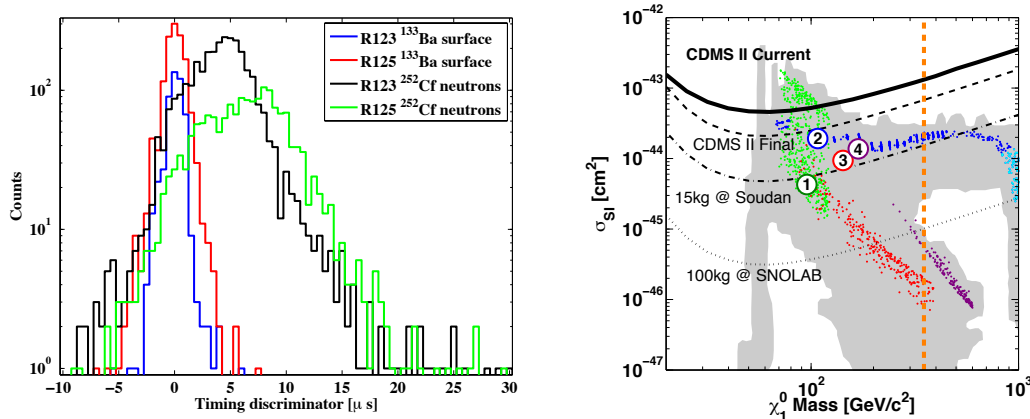


Figure 1: Left panel: Comparison of the simple timing discriminator for the last analysis with the current analysis. The separation of the surface event distribution and nuclear recoil distribution shows an improvement for the current data, yielding a possible higher selection efficiency for nuclear recoils. Right panel: Mass vs spin-independent WIMP nucleon cross section parameter space. The horizontal curves represent current and projected sensitivities of the CDMS experiment. The vertical (orange/dotted) line represent the approximate upper limit of the LHC reach in neutralino mass. The gray shaded region and colored points are scans of the CMSSM [6] along with four Linear Collider Cosmology benchmark points (numbered points)[7].

mizes the active phonon collection area, and new sensor configurations are expected to improve the discrimination between surface events and nuclear-recoils. With a runtime of 2 years the five SuperTower setup with a total mass of 15kg of Ge is expected to break the benchmark sensitivity of $1 \times 10^{-45} \text{cm}^2$ and probe parameter space down to a level of $5 \times 10^{-45} \text{cm}^2$. At the SuperCDMS 100 kg stage, operated at SNOLAB, it is expected that the CDMS experiment reaches the zeptobarn sensitivity. As shown in figure 1, SuperCDMS 100kg aims to reach a sensitivity of $3 \times 10^{-46} \text{cm}^2$ at a WIMP mass of $60 \text{GeV}/c^2$.

4 Electromagnetic signatures of dark matter

The annual modulation signature observed by DAMA [8] may be interpreted as the conversion of a dark matter particle into electromagnetic energy in the detector. In this case the corresponding signal should also be observable in the electron-recoil spectrum of CDMS. The possibility of an electron-recoil signal from axion-like dark matter particles has recently been investigated [9]. A general analysis of the low-energy electron recoil spectrum of the germanium detectors from 2-8.5 keV resulted in 90% CL upper limits on an excess rate above background [10]. These upper limits are directly compared to the total rate observed by DAMA in figure 2. It should be stressed that the DAMA rate may contain a contribution of ^{40}K decays at an energy of 3.2 keV, but no information on the actual rate from this background is provided by the DAMA collaboration. Thus no subtraction is performed, which would reduce the difference between the upper limit from CDMS and the excess rate in DAMA. The event rates in CDMS and DAMA detection media may differ depending on the coupling of the dark matter particle. For an electromagnetic conversion a Z^2 (where Z is the atomic number) scaling of the cross section

is natural and thus considered here. Another scaling can be trivially considered. The scaled limits from CDMS to the rate in NaI are shown as the blue lines in figure 2. The inset in figure 2 shows the upper limits on a possible modulation amplitude under the assumption of a standard halo model, yielding a conservative upper bound on the modulation amplitude of 6% of the total rate. The upper limits set by CDMS are about a factor of 2 lower than the modulation amplitudes observed by DAMA. This constraints are not affected by any residual background rate in the DAMA data.

5 Summary

The CDMS-II experiment has maintained high dark matter discovery potential by limiting expected backgrounds to less than one event in the signal region. The current data sets the world's most stringent upper limit on the spin-independent WIMP-nucleon cross-section for WIMP masses above $42 \text{ GeV}/c^2$ with a minimum of $4.6 \times 10^{-44} \text{ cm}^2$ for a WIMP mass of $60 \text{ GeV}/c^2$. The analysis of a dataset with a factor of 2.5 more Ge exposure is ongoing, it is expected to increase the sensitivity to the low 10^{-44} cm^2 range. The first super tower with 6 new 1 inch thick detectors was successfully installed at the Soudan site and is currently tested in terms of rejection efficiency of surface events. These detectors will be used in the next upgrades of the CDMS experiment which aims to reach the zeptobarn sensitivity with a SuperCDMS 100 kg stage operated at SNOLAB.

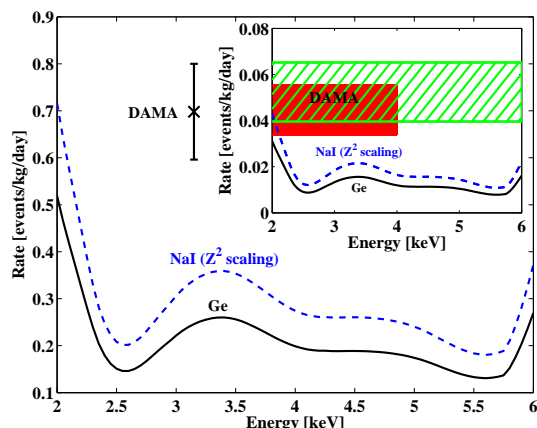


Figure 2: Direct comparison between the 90% CL upper limit in CDMS (black/solid) with the total counting rate observed by DAMA/LIBRA (black data point, shown with 2σ error bars). The inset compares the upper limit on the modulation, amplitude assumed to be 6% of the upper limit on the total rate, with the 2σ regions of the annual modulation amplitude observed by DAMA. The blue/dashed lines give the upper limits in Ge scaled to NaI (see text).

Although being designed for the search for nuclear recoils, the CDMS experiment has started to look for electromagnetic signatures of dark matter particles. The analysis of the low-energy electron-recoil spectrum of CDMS may help to identify or constrain possible models which can explain the annual modulation signature observed by DAMA.

References

- [1] D.N. Spergel *et al.*, *Astrophys. J. Suppl.* 148, 175 (2003).
- [2] G. Jungman *et al.*, *Phys. Rep.* 267, 195 (1996).
- [3] D.S. Akerib *et al.*, *Phys. Rev. D* 72, 052009 (2005)
- [4] CDMS Collab., in preparation.
- [5] Z. Ahmed *et al.*, *Phys. Rev. Lett.* 102, 011301 (2009).
- [6] E. A. Baltz & P. Gondolo, *JHEP* 10, 052 (2004).
- [7] E. A. Baltz *et al.*, *Phys. Rev. D* 74, 103521 (2006).
- [8] R. Bernabei *et al.*, *Eur. Phys. J. C* 56, 333 (2008).
- [9] Z. Ahmed *et al.*, *Phys. Rev. Lett.* 103, 141802 (2009).
- [10] Z. Ahmed *et al.*, arXiv:0907.1438.

The XENON100 Detector for Dark Matter Searches

Alexander Kish for the XENON100 collaboration

University of Zürich, Winterthurerstrasse 190, 8057 Zürich, Switzerland

DOI: http://dx.doi.org/10.3204/DESY-PROC-2009-05/kish_alexander

The XENON100 detector, which has replaced the XENON10 prototype in the same location and improved shield at Laboratori Nazionali del Gran Sasso (Italy), is a dual phase (liquid-gas) xenon time-projection chamber for particle detection. The total amount of liquid xenon is 165 kg, of which 65 kg are in the target volume enclosed by a teflon/copper structure, the rest being in the surrounding active veto. The direct and proportional VUV light signal produced by particle interactions is detected by 242 PMTs. The expected sensitivity of the XENON100 for spin-independent WIMP-nucleon couplings is $2 \cdot 10^{-45} \text{ cm}^2$ for a 100 GeV WIMP with a background-free exposure of 6000 kg-days. In this paper, the principle of the XENON experiment and its main components are described, and a Monte Carlo study of the various types and sources of the background is summarized.

1 Introduction

The XENON100 detector [1], which is installed in the Laboratori Nazionali del Gran Sasso (LNGS) in Italy, is a second generation detector within the XENON program which aims at the direct detection of particle dark matter in the form of Weakly Interacting Massive Particles (WIMPs) [2], [3]. It is the successor of XENON10, which has set a limit on the WIMP-nucleon spin-independent cross-section of $8.8 \times 10^{-44} \text{ cm}^2$ for a WIMP mass of 100 GeV/c² [4]. XENON100 aims to improve this sensitivity by more than one order of magnitude due to increase of the target mass by a factor of 10 and reduction of the background in the target volume by a factor of 100.

The noble gas xenon has many advantages for particle detection, and in particular for dark matter search. It is an efficient and fast scintillator: $\lambda = 178 \text{ nm}$, decay time of the fast (slow) component is 2.2 ns (27 ns) [5]. Availability of both scintillation and ionization signals provides event-by-event discrimination based on the amount of signals in both channels. High density of liquid xenon ($\sim 3 \text{ g/cm}^3$) provides powerful self-shielding in a compact detector geometry, in addition to the absence of the naturally occurring long-lived radioactive isotopes.

2 XENON100 Detector and Shield Design

The XENON100 shield (schematically shown in figure 1, with 4π coverage of the detector, consists (from outside to inside) of tanks filled with water (thickness 20 cm) to moderate ambient neutrons, two layers of lead (15 cm outer layer and 5 cm inner layer with a lower contamination of the radioactive isotope ²¹⁰Pb), 20 cm of polyethylene, and a 5 cm thick copper layer.

THE XENON100 DETECTOR FOR DARK MATTER SEARCHES

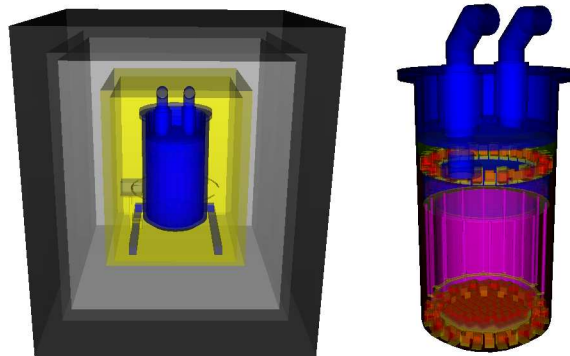


Figure 1: Left: The XENON100 detector inside its shield as it was simulated within the GEANT4 framework (the colors represent: two layers of lead - dark grey, polyethylene - light grey, and copper - yellow, water tanks are not shown; on the left side of the cryostat - lead brick for calibration with Am-Be source); Right: The closeup view of the detector (blue - stainless steel, magenta - PTFE, yellow - copper, orange - PMTs).

The XENON100 detector is a dual phase (liquid-gas) time-projection chamber (TPC). The total amount of liquid xenon (LXe) enclosed in the stainless steel vacuum cryostat is 165 kg. The liquid xenon in the target volume is 65 kg, enclosed by a cylindrical PTFE and copper structure. PTFE reflects scintillation light (with high efficiency for VUV region [6]) and optically separates the target volume from the surrounding LXe, which has a mass of 100 kg (~ 4 cm thick). In addition to self-shield capability of LXe due to its high density, light sensors installed in the xenon volume around the target provide an active veto for additional background discrimination.

The TPC is installed in a double walled low activity stainless steel cryostat vessel sitting on the stainless steel support bars fixed to the shield door. The total weight of the vessel is 73.6 kg, which is only 30% of that of the XENON10 prototype [4].

Electrons created by ionization in the LXe target are drifted upwards by a strong electric field applied across the TPC. The cathode is located in the liquid phase below the target. In order to shield the bottom PMTs from the electric field, an additional (screening) mesh is installed below the cathode. The anode stack is placed in the gas phase maintained inside the 'diving bell' [7]. An extraction field is created across the liquid-gas interface by applying high voltage on the anode. Two additional meshes are installed below and above the anode and kept at ground potential, to close the field cage, and shield the top PMT array from the high electric field.

The scintillation light generated by particles interacting with the xenon atoms is detected by 242 one square inch R8520-06-Al Hamamatsu photomultiplier tubes (PMT). The top PMT array consists of 98 PMTs. 80 PMTs are immersed in liquid xenon below the target volume. Additionally, 64 PMTs view the veto volume: 16 PMTs above and below the TPC and 32 observing the sides.

3 Background Predictions

The background of the XENON100 experiment consists of two types: electron recoils (gamma, beta radiation) and nuclear recoils (elastic neutron scatters).

Electron recoil background originates from radioactive contamination of detector and shield materials (^{232}Th , ^{238}U , ^{60}Co , and ^{40}K), radioactive contamination in liquid xenon (^{232}Th , ^{238}U and ^{85}Kr), and the decays of ^{222}Rn and its progeny inside the shield cavity.

The main source of nuclear recoil background is neutron production with (α, n) reactions from ^{232}Th , ^{238}U , and ^{235}U decays and spontaneous fission of ^{238}U in materials of the detector, shield and rock and concrete of the underground laboratory. Another contribution comes from muon-induced neutrons.

The majority of materials planned to be used in the construction of the XENON100 detector and its shield were screened with low background Ge detectors in order to determine their radioactivity. Table 1 shows the results of the measured radioactive contamination, including contamination in LXe, determined with a β - α delayed coincidence technique.

These values are used as an input information for the Monte Carlo simulations with GEANT4 toolkit and predictions of the background from various sources.

Dangerous background comes only from single scatter events, as this is the predicted behavior of a WIMP. Multiple scatter events are rejected taking into account the position resolution of the detector.

The fiducial volume cuts used in the analysis of the Monte Carlo data are preliminary, as appropriate for such a study. In addition, the effect of the active veto is not considered in the

Table 1: Radioactive contamination of the materials used in the construction of XENON100. The PMT signal cables additionally contain (5.0 ± 0.9) mBq/kg of ^{108m}Ag . Lead used for the shield is contaminated with ^{210}Pb : (530 ± 70) Bq/kg in the outer layer and (26 ± 6) Bq/kg in the inner layer.

Material	Unit	^{238}U	^{232}Th	^{60}Co	^{40}K
		[mBq/unit]	[mBq/unit]	[mBq/unit]	[mBq/unit]
Stainless steel	kg	< 1.7	< 1.9	5.5 ± 0.6	< 9.0
PTFE	kg	< 0.31	< 0.16	< 0.11	< 2.25
PMTs	piece	0.15 ± 0.02	0.17 ± 0.04	0.6 ± 0.1	11 ± 2
PMT bases	piece	0.16 ± 0.02	0.07 ± 0.02	< 0.01	< 0.16
Support bars (steel)	kg	< 1.3	2.9 ± 0.7	1.4 ± 0.3	< 7.1
Copper (inside)	kg	< 0.22	< 0.16	0.20 ± 0.08	< 1.34
Resistor chain	piece	0.027 ± 0.004	0.014 ± 0.003	< 0.003	0.19 ± 0.03
Cathode support ring	kg	3.6 ± 0.8	1.8 ± 0.5	7.3 ± 1.3	< 4.92
Top grids support rings	kg	< 2.7	< 1.5	13 ± 1	< 12
PMT signal cables	kg	< 1.6	3.7 ± 1.8	< 0.69	35 ± 13
Polyethylene shield	kg	0.23 ± 0.05	< 0.094	< 0.89	0.7 ± 0.4
Copper shield	kg	< 0.07	< 0.03	< 0.0045	< 0.06
Lead shield (outer)	kg	< 0.92	< 0.72	< 0.12	14 ± 3
Lead shield (inner)	kg	< 0.66	< 0.55	< 0.11	< 1.46
Liquid xenon		< 2.90 ppt	< 1.95 ppt		

present analysis. For the detailed study, see [8].

The total single nuclear recoil rate, from all sources listed in table 2, is 1.43 (0.55) event/year for 50 kg (30 kg) fiducial volume. It is dominated by the neutrons originating from the radioactive contamination in the detector, shield, and laboratory materials. It is concluded that no muon veto is required for the XENON100, but will be relevant in the next generation of the XENON dark matter experiments.

Table 2: Nuclear recoil background.

	Single nuclear recoils per year in	
	50 kg FV	30 kg FV
Detector and shield materials	< 0.68	< 0.28
Cavern	0.48 ± 0.15	0.20 ± 0.09
Cosmic ray muons	0.27 ± 0.13	< 0.07
All sources	< 1.43	< 0.55

The dominant background of the XENON100 dark matter search experiment is the electron recoil background. As it is shown in table 3, the main background source is radioactive contamination in the detector materials (dominated by PMTs). Background rate from beta-decay of ^{85}Kr in liquid xenon is scaled to 0.7 ppb of Kr, the value determined with a delayed coincidence analysis before purification with a dedicated distillation column, which is expected to reduce krypton concentration down to ppt level [9].

Table 3: Electron recoil background.

	events/(kg·day·keVee)	
	50 kg FV	30 kg FV
Detector and shield materials	< 21.01	< 7.73
^{238}U and ^{232}Th in LXe	< 5.57	< 3.24
^{85}Kr in LXe	< 11.85	< 7.05
^{222}Rn in the cavity	< 2.56	< 1.24
All sources	< 40.99	< 19.26

References

- [1] E. Aprile, L. Baudis, arXiv:0902.4253 (2008).
- [2] G. Steigman and M.S. Turner, Nucl. Phys. **B253** 375 (1985).
- [3] D. Clowe *et al.* Astrophys. J. **648** L109 (2006).
- [4] J. Angle *et al.* (XENON10 Collaboration), Phys. Rev. Lett. **100**, 021303 (2008).
- [5] T. Doke *et al.*, NIM **A420** 62 (1999).
- [6] M. Yamashita *et al.*, NIM **A535** 692 (2004).
- [7] J. Angle *et al.* (XENON10 Collaboration) 'Design and performance of the XENON10 dark matter experiment'. In preparation.
- [8] E. Aprile *et al.* 'A Monte Carlo study of the electron and nuclear recoil background for the XENON100 dark matter search experiment'. In preparation.
- [9] K. Abe *et al.* (XMASS Collaboration), Astrop. Phys. **31**, 290 (2009).

SUSY dark matter and the LHC

Howard Baer

Dep't of Physics and Astronomy, University of Oklahoma, Norman, OK 73019

DOI: http://dx.doi.org/10.3204/DESY-PROC-2009-05/baer_howard

Weak scale supersymmetry is a highly motivated extension of the Standard Model that has a strong degree of support from data. It provides several viable dark matter candidates: the lightest neutralino (a WIMP), the gravitino, and the axion/axino supermultiplet. The LHC turn-on is imminent. The discovery of supersymmetry at the LHC will go a long way towards establishing the nature of dark matter. I present arguments why mainly axion cold dark matter is a better fit for supersymmetric models than neutralinos. I also argue that Yukawa-unified SUSY GUT theories based on $SO(10)$ with mixed axion/axino cold dark matter are extremely compelling, and present distinctive signatures for gluino pair production at the LHC.

1 Introduction

Astrophysical evidence for the existence of dark matter is now overwhelming, and comes from disparate sources: galactic clustering, galactic rotation curves, anisotropies in the CMB, microlensing, large scale structure, to name a few. The dark matter clusters on large scales, and helps seed structure formation in the universe. While the identity of the dark matter particle, or particles, is unknown, we do know several of its properties: it must be massive, non-relativistic (cold or warm), electric and color neutral, and stable at least on cosmic time-scales.

Of all the fundamental particles in the Standard Model (SM) of particle physics, only the neutrinos come close to having these properties. However, neutrinos are exceedingly light and engage in weak interactions: relic neutrinos would move at highly relativistic velocities, and so couldn't clump enough to seed structure formation. Their measured abundance from WMAP analyses is only a tiny fraction of the universe's energy budget. Thus, the existence of dark matter is also evidence for physics Beyond the Standard Model (BSM).

While there exist a plethora of candidate DM particles from BSM theories (examples include black hole remnants, Q-balls, sterile neutrinos, axions, KK gravitons, gravitinos, neutralinos, KK photons, branons and the lightest T -parity odd particle of Little Higgs theories. Two of these stand out in that they arise naturally due to very elegant solutions to long-standing problems in particle physics. These include the *axion*, which arises from the Peccei-Quinn (PQ) solution to the strong CP problem of QCD[1], and the *lightest supersymmetric particle*, or LSP, of R -parity conserving supersymmetric (SUSY) theories[2]. The SUSY theories solve the problematic quadratic divergences associated with scalar fields by introducing a new symmetry which relates bosons to fermions, thus giving scalar fields the milder divergence structure which is held by chiral fermions and gauge fields. SUSY also provides a means to unification with gravity, is an essential part of superstring theory, and in concert with Grand Unified Theories

(GUTs), receives some experimental support in the unification of gauge couplings under MSSM renormalization group evolution.

In fact, the PQ strong CP solution and supersymmetry are in many ways made for each other, so these two schemes are not mutually exclusive, and both may well be right. In that case, the axion occurs as part of an axion supermultiplet, which contains along with the axion an R -parity odd axino \tilde{a} , which may serve as LSP. In SUSY theories, the neutralino, the gravitino and the axino are all possible LSP candidates. In this talk, I will restrict my comments to supersymmetric dark matter (which includes axions and axinos), and comment on how it relates to LHC physics.

2 SUSY WIMP (neutralino) cold dark matter

In SUSY theories with neutralino CDM, the $\tilde{\chi}_1^0$ is considered a natural WIMP candidate for dark matter. The neutralino relic density can be calculated by solving the Boltzmann equation as formulated for a FRW universe. Central to the calculation is computation of the thermally averaged neutralino annihilation (and co-annihilation) cross section. The fact that the relic density comes out approximately in the right ballpark is often referred to as the “WIMP miracle”.

The paradigm model for SUSY phenomenology is called minimal supergravity (mSUGRA) or CMSSM. It is defined by just a few parameters: $m_0, m_{1/2}, A_0, \tan\beta$ and $sign(\mu)$. In the mSUGRA model, the WIMP miracle is actually no miracle at all! The relic density turns out to be much too large over most parameter space. In fact, only in regions where the neutralino annihilation rate is highly enhanced will the relic density match the measured value. These regions are termed: the stau co-annihilation region at low m_0 , the HB/FP region at large m_0 where μ becomes small and we get mixed bino-higgsino CDM, the A -resonance region at large $\tan\beta$ where $\tilde{\chi}_1^0\tilde{\chi}_1^0$ annihilation through the A -resonance is enhanced, and the (largely excluded) bulk region, where annihilation is through t -channel exchange of light sleptons.

Direct production of WIMP dark matter at LHC (*e.g.* $pp \rightarrow \tilde{\chi}_1^0\tilde{\chi}_1^0 X$) is usually not interesting since there is no hard energy deposition for detectors to trigger upon. However, if SUSY exists, then LHC may be able to produce many or all of the *other* SUSY particles. The SUSY particle’s subsequent cascade decays[3] should lead to collider events with high p_T jets, high p_T isolated e s and μ s. Since each sparticle cascade decay terminates at the LSP (the putative DM particle), the SUSY events should also contain large missing transverse energy (E_T^{miss}) due to non-detection of the DM particles.

At each point in mSUGRA (or any other SUSY model) parameter space, we can simulate LHC production of the entire array of superparticles, along with their cascade decays[4]. By looking for signals with high p_T jets, isolated leptons and E_T^{miss} – beyond levels expected in the SM– we can test if a signal can be seen for an assumed value of integrated luminosity. In Fig. 1[5, 6], such a calculation has been made assuming 100 fb^{-1} of integrated luminosity. LHC should be able to see the parameter space below the contour marked “LHC”, which corresponds to $m_{\tilde{g}} \sim 3 \text{ TeV}$ when $m_{\tilde{g}} \sim m_{\tilde{q}}$, or $m_{\tilde{g}} \sim 1.8 \text{ TeV}$ when $m_{\tilde{g}} \gg m_{\tilde{q}}$. We also show contours of direct WIMP detection rates and indirect WIMP detection rates via high energy neutrino detection at IceCube, or via detection of γ s, e^+ s or \bar{p} s arising from neutralino annihilation in the galactic halo.

It is noteworthy that in the DM-favored HB/FP region at large m_0 , the LHC can only cover a portion of allowed parameter space. However, in this region, direct detection via Xenon-100

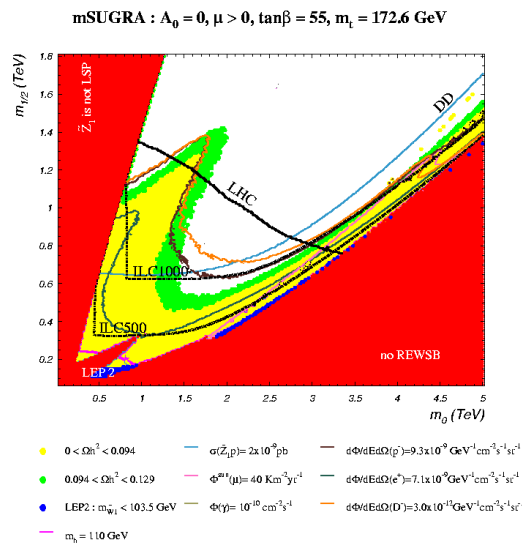


Figure 1: Contours of direct and indirect detection rates along with reach of LHC and ILC for SUSY in the mSUGRA model for $\tan\beta = 55$.

or indirect detection via IceCube is likely. In the A -annihilation region— the large bump in the center of the plot— detection of halo annihilations via γ , e^+ and \bar{p} is enhanced[7].

The enhancement of DD and IDD in the higgsino-like region is a general feature of a large assortment of models going beyond mSUGRA. In Fig. 2, we show predicted rates in models with a *well-tempered* neutralino[8]. The large cluster of models around 10^{-8} pb shows that the next set of DD experiments can either discover or rule out an entire class of well-motivated SUSY models[9].

3 The gravitino problem for WIMP and gravitino dark matter

A potential pit-fall in the mSUGRA model is known as the gravitino problem. If we assume a SUGRA-type model, with a TeV scale gravitino \tilde{G} , then gravitinos can be produced thermally in the early universe (even though they are never in thermal equilibrium). If the \tilde{G} is not the LSP, then it will decay into particle-particle pairs, and the sparticle cascade decays will contribute additional LSPs to the relic density. The relic density is too much if the re-heat temperature $T_R \gtrsim 10^{10}$ GeV. Even if T_R is lower, the late-time gravitino decays inject high energy particles into the cosmic soup during or after BBN, which can destroy the successful BBN predictions which match so well with data. Detailed calculations[10] show that one needs $T_R \lesssim 10^5$ GeV (which conflicts with many baryogenesis mechanisms) or $10^5 < T_R < 10^9$ GeV as long as $m_{\tilde{G}} \gtrsim 5$ TeV (the large $m_{\tilde{G}}$ suppresses the gravitino lifetime to less than 1 sec, so $\tilde{G} \rightarrow f\bar{f}$ decays occur at the onset or even before BBN starts). Since in SUGRA models the

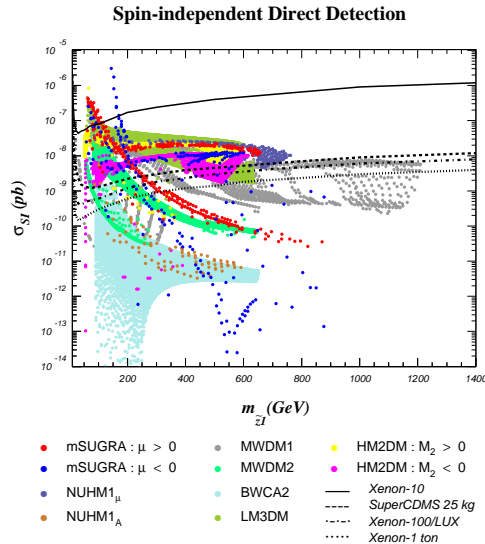


Figure 2: Direct detection rates for SUSY models with a well-tempered neutralino. Each point represents a relic-density consistent model with $\Omega_{\tilde{\chi}_1^0} h^2 \simeq 0.11$.

gravitino mass sets the scale for all the SSB terms, then we would naively expect all the SUSY particles to be at masses > 5 TeV (beyond LHC reach).

One way out might be to assume the gravitino is the LSP. But this results in the gravitino problem in reverse. Then neutralinos or other sparticles in the early universe would decay with long lifetimes in particle-gravitino pairs, and again disrupt BBN. Detailed calculations[10] show that $m_{\tilde{G}}$ should be $\lesssim 1$ GeV for $m_{\tilde{\chi}_1^0} \sim 100 - 1000$ GeV. Since $m_{\tilde{G}}$ sets the scale for the other sparticle, we would expect all the sparticles to have mass $\lesssim 1$ GeV, in contradiction to experimental limits.

4 Mainly axion CDM in minimal supergravity model

Another possibility is to assume some form of PQ solution to the strong CP problem. In the SUGRA context, we will add an axion supermultiplet to the model, which also contains an R -odd spin $\frac{1}{2}$ axino \tilde{a} [11, 12]. Then, axions will be produced as usual via vacuum misalignment[13], and can contribute to the relic density. Their relic abundance depends on the PQ breaking scale f_a , or alternatively on m_a . A value of $f_a \sim 10^{12}$ GeV, corresponding to $m_a \sim 10^{-6}$ eV, would saturate the measured DM abundance.

The value of the axino mass $m_{\tilde{a}}$ is very model-dependent: estimates range from the MeV to the multi-GeV scale[12]. In mSUGRA, if \tilde{a} is the LSP, then $\tilde{\chi}_1^0 \rightarrow \tilde{a}\gamma$ can occur with a lifetime of order a fraction of a second: it is then BBN-safe. The \tilde{a} can also be produced thermally like the gravitino[14]. Its thermal abundance depends on f_a , $m_{\tilde{a}}$ and T_R . Thus, DM would have three components: cold axions, cold axinos from thermal production and warm axinos from

neutralino decay.

The scenario works well if $m_{\tilde{a}} \sim$ the MeV scale. Then, we find the mSUGRA model can have dominant axion CDM with a small mixture of warm and cold axinos[15]. The resulting value of T_R is plotted in mSUGRA space in Fig. 3. The regions of mSUGRA space that are most neutralino dis-favored lead to the highest values of $T_R > 10^6$ GeV. This is enough to sustain non-thermal or Affleck-Dine leptogenesis! Thus, the most dis-favored neutralino DM regions are precisely the *most favored* axion/axino regions! Also, consequently, we expect quite different collider signatures at LHC in the case of mixed axion/axino CDM, as compared to neutralino DM. We remark here that calculating the amount of fine-tuning of the neutralino relic abundance also shows a preference for mixed axion/axino CDM over neutralino CDM[16].

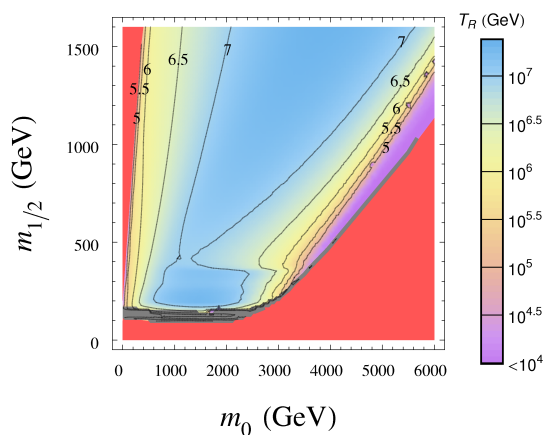


Figure 3: Contours of $\log_{10} T_R$ (the re-heat temperature) in the mSUGRA model with mainly axion CDM, for $\tan\beta = 10$.

5 Yukawa-unified SUSY, mixed axion/axino CDM and the LHC

SUSY GUT models based on the gauge group $SO(10)$ are extremely compelling, since these models allow for matter unification into the 16 dimensional spinor of $SO(10)$, give rise naturally to see-saw neutrinos, and yield automatic cancellation of triangle anomalies[17]. The simplest $SO(10)$ SUSY GUT models also contain $t-b-\tau$ Yukawa coupling unification. Scans over SUSY model parameter space reveal that Yukawa unification only occurs for a very specific spectra: first/second generation scalars at the 10 TeV level, third gen. scalars and Higgs at the TeV scale, while gauginos are quite light, with $m_{\tilde{g}} \sim 300 - 500$ GeV and $m_{\tilde{\chi}_1^0} \sim 50 - 80$ GeV[18, 19]. The neutralino relic abundance turns out to be much too high: $\Omega_{\tilde{\chi}_1^0} h^2 \sim 10^3 - 10^4$, about 4-5 orders of magnitude too much. The problem can be solved by invoking mixed axion/axino CDM[19]. Then, $\tilde{\chi}_1^0 \rightarrow \tilde{a}\gamma$ decays reduce the relic abundance by factors of $10^4 - 10^5$. The scenario works best if the CDM is mainly axions, with a small admixture of thermal and non-

thermal axinos[20]. Values of $T_R \sim 10^7 - 10^8$ are possible, allowing for baryogenesis. And since $m_{\text{particle}} \sim 10$ TeV, we also expect $m_{\tilde{G}} \sim 10$ TeV, thus solving the gravitino problem!

In this model, the light gluinos lead to robust signatures at both the Tevatron[21] and LHC colliders[22], and the whole scenario should be largely tested within year 1 of LHC operation, or even sooner if a Tevatron analysis is performed.

References

- [1] R. Peccei and H. Quinn, PRL**38** (1977) 1440 and *Phys. Rev.* **D 16** (1977) 1791.
- [2] See *e.g.* H. Baer and X. Tata, *Weak Scale Supersymmetry*, (Cambridge Univ. Press, 2006).
- [3] H. Baer *et al.*, *Phys. Lett.* **B 161** (1985) 175; G. Gamberini, *Z. Physik* **C 30** (1986) 605; H. Baer, V. Barger, D. Karatas and X. Tata, *Phys. Rev.* **D 36** (1987) 96; H. Baer, X. Tata and J. Woodside, *Phys. Rev.* **D 45** (1992) 142.
- [4] For recent work, see H. Baer, V. Barger, A. Lessa and X. Tata, JHEP**0909** (2009) 063.
- [5] H. Baer, C. Balázs, A. Belyaev, T. Krupovnickas and X. Tata, JHEP**0306** (2003) 054.
- [6] H. Baer, E. K. Park and X. Tata, *New J. Phys.* **11** (2009) 105024.
- [7] H. Baer and J. O’Farrill, JCAP **0404** (2004) 005; H. Baer, A. Belyaev, T. Krupovnickas and J. O’Farrill, JCAP **0408** (2004) 005.
- [8] N. Arkani-Hamed, A. Delgado and G. F. Giudice, *Nucl. Phys.* **B 741** (2006) 108.
- [9] H. Baer, A. Mustafayev, E. Park and X. Tata, JCAP **0701**, 017 (2007) and JHEP**0805** (2008) 058.
- [10] M. Kawasaki, K. Kohri, T. Moroi and A. Yotsuyanagi, *Phys. Rev.* **D78** (2008) 065011.
- [11] K. Rajagopal, M. Turner and F. Wilczek, *Nucl. Phys.* **B 358** (1991) 447.
- [12] L. Covi, H. B. Kim, J. E. Kim and L. Roszkowski, JHEP**0105** (2001) 033.
- [13] L. F. Abbott and P. Sikivie, *Phys. Lett.* **B 120** (1983) 133; J. Preskill, M. Wise and F. Wilczek, *Phys. Lett.* **B 120** (1983) 127; M. Dine and W. Fischler, *Phys. Lett.* **B 120** (1983) 137; M. Turner, *Phys. Rev.* **D 33** (1986) 889.
- [14] A. Brandenburg and F. Steffen, JCAP**0408** (2004) 008.
- [15] H. Baer, A. Box and H. Summy, JHEP**0908** (2009) 080.
- [16] H. Baer and A. Box, arXiv:0910.0333 (2009).
- [17] For a review, see S. Raby, in *Phys. Lett.* **B 667** (2008) 1.
- [18] D. Auto *et al.*, *J. High Energy Phys.* **0306** (2003) 023.
- [19] H. Baer, S. Kraml, S. Sekmen and H. Summy, JHEP**0803** (2008) 056.
- [20] H. Baer, M. Haider, S. Kraml, S. Sekmen and H. Summy, JCAP**0902** (2008) 002.

- [21] H. Baer, S. Kraml, S. Sekmen and H. Summy, arXiv:0910.2988 (2009).
- [22] H. Baer, S. Kraml, S. Sekmen and H. Summy, JHEP**0810** (2008) 079.

The ArDM - a ton - scale liquid argon experiment for direct Dark Matter Detection

Polina Otyugova, on behalf of ArDM collaboration

Physik-Institut der Universität Zürich, Winterthurerstrasse 190, CH-8057 Zürich, Switzerland

DOI: <http://dx.doi.org/10.3204/DESY-PROC-2009-05/otyugova.polina>

The ArDM is a ton-scale double phase detector for the direct search of the Weakly Interacting Massive Particle (WIMPs) as Dark Matter candidates. The detector is based on a liquid Argon (LAr) target. The present goal is to assemble, fully characterize the detector on the surface and then operate it at an underground facility. The scintillation light and ionization charge produced by recoiling nuclei in WIMP-Ar collision can be measured independently. The discrimination of the WIMP induced nuclear recoils from the electron/gamma background is done using the pulse discrimination technique and the ratio between the produced light and charge. The experiment and the last results from the detector commissioning are presented.

1 Direct Dark Matter Detection Principle Based on Liquid Argon Technology

Understanding the nature of Dark Matter is one of the most exciting problems of particle physics. One of the main evidences for Dark Matter comes from the observations of clusters of galaxies. Weak lensing observations of 1E0657-558, a system of two merged galaxy clusters, enabled a direct detection of Dark Matter [1].

A reasonable hypothesis is that Dark Matter is composed of a new kind of matter, made of so-called Weakly Interacting Massive Particles (WIMPs). The most favored candidate for these particles is the lightest supersymmetric (SUSY) particle, the neutralino. The idea of a direct detection of the Dark Matter with noble liquids is based on the detection of a nuclear recoil induced by the interaction of a WIMP with the nuclei of the target. The nuclear recoil results in the emission of scintillation light and the ionization charge which can be detected in the detector medium. The typical recoil energies are of the order of 10-100 keV.

The scintillation of LAr occurs through the radiative decays of excited molecular states Ar_2^* . The radiatively excited molecules are created in 2 spin states: $^1\Sigma_u^+$ (singlet state) and $^3\Sigma_u^+$ (triplet state). The luminescence light is in the vacuum ultra violet (VUV) region with a wavelength of 128 nm. The two spin states have different decay times: $\tau_1 \simeq 5$ ns for the singlet state and $\tau_2 \simeq 1.6$ μ s for the triplet state. The significant difference in the decay time allows a possibility to do an efficient pulse shape analysis. In addition LAr is characterized by a low ionization potential and a long electron lifetime. The decay time of the triplet state and the electron lifetime strongly depend on the purity of the liquid or gas as demonstrated in [2].

The combination of pulse shape discrimination with the analysis of the ratio of the scintillation to ionization yields leads to the efficient background rejection. These features and the

low cost of argon makes LAr an extremely promising target material for direct Dark Matter detection.

2 The ArDM Experiment

The design of the ArDM detector [3] is based on the possibility to measure both signals of scintillation and ionization independently. The layout of the detector with its components are shown in the Fig.1. The high voltage for the drift field is supplied from the Greinacher [4]

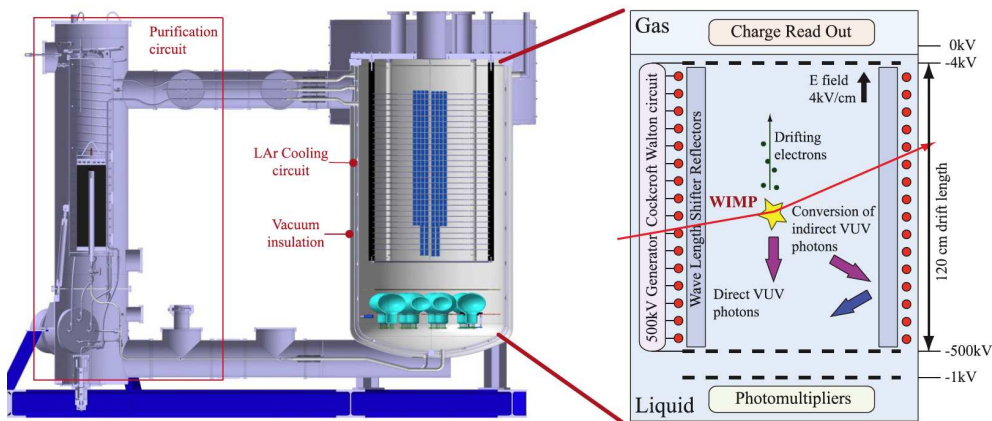


Figure 1: Conceptual layout of the ArDM experiment.

(Cockcroft-Walton) chain which consists of 210 stages. The high electric drift field of about 4 kV/cm ensures the drift of ionization charges towards the gas phase. The maximum drift distance does not exceed 120 cm. The field shaping rings are covered on the inner side with reflectors in order shift the light in to the visible range and to increase the light collection efficiency. Fourteen PMTs are located below the HV cathode. The charge readout system is located in the top of the detector. The charge is extracted from the liquid phase into the gas by the high electric field between the extraction grid and the first electrode of the charge readout system. The extraction grid is immersed in the LAr and placed 1 mm below the liquid surface. The fiducial mass of the detector is estimated to be about 850 kg.

The LAr recirculation and purification system based on a CuO filled cartridge, provides the necessary purity of the LAr for long drift paths upto 120 cm. The monitoring of the LAr purity is independently done using the electron drift path and the decay time of slow component of the light signal (τ_2) see [2].

3 First Test of the ArDM Detector in Liquid Argon

For the first time the ArDM detector was filled with 1 ton of LAr and tested in May 2009. The test was performed with a partial light readout assembly (8 PMTs instead of 14), zero drift electric field and no charge readout system installed. The side reflectors and the light readout

DAQ were complete. The light readout assembly contained 7 Hamamatsu R5912. The side reflectors and the windows of the PMTs were coated with tetraphenyl Butadien (TPB) WLS.

The side reflector was made of 15 Tetratex® foils¹ (120×25 cm²). The foils were coated with an optimal thickness of WLS [5] using the evaporation technique. A custom made evaporator was used for the TPB deposition.

The setup was filled with LAr so that the side reflectors were fully immersed. The detector was kept full for about 3 weeks and various measurements using different radioactive sources were performed. The purity of LAr (τ_2) was constantly monitored within 600 hours and the constant value of $\tau_2 \simeq 1.5$ μ s was measured in agreement with expectations [2]. This indicates a good purity of the used LAr taking into account that no purification system was involved during the test. To study the detector response on γ radiation we used ^{137}Cs ($E_\gamma = 661$ keV) and ^{22}Na ($E_\gamma = 511$ keV and 1274 keV) sources and Am-Be source for neutron studies. The γ energy spectra are shown in Fig.2. The spectrum for ^{137}Cs was obtained with the detector self-trigger. For the spectra for ^{22}Na the trigger was set up to the detector in coincidence with an external NaI scintillator. From these spectra a preliminary estimation of the lower limit for

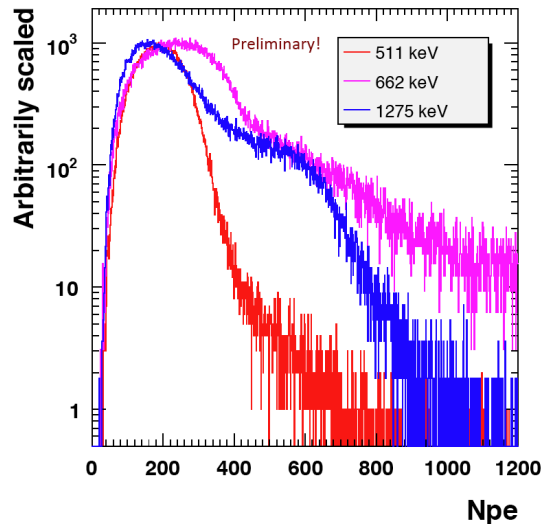


Figure 2: The energy spectra for ^{137}Cs and ^{22}Na

light yield is ~ 0.5 photoelectrons/keV for electrons (pe/keVee) with the 7 PMTs assembly.

Another important measurement was performed using ^{22}Na triggering on the external scintillator crystal. The triggering was done by requiring from the NaI crystal an energy given by the sum of 511 keV and 1275 keV γ energies. This then allowed the detection of the second 511 keV γ in argon. The spectrum is shown in Fig.3. Taking into account the light yield of 0.5 pe/keVee events with the energy deposit ~ 50 keV can be observed with a 1- ton detector.

A large data sample was taken in to study the detector response to fast neutrons from Am-Be source. The analysis of these data is in progress but a preliminary evidence for neutron-induced nuclear recoils was obtained.

¹ePTFE membrane, Donaldson Company, Inc.

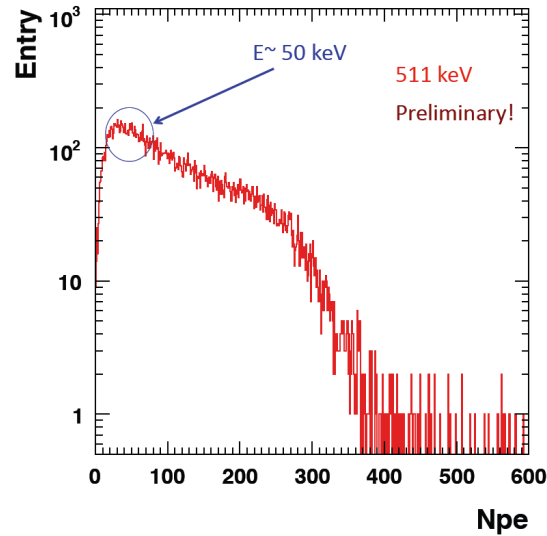


Figure 3: Energy spectra for ^{22}Na 511 keV γ s in photoelectrons obtained with the external trigger. Events with the energy of ~ 50 keV can be observed.

4 Conclusions

The ArDM detector was recently tested fully filled with liquid argon. Various studies of the detector response on neutrons and electromagnetic radiation were performed. The tests proved a good constant purity of LAr during ~ 600 hours of operation. The preliminary calibration showed the lower limit on the light yield ~ 0.5 phe/keVee. It was also demonstrated that the events with an energy deposit of ~ 50 keV can be observed with the 1-ton detector. Evidence for neutron-induced nuclear recoils was also obtained.

References

- [1] D. Clowe *et al.*, *Title: A direct empirical proof of the existence of dark matter*, [arXiv:astro-ph/0608407v1].
- [2] C. Amsler *et al.* *Luminescence quenching of the triplet excimer state by air traces in gaseous argon*, JINST **3**, (2008) P02001.
- [3] A. Rubbia, *ArDM: A ton-scale liquid argon experiment for direct detection of dark matter in the universe*, J. Phys. Conf. Ser. **39**, (2006) 129.
- [4] *Negotiations of the Swiss Society of Natural Sciences*. Issue 154 (1974), p. 239-251.
- [5] V. Boccone *et al.* *Development of wavelength shifter coated reflectors for the ArDM argon dark matter detector*, JINST **4** (2009) P06001

Particle dark matter in the galactic halo: results from DAMA/LIBRA

R. Bernabei^{1,2}, P. Belli², F. Cappella^{3,4}, R. Cerulli⁵, C. J. Dai⁶, A. d'Angelo^{3,4}, H. L. He⁶, A. Incicchitti⁴, X. H. Ma⁶, F. Montecchia^{2,7}, F. Nozzoli^{1,2}, D. Prospero^{3,4}, X. D. Sheng⁶, R. G. Wang⁶, Z. P. Ye^{6,8}

¹Dip. di Fisica, Università di Roma “Tor Vergata”, I-00133 Rome, Italy

²INFN, sez. Roma “Tor Vergata”, I-00133 Rome, Italy

³Dip. di Fisica, Università di Roma “La Sapienza”, I-00185 Rome, Italy

⁴INFN, sez. Roma, I-00185 Rome, Italy

⁵Laboratori Nazionali del Gran Sasso, I.N.F.N., Assergi, Italy

⁶IHEP, Chinese Academy, P.O. Box 918/3, Beijing 100039, China

⁷Laboratorio Sperimentale Policentrico di Ingegneria Medica, Università di Roma “Tor Vergata”

⁸University of Jing Gangshan, Jiangxi, China

DOI: http://dx.doi.org/10.3204/DESY-PROC-2009-05/belli_pierluigi

The DAMA/LIBRA experiment at the Gran Sasso National Laboratory of the I.N.F.N. has confirmed with higher sensitivity the model independent evidence for Dark Matter (DM) particles in the galactic halo obtained by the former DAMA/NaI experiment by investigating the DM annual modulation signature. Considering the data collected by DAMA/NaI and by DAMA/LIBRA (cumulative exposure of $0.82 \text{ ton} \times \text{yr}$), a confidence level of 8.2σ has been achieved. No systematics or side reactions able to account for the measured modulation amplitudes and to simultaneously satisfy all the many peculiarities of the signature have been found or suggested by anyone over more than a decade.

DAMA is an observatory for rare processes operating deep underground in the Gran Sasso National Laboratory of the I.N.F.N.. The experiment is mainly devoted to the development and use of low background scintillators. The main experimental set-ups are: i) the first generation DAMA/NaI set-up[1, 2]; ii) DAMA/LXe[3, 4]; iii) DAMA/R&D[5]; iv) DAMA/Ge[6]; v) the new second generation DAMA/LIBRA set-up ($\simeq 250 \text{ kg}$ highly radiopure NaI(Tl))[7, 8, 9]. Many rare processes have been investigated obtaining often competitive results. In particular, DAMA/LIBRA is further investigating the presence of DM particles in the galactic halo by exploiting the model independent DM annual modulation signature. This signature – originally suggested in the middle of '80 in ref. [10] – exploits the effect of the Earth revolution around the Sun on the flux of DM particles in the detectors. In fact, as a consequence of its annual revolution, the Earth should be crossed by a larger flux of DM particles around ~ 2 June (when its rotational velocity is summed to the one of the solar system with respect to the Galaxy) and by a smaller one around ~ 2 December (when the two velocities are subtracted). This offers an efficient model independent signature and allows to test large intervals of cross sections and halo densities.

In particular, the DM annual modulation signature is very distinctive since the corresponding signal must simultaneously satisfy all the following requirements: i) the rate must contain

a component modulated according to a cosine function; ii) the period is one year; iii) the phase is roughly \simeq 2nd June; iv) this modulation must only be found in a well-defined low energy range, where DM particle induced events can be present ; v) it must apply only to those events in which just one detector of many actually "fires" (*single-hit events*), since the DM particle multi-interaction probability is negligible; vi) the modulation amplitude in the region of maximal sensitivity must be $\lesssim 7\%$ for usually adopted halo distributions, but it can be larger in case of some possible scenarios as e.g. those in refs. [11, 12]. Only systematic effects or side reactions able to account for the whole observed modulation amplitude and to contemporaneously fulfil all the requirements given above might mimic this signature; thus, no other effect investigated so far in the field of rare processes offers a so stringent and unambiguous signature. It is worth noting that the DM annual modulation is not – as often naively said – a “seasonal” variation and it is not a “winter-summer” effect. In fact, the DM annual modulation is not related to the relative Sun position, but it is related to the Earth velocity in the galactic frame. Moreover, the phase of the DM annual modulation (roughly 2nd June) is well different than those of physical quantities (such as temperature of atmosphere, pressure, other meteorological parameters, cosmic rays flux, ...) instead correlated with seasons.

Detailed descriptions of DAMA/NaI[13, 14, 15, 16] and of DAMA/LIBRA[7] performances have been published. The DAMA/NaI experiment collected an exposure of $0.29 \text{ ton}\times\text{yr}$ running over 7 annual cycles, while DAMA/LIBRA has released so far the data of its first 4 annual cycles for an exposure of $0.53 \text{ ton}\times\text{yr}$. The total exposure of the two experiments is $0.82 \text{ ton}\times\text{yr}$, which is orders of magnitude larger than the exposure typically collected in the field.

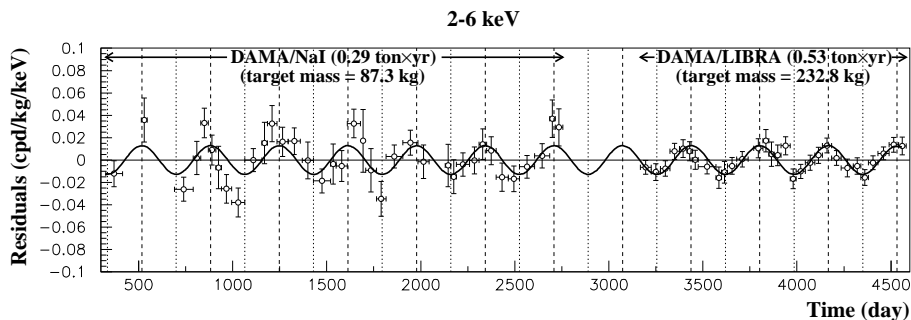


Figure 1: Experimental model-independent residual rate of the *single-hit* scintillation events, measured by DAMA/NaI and DAMA/LIBRA in the (2 – 6) keV energy intervals as a function of the time. The zero of the time scale is January 1st of the first year of data taking of the former DAMA/NaI experiment. The superimposed curve is the cosinusoidal functions with 1 year period, June 2nd phase and fitted amplitude $(0.0129 \pm 0.0016) \text{ cpd/kg/keV}$. The dashed vertical lines correspond to the maximum of the signal (June 2nd), while the dotted vertical lines correspond to the minimum. For details see[8].

Several model-independent analyses have been performed[8]. Figure 1 shows the time behaviour of the experimental (2–6) keV residual rates for *single-hit* events collected by DAMA/NaI and by DAMA/LIBRA. The superimposed curve represents the cosinusoidal functions: $A \cos \omega(t - t_0)$ with $T = \frac{2\pi}{\omega} = 1 \text{ yr}$ and phase $t_0 = 152.5 \text{ day}$ (June 2nd), while the modulation amplitudes, A , is the best fit value obtained over the DAMA/NaI and DAMA/LIBRA data. When the period and the phase parameters are released in the fit, values well compatible with those expected

for a DM particle induced effect are obtained[8]: $T = (0.998 \pm 0.003)$ yr and $t_0 = (144 \pm 8)$ day in the (2–6) keV energy interval. The same data of Figure 1 have also been investigated by a Fourier analysis[8]. For all the performed analyses and for details see ref. [8]. In particular, a relevant investigation has been performed by applying the same hardware and software procedures, used to acquire and to analyse the *single-hit* events, to the *multiple-hits* ones. In fact, since the probability that a DM particle interacts in more than one detector is negligible, a DM signal can be present just in the *single-hit* residual rate. Thus, this allows the study of the background behaviour in the same energy interval where the positive effect is observed. In particular, while a clear modulation with proper features is present in the 2 – 6 keV *single-hit* events, the modulation amplitude of the *multiple-hits* ones in the same energy interval is well compatible with zero[8] (see Figure 2). Similar results were previously obtained also for the

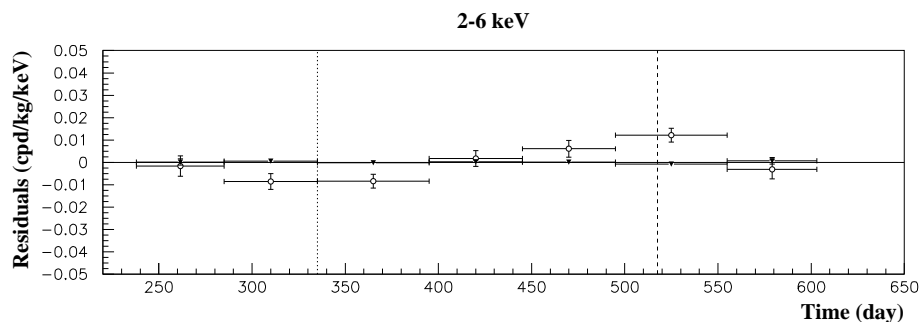


Figure 2: Experimental model-independent residual rates of the (2 – 6) keV *single-hit* events (open circles) (class of events to which DM events belong) and of the (2 – 6) keV *multiple-hits* events (filled triangles) (class of events to which DM events do not belong), measured in the four DAMA/LIBRA annual cycles (as collected in a single cycle; the initial time of the scale is taken on August 7th). The same identical hardware and the same identical software procedures have been applied in both cases. In the plots the experimental points present the errors as vertical bars and the associated time bin width as horizontal bars. For details see[8].

DAMA/NaI data[16]. Thus, again evidence of annual modulation with proper features, as required by the DM annual modulation signature, is present in the *single-hit* residual rate (events class to which the DM particle induced events belong), while it is absent in the *multiple-hits* one (event class to which only background events belong). Since the same identical hardware and the same identical software procedures have been used to analyse the two classes of events, the obtained result offers an additional strong support for the presence of a DM particle component in the galactic halo further excluding any side effect either from hardware or from software procedures or from background.

All the performed analyses[8] confirm that a modulation amplitude is present in the lower energy intervals with the period and the phase in agreement with those expected for DM induced signals; in addition, the observed annual modulation fulfills the requirements of the DM signature.

As previously done for the case of DAMA/NaI[14, 15, 16], careful investigations on absence of any significant effect from systematics or side reactions have been quantitatively carried out also for DAMA/LIBRA; it is reported in details in ref. [8]. No systematics or side reactions able to account for the measured modulation amplitude and to simultaneously satisfy all the

requirements of the signature have been found or suggested by anyone over more than a decade.

In September 2008 a first upgrading of the DAMA/LIBRA set-up has been realized by substituting some PMTs and replacing the transient digitizers with new ones. A new DAQ system with optical readout has also been installed.

Moreover, mainly in order to lower the energy threshold of the experiment, the replacement of all the PMTs with new ones having higher quantum efficiency is planned for the next year; this will also improve other significant experimental aspects. The increasing of the exposure and the hardware improvements will allow the further investigation of some open aspects in the DM field and of second order effects.

Finally, other processes are also investigated by DAMA/LIBRA; in particular, recently new results on the search for possible processes violating the Pauli-Exclusion-Principle in Sodium and in Iodine have been presented in ref. [9].

References

- [1] R. Bernabei et al., Phys. Lett. B 389 (1996) 757; Phys. Lett. B 424 (1998) 195; Phys. Lett. B 450 (1999) 448; P. Belli et al., Phys. Rev. D 61 (2000) 023512; R. Bernabei et al., Phys. Lett. B 480 (2000) 23; Phys. Lett. B 509 (2001) 197; Eur. Phys. J. C 23 (2002) 61; P. Belli et al., Phys. Rev. D 66 (2002) 043503. R. Bernabei et al., La Rivista del Nuovo Cimento 26 n.1 (2003) 1-73. Int. J. Mod. Phys. D 13 (2004) 2127. Int. J. Mod. Phys. A 21 (2006) 1445. Eur. Phys. J. C 47 (2006) 263. Int. J. Mod. Phys. A 22 (2007) 3155. Eur. Phys. J. C 53 (2008) 205. Phys. Rev. D 77 (2008) 023506. Mod. Phys. Lett. A 23 (2008) 2125.
- [2] R. Bernabei et al., Phys. Lett. B 408 (1997) 439; Phys. Rev. Lett. 83 (1999) 4918; Il Nuovo Cimento A112 (1999) 1541; Phys. Lett. B 515 (2001) 6; Eur. Phys. J. A 23 (2005) 7. Eur. Phys. J. A 24 (2005) 51. P. Belli et al., Phys. Lett. B 460 (1999) 236; Phys. Rev. C 60 (1999) 065501; F. Cappella et al., Eur. Phys. J.-direct C14 (2002) 1.
- [3] P. Belli et al., Astropart. Phys. 5 (1996) 217; Nuovo Cim. C 19 (1996) 537; Phys. Lett. B 387 (1996) 222; Phys. Lett. B 389 (1996) 783 (err.); Phys. Lett. B 465 (1999) 315; Phys. Rev. D 61 (2000) 117301; R. Bernabei et al., New J. of Phys. 2 (2000) 15.1; Phys. Lett. B 493 (2000) 12; Nucl. Instr. & Meth A 482 (2002) 728; Eur. Phys. J. direct C 11 (2001) 1; Phys. Lett. B 527 (2002) 182; Phys. Lett. B 546 (2002) 23; in the volume *Beyond the Desert 2003*, Springer, Berlin (2003) 365; Eur. Phys. J. A 27, s01 (2006) 35.
- [4] R. Bernabei et al., Phys. Lett. B 436 (1998) 379.
- [5] R. Bernabei et al., Astropart. Phys. 7 (1997) 73; Nuovo Cim. A 110 (1997) 189; P. Belli et al., Astropart. Phys. 10 (1999) 115; Nucl. Phys. B 563 (1999) 97; R. Bernabei et al., Nucl. Phys. A 705 (2002) 29; P. Belli et al., Nucl. Instr. & Meth A 498 (2003) 352; R. Cerulli et al., Nucl. Instr. & Meth A 525 (2004) 535; R. Bernabei et al., Nucl. Instr. & Meth A 555 (2005) 270; Ukr. J. Phys. 51 (2006) 1037; P. Belli et al., Nucl. Phys. A 789 (2007) 15; Phys. Rev. C 76 (2007) 064603; Phys. Lett. B 658 (2008) 193; Eur. Phys. J. A 36 (2008) 167; Nucl. Phys. A 826 (2009) 256.
- [6] P. Belli et al., Nucl. Instr. & Meth. A 572 (2007) 734; Nucl. Phys. A 806 (2008) 388; Nucl. Phys. A 824 (2009) 101.
- [7] R. Bernabei et al., Nucl. Instr. & Meth. A 592 (2008) 297.
- [8] R. Bernabei et al., Eur. Phys. J. C 56 (2008) 333.
- [9] R. Bernabei et al., Eur. Phys. J. C 62 (2009) 327.
- [10] K.A. Drukier et al., Phys. Rev. D 33 (1986) 3495; K. Freese et al., Phys. Rev. D 37 (1988) 3388.
- [11] D. Smith and N. Weiner, Phys. Rev. D 64 (2001) 043502; D. Tucker-Smith and N. Weiner, Phys. Rev. D 72 (2005) 063509.
- [12] K. Freese et al. astro-ph/0309279; Phys. Rev. Lett. 92 (2004) 11301.
- [13] R. Bernabei et al., Il Nuovo Cim. A 112 (1999) 545.
- [14] R. Bernabei et al., Eur. Phys. J. C 18 (2000) 283.
- [15] R. Bernabei et al., La Rivista del Nuovo Cimento 26 n.1 (2003) 1-73.
- [16] R. Bernabei et al., Int. J. Mod. Phys. D 13 (2004) 2127.
- [17] R. Bernabei et al., ISBN 978-88-95688-12-1, pages 1-53 (2009) Exorma Ed. (arXiv:0806.0011v2).

Dark Matter Search with Germanium Detector at O(100eV) threshold

Shin-Ted Lin, Henry T. Wong (for the TEXONO Collaboration)

Institute of Physics, Academia Sinica, Taipei 11529, Taiwan.

DOI: http://dx.doi.org/10.3204/DESY-PROC-2009-05/lin_shin-ted

The current goals of the TEXONO research program are on the development of germanium detectors with sub-keV sensitivities to realize experiments on neutrino magnetic moments, neutrino-nucleus coherent scattering, as well as WIMP dark matter searches. New limits were placed for the couplings of low-mass WIMPs with matter with a ultra-low-energy germanium prototype detector. Data are being taken with a 500 g Point Contact Germanium detector, where a threshold of ~ 350 eV was demonstrated. The dark matter program will evolve into a dedicated experiment at an underground laboratory under construction in Sichuan, China.

1 Introduction

A research program on low energy neutrino and dark matter physics is pursued at the Kuo-Sheng Neutrino Laboratory (KSNL) by the TEXONO Collaboration[1]. The laboratory is located at a distance of 28 m from a 2.9 GW reactor core and has an overburden of about 30 meter-water-equivalent. Results on neutrino magnetic moments[2] and neutrino-electron scattering cross-section have been obtained[3]. The present goals are to develop advanced detectors with kg-size target mass, 100 eV-range threshold and low-background specifications[4] for searches of Weakly Interacting Massive Particles (WIMPs)[5] at the low-mass region as well as studies of neutrino-nucleus coherent scattering[6] and neutrino magnetic moments.

2 Results on Dark Matter Searches

A four-channel Ultra-Low-Energy Germanium (ULEGe) prototype detector with a total active mass of 20 g has collected low-background data at KSNL[5]. The trigger and analysis efficiencies are shown in Figure 1. An energy threshold of (220 ± 10) eV was achieved at an efficiency of 50%. The background spectrum with 0.338 kg-day of exposure is displayed in Figure 2. Constraints on WIMP-nucleon spin-independent $[\sigma_{\chi N}^{SI}]$ and spin-dependent $[\sigma_{\chi N}^{SD}(n)]$ couplings as functions of WIMP-mass (m_{χ}) were derived, as depicted in Figures 3&4, respectively. Overlaid on the plots are results from experiments which define the current exclusion boundaries, the DAMA-allowed regions and that favored by SUSY models[5, 7]. The KSNL limits improve over previous results at $m_{\chi} \sim 3 - 6$ GeV. Sensitivities for full-scale experiments at 1 cpd background level are projected as dotted lines. The observable nuclear recoils at $m_{\chi}=5$ GeV

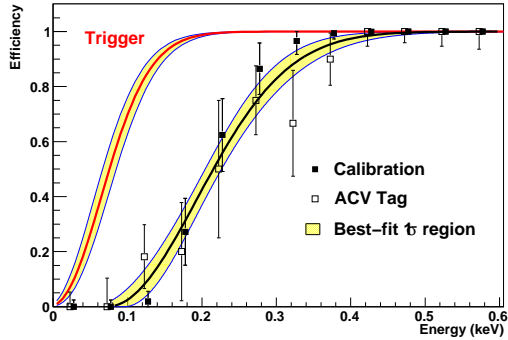


Figure 1: The trigger efficiency for physics events recorded by the DAQ system and analysis efficiency of the PSD cut with the best-fit 1σ region, using the 20 g ULEGe prototype detector, as derived by the the ^{55}Fe -calibration and *in situ* background events with ACV tags, respectively.

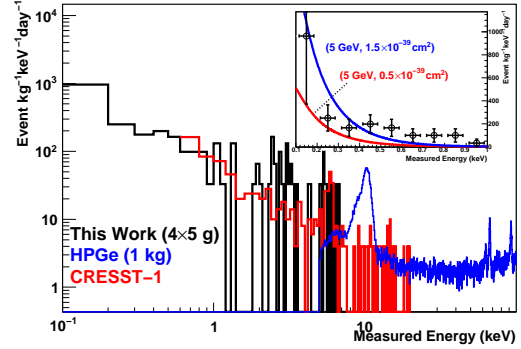


Figure 2: The measured spectrum of ULEGe with 0.338 kg-day of data, after various background suppression procedures. Background spectra of the CRESST-I experiment[7] and the HPGe[2] are overlaid for comparison. The expected spectra for two cases of $(m_\chi, \sigma_{\chi N}^{\text{SI}})$ are superimposed onto the inset.

and $\sigma_{\chi N}^{\text{SI}} = 0.5 \times 10^{-39} \text{ cm}^2$ (allowed) and $1.5 \times 10^{-39} \text{ cm}^2$ (excluded) are superimposed with the measured spectrum in the inset of Figure 2 for illustrations.

3 Performance of Point-Contact Germanium Detectors

The design of Point-Contact Germanium (PCGe) detectors was first proposed in the 1980's[8], offering the potential merits of sub-keV sensitivities with kg-scale target mass. There is intense recent interest triggered by successful realization and demonstration of the detector technique[9]. A PCGe of target mass 500 g was constructed and has been collecting data in KSNL since early 2009.

Similar procedures to those developed for the ULEGe were adopted to study the efficiency factors below the electronic noise edge. The results, analogous to those of Figure 1, are displayed in Figure 5. The trigger efficiencies were measured with two methods. The fractions of calibrated pulser events above the discriminator threshold provided the first measurement, while the studies on the amplitude distributions of *in situ* data contributed to the other. The relative timing between the PCGe and anti-Compton (ACV) NaI(Tl) detectors is shown in Figure 6, for “sub-noise edge” events at 200-400 eV before and after the pulse shape discrimination (PSD) selection processes. Events in coincidence with ACV at the “50–200 ns” window are due to multiple Compton scatterings, which are actual physical processes having similar pulse shapes as the neutrino and WIMP signals. It can be seen that only these events have substantial probabilities of surviving the cuts, and the fractions constitute to the PSD efficiencies. The threshold at $\sim 50\%$ combined efficiencies is ~ 350 eV. Intensive background and optimization studies with the PCGe at KSNL are underway.

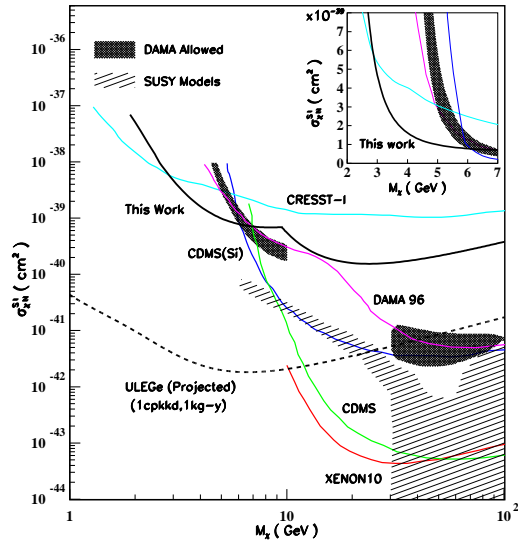


Figure 3: Exclusion plot of the spin-independent χN cross-section versus WIMP-mass.

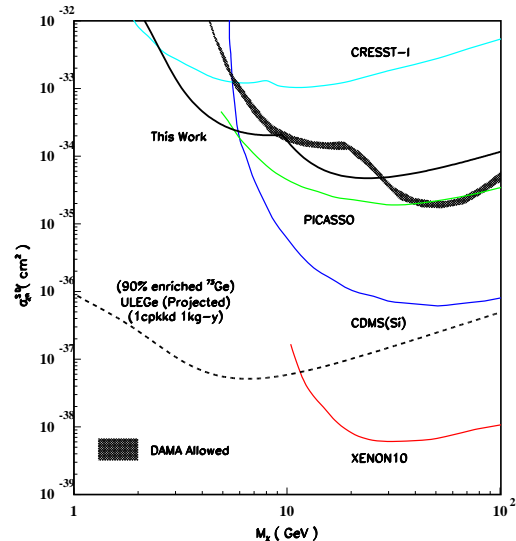


Figure 4: Exclusion plot of the spin-dependent χ -neutron cross-section versus WIMP-mass.

4 China Jin-Ping Underground Laboratory

The dark matter limits of Ref. [5] are by-product results of an experimental configuration optimized for neutrino physics. It is essential that the program will evolve into a dedicated dark matter search experiment in an underground location.

An excellent candidate site for a deep underground laboratory was recently identified in Sichuan, China where the China Jin-Ping Laboratory (CJPL) is being constructed[10]. The laboratory has more than 2500 m of rock overburden, is accessible by a road tunnel built for public traffic, and is supported by excellent infrastructures already available near the entrance. The first cavern of size 6 m(height)X6 m(width)X40 m(depth) is scheduled for completion in early 2010.

5 Status and Plans

A detector with 1 kg mass, 100 eV threshold and 1 cpd background level has important applications in neutrino and dark matter physics, as well as in the monitoring of reactor operation. Crucial advances have been made in adapting the Ge detector technology to satisfy these requirements. Competitive limits have been achieved in prototype studies on the WIMP couplings with matter. Intensive research programs are being pursued along various fronts towards realization of experiments which can meet all the technical challenges.

The low energy neutrino physics program will continue at KSNL, where a 900 g PCGe detector will be installed in 2010. Dedicated dark matter search with both 20 g ULEGe and 500 g PCGe detectors will be the first experimental program conducted at CJPL commencing 2010.

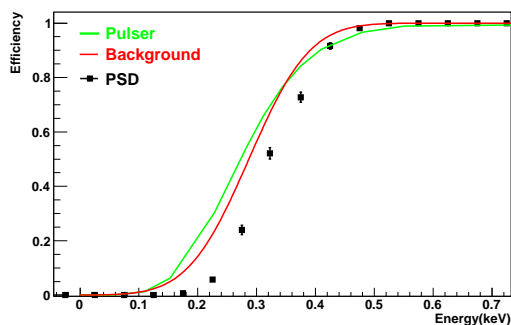


Figure 5: The trigger and analysis efficiencies of the 500 g PCGe detector, as derived from the test pulser and *in situ* events, respectively.

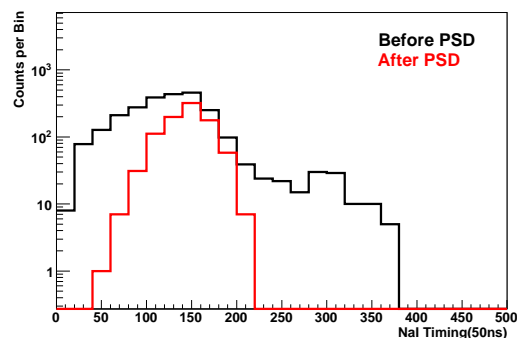


Figure 6: Events as a function of relative timing between ACV-NaI(Tl) and PCGe systems, before and after PSD selection.

6 Acknowledgments

I would like to thank Prof. Tsz-King Wong for his helpful consultations and full financial support for me attending this workshop; Dr. Muhammed Deniz for useful discussions. This work is supported by contracts of Prof. Tsz-King Wong NSC 97-2112-M-001-010 and NSC 98-2628-M-001-013 from the National Science Council, Taiwan, as well as by the Theme Project Scheme 2008-10 from the Academia Sinica, Taiwan.

References

- [1] H. T. Wong, *Mod. Phys. Lett. A* **19** (1207) 2004.
- [2] H. B. Li et al., *Phys. Rev. Lett.* **90** (131802) 2003; H. T. Wong et al., *Phys. Rev. D* **75** (012001) 2007.
- [3] H. B. Li et al., *Nucl. Instrum. Methods A* **459**, (93) 2001; M. Deniz, H. T. Wong, [arXiv:0810.0809] 2008 ;
- [4] H. T. Wong, *Mod. Phys. Lett. A* **23** (1431) 2008.
- [5] S. T. Lin et al., *Phys. Rev. D* **76** (061101 R) 2009 and references therein.
- [6] H. T. Wong et al., *J. Phys. Conf. Ser.* **39** (266) 2006.
- [7] M. Drees and G. Gerbier *Phys. Lett. B* **667** (241) 2008 and references therein.
- [8] P.N. Luke et al., *IEEE Trans. Nucl. Sci.* **36** (926) 1989.
- [9] P. A. Barbeau, J. I. Collar and O. Tench *JCAP* **09** (009) 2007.
- [10] D. Normile, *Science* **324** (1246) 2009.

Status of the KIMS experiment

SeungCheon Kim

(for the KIMS collaboration)

Department of Physics and Astronomy, Seoul National University, Seoul 151-747

DOI: http://dx.doi.org/10.3204/DESY-PROC-2009-05/kim_seungcheon

KIMS(Korea Invisible Mass Search) is the research project to search for the direct interaction of WIMPs (Weakly Interacting Massive Particles), one of the strongest candidates for the missing matter in the universe. The experiment has been carried out at the Yangyang underground laboratory in Korea using CsI(T ℓ) crystal scintillators whose total mass is 104.4kg. The status is reported here.

1 Introduction

The existence of dark matter is the prevailing hypothesis about the missing matter of our universe, which is supported by various cosmological observations, such as, galaxy velocity distribution [1], observations of X-rays from hot clusters [2], observation of the bullet cluster [3] and CMB anisotropy measurements [4].

The dark matter is very likely to be a WIMP(Weakly Interacting Massive Particle). And, candidates for WIMPs are very abundant, for example, the lightest supersymmetric particle, lightest kaluza-klein particle, massive sterile neutrino and axino, which are introduced from various motivations other than the dark matter problem. WIMPs are expected to recoil the nucleus and deposit a few tens keV of recoil energy. Since its interaction rate is known to be very rare, the detector material must be carefully chosen to avoid radioisotope background and proper passive and active shielding is required.

KIMS is a research project to search for this direct interaction of WIMPs using CsI(T ℓ) crystal scintillators, whose total mass is 104.4kg. The experiment has been carried out in the Yangyang underground laboratory(Y2L) which is at 2000 m water-equivalent-depth. CsI(T ℓ) crystal is a very popular scintillator well-known for its high scintillation yield. It is relatively easy to get large mass with an affordable cost. Also, it enables the pulse shape discrimination so that we can estimate nuclear recoil event rate. Furthermore, the spin expectation value of protons in Cs and I is relatively high compared to other target materials used for WIMP searches. Therefore, currently the most stringent limits on spin dependent WIMP interactions with pure protons is set with CsI(T ℓ) detector [6]. But, CsI crystal has intrinsic radioisotope backgrounds such as ^{137}Cs , ^{134}Cs and ^{87}Rb . We found that ^{137}Cs comes into the crystal through the processing water in manufacturing CsI powder. With ultra clean water, we obtained $\sim 2\text{counts}/(\text{keV} \cdot \text{kg} \cdot \text{day})$ level of background for CsI powder around 10keV region [5].

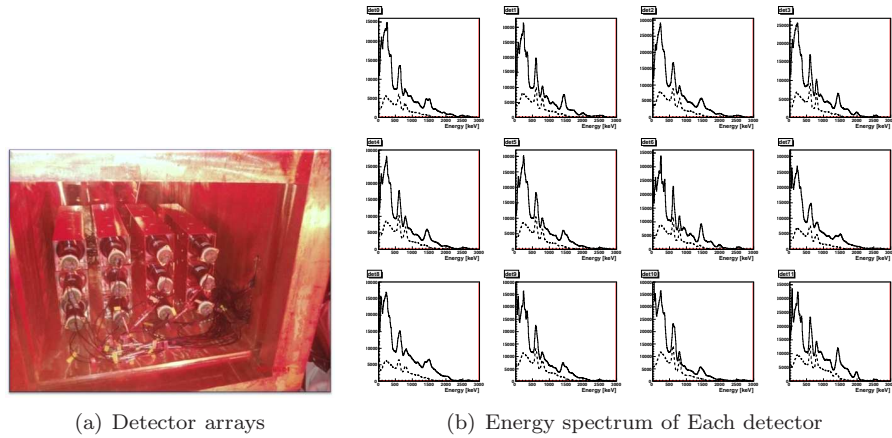


Figure 1: Detector arrays and their energy spectrum, at (b) dashed line represents multiple events.

2 Detector description

The whole detector system is composed of 3×4 CsI(Tl) detector arrays shielded adequately with Cu, Polyethylene, lead and Muon veto layer made of liquid scintillator covering the whole system with 4π coverage, which also acts as a neutron moderator. Details of the KIMS detector can be found in other documents [7]. Each detector module consists of a crystal and two PMTs mounted at both ends of the crystal. The crystal weighs 8.7kg, and its size is $8 \text{ cm} \times 8 \text{ cm} \times 30 \text{ cm}$. The PMT has green-enhanced photocathodes and their photoelectron yields are about 5 per keV. At present, events are recorded for a period of $40 \mu\text{s}$ and digitized with 400MHz FADC. We required 2 photoelectrons within $2 \mu\text{s}$ in each PMT for an event trigger condition. We applied 8ms dead time after high energy event trigger. The efficiency of this dead time application is more than 99% .

Figure 1 shows the detector array and their energy spectrum. The dashed line is the energy spectrum of multiple hit events. Here one can see the two dominant peaks correspond to ^{134}Cs , 604 and 795keV. The Compton scattered and full-peak events of these gammas are very useful in various calibration. As seen in Figure 2 (a), a plot of the energy spectrum of one detector versus that of the others, one can see various decay modes of ^{134}Cs . Each circle in the plot (a) represents the decay mode of same letter in (b).

Since neutron events mimic WIMPs, we measured the neutron background inside the detector shield using BC501A liquid detectors. Though the passive shield blocks neutron background sufficiently, there can be neutron background inside the shield due to high energy muon interactions with the shield structure. From the coincidence between Muon detector and neutron detector, we measured the muon induced neutron rate, $(3.8 \pm 0.7) \times 10^{-2}$ counts/day/liter for 0.4 MeV - 2.75 MeV neutron. It is roughly consistent with our GEANT4 simulation results, $(2.0 \pm 0.2) \times 10^{-2}$ counts/day/liter.

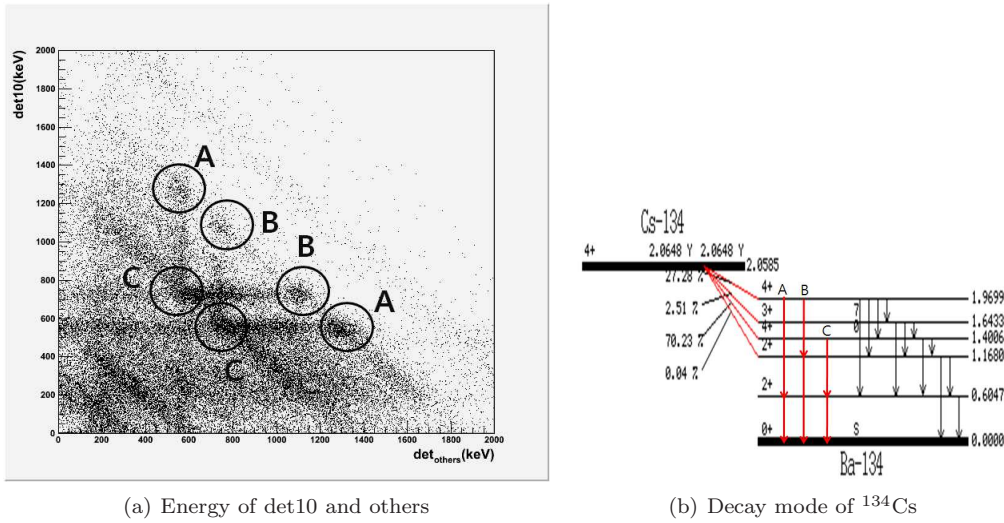


Figure 2: Identification of decay mode of ^{134}Cs with detector arrays.

3 PMT noise background study

In a rare phenomena search experiment with low energy threshold using PMTs, the background from PMT noise limits the sensitivity seriously. There are several main sources for PMT noise background. These are thermionic emission, afterpulse, Cerenkov radiation from Cosmic rays or background radioisotopes. Scintillation from the glass envelope also can cause PMT noise. For thermionic emission, since it is seen as one single photo electron(SPE) and its typical rate is a few kHz, the probability of several thermionic emissions in the $40\mu\text{s}$ event window for both PMTs contributing to energy range higher than 2keV is negligible. Afterpulse is produced by the collision of the residual gas ion in the PMT with the photocathode. After collision, several SPEs are released at the same time. Therefore, it forms big cluster signals compared to the normal SPE. Figure 3 shows the 2-dimensional scatter plot between the size of a cluster and the time from the previous cluster. The cluster size is indicated by the number of SPEs. Usually, the cluster size is one SPE. But, one can find clusters whose size are equivalent to several SPEs and which show up in a fixed time span from the previous cluster. These time spans depend on ion colliding with a photocathode. Cerenkov radiation also produces several SPEs in a very short time, less than a few ns, it also shows big clusters in its signal.

For PMT background study, We took about 2 month data putting clean acrylic boxes in place of crystals. We call it PMT-only-detector. From these data, we found PMT noise event has big clusters in it, and it can be understandable with above explanation. Since it is almost random coincident between two PMTs, the event is asymmetric in signal size and time distribution along two PMTs. Based on these facts, we developed the event selection cuts to reject the PMT noise event. We applied these cuts to 25 days of PMT-only-detector data and for most of detectors, less than 10 events survived equivalent to ~ 0.05 count/kg/day. After applying PMT noise rejection cut and other cuts (e.g multiple hit rejection), our preliminary background level is $2\text{--}4$ counts/(keV · kg · day) after efficiency correction.

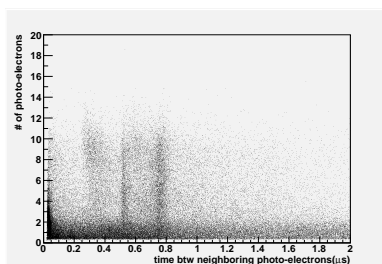


Figure 3: Signal size and time distribution of afterpulse.

4 Status and plan

We have collected about one year data with 104.4kg of detector. Based on better understanding of PMT noise background, we have developed more efficient cuts. Background level is $2\text{--}4 \text{ counts}/(\text{keV} \cdot \text{kg} \cdot \text{day})$. Now, various analysis is going on for the accumulated data. More time is required to analyze the annual modulation to cover the whole time bins of a year. Currently, we are testing new PMT known for higher quantum efficiency in metal packaging. If it shows better performances, it will be adopted in the future upgrade.

References

- [1] K. G. Begeman *et al.*, Mon. Not. Roy. Astron. Soc. **249** 523 (1991).
- [2] S. W. Allen *et al.*, Mon. Not. Roy. Astron. Soc. **334** L11 (2002).
- [3] D. Clowe *et al.*, ApJL. **648**, L109-L113 (2006), arXiv:astro-ph/0608407v1
- [4] E. Komatsu *et al.*, ApJS **180** 330 (2009).
- [5] H.S.Lee *et al.*, Nucl. Instrum. Methods A **571** 644 (2007).
- [6] H.S.Lee *et al.*, Phys. Rev. Lett. **99** 091301 (2007).
- [7] H.S.Lee, Dark Matter Search with CsI(Tl) Crystals, Ph.D, Dissertation, Department of Physics, Seoul National University, (2007)

Chapter 3

Indirect Searches for WIMPs

Search for Dark matter in the sky in the Fermi era

Aldo Morselli

INFN Roma Tor Vergata

DOI: http://dx.doi.org/10.3204/DESY-PROC-2009-05/morselli_ald

The Fermi Large Area Telescope is providing the measurement of the high energy (20 GeV to 1 TeV) cosmic ray electrons and positrons spectrum with unprecedented accuracy. This measurement represents a unique probe for studying the origin and diffusive propagation of cosmic rays as well as for looking for possible evidences of Dark Matter. In this framework, we discuss possible interpretations of Fermi results in relation with other recent experimental data on energetic electrons and positrons and in the searches of gamma-ray fluxes coming from WIMP pair annihilations in the sky.

1 Electron and positron flux

Recently the experimental information available on the Cosmic Ray Electron (CRE) spectrum has been dramatically expanded as the Fermi-LAT Collaboration [1, 2] has reported a high precision measurement of the electron spectrum from 20 GeV to 1 TeV performed with its Large Area Telescope (LAT) [3]. The spectrum shows no prominent spectral features and it is significantly harder than that inferred from several previous experiments. These data together with the PAMELA data on the rise above 10 GeV of the positron fraction[4] are quite difficult to explain with just secondary production [5],[6], [7]. The temptation to claim the discovery of dark matter is strong but there are competing astrophysical sources, such as pulsars, that can give strong flux of primary positrons and electrons (see [8], [9], [10], [11] and references therein). At energies between 100 GeV and 1 TeV the electron flux reaching the Earth may be the sum of an almost homogeneous and isotropic component produced by Galactic supernova remnants and the local contribution of a few pulsars with the latter expected to contribute more and more significantly as the energy increases.

Two pulsars, Monogem, at a distance of $d=290$ pc and Geminga, at a distance of $d=160$ pc, can give a significant contribution to the high energy electron and positron flux reaching the Earth and with a set of reasonable parameters of the model of electron production we can have a nice fit of the PAMELA positron fraction[4] and Fermi data (see figures 1 and 2) , but it is true that we have a lot of freedom in the choice of these parameters because we still do not know much about these processes, so further study on high energy emission from pulsars are needed in order to confirm or reject the pulsar hypothesis.

Nevertheless a dark matter interpretation of the Fermi-LAT and of the PAMELA data is still an open possibility. In Figure 3 is shown the parameter space of particle dark matter mass versus pair-annihilation rate, for models where dark matter annihilates into monochromatic e^\pm [11]. The preferred range for the dark matter mass lies between 400 GeV and 1-2 TeV, with

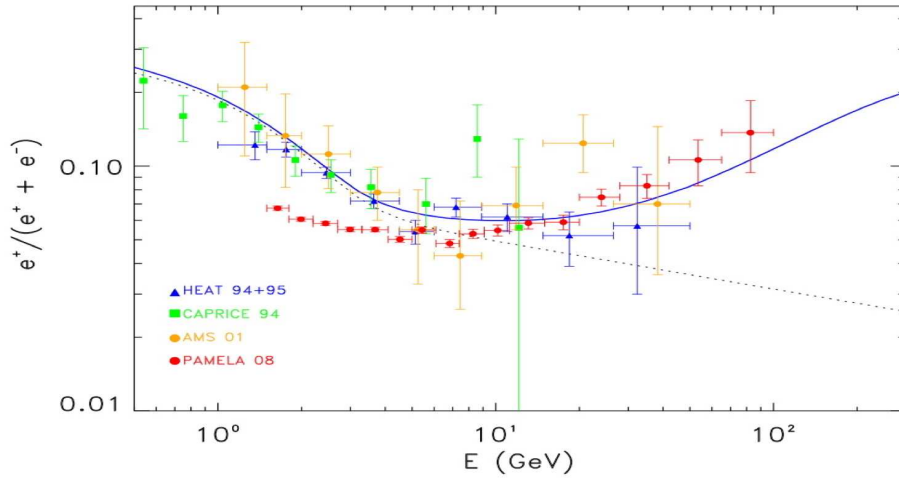


Figure 1: PAMELA data and a possible contribution from Monogem and Geminga pulsars [11]. Black-dotted line shows the background from secondary positrons in cosmic rays from GALPROP

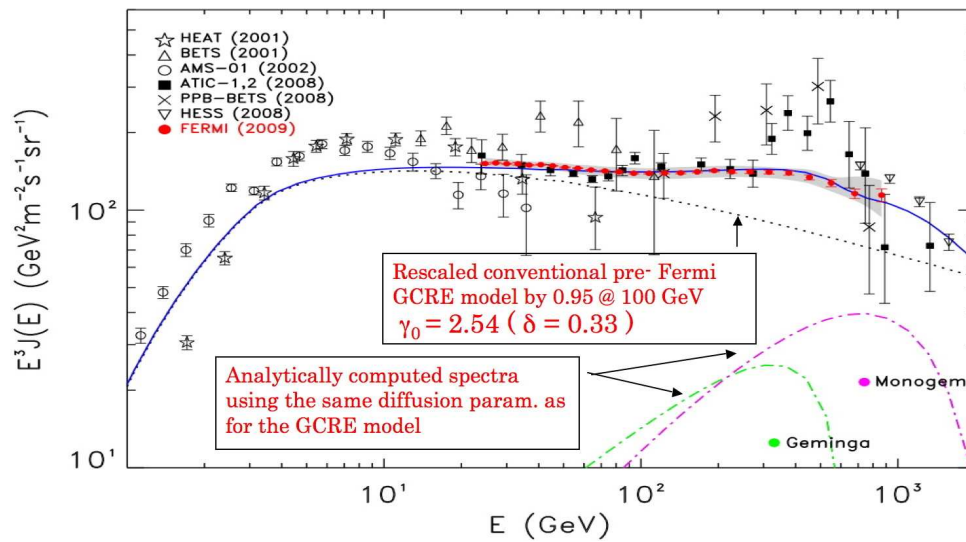


Figure 2: Electron-plus-positron spectrum (blue continuous line) for the same scenario as in figure 1. The gray band represents systematic errors on the Fermi-LAT data [3]

larger masses increasingly constrained by the H.E.S.S. results. The required annihilation rates, when employing the dark matter density profile imply typical boost factors ranging between 20 and 100, when compared to the value $\langle\sigma v\rangle \sim 3 \times 10^{-26} \text{ cm}^3/\text{sec}$ expected for a thermally produced dark matter particle relic.

How can one distinguish between the contributions of pulsars and dark matter annihilations?

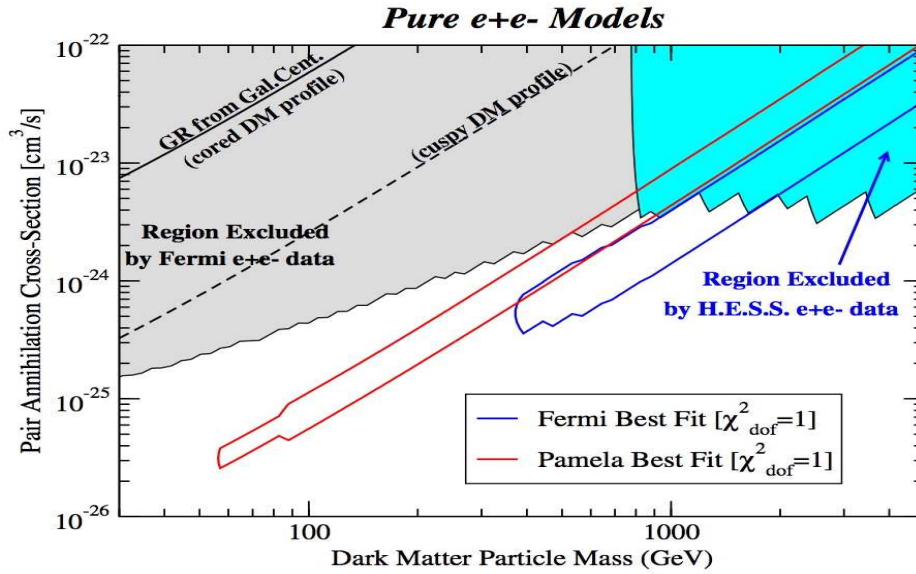


Figure 3: The parameter space of particle dark matter mass versus pair-annihilation rate, for models where dark matter annihilates into monochromatic e^\pm . Models inside the regions shaded in gray and cyan over-produce e^\pm from dark matter annihilation with respect to the Fermi-LAT and H.E.S.S. measurements, at the $2\text{-}\sigma$ level. The red and blue contours outline the regions where the χ^2 per degree of freedom for fits to the PAMELA and Fermi-LAT data is at or below 1.

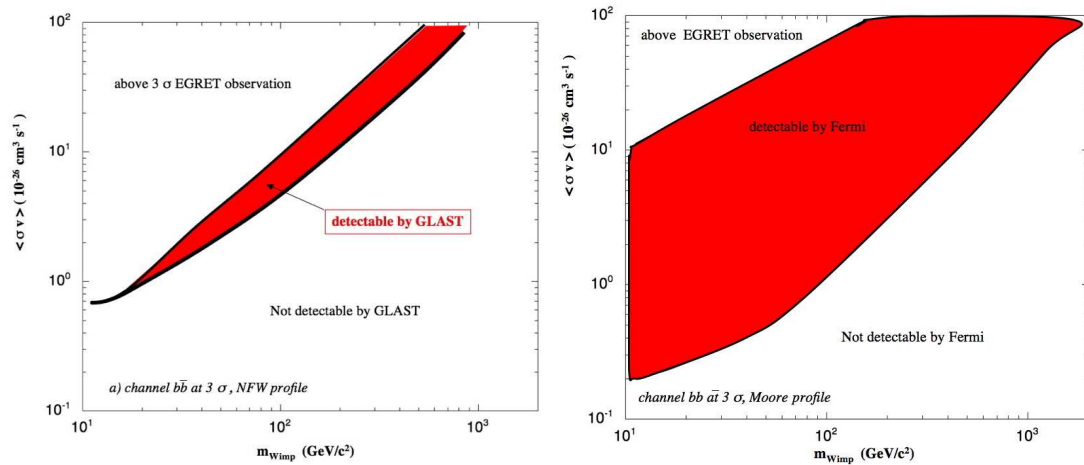


Figure 4: *Left*: Cross Section times WIMP velocity versus the WIMP mass for the $b\bar{b}$ annihilation channel. The red region is allowed by EGRET data and detectable by GLAST for 3σ significance and 5 years of Fermi operation. *Right*: Same as figure on the left but for Sagittarius Dwarf assuming a Moore profile as described in [12]

Most likely, a confirmation of the dark matter signal will require a consistency between different

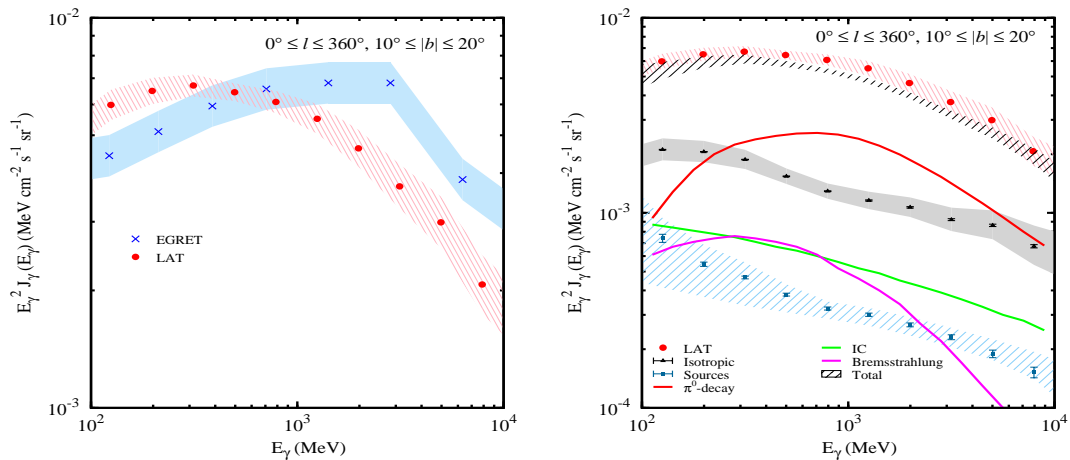


Figure 5: *Left*: Preliminary diffuse emission intensity averaged over all Galactic longitudes for latitude range $10^\circ \leq |b| \leq 20^\circ$. Data points: Fermi LAT, red dots; EGRET, blue crosses. Systematic uncertainties: Fermi LAT, red; EGRET, blue. *Right*: Preliminary Fermi LAT data with model, source, and isotropic components for same sky region.

experiments and new measurements of the reported excesses with large statistics. The observed excess in the positron fraction should be consistent with corresponding signals in absolute positron and electron fluxes in the PAMELA data and all lepton data collected by Fermi. Fermi has a large effective area and long projected lifetime, 5 years nominal with a goal 10 years mission, which makes it an excellent detector of cosmic-ray electrons up to ~ 1 TeV. Future Fermi measurements of the total lepton flux with large statistics will be able to distinguish a gradual change in slope with a sharp cutoff with high confidence [12]. The latter, can be an indication in favor of the dark matter hypothesis. A strong leptonic signal should be accompanied by a boost in the γ -ray yield providing a distinct spectral signature detectable by Fermi.

The Galactic center (GC) is expected to be the strongest source of γ - rays from DM annihilation, due to its coincidence with the cusped part of the DM halo density profile [13, 14].

An excess in gamma-ray should also be seen in the Galactic diffuse spectrum. Figure 5 (left) shows the LAT data averaged over all Galactic longitudes and the latitude range $10^\circ \leq |b| \leq 20^\circ$. The hatched band surrounding the LAT data indicates the systematic uncertainty in the measurement due to the uncertainty in the effective area described above. Also shown on the right are the EGRET data for the same region of sky where one can see that the LAT-measured spectrum is significantly softer than the EGRET measurement [15]. Figure 5 (right) compares the LAT spectrum with the spectra of an *a priori* diffuse Galactic emission (DGE) model. While the LAT spectral shape is consistent with the DGE model used in this paper, the overall model emission is too low thus giving rise to a $\sim 10 - 15\%$ excess over the energy range 100 MeV to 10 GeV. However, the DGE model is based on pre Fermi data and knowledge of the DGE. The difference between the model and data is of the same order as the uncertainty in the measured CR nuclei spectra at the relevant energies. Overall, the agreement between the LAT-measured spectrum and the model shows that the fundamental processes are consistent with our data, thus providing a solid basis for future work understanding the DGE.

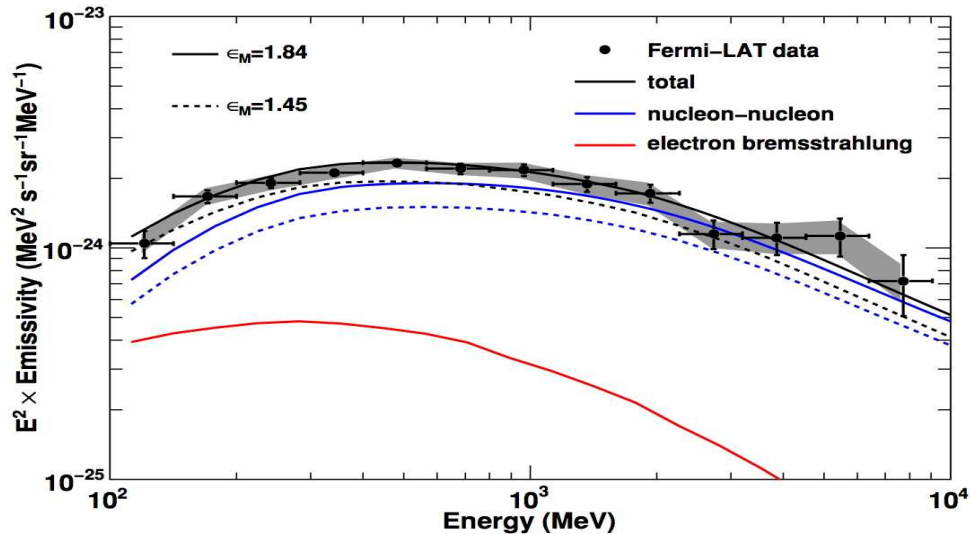


Figure 6: Differential γ -ray emissivity from the local atomic hydrogen gas compared with the calculated γ -ray production. The horizontal and vertical error bars indicate the energy ranges and 1σ statistical errors, respectively. Estimated systematic errors of the LAT data are indicated by the shaded area. A nucleus enhancement factor ϵ_M of 1.84 is assumed for the calculation of the γ -rays from nucleon-nucleon interactions. Dotted lines indicate the emissivities for the case of $\epsilon_M = 1.45$, the lowest values in the referenced literature.

Also at higher latitudes for the moment we did not observe any excess. Figure 6 shows the diffuse γ -rays in a mid-latitude region in the third quadrant (Galactic longitude l from 200° to 260° and latitude $|b|$ from 22° to 60°). The region contains no known large molecular cloud and most of the atomic hydrogen is within 1 kpc of the solar system. The contributions of γ -ray point sources and inverse Compton scattering are estimated and subtracted. The residual γ -ray intensity exhibits a linear correlation with the atomic gas column density in energy from 100 MeV to 10 GeV. The differential emissivity from 100 MeV to 10 GeV agrees with calculations based on cosmic ray spectra consistent with those directly measured, at the 10 % level. The results obtained indicate that cosmic ray nuclei spectra within 1 kpc from the solar system in regions studied are close to the local interstellar spectra inferred from direct measurements at the Earth within $\sim 10\%$ [16].

Finally a line at the WIMP mass, due to the 2γ production channel, could be observed as a feature in the astrophysical source spectrum [12]. Such an observation is a “smoking gun” for WIMP DM as it is difficult to explain by a process other than WIMP annihilation or decay and the presence of a feature due to annihilation into γZ in addition would be even more convincing.

2 Conclusion

Recent accurate measurements of cosmic-ray positrons and electrons by PAMELA, and Fermi have opened a new era in particle astrophysics. The CRE spectrum measured by Fermi-LAT

is significantly harder than previously thought on the basis of previous data. Adopting the presence of an extra e^\pm primary component with ~ 2.4 spectral index and $E_{cut} \sim 1TeV$ allow to consistently interpret Fermi-LAT CRE data (improving the fit), HESS and PAMELA. Such extra-component can be originated by pulsars for a reasonable choice of relevant parameters or by annihilating dark matter for model with $M_{DM} \sim 1TeV$. Improved analysis and complementary observations (CRE anisotropy, spectrum and angular distribution of diffuse γ , DM sources search in γ) are required to possibly discriminate the right scenario. Their exotic origin has to be confirmed by complimentary findings in γ -rays by Fermi and atmospheric Cherenkov telescopes, and by LHC in the debris of high-energy proton destructions. A positive answer will be a major breakthrough and will change our understanding of the universe forever. On the other hand, if it happens to be a conventional astrophysical source of cosmic rays, it will mean a direct detection of particles accelerated at an astronomical source, again a major breakthrough. In this case we will learn a whole lot about our local Galactic environment. However, independently on the origin of these excesses, exotic or conventional, we can expect very exciting several years ahead of us.

References

- [1] W.B.Atwood et al. [Fermi Coll.] ApJ 697 No 2 (2009 June 1) 1071-1102 [arXiv:0902.1089]
- [2] A.A.Abdo et al. [Fermi Coll.] Astroparticle Physics 32 (2009) 193-219 [arXiv:0904.2226]
- [3] A.A.Abdo et al. [Fermi Coll.], Phys. Review Letters, 102, 181101 (2009) [arXiv:0905.0025]
- [4] O. Adriani et al. [PAMELA Coll.] Nature 458, 607, 2009 [arxiv:0810.4995]
- [5] A. W. Strong and I. V. Moskalenko, ApJ 509 (1998) 212, ApJ 493 (1998) 694
- [6] A. Lionetto, A. Morselli, and V. Zdravkovic, JCAP09 (2005) 010 [astro-ph/0502406] V. S. Ptuskin et al., ApJ 642 (2006) 902
- [7] A. Morselli, I.Moskalenko, PoS(idm2008)025 [arXiv:0811.3526]
- [8] A.Boulares APJ 342 (1989) 807-813
- [9] F. A. Aharonian, A. M. Atoyan and H. J. Völk, Astron. Astrophys. 294 (1995) L41
- [10] S. Coutu et al., Astropart. Phys. 11 (1999) 429
- [11] D.Grasso et al. Astroparticle Physics 32 (2009), pp. 140-151 [arXiv:0905.0636]
- [12] E. Baltz et al. , JCAP07 (2008) 013 [arXiv:0806.2911]
- [13] A. Morselli at al., Nucl. Phys. 113B (2002) 213
- [14] A.Cesarini, F.Fucito, A.Lionetto, A.Morselli, P. Ullio, Astropart. Phys. 21 (2004) 267 [astro-ph/0305075]
- [15] A.Abdo et al. [Fermi Coll.], PRL accepted [arXiv:0912.0973]
- [16] A.A.Abdo et al., [Fermi Coll.], ApJ 703 (2009) 1249-1256 [arXiv:0908.1171]

Dark Matter Searches with Imaging Atmospheric Cherenkov Telescopes and Prospects for Detection of the Milky Way Halo

Ullrich Schwanke

Humboldt University Berlin, Newtonstrasse 14, 12489 Berlin, Germany

DOI: http://dx.doi.org/10.3204/DESY-PROC-2009-05/schwanke_ullrich

Gamma rays lend themselves to indirect Dark Matter (DM) searches due their wide range, propagation on straight lines, and comparatively easy detection. This article provides references to DM searches with imaging atmospheric Cherenkov telescopes (IACTs) at very high energies (VHE; > 100 GeV) and argues that the halo of the Milky Way is a promising target for searches if the results of recent supercomputer simulations of DM halos are correct.

1 Dark Matter Searches with Cherenkov Telescopes

DM searches with IACTs have targeted the Galactic Centre [1], globular clusters [2], dwarf spheroidal galaxies [3, 4, 5, 6] and galaxy clusters [7], and allowed the calculation of upper limits on the annihilation cross-section of weakly interacting massive particles (WIMPs) in specific scenarios. The sensitivity of current instruments and order-of-magnitude uncertainties in the modelling of DM densities inside the above astrophysical objects imply that the obtained limits are at least one order of magnitude higher than the cross-section predicted by theories beyond the Standard Model (supersymmetry, supergravity, extra dimensions).

2 Prospects for DM Searches in the Galactic Halo

In the VHE domain, DM searches close to the Galactic Centre are made difficult by the presence of the Galactic Centre source HESS J1745–290 [1] and of diffuse emission from the Galactic plane that can be plausibly explained by hadronic cosmic rays interacting in giant molecular clouds [8]. Searches at larger distances from the Galactic Center ($\sim 1^\circ$) appear still promising in the light of recent high-resolution N-body simulations of Cold Dark Matter (CDM) halos featured by galaxies like the Milky Way. The simulations performed within the framework of the Virgo Consortium’s Aquarius Project [9] attained a minimal particle mass of $1712 M_\odot$ and a converged length of 120 pc [10]. A factor of three improvement over the *Via Lactea II* simulations [11] resulted in predictions that contrast earlier findings, in particular that the annihilation signal seen by an observer located within the halo is not dominated by small clumps (whose clustering in DM halos would make dwarf galaxies attractive targets), but is dominated by the radiation produced by diffuse DM in the main halo.

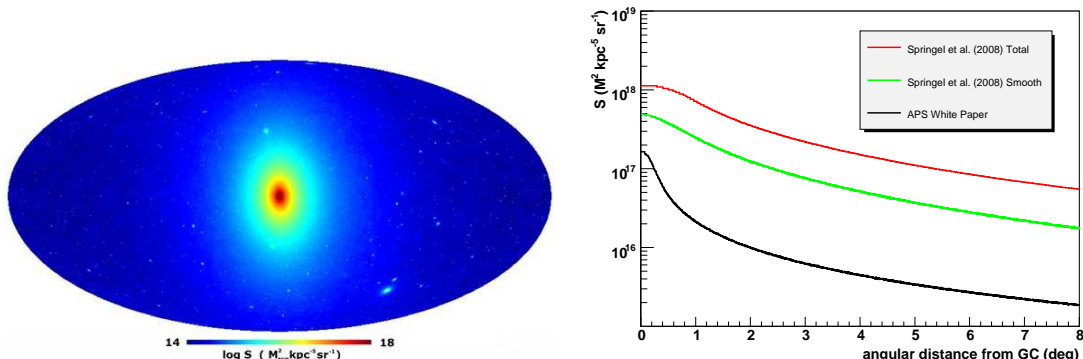


Figure 1: **(Left:)** Visualization of the astrophysical factor (Eq. (1)) for the Aquarius Simulation. (Taken from [9].) **(Right:)** Astrophysical factor as function of the distance from the Galactic Centre. See text for details.

The left panel of Figure 1 shows (in galactic coordinates) the astrophysical factor

$$S = \frac{1}{4\pi} \int_{\text{los}} \rho^2(r(s)) ds \quad (1)$$

inferred from the simulation of one particular halo (*Aq-A-1*) which is thought to roughly resemble the Milky Way. The astrophysical factor was calculated for an observer placed at a distance of ~ 8 kpc from the halo centre and depends to first order only in the angular distance from the Galactic Centre, as illustrated in Fig. 1 (right). The total astrophysical factor from the *Aq-A-1* simulation (red line in right panel of Fig. 1) exceeds earlier estimates (e.g. from [12] (black line)) by an order of magnitude and includes a factor of ~ 3 enhancement due to substructure in the DM distribution when compared to estimates of the smooth component only (green line). It is also evident that the astrophysical factor and hence any diffuse photon flux falls by more than one order of magnitude when going from an angular distance of 1° to 7° .

Under the assumption of a Majorana WIMP and negligible line emission, the astrophysical factor translates itself into a differential continuum photon flux according to

$$\frac{d\Phi}{dE} = \frac{\langle\sigma v\rangle}{2} \frac{1}{M^2} \frac{dN_\gamma}{dE} \cdot S$$

where $\langle\sigma v\rangle$ is the velocity-averaged self annihilation cross-section, M the WIMP mass and dN_γ/dE the differential photon spectrum produced in the WIMP annihilation. In order to estimate the photon flux from annihilation in the halo at H.E.S.S. energies the velocity-averaged annihilation cross-section was set to $\langle\sigma v\rangle = 4 \cdot 10^{-26} \text{ cm}^3 \text{ s}^{-1}$ (see, e.g., Fig. 13 of [12] for an overview of annihilation cross-sections in supersymmetric models that satisfy current accelerator and WMAP constraints) and WIMP masses above 0.5 TeV (i.e. well above the H.E.S.S. threshold) were investigated. For the H.E.S.S. array which measures photon energies above an analysis threshold of $E_t \simeq 0.2$ TeV up to the WIMP mass the accessible flux is proportional to

$$G(E_t|M) = \frac{1}{M^2} \int_{E_t}^M \frac{dN_\gamma}{dE} dE. \quad (2)$$

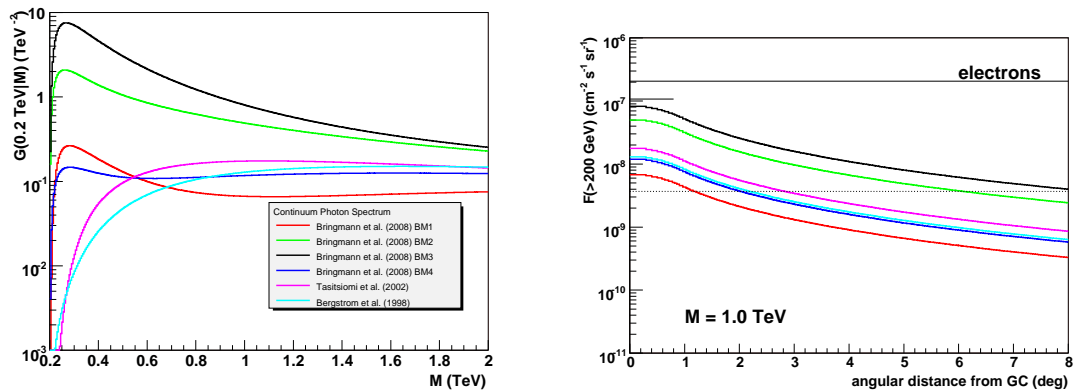


Figure 2: **(Left:)** The quantity $G(E_t|M)$ (Eq. (2)) for $E_t = 0.2 \text{ TeV}$ and six different photon spectra produced in WIMP annihilations. The models BM1–BM2 include internal bremsstrahlung, the other two models do not. See text for details. **(Right:)** Diffuse photon and electron fluxes as a function of the angular distance from the Galactic Centre. The same color coding as in the left panel was used. See text for a detailed discussion.

The quantity $G(E_t|M)$ as a function of the WIMP mass M is shown in the left panel of Fig. 2 for six assumptions for the photon spectrum dN_γ/dE from the WIMP annihilation. It is seen that the interplay of dN_γ/dE and the $1/M^2$ term produces a peak close to E_t for MSSM and mSUGRA benchmark models with internal bremsstrahlung (BM1–BM4, taken from [13]). This peak is due to a high fraction of bremsstrahlung photons close to the kinematic limit at $E_\gamma = M$, but it is also known that models with enhanced bremsstrahlung tend to have smaller values of $\langle\sigma v\rangle$. As examples for two models without sizable bremsstrahlung the Tasitsiomi spectrum [14] (magenta line, photon emission primarily from π^0 s created in quark jets) and an approximation [15] for dominant annihilation into W -bosons (cyan line) are shown. These models have a suppressed photon yield close to E_t but also reach a level of $G(0.2 \text{ TeV}|M) \sim 0.1 \text{ TeV}^{-2}$ for WIMP masses well above 0.2 TeV , so in the following discussion the Tasitsiomi spectrum will be emphasised as a reasonably conservative estimate of the photon yield.

It is instructive to compare the predicted photon flux from WIMP annihilation with other diffuse fluxes. Using the above assumption for $\langle\sigma v\rangle$ and a WIMP mass of $M = 1 \text{ TeV}$, Fig. 2 (right) shows integral fluxes above $E_t = 0.2 \text{ TeV}$ as a function of the angular distance from the Galactic center. The shape of the six different models curves (with the same color coding as in the left panel) is given by the angular dependence of the astrophysical factor and its convolution with the angular resolution of the photon detector. In the intermediate case of the Tasitsiomi annihilation spectrum (magenta line), the photon flux at an angular distance of 1° is a factor ~ 20 smaller than the diffuse electron flux (long black line, [16]) and lies about one order of magnitude below the diffuse emission from the Galactic plane (black line up to 1° , [8]).

The detection of such a tiny diffuse flux presents a substantial challenge. Clearly, the regions of diffuse emission from the Galactic plane should be avoided (unless one tries to identify WIMP signatures on top of the diffuse photon spectrum which can be described by a power-law [8]), but a search at distances of $\sim 1^\circ$ from the Galactic Centre could be promising. Rough estimates using the above assumptions and the known effective area of the H.E.S.S. array indicate that

a photon rate close to ~ 100 events/h is predicted in the inner 4° of the 5° -diameter field of view when regions with galactic latitude $|b| < 0.8^\circ$ are disregarded. This rate is tiny in comparison with the hadron and electron rate of ~ 10 Hz and ~ 1 Hz, respectively, that remain after application of cuts that seek to enrich photon events, but one can plausibly show that H.E.S.S. has sensitivity for a DM searches at a boost factor of essentially one.

One of the most difficult aspects of such a search for DM annihilation radiation from the Milky Way halo is the need for an absolute subtraction of the remaining proton and electron background. The background subtraction can only be achieved by comparing the data rate of field of views close to the Galactic Centre (i.e. an ON region with a sizable contribution from DM annihilation) with OFF regions at larger angular distances where the annihilation flux is much smaller. Currently, two approaches are investigated that could provide suitable data sets for the calculation of first limits on the flux of annihilation photons. The first approach is data-taking in an ON-OFF mode with an offset in Right Ascension which ensures the same zenith and azimuth coverage for the ON and the OFF regions. The second approach is data-taking in the so-called drift-scan mode [17] where constant acceptance is obtained by pointing the telescopes to a fixed observation position. In this setting, regions of varying annihilation flux pass through the field of view and the residual rate at large distances from the Galactic Centre can be used to normalize the background rate. Clearly, many additional factors (absolute stability of detector and atmosphere in one observation night, variations of sky brightness between ON and OFF regions, presence of bright stars that switch off camera pixels etc.) must be controlled and understood but it is hoped that first results will be available in the not too distant future.

References

- [1] F. Aharonian *et al.*, Phys. Rev. D **97**, 221102 (2006)
- [2] M. Wood *et al.*, Astrophys. J. **678**, 594 (2008)
- [3] H.E.S.S. collaboration, F. Aharonian *et al.*, Astropart. Phys. **29**, 55–62 (2008)
- [4] J. Albert *et al.*, Astrophys. J. **679**, 428 (2008)
- [5] E. Aliu *et al.*, Astrophys. J. **697**, 1299 (2009)
- [6] H.E.S.S. collaboration, F. Aharonian *et al.*, Astrophys. J. **691**, 175–181 (2009)
- [7] J. Aleksic (MAGIC Coll.) *et al.*, submitted to Astrophys. J. (09/2009)
- [8] F. Aharonian *et al.*, Nature **439**, 695–698 (2006)
- [9] <http://www.mpa-garching.mpg.de/aquarius>
- [10] V. Springel *et al.*, Nature **456**, 73–76 (2008)
- [11] J. Diemand *et al.*, Nature **454**, 735–738 (2008)
- [12] <http://cherenkov.physics.iastate.edu/wp>
- [13] T. Bringmann, L. Bergström and J. Edsjö, JHEP **0801**, 049 (2008)
- [14] A. Tasitsiomi and A.V. Olinto, Phys. Rev. D **66**, 083006 (2002)
- [15] L. Bergström, P. Ullio and J.H. Buckley, Astropart. Phys. **9**, 137–162 (1998)
- [16] H.E.S.S. collaboration, F. Aharonian *et al.*, Phys. Rev. Lett. **101**, 261104 (2008)
- [17] M.P. Kertzman for the VERITAS Collaboration, Proc. of the 30th ICRC, Vol. 2, 743–746 (2008).

Dark matter and the PAMELA data

Julien Lavalle

Dipartimento di Fisica Teorica, Torino University & INFN-Torino
Via Giuria 1, I-10125 Torino — Italia

DOI: <http://dx.doi.org/10.3204/DESY-PROC-2009-05/lavalle-julien>

The recent observation of a rising positron fraction up to ~ 100 GeV by the PAMELA experiment has triggered a considerable amount of interpretation attempts in terms of dark matter (DM) annihilation or decay, though most of the “natural” DM candidates arising in particle physics beyond the standard model are not expected to be observed in the cosmic antimatter spectrum. Here, we make a critical reassessment of such a possibility.

Introduction: Among interesting *astroparticle* signatures of DM annihilation or decay, antimatter cosmic rays (CRs) have long been considered as promising tracers [1], but it is only recently that precision data have become available to look for non-standard features [2]. Although the rise in the local cosmic positron fraction at GeV energies has been observed for a long time (*e.g.* [3]), the statistics accumulated by the PAMELA satellite experiment [4] is unprecedented and covers a much larger energy range, up to 100 GeV. A secondary origin of these positrons seems unlikely [5, 6], even when considering theoretical uncertainties. The main questions are therefore (i) whether or not standard astrophysics may supply for such a signal and (ii) whether or not DM annihilation or decay is expected to be (also) observed in this channel. It is noteworthy that this was already discussed by [7] twenty years ago, where the author pointed out that a pulsar origin was the best explanation to a rising positron fraction. It is not less interesting and sociologically striking to take a census of the articles addressing point (i) versus those focused on point (ii).

Astrophysical positrons: The general formalism of CR transport was designed a long time ago in the seminal book of Ginzburg & Syrovatskii [8], and refined many times since then (*e.g.* [9, 10]). In some cases, analytical solutions to the diffusion equation can be found in terms of Green functions \mathcal{G} . This is the case for electrons and positrons above a few GeV, for which all processes but spatial diffusion and energy losses (inverse Compton scattering on interstellar radiation fields, synchrotron) can safely be neglected. The infinite 3D Green function, valid at high energy when spatial boundaries of the diffusion zone cannot be reached, reads: $\mathcal{G}_e(E, \vec{x} \leftarrow E_s, \vec{x}_s) = \frac{1}{b(E)\{\pi\lambda^2\}^{3/2}} \exp\left\{-\frac{|\vec{x}-\vec{x}_s|^2}{\lambda^2}\right\}$, where $b(E) = -dE/dt$ is the energy loss function. Diffusion effects, set by the energy-dependent diffusion coefficient $K_d(E) = K_0(E/E_0)^\delta$, are hidden in the propagation scale $\lambda(E, E_s) = \left\{4 \int_E^{E_s} dE' K_d(E')/b(E')\right\}^{1/2}$. In the solar neighborhood, the typical energy loss timescale at $E_0 = 1$ GeV is $\tau \simeq 315$ Myr. With a typical diffusion coefficient of $K_0 \simeq 0.01$ kpc²/Myr [11], one finds $\lambda \sim 3.5$ kpc, which justifies *a posteriori* the use of the local interstellar properties to compute the energy losses [6]. In the Thomson approximation, that we will use throughout this proceeding, $b(E) = (E_0/\tau) \{\epsilon \equiv E/E_0\}^2$ [12], which implies that the propagation scale strongly decreases with energy ($\delta < 0.8$): in contrast to protons,

high energy electrons have a short range propagation.

Positrons of astrophysical origin can be secondaries or primaries. Secondaries are produced from spallation reactions between the CR nuclei and the ISM gas. Primaries are those CRs which are accelerated in the shocked medium surrounding classical sources like supernova remnants (SNRs), pulsar wind nebulae (PWNe), *etc.* Up to a good approximation, the source term of these primary and secondary components can be approximated as a power law spectrum of index γ homogeneously distributed in the thin Galactic disk: $\mathcal{Q}(E, \vec{x}) = 2h\delta(z)Q_0\epsilon^{-\gamma}$, where $h \sim 100$ pc is the half-thickness of the disk — the normalization and the spectral index are of course different for secondaries and primaries. Convoluting this source term with the 3D propagator, we readily get the flux: $\phi(E) \simeq ochQ_0\epsilon^{-\tilde{\gamma}}/\sqrt{K_0/\tau}$, where $o = \sqrt{1-\delta}/4\pi^{3/2}(\gamma-1)$ and where the propagated spectral index is $\tilde{\gamma} = \gamma + (\delta + 1)/2$, much softer than at source. For secondary positrons, since the $p-p$ cross section is almost constant at high energy, their source index is close to the CR proton index, which is not expected to vary significantly about its local value, *i.e.* $\gamma_s \sim 2.7$: with a typical diffusion slope of $\delta = 0.7$, we get $\tilde{\gamma}_s \sim 3.55$, close to the accurate prediction. Such a spectral behavior cannot explain the rising positron fraction measured by PAMELA. For primaries, the source index is close to 2.1 from shock wave acceleration theory and from observations of SNRs. We therefore get $\tilde{\gamma}_p \sim 2.95$, not far from current measurements. From the flux expression above, we can also understand why a large diffusion halo model, which must have a large K_0 , gives a lower flux than a small diffusion halo model. Nevertheless, this simple smooth picture fails at high energy because of the short range of electrons, and contributions from discrete local sources are expected to dominate the flux above ~ 50 GeV, which is known for a long time [13]. A complete modeling including secondaries and primaries from SNRs and pulsars (which produce electron-positron pairs) in a self-consistent way can actually easily fit all the available data on electrons and positrons (see [14] and references therein). It is therefore not relevant anymore to talk about “excesses” as far as astrophysics is concerned.

To summarize this part, we emphasize that the background to consider when looking for exotic signatures in the positron (or electron) spectrum is not only made of secondaries, but also of astrophysical primaries. Moreover, standard astrophysics can naturally explain the current data without over-tuning the parameters [14]. This means that no exotic source of positrons is needed at this stage. Finally, not only are astrophysical primaries expected in significant amount and with various spectral features, but also the associated predictions are not yet under control: this is bad news for DM searches in the local positron spectrum. To make it clearer to us, particle physicists, it is like trying to interpret features in the products of $p-p$ collisions, in a phase-space zone where the QCD background is expected to be large, but without knowing it accurately. Would anybody bet on a discovery there?

Positrons from dark matter annihilation: The conditions for a cosmic messenger to be a good tracer of any exotic signal are: (i) the signal to background ratio is favorable, given the experimental capability; (ii) the background is known/calculable, and controled; (iii) specific features make the signal distinguishable from the background. It is already clear that conditions (ii) and (iii) are not fulfilled. It is therefore difficult to hope to identify a DM signal in the current *local* positron data. Nevertheless, we can still ask whether DM is about to provide a sizable contribution (or use the data as pure constraints), should it be subdominant. If so, there might still be some hopes for isolating it with future experiments, provided improvements in the understanding of the background.

One important ingredient for indirect detection predictions is the DM density profile. Since we deal with short propagation scales here, we will only consider the local environment. The

local source term associated with DM annihilation reads: $\mathcal{Q}_\chi(\odot, E) = \mathcal{S} \frac{dN(E)}{dE}$ with $\mathcal{S} \equiv \delta \frac{\langle \sigma v \rangle}{2} \left\{ \frac{\rho_\odot}{m_\chi} \right\}^2$ where $\delta = 1/2$ for Dirac fermionic WIMPs, 1 otherwise; $\langle \sigma v \rangle$ is the WIMP annihilation cross section, m_χ the WIMP mass and $dN(E)/dE$ is the injected spectrum of positrons. In the local limit (*i.e.* vanishingly small propagation scale), the positron propagator is $\mathcal{G}_e(E, \vec{x} \leftarrow E_s, \vec{x}_s) \xrightarrow{\lambda \rightarrow 0} \delta(E_s - E) \delta^3(\vec{x}_s - \vec{x})/b(E)$. Assuming annihilation in e^+e^- , then $dN(E)/dE = \delta(E - m_\chi)$ and the positron flux in the local limit is analytical: $\phi_\odot^\chi(E \rightarrow m_\chi) \xrightarrow{\chi\chi \rightarrow e^+e^-} \frac{c}{4\pi} \frac{\mathcal{Q}_\chi(\vec{x}_\odot, E)}{b(E)} \approx 3.2 \times 10^{-10} \text{cm}^{-2} \cdot \text{GeV}^{-1} \cdot \text{s}^{-1} \cdot \text{sr}^{-1} \times \frac{\langle \sigma v \rangle}{3 \times 10^{-26} \text{cm}^3/\text{s}} \frac{\tau}{10^{16} \text{s}} \left[\frac{\rho_\odot}{0.3 \text{GeV}/\text{cm}^3} \right]^2 \left[\frac{m_\chi}{100 \text{GeV}} \right]^{-4}$. For these values, the result is very close to the prediction of the secondary positron flux at 100 GeV, which means that boosting the local DM density by a factor of a few is enough to feed the PAMELA data significantly. Nevertheless, this is, at least to our knowledge, the unique (still contrived) example for which one may recover the observed positron fraction up to 100 GeV without over-tuning the annihilation cross section. The presence of DM substructures (also called subhalos or clumps), expected from structure formation theory, could boost the annihilation rate. Extensive calculations of the effects of subhalos on the antimatter signatures of DM annihilation can be found in [15, 16], where the mass and spatial distributions of the objects are crucial inputs. Here, we will again focus on the local impact of subhalos. Any subhalo can be modeled from its mass m , inner density profile ρ and radius R in the Galaxy, such that the resulting DM annihilation rate is set by its *annihilation volume*: $\xi(m, R) = 4\pi \int_0^{r_v} dr r^2 \left\{ \frac{\rho_{\text{cl}}(m, R, r)}{\rho_\odot} \right\}^2$, which measures the ratio of its intrinsic emissivity to the local DM emissivity. The local subhalo flux is then: $\phi_{\text{cl}, \odot}^\chi(E) \xrightarrow{\lambda \rightarrow 0} \frac{\beta c}{4\pi} \mathcal{S} N_{\text{cl}} \frac{d\mathcal{P}_V(\vec{x}_\odot)}{dV} \frac{\langle \xi(\vec{x}_\odot) \rangle_m}{b(E)} \frac{dN(E)}{dE}$, where $\langle \rangle_m$ denotes the average over the mass distribution. The so-called *boost factor* is defined by the ratio of smooth+subhalo to smooth-only flux predictions. Since the effective volume contributing to the flux depends on the positron propagation scale, and therefore on energy, the boost factor depends on energy. We have in the short range limit, which turns out to be an average upper limit: $\mathcal{B}_\odot \xrightarrow{\lambda \rightarrow 0} 1 + N_{\text{cl}} \frac{d\mathcal{P}_V(\vec{x}_\odot)}{dV} \langle \xi(\vec{x}_\odot) \rangle_m$. The boost limit is naturally given by the local number density of objects $N_{\text{cl}} d\mathcal{P}_V(\vec{x}_\odot)/dV$ times the average annihilation volume of a single object $\langle \xi(\vec{x}_\odot) \rangle_m$ (already normalized to the local smooth luminosity). For large propagation scales, *i.e.* low energy, the signal coming from the cuspy smooth distribution in the Galactic center will have larger contribution to the total flux, lowering the boost factor. This is an important trend which is very often neglected. The global subhalo flux should be associated with a statistical variance σ related to the number of objects *seen* in positrons; σ therefore increases with energy [15, 16]. This translates into a large variance for the boost factor at high energy if the subhalo contribution dominates. One can play with any subhalo model, but it turns out that even in extreme cases, $\mathcal{B}_\odot \lesssim 20$ [16]. Using results from high resolution N-body simulations, it was shown in [17] that $\mathcal{B}_\odot \lesssim 5$ (enough for direct annihilation in e^+e^- only). One can still invoke the presence of massive nearby subhalos or other dark objects, but such a improbable possibility is in tension with gamma-ray constraints [18].

Conclusion: We have argued that the rising local positron fraction observed by the PAMELA experiment can be explained by properly including known astrophysical sources of primary positrons like pulsars, as already suggested twenty years ago [7]. Therefore, it seems that understanding this measurement, as well as the so-called “electron excess” sometimes *seen* in the Fermi data [19], are no longer theoretical issues, since standard and not contrived explanations are available. Remains open the question of identifying and modeling more accurately

the local sources in order to sustain this solution on more detailed grounds. These are good news for this research domain.

Regarding the DM hypothesis, we have shown that usual thermal WIMP candidates are not expected to contribute significantly to the local positron flux, even when treated in a self-consistent framework including subhalos. The only possibility without over-tuning the annihilation cross section allowed for thermal relics is to consider direct production of e^+e^- and a mass scale ~ 100 GeV, a quite contrived case. Likewise, we have also emphasized that should DM yield a sizable positron signal, it would be difficult to disentangle it from standard astrophysical sources; the background is not yet under control.

Nevertheless, WIMPs remain excellent DM candidates, far from excluded. The crucial issue of their detection is still challenging, since their expected properties have made them continuously escape from observations despite the advent of new experimental techniques. It seems important to develop more complex strategies based on multi-messenger, multi-wavelength and multi-scale approaches, for which big efforts should be made (i) to quantify and minimize the associated theoretical uncertainties and (ii) to control the backgrounds. Other detection methods are also very important, among which the LHC results are particularly expected.

Acknowledgments: It is a pleasure to thank all the organizers of the Patras workshop held in Durham for their warm welcoming.

References

- [1] J. Silk and M. Srednicki. *Physical Review Letters*, 53:624–627, August 1984.
- [2] J. Carr, G. Lamanna, and J. Lavalle. *Reports on Progress in Physics*, 69:2475–2512, August 2006.
- [3] J. L. Fanselow *et al.*. *Astrophys. J.*, 158:771–+, November 1969.
- [4] O. Adriani *et al.*. *Nature*, 458:607–609, April 2009.
- [5] I. V. Moskalenko and A. W. Strong. *Astrophys. J.*, 493:694–+, January 1998.
- [6] T. Delahaye *et al.*. *Astron. Astrophys.*, 501:821–833, July 2009.
- [7] A. Boulares. *Astrophys. J.*, 342:807–813, July 1989.
- [8] V. L. Ginzburg and S. I. Syrovatskii. New York: Macmillan, 1964, 1964.
- [9] V. S. Berezinskii *et al.*. Amsterdam: North-Holland, 1990, edited by Ginzburg, V.L., 1990.
- [10] A. W. Strong, I. V. Moskalenko, and V. S. Ptuskin. *Annual Review of Nuclear and Particle Science*, 57:285–327, November 2007.
- [11] D. Maurin *et al.*. *Astrophys. J.*, 555:585–596, July 2001.
- [12] G. R. Blumenthal and R. J. Gould. *Reviews of Modern Physics*, 42:237–271, 1970.
- [13] C. S. Shen. *Astrophys. J. Lett.*, 162:L181+, December 1970.
- [14] T. Delahaye *et al.*. *arXiv:1002.1910*, February 2010.
- [15] J. Lavalle *et al.*. *Astron. Astrophys.*, 462:827–840, February 2007.
- [16] J. Lavalle *et al.*. *Astron. Astrophys.*, 479:427–452, February 2008.
- [17] L. Pieri, J. Lavalle, G. Bertone, and E. Branchini. *arXiv:0908.0195*, August 2009.
- [18] T. Bringmann, J. Lavalle, and P. Salati. *Physical Review Letters*, 103(16):161301–+, October 2009.
- [19] A. A. Abdo *et al.*. *Physical Review Letters*, 102(18):181101–+, may 2009.

Dark Matter Decay and Cosmic Rays

Christoph Weniger

DESY, Notkestraße 85, 22607 Hamburg, Germany

DOI: http://dx.doi.org/10.3204/DESY-PROC-2009-05/weniger_christoph

The decay of dark matter is predicted by many theoretical models and can produce observable contributions to the cosmic-ray fluxes. I shortly discuss the interpretation of the positron and electron excess as observed by PAMELA and Fermi LAT in terms of decaying dark matter, and I point out the implications for the Fermi LAT observations of the γ -ray flux with emphasis on its dipole-like anisotropy.

1 Introduction

The most popular type of dark matter (DM) candidate, the weakly interacting massive particle (WIMP), can naturally reproduce the observed DM abundance due to effective self-annihilation in the early Universe, and today this same annihilation process could produce an observable contribution to the measured cosmic-ray fluxes on Earth. Such an indirect detection of DM is also possible if DM *decays* with a sufficiently large rate. There exist a number of interesting DM models (see *e.g.* [1] and references therein) that predict the decay of DM on cosmological time scales, namely with lifetimes around and above $\tau_{\text{DM}} \simeq \mathcal{O}(10^{26} \text{ s})$, which are typically required to be not in conflict with current observational limits. Among these models is the gravitino with a small violation of R -parity, motivated by requiring a consistent thermal history of the Universe, and the sterile neutrinos, whose long lifetime is due to tiny Yukawa couplings. The typical masses for these DM candidates lie in the 100 GeV and the 10 keV regime, respectively. Another interesting model with kinetically mixed hidden gauginos was also recently studied [2]. Even in models where DM is stable in the first place, the consideration of higher-dimensional operators often renders the DM particle unstable with cosmological lifetimes. Since the indirect detection signals from decay differ in general from the ones of annihilation, a dedicated study of decaying DM signals is mandatory. Below I will shortly review the γ -ray and e^\pm -signals that can come from DM decay, and I will discuss them in light of recent observations.

2 Cosmic rays from dark matter decay

Provided the decays occur at a sufficiently large rate, their products could be observable as an exotic contribution to the high energy cosmic ray fluxes of γ -rays, electrons, positrons, antiprotons, neutrinos or antideuterons. Among the different cosmic-ray species, γ -rays play a distinct role, due to their sensitivity to far-distant sources and their potential to discriminate between astrophysical and DM signals. The *gamma-ray* signal from DM decay consists of several components. The most important one is related to the prompt radiation (*e.g.* final state radiation) produced in the decay of DM particles inside the Milky Way halo. It depends on the

halo density profile, and although the halo profile is expected to be approximately isotropic, the corresponding flux at Earth exhibits a strong dipole-like anisotropy due to the offset between sun and galactic center. In contrast, the extragalactic prompt component of the γ -ray signal, which stems from the decay of DM particles at cosmological distances, is largely isotropic. At energies around 10 GeV or below, the magnitude of the halo and extragalactic fluxes are of the same order, whereas at much higher energies around 1 TeV the inelastic scattering between γ -rays and the intergalactic background light renders the extragalactic component negligible. Decaying DM in general also produces electrons and positrons, which give rise to another contribution of the γ -ray signal, coming from the inverse Compton scattering (ICS) between the electrons and positrons and the interstellar radiation field (ISRF). This component is highly anisotropic and usually lower in energy than the component from prompt radiation. The main background in the γ -ray channel is the diffuse emission of our Galaxy, which is mainly due to interactions of cosmic rays with the galactic gas and the ISRF. This component is by far strongest in the galactic disk region, and it turns out that exotic fluxes from DM decay would dominantly show up at higher latitudes, away from the disk. This is in contrast to annihilation signals, which are often expected to be best seen very near to the galactic center.

The *electrons and positrons* produced in the Milky Way halo by DM decay scatter on irregularities of the Galactic magnetic field, which results in a wash-out of directional information before they reach the Earth. Their propagation is commonly described by a diffusion model, whose free parameters are tuned to reproduce the observed cosmic-ray nuclei fluxes. The astrophysical background in this channel is mainly due to primary electrons, which are presumably produced in supernova remnants, and due to secondary positrons, produced in the interaction of cosmic-rays with the galactic gas.

Recently it has become apparent that state-of-the-art propagation models fail to reproduce the PAMELA measurements of the *positron fraction* at energies larger than 10 GeV [3]. Together with the more recent Fermi LAT and HESS data [4] for the total e^\pm -flux the experiments suggest an excess of electrons and positrons up to energies around a few 1 TeV. The most common astrophysical explanation of this excesses is the electron-positron pair production by the interactions of high-energy photons in the strong magnetic field of nearby pulsars, such as Geminga or Monogem (see *e.g.* [5] and references therein). However, an arguably more exciting explanation of the cosmic-ray electron/positron excesses is the possibility that the electrons and positrons are produced in the annihilation or the decay of DM particles.

3 Positron excess and gamma-ray prospects

If the observed excess of positrons and electrons is entirely due to DM decay, one obtains clear predictions for the γ -ray signal that should be observable at Fermi LAT. In Ref. [6] we analyzed the predictions for the positron fraction and the total electron plus positron flux including a possible contribution from DM decay in order to account for the anomalies observed by PAMELA and Fermi. We considered several scenarios of de-

Decay Channel	M_{DM} [GeV]	τ_{DM} [10^{26} s]
$\psi_{\text{DM}} \rightarrow \mu^+ \mu^- \nu$	3500	1.1
$\psi_{\text{DM}} \rightarrow \ell^+ \ell^- \nu$	2500	1.5
$\phi_{\text{DM}} \rightarrow \mu^+ \mu^-$	2500	1.8
$\phi_{\text{DM}} \rightarrow \tau^+ \tau^-$	5000	0.9
$\psi_{\text{DM}} \rightarrow W^\pm \mu^\mp$	3000	2.1

Table 1: DM decay channels that we found to best fit the Fermi LAT and PAMELA data [6].

caying DM, being it either a fermionic or a bosonic particle, which decays into various channels with a branching ratio of 100%. Our results are summarized in Tab. 1, an example is shown in Fig. 1. From the data leptonic, and in particular muonic, modes are favored. Note that the decay into $W^\pm\mu^\mp$ is in some tension with the anti-proton/proton ratio observed by PAMELA.

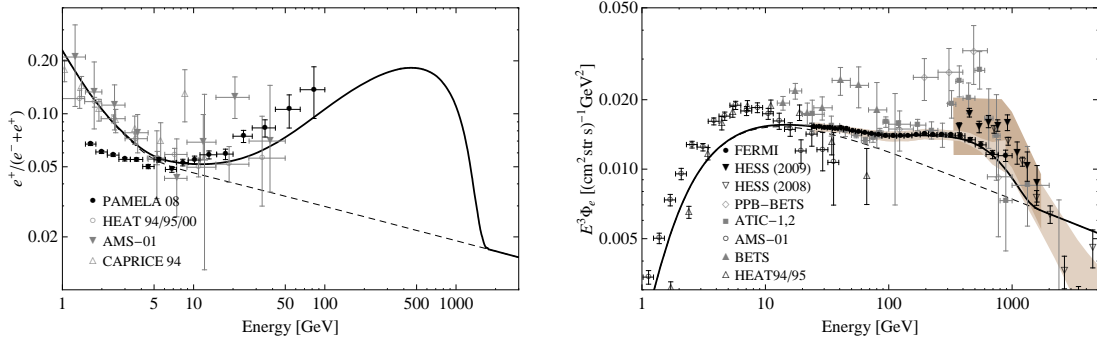


Figure 1: Positron fraction (*left panel*) and electron+positron flux (*right panel*) for DM decay $\psi_{\text{dm}} \rightarrow \mu^+\mu^-\nu$ (see Tab. 1). The dashed line shows the astrophysical background. Details are given in Ref. [6].

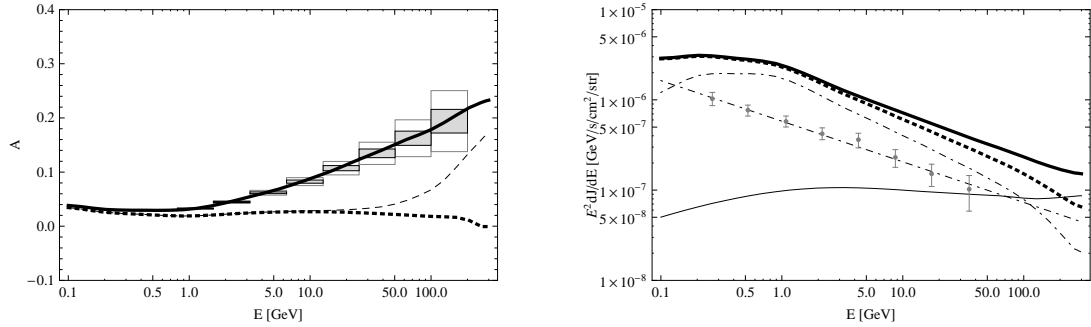


Figure 2: *Left panel*: Anisotropy of γ -ray signal for the decay mode $\psi_{\text{dm}} \rightarrow \mu^+\mu^-\nu$ [7]. The *solid* line shows the anisotropy of the total signal, including the galactic foreground, the *dotted* line shows the anisotropy of the foreground alone. The *thin dashed* line is the anisotropy of the total signal when neglecting ICS radiation of electrons and positrons from DM decay. *Right panel*: Averaged fluxes of the different γ -ray components. Line coding as in left panel, in addition the *thin solid* line shows the pure DM signal and the *dot-dashed* lines show the adopted extragalactic background flux and the galactic foreground. Data points correspond to the preliminary Fermi LAT results for the extragalactic γ -ray background [8].

The production of electrons and positrons in the DM decay inevitably produces also contributions to the cosmic γ -rays. In particular the γ -ray signal of the decay modes shown in Tab. 1 should give rise to a clear signal in the Fermi LAT observations at higher latitudes. Furthermore this signal is expected to be anisotropic, which can be used to discriminate it from the galactic foreground and the extragalactic γ -ray background. To illustrate this we define

the anisotropy parameter $A = (\bar{J}_{\text{GC}} - \bar{J}_{\text{GAC}})/(\bar{J}_{\text{GC}} + \bar{J}_{\text{GAC}})$, where \bar{J}_{GC} and \bar{J}_{GAC} denote the diffuse γ -ray flux averaged over the hemisphere in direction of the Galactic center (GC) and anticenter (GAC), respectively. The galactic disk, with latitudes $|b| < 10^\circ$, is excluded from the average. The left panel of Fig. 2 shows our results for the anisotropy parameter which is expected to be observed by the Fermi LAT if the DM particle decays into $\mu^+\mu^-\nu$ (see Ref. [7] for details). Although the decay channel is marginally consistent with preliminary data (right panel), a sizeable anisotropy, around $A \simeq 0.2-0.3$, is predicted at energies $E_\gamma \simeq 100$ GeV. This can be significantly different from the anisotropy of the astrophysical foreground (we adopt the conventional model 44_500180 from `galprop.stanford.edu`). As indicated by our estimates of the statistical error bars for one-year and five-year Fermi LAT observation, this deviation should be clearly visible in the upcoming results for the diffuse γ -ray sky.

4 Conclusions

Many theoretical models predict the decay of DM on cosmological timescales, giving rise to an anomalous contribution to the observed cosmic-ray fluxes. The corresponding γ -ray signals could show up as broad features over large angular distance in the γ -ray sky. If decaying DM is the right explanation of the positron and electron excess observed by PAMELA and Fermi LAT, a corresponding γ -ray signal with a large dipole-like anisotropy should be observed in the very near future with Fermi LAT. This anisotropy would be due to prompt radiation at high latitudes, and due to ICS radiation at lower latitudes, most prominent in a region of a few kpc around the galactic center. It is tempting to speculate that such an ICS signal already showed up in the Fermi LAT data, see Ref. [9].

Acknowledgments

The author likes to thank the organizers of the *5th Patras Workshop on Axions, WIMPs and WISPs* for an enlightening conference, and Alejandro Ibarra and David Tran for very fruitful collaboration.

References

- [1] W. Buchmüller, L. Covi, K. Hamaguchi, A. Ibarra and T. Yanagida, *JHEP* **0703** (2007) 037 [arXiv:hep-ph/0702184]; A. Boyarsky, O. Ruchayskiy and M. Shaposhnikov, arXiv:0901.0011 [hep-ph]; A. Arvanitaki, S. Dimopoulos, S. Dubovsky, P. W. Graham, R. Harnik and S. Rajendran, *Phys. Rev. D* **79** (2009) 105022 [arXiv:0812.2075 [hep-ph]].
- [2] A. Ibarra, A. Ringwald, D. Tran and C. Weniger, *JCAP* **0908** (2009) 017 [arXiv:0903.3625 [hep-ph]]. A. Ibarra, A. Ringwald and C. Weniger, *JCAP* **0901** (2009) 003 [arXiv:0809.3196 [hep-ph]].
- [3] O. Adriani *et al.* [PAMELA Collaboration], *Nature* **458** (2009) 607 [arXiv:0810.4995 [astro-ph]].
- [4] A. A. Abdo *et al.* [The Fermi LAT Collaboration], *Phys. Rev. Lett.* **102**, 181101 (2009) [arXiv:0905.0025 [astro-ph.HE]]; F. Aharonian *et al.* [H. E. S. S. Collaboration], arXiv:0905.0105 [astro-ph.HE].
- [5] D. Grasso *et al.* [FERMI-LAT Collaboration], *Astropart. Phys.* **32** (2009) 140 [arXiv:0905.0636 [astro-ph.HE]].
- [6] A. Ibarra, D. Tran and C. Weniger, arXiv:0906.1571 [hep-ph] (2009).
- [7] A. Ibarra, D. Tran and C. Weniger, arXiv:0909.3514 [hep-ph] (2009).
- [8] M. Ackermann, Talk given at TeV Particle Astrophysics 2009.
- [9] G. Dobler, D. P. Finkbeiner, I. Cholis, T. R. Slatyer and N. Weiner, arXiv:0910.4583 [astro-ph.HE].

Chapter 4

Photon Regeneration and Laser Polarization Experiments

The CAST experiment: status and perspectives

Esther Ferrer Ribas on behalf of the CAST Collaboration

IRFU, CEA/Saclay, 91190 Gif sur Yvette, France

DOI: http://dx.doi.org/10.3204/DESY-PROC-2009-05/ferrer-ribas_esther

The status of the solar axion search with the CERN Axion Solar Telescope (CAST) will be discussed. Results from the first part of CAST phase II where the magnet bores were filled with ^4He gas at variable pressure in order to scan m_a up to 0.4 eV will be presented. From the absence of excess X-rays when the magnet was pointing to the Sun, we set a typical upper limit on the axion-photon coupling of $g_{a\gamma} \lesssim 2.17 \times 10^{-10} \text{GeV}^{-1}$ at 95% CL for $m_a < 0.4$ eV, the exact result depending on the pressure setting. Our search for axions with masses up to about 1.2 eV using ^3He as a buffer gas is, since last year, in progress in the second part of CAST phase II. Expectations for sensitivities will be given. Near future perspectives as well as more long term options for a new helioscope experiment will be evoked.

1 Introduction

The CAST (Cern Axion Solar Telescope) experiment is using a decommissioned LHC dipole magnet to convert solar axions into detectable x-ray photons. Axions are light pseudoscalar particles that arise in the context of the Peccei-Quinn[1] solution to the strong CP problem and can be Dark Matter candidates[2]. Stars could produce axions via the Primakoff conversion of the plasma photons. The CAST experiment is pointing at our closest star, the Sun, aiming to detect solar axions. The detection principle is based on the coupling of an incoming axion to a virtual photon provided by the transverse field of an intense dipole magnet, being transformed into a real, detectable photon that carries the energy and the momentum of the original axion. The axion to photon conversion probability is proportional to the square of the transverse field of the magnet and to the active length of the magnet. Using an LHC magnet (9 T and 9.26 m long) improves the sensitivity by a factor 100 compared to previous experiments. The CAST experiment has been taking data since 2003 providing the most restrictive limits on the axion-photon coupling [3, 4] for masses $m_a \lesssim 0.02$ eV. At this mass the sensitivity is degraded due to coherence loss. In order to restore coherence, the magnet can be filled with a buffer gas providing an effective mass to the photon[5]. By changing the pressure of the buffer gas in steps, one can scan an entire range of axion mass values. At the end of 2005 the CAST experiment started such a program, entering its phase II by filling the magnet bore with He gas. From 2005 to 2007, the magnet bore was filled with ^4He gas extending our sensitivity to masses up to 0.4 eV, final results will be presented here. From March 2008 onwards the magnet bore has been filled with ^3He and the sensitivity should be increased to sensitivities up to $m_a \lesssim 1.2$ eV by the end of the ^3He run in 2010.

2 The CAST experimental set-up: recent upgrades

The CAST set up has been described elsewhere [3, 9]. From 2002 to 2006 three X-ray detectors were mounted on the two sides of the magnet: a conventional TPC[10] covering both magnet bores looking for sunset axions; in the sunrise side one of the bores was covered by a Micromegas detector[11] and in the other bore a CCD detector coupled to a telescope[12] improving the signal to background ratio by a factor 150. In 2006 the TPC started to show a degraded performance due to aging. It was then decided to replace the sunset TPC and the existing Micromegas detector in the sunrise side by a new generation of Micromegas detectors[13, 14] that coupled with suitable shielding would improve greatly their performance. The new detectors were commissioned end of 2007 and by mid 2008 they have already shown an improvement in performance that has been translated in a background reduction of a factor 15 compared to the TPC performances and a factor 3 compared to the standard Micromegas detector used without shielding till 2006. The CCD detector will also be upgraded by the fall 2009 by a new detector with improved performance: better low energy response, lower intrinsic background by using more radio-pure materials and less out of time events.

In 2005, the experiment went through a major upgrade to allow operation with He buffer gas in the cold bore. This upgrade was done in two steps: first the system was designed for operation using ^4He and in 2007 the system was upgraded for operation at higher buffer gas densities using ^3He . The system has been designed to control the injection of He in the magnet bores with precision and to monitor accurately the gas pressure and temperature[15, 16]. Special care has been taken to achieve high precision in the reproducibility of steps (< 0.01 mbar) and to protect the system for ^3He loss. The ^3He system has been operating successfully since december 2007.

3 Results

As during phase I, the tracking data (magnet pointing the sun) represented about 2×1.5 hours per day while the rest of the day was used to measure background. The procedure was to daily increase the ^4He density so that sunrise and sunset detectors measure every pressure. Every specific pressure of the gas allows to test a specific axion mass having a new discovery potential. The ^4He data recorded end of 2005 and 2006 represents around 300 hours of tracking data and 10 times more hours of background data for each detector, covering 160 pressure settings allowing to scan a new axion mass range between 0.02 and 0.39 eV.

An independent analysis was performed for each data set of the three different detectors. A combined preliminary result was derived where from the absence of a signal above background CAST excludes a new range in the $g_{a\gamma}-m_a$ plane shown in figure 1 from axion masses of 0.02 eV (Phase I) up to masses of 0.39 eV. This parameter space was not previously explored in laboratory experiments. CAST has therefore entered the QCD axion band for the first time in this range of axion masses, excluding an important portion of the axion parameter space. The final results have been published in [17].

The collaboration has performed by-product analysis of the data taken, to look for other axion scenario to which CAST would also be sensitive. The TPC phase I data has been reanalysed in order look for 14 keV axions coming from M1 transitions. In addition, data taken with a calorimeter during the phase I, were used to search for high energy (MeV) lines from high energy axion conversion [6, 7]. More recently a few days of data were taken with a visible detector coupled to one end of the CAST magnet [8], in search for axions with energy in the

”visible” range. It is foreseen that a permanent setup will be installed in the experiment in order to take data without interfering with the standard program of CAST.

At present, we are running with ^3He since 2008 and by the end of this year we should have reached sensitivities of around $m_a < 0.8\text{ eV}$.

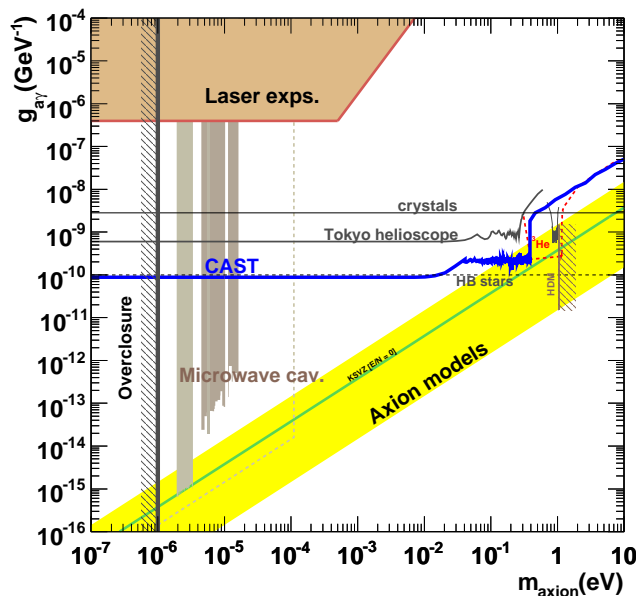


Figure 1: Exclusion plot in the axion-photon coupling versus the axion mass plane for a wide range of parameters. The limit achieved by the CAST experiment (combined result of the CAST phase I and ^4He part of phase II) is compared with constraints obtained from the Sumico experiment (the Tokyo helioscope) and HB stars. The red dashed line shows our prospects for the ^3He run started in March 2008. The vertical line (HDM) is the hot dark matter limit for hadronic axions $m_a < 1.0\text{ eV}$ inferred from observations of the cosmological large-scale structure. The yellow band represents typical theoretical models with $|E/N - 1.95|$ in the range 0.07–7 where the green solid line corresponds to the case when $E/N = 0$ is assumed. Limits from laser, microwave and underground detectors [18] for axion searches have been included.

4 After CAST?

CAST original physics program will finish at the end of 2011. The CAST collaboration is looking into possibilities in order to achieve greater sensitivities. The sensitivity of helioscope axion searches depends strongly on the magnet’s characteristics. Ongoing R & D on dipoles will lead to stronger and bigger magnets in the coming years (2013-2015). Such magnets could either be adopted to the existing infrastructure of CAST, thus eliminating the cost to the magnet itself, or be used with a new tracking and cryogenics system, improving thus many characteristics (like daily tracking time, safety etc) but increasing the cost. In parallel, effort

will be devoted on the development of high efficiency focusing devices and new electronics for the detectors, aiming to achieve very low background levels. All this would allow pushing the sensitivity of the experiment to the level of 10^{-11}GeV^{-1} , probing the QCD axion model region for masses higher than 10^{-2}eV . In order to exceed the limit of 10^{-11}GeV^{-1} with a helioscope, specially developed magnets are necessary. Taking advantage of the fact that the important parameter is the strength and not the homogeneity of the magnetic field, a stronger magnet with bigger aperture, could be designed and constructed especially for such an experiment. This is a more expensive and long term option, which would allow reaching the limits of the helioscope axion searches with an increased discovery potential. These different options as well as expected sensitivities were presented in detail in [19].

5 Conclusions

The CAST experiment has established the most stringent experimental limit on the axion coupling constant over a wide range of masses, exceeding astrophysical constraints. The ^4He phase has allowed to enter in an unexplored region favoured by the theory axion models. From the absence of excess X-rays when the magnet was pointing to the Sun, we set a preliminary upper limit on the axion-photon coupling of $g_{a\gamma} \lesssim 2.22 \times 10^{-10} \text{GeV}^{-1}$ at 95% CL for $m_a \lesssim 0.4 \text{eV}$, the exact result depending on the pressure setting. At present, with the ^3He run we are exploring deeper this region to reach sensitivities of $m_a < 1.2 \text{eV}$. The Collaboration is looking into developing a new generation of helioscopes in order to reach sensitivities of the order of 10^{-11}GeV^{-1} leading to explore a large part of the QCD favoured model region including the otherwise non-accessible sub-eV range.

References

- [1] R.D. Peccei and H.R. Quinn, Phys. Rev. Lett. **38**, 1440 (1977).
- [2] P. Sikivie, Int. J. Mod. Phys. **D3 S**, 1 (1994) and Phys. Rev. Lett. **51**, 1415 (1983).
- [3] K. Zioutaset *et al.* (CAST collaboration), Phys. Rev. Lett. **94**, 121301 (2005), arXiv: hep-ex/0411033.
- [4] S. Andriamonjeet *et al.* (CAST collaboration), JCAP **04** 10 (2007), arXiv:hep-ex/0702006.
- [5] K. van Bibber, P.M McIntyre, D.E. Morris and G.G Raffelt, Phys. Rev. D **39**, 2089 (1989).
- [6] S. Andriamonje *et al.* (CAST collaboration), accepted for publication at JCAP, arXiv:hep-ex/09064488
- [7] K. Jakovic *et al.* (CAST collaboration), these proceedings.
- [8] M. Karuza *et al.* (CAST collaboration), these proceedings.
- [9] K. Zioutas *et al.*, Nucl. Instrum. Methods Phys. Res., A **425** 480 (1999), arXiv:astro-ph/9801176.
- [10] D. Autiero *et al.*, New J. Phys **9**, 171 (2007) arXiv: hep-ex/0702189.
- [11] P. Abbon *et al.*, New J. Phys **9**, 170 (2007), arXiv: hep-ex/0702190.
- [12] M. Kuster *et al.*, New J. Phys **9**, 169 (2007), arXiv: hep-ex/0702188.
- [13] J. Galán *et al.*, Nucl. Instr. and Meth. A **604** 15-19 (2009).
- [14] S. Aune *et al.*, J. Phys. Conf. Ser. **179** 012015 (2009).
- [15] T.O. Niinikoski *et al.*, Submitted to Proc. ICEC 22, Seoul (2008).
- [16] CAST Collaboration, SPSC-TDR-001, CERN-SPSC-2006-029.
- [17] E. Arik *et al.* (CAST collaboration), JCAP 0902, 008 (2009).
- [18] Z. Ahmed *et al.* (CDMS Collaboration), Phys. Rev. Lett. **103** 141802 (2009), arXiv: hep-ex/0902.4693.
- [19] T. Papaevangelou (CAST collaboration), Presentation at “New opportunities in the Physics Landscape at CERN”.

Search for Solar ALPs in the Low Energy Range at CAST

Giovanni Cantatore^{1,2}, Marin Karuza¹, Valentina Lozza^{1,2} for the CAST collaboration

¹INFN Sezione di Trieste, Via A. Valerio 2, 34127 Trieste, Italy

²Università di Trieste, Dipartimento di Fisica, Via A. Valerio 2, 34127 Trieste, Italy

DOI: http://dx.doi.org/10.3204/DESY-PROC-2009-05/karuza_marin

It has been shown that a detector system, sensitive to single photons in the eV range can be coupled to the CAST experiment [1]. However the detectors used had high background rates compared with the expected signal, thus a search for a detector suitable for integrating in the present setup and with a low background rates was initiated. A suitable detector candidate was found and results from first tests are presented.

1 Introduction

Although it has been observed and studied from the very beginning of civilization, the Sun is far from being completely understood thus leaving space for some surprises. One of them might be the production of yet experimentally undiscovered particles that could be the axion or particles that have some of its properties (Axion Like Particles).

The differential Solar axion flux at the Earth is expected to be peaked at 3.0 keV with the average energy being 4.2 keV [2]. However there are many not completely understood phenomena taking place in the Sun [3] that could affect the calculated axion spectrum. One of possibilities is related to one of the most puzzling questions of modern physics: the high temperature of the Solar corona and its existence alone. The proposed explanations for the temperature difference of three orders of magnitude between corona and surface of the Sun, include wave heating theory, proposed back in 1949 [4], magnetic reconnection [5] and the axion production related to the magnetic fields near the surface of the Sun [6][7]. The last one is, obviously, also the most interesting as far as this work is concerned. The mechanisms that could contribute to the axion spectrum at low energies (\approx eV), with respect to the peak of the theoretical forecast, are either the oscillation of axions from the solar core in X-ray photons and their scattering off free electrons in the solar corona or the production of axions by the Primakoff effect [8]. These two processes could also explain the reduction in the solar luminosity near sunspots in the visible part of the electromagnetic spectrum.

Furthermore, there are also theoretical mechanisms that include axions affecting the high energy tail of the expected axion spectrum. However they are not of interest for this work and are described elsewhere, as for example the production of axions by the deexcitation of the thermally excited ^{57}Fe nuclide [9].

Since the preliminary tests have shown the feasibility of integrating another detector to the CERN Axion Solar Telescope (CAST) without interfering with its scientific programme the

3 Detector developments

From the obtained results it can be clearly seen that the proposed setup is working and that interesting limits in the axion mass-coupling constant plane cannot be reached by simple integration, the limit being inversely proportional to the eighth root of measurement time, thus a detector with lower background has to be considered. Among the possible choices, a G-APD was chosen as the most promising due to its relative simplicity of operation and commercial availability. In particular the id101-50 model produced by IdQuantique was selected. Although the best sensors of this type have a background count rate still too high for considerably lowering the coupling constant limit, this detector is interesting since its background is mainly due to thermally emitted carriers and thus it is possible to further reduce it by cooling the detector to cryogenic temperatures. For this purpose a cryostat was constructed (Fig. 2) with a copper cold finger that holds about one liter of liquid nitrogen that is sufficient for about one hour long operation without refilling. The detector is placed in a seat in the cold finger and its temperature is read by thermocouples attached to the cold finger. The temperature of liquid nitrogen was reached, but the temperature of the G-APD active area could not be directly measured thus leaving us only with an estimate that was obtained from the measured temperature dependency of the breakdown voltage. It results that the sensor was cooled down at least to 130 K. The cooling of the detector is not free of drawbacks since it results in raising the afterpulsing rate, however the detector is to be operated at a low signal rate and the problem can be solved by increasing the detector dead time. The solution adopted selects and discards the afterpulses by software, thus leaving the hardware of the detector unaltered and providing the control of the dead time as well as raw and corrected counting rates.



Figure 2: Custom made liquid nitrogen cryostat. The coolant is inserted from the aperture in the upper part that is connected to a hollow copper cold finger which is also holding the detector.

As can be seen in the following plot (Fig. 3) cooling to cryogenic temperature resulted in lowering the Dark Count Rate (DCR) by five orders of magnitude (blue symbols) with respect to the DCR at room temperature while maintaining the quantum efficiency (red symbols). The fact that the counts remain unchanged while lowering the temperature guarantees also that the dead time was set correctly and that it does not affect the efficiency.

It has to be stressed that the detector under study is an off-specs detector with a DCR of

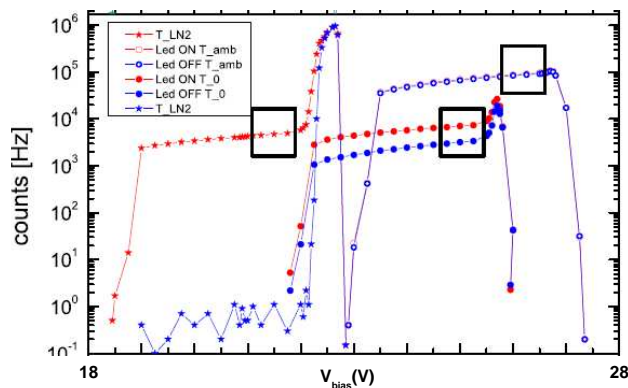


Figure 3: Characterization of a test G-APD detector at three different temperatures. The chosen working bias voltage regions are indicated by a rectangle. A reduction of five orders of magnitude in DCR with respect to that at room temperature is obtained when cooling the detector.

almost 100 kHz at room temperature, while tests with detectors with low DCR also at room temperature are to be conducted yet. It is not clear whether the same order of magnitude reduction can be obtained.

4 Conclusion and prospects

In order not to interfere with the CAST original scientific programme, a permanent installation for the low energy photon counter was devised with a modification, to the original BaRBE setup. It consists of a $5\ \mu\text{m}$ thick polypropylene support for a 20 nm aluminum mirror (Fig. 4) that should be placed in the reconverted photon beam. It is transparent to X-rays while it is reflective for $\approx\text{eV}$ photons, thus steering them to the telescope that conveys them in the optical fiber leading to the detector. With a detector that has a sufficiently low background

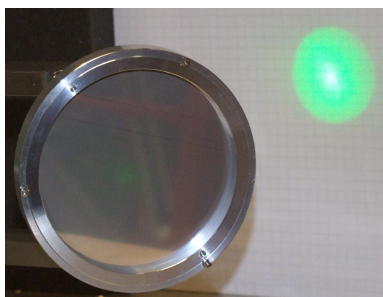


Figure 4: Semitransparent mirror placed in its support. A steered laser beam coming from telescope can be seen.

and the semitransparent mirror in place the search for Solar axions in the low energy range can start, still with no hope of lowering the limit, when only standard axion model is considered, but with an enhanced probability of detecting axions coming from processes discussed in the introduction.

5 Acknowledgments

Funding for the BaRBE project has been provided by INFN (Italy). Special thanks to the CAST collaboration for support and assistance, Saclay group for providing us with this mirror and the Trieste mechanical workshop and its head D. Iugovaz for fulfilling all our requests.

References

- [1] Cantatore G. et al. http://dx.doi.org/10.3204/DESY-PROC-2008-02/cantatore_giovanni_lea
- [2] Raffelt G. G., Axions motivation, limits and searches, *J. Phys. A:Math.Theor.* 40 (2007), 66076620
- [3] Zioutas K., The enigmatic Sun: a crucible for new physics, *CERN Courier* (May 2008)
- [4] Klimchuck J.A., On solving the coronal heating problem, *Solar Physics* 234 (2006) 41-77
- [5] Manoharan P.K., Evidence for Large-Scale Solar Magnetic Reconnection from Radio and X-Ray Measurements, *The Astrophys. Journal* 468, 73-76, (September 1996)
- [6] Zioutas K., Axions could shed light on solar mysteries, interview for *Physicsworld*, 2009
- [7] DiLella L., Zioutas K., Observational evidence for gravitationally trapped massive axion(like) particles, *Astroparticle physics* 19, 145-170, 2002
- [8] Primakoff H., Photo-Production of Neutral Mesons in Nuclear Electric Fields and the Mean Life of the Neutral Meson, *Phys. Rev.* 81, 899, 1951
- [9] Jakovcic K., Prospects for the CERN Axion Solar Telescope to 14.4 keV Axions, *Nucl. Instrum. Meth.* A580 (2007) 37-39

Search for Monoenergetic Solar Axions with CAST

Krešimir Jakovčić on behalf of the CAST Collaboration

Rudjer Bošković Institute, 10000 Zagreb, Croatia

DOI: http://dx.doi.org/10.3204/DESY-PROC-2009-05/jakovcic_kresimir

We present the results of the CERN Axion Solar Telescope (CAST) search for monoenergetic axions or axion-like particles that could be emitted from the Sun by ^{57}Fe (14.4 keV) and ^7Li (0.478 MeV) nuclear de-excitations and $\text{D}(p, \gamma)^3\text{He}$ (5.5 MeV) reaction. The non-observation of the signal above background allowed us to set model-independent limits on the coupling constants of pseudoscalar particles that couple to a nucleon and to two photons.

1 Introduction

Axions are neutral pseudoscalar particles that emerge as an inevitable consequence of the Peccei-Quinn solution [1] to the strong CP problem and are viable dark matter candidates. Despite the exhaustive search that has been going on for more than 30 years, there is still no positive signal for the axion or axion-like particles (ALPs). It is expected that pseudoscalars like axions should be abundantly produced in stars by nuclear and thermal processes. Hence, as the closest star, the Sun would be a strong axion emitter suitable for axion searches. As these particles couple to two photons, they could be produced in the solar core via Primakoff conversion of thermal photons in the Coulomb fields of the solar plasma. Such axions would have a continuous energy spectrum with a peak at 3 keV, mean energy of 4.2 keV, and dying off above ~ 10 keV. Due to the axion-nucleon coupling, there are additional components of solar axions emitted in nuclear de-excitations and reactions. The energy of these monoenergetic axions corresponds to the energy of the particular process. With axions being pseudoscalar particles, axion emission from nuclear processes is expected to occur predominantly via M1 nuclear transitions. Several such processes have been proposed as sources of monoenergetic solar axions [2, 3]. Here we focus on the search for solar axions and more general ALPs which may be emitted from de-excitation of ^{57}Fe (14.4 keV) and ^7Li (0.478 MeV) nuclei, and from $\text{D}(p, \gamma)^3\text{He}$ (5.5 MeV) reaction.

2 CAST experiment

The CERN Axion Solar Telescope (CAST) is the most recent implementation of the axion helioscope technique [4]. When its 9.26 m long LHC dipole prototype magnet is pointed towards the Sun, solar axions could coherently convert to photons of the same energy via the inverse Primakoff process, while traversing the 9 T magnetic field produced in the two parallel bores inside the magnet. To detect these photons, several low-background X-ray detectors are installed on both ends of the magnet. The CAST experiment is primarily designed to search for axions or ALPs that could be produced in the Sun by the Primakoff conversion of thermal photons and

it set the most restrictive experimental limits on the axion-photon coupling constant for masses $m_a < 0.4$ eV. Details about these results and experimental set-up can be found in [5, 6, 7].

3 Search for 14.4 keV solar axions

It is estimated that the most dominant component of monoenergetic solar axions is given by the 14.4 keV axions which may be emitted in the M1 nuclear transition between the first and the ground state of thermally excited ^{57}Fe nuclei [3]. This stable iron isotope can be a suitable emitter of solar axions due to its exceptional abundance among heavy elements in the Sun (2.8×10^{-5}) and the fact that its first excited nuclear state ($E^* = 14.4$ keV) is low enough to be relatively easily thermally excited in the hot interior of the Sun ($kT \sim 1.3$ keV). The excited ^{57}Fe nucleus relaxes to its ground state mainly through the emission of the 14.4 keV photon or an internal conversion electron. Since this de-excitation occurs dominantly via an M1 transition, an axion could also be emitted. Following the calculations in [8], the expected total flux of ^{57}Fe solar axions at the Earth is

$$\Phi_a^{14.4\text{ keV}} = 4.56 \times 10^{23} (g_{aN}^{\text{eff}})^2 \text{ cm}^{-2} \text{ s}^{-1},$$

where $g_{aN}^{\text{eff}} \equiv (-1.19g_0 + g_3)$ is the effective axion-nucleon coupling constant for this particular process, while g_0 and g_3 are the isoscalar and isovector axion-nucleon coupling constants and they are model dependent parameters.

Our search for ^{57}Fe solar axions was based on the data acquired during the Phase I of the CAST experiment with the conventional TPC detector mounted on one end of the magnet covering both bores. The axion signal, i.e., an excess of 14.4 keV X-rays when the magnet was pointing to the Sun was not found. Hence we set model-independent limits on the product of the axion-photon and axion-nucleon coupling constants as a function of the axion mass (shown in Fig. 1 on the left side). In the mass range $m_a \lesssim 0.03$ eV, where the axion-to-photon conversion process is coherent and has maximum probability, the limit is mass-independent and its value is $g_{a\gamma} g_{aN}^{\text{eff}} < 1.36 \times 10^{-16} \text{ GeV}^{-1}$ (95% CL). For higher axion masses, the coherence of the process is lost, which suppresses the conversion probability and, as a consequence, the sensitivity of the experiment to 14.4 keV axions diminishes rapidly with the increase of the axion mass above ~ 0.03 eV, thus providing weaker, mass-dependent limit. From the above limit we also set the constraint on $g_{a\gamma}$ as a function of g_{aN}^{eff} for axion masses $m_a \lesssim 0.03$ eV. This limit, labeled as ‘‘CAST-Fe’’, is shown on the right side in Fig. 1. It is constrained with the vertical boundary at $g_{aN}^{\text{eff}} = 3.6 \times 10^{-6}$, denoted as ‘‘Lum-Fe’’, due to the requirement based on the solar neutrino flux measurements that the axion emission from ^{57}Fe nuclei in the Sun should not exceed 10% of the solar photon luminosity. Due to the finite energy resolution of the TPC detector, our method to search for ^{57}Fe solar axions is significantly sensitive in the region of $g_{a\gamma} - g_{aN}^{\text{eff}}$ parameter space below the line denoted as ‘‘Det’’, where the ^{57}Fe solar axion flux exceeds the tail of the Primakoff solar axion flux in the energy range of the expected ^{57}Fe axion signal. In the region above the ‘‘Det’’ line (light grey), the Primakoff axion contribution dominates and thus suppresses the sensitivity to the ^{57}Fe axions. This resulted in the upper limit of $g_{a\gamma} < 3.5 \times 10^{-10} \text{ GeV}^{-1}$ (95% CL) which is displayed as a red horizontal line in Fig. 1 (right side).

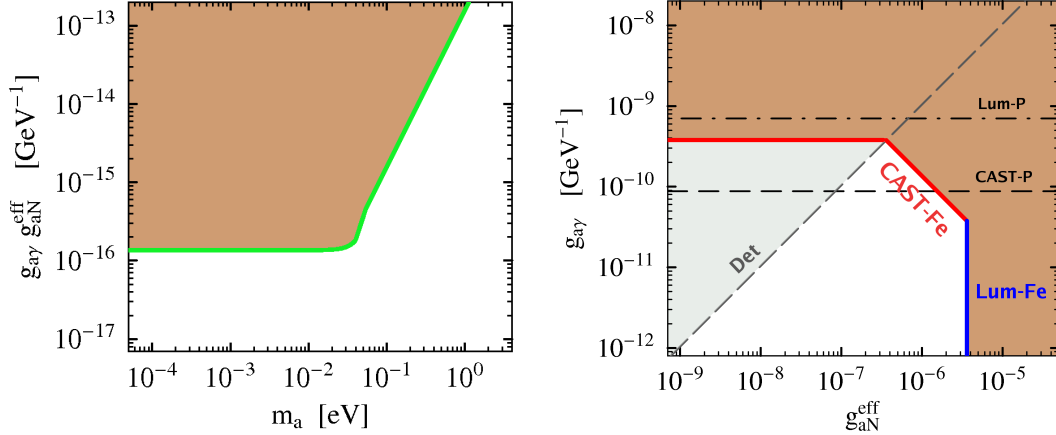


Figure 1: Left: The 95% CL upper limit on the product $g_{a\gamma} g_{aN}^{\text{eff}}$ as a function of the axion mass m_a , imposed by the CAST's search for ^{57}Fe solar axions. Right: The upper limit on $g_{a\gamma}$ versus g_{aN}^{eff} , based on the relations $g_{a\gamma} g_{aN}^{\text{eff}} < 1.36 \times 10^{-16} \text{ GeV}^{-1}$ and $g_{a\gamma} < 3.5 \times 10^{-10} \text{ GeV}^{-1}$ for $m_a \lesssim 0.03 \text{ eV}$, is shown as the red line CAST-Fe. The dark brown area is excluded. Lines denoted as Lum-Fe and Det are described in the text. Upper limits from the Primakoff solar axion luminosity (Lum-P) and CAST's search for the Primakoff solar axions (CAST-P) [6], that rely solely on $g_{a\gamma}$, are also displayed for comparisons.

4 Search for high-energy solar axions

In addition to the search for ^{57}Fe axions, CAST also performed a similar search for high-energy monoenergetic solar axions and ALPs. Two processes were considered: a) de-excitation of the first excited state of ^7Li nuclei produced in the Sun by the ^7Be electron capture, and b) radiative capture of proton on deuteron $\text{D}(p, \gamma)^3\text{He}$. The energies of axions that may be emitted instead of photons in both processes are 0.478 MeV and 5.5 MeV, respectively. Following the calculations in [9], the expected total fluxes of these solar axions at the Earth are

$$\Phi_a^{0.478 \text{ MeV}} = 5.23 \times 10^8 (g_0 + g_3)^2 \text{ cm}^{-2} \text{ s}^{-1} \quad \text{and} \quad \Phi_a^{5.5 \text{ MeV}} = 2.03 \times 10^{10} g_3^2 \text{ cm}^{-2} \text{ s}^{-1},$$

which is many orders of magnitude smaller than the ^{57}Fe solar axion flux. To detect photons produced by conversion of high-energy axions in the magnet bores, a special low-background γ -ray calorimeter based on CWO crystal was installed on one end of the magnet during the CAST Phase I. Since no evidence of an axion signal was observed for any of the two considered processes, an upper limit on the axion-photon coupling constant was set as a function of axion mass and axion-nucleon coupling constant. Figure 2 shows the exclusion plots of $g_{a\gamma}$ versus m_a obtained for two indicated values of the parameter $g_0 + g_3$ (for ^7Li axions) and g_3 (for proton-deuteron fusion axions). These values are chosen as representative of the range of couplings corresponding to the Peccei-Quinn symmetry breaking scale of $f_a = 10^6 - 10^8 \text{ GeV}$. The presented contours serve as an example to show how the excluded region in the $g_{a\gamma} - m_a$ parameter space can be scaled for various choices of g_0 and g_3 . In this manner, our results can also be generally applied to impose the constraints on light pseudoscalars that couple to a nucleon and to two photons.

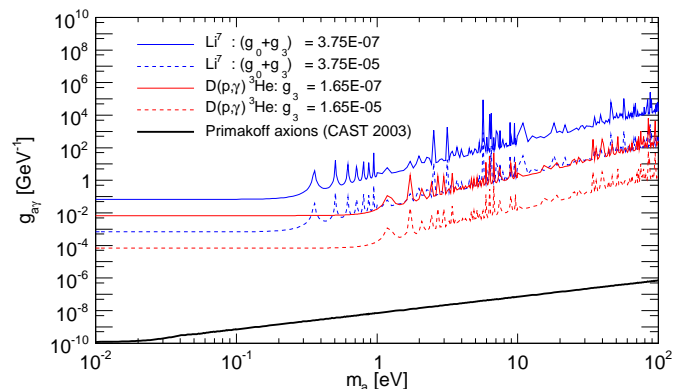


Figure 2: Exclusion plot (95% CL) in the axion-photon coupling versus axion mass plane imposed by the CAST’s search for 0.478 MeV axions from ${}^7\text{Li}$ de-excitation (blue lines) and 5.5 MeV axions from proton-deuteron fusion (red lines). The limit obtained from each of the processes is presented for two indicated values of the axion-nucleon coupling constants g_0 and g_3 . The upper limit from the CAST’s search for the Primakoff solar axions (black line) is also shown for the comparison.

5 Conclusions

As extension to its main research program, i.e., the search for the Primakoff solar axions and ALPs, CAST also performed the first search for monoenergetic axions using a helioscope approach. Three nuclear processes were considered as sources of monoenergetic solar axions: de-excitation of ${}^{57}\text{Fe}$ (14.4 keV) and ${}^7\text{Li}$ (0.478 MeV) nuclei, and proton-deuteron fusion (5.5 MeV). The search was sensitive to axion interactions both with a nucleon (in the emission processes) and photons (in the detection process). This allowed us to explore the relation between axion-nucleon and axion-photon coupling constants for a wide range of axion masses and set the model-independent limits that can generally apply not only to axions but also to similar exotic pseudoscalar particles that couple to two photons and can be emitted in the nuclear magnetic transitions.

References

- [1] R.D. Peccei and H.R. Quinn, Phys. Rev. Lett. **38** 1440 (1977) and Phys. Rev. **D16** 1791 (1977).
- [2] G. Raffelt and L. Stodolsky, Phys. Lett. **119B** 323 (1982).
- [3] W.C. Haxton and K.Y. Lee, Phys. Rev. Lett. **66** 2557 (1991).
- [4] P. Sikivie, Phys. Rev. Lett. **51** 1415 (1983) and Phys. Rev. Lett. **52** 695 (1984).
- [5] K. Zioutas *et al.* (CAST Collaboration), Phys. Rev. Lett. **94** 121301 (2005).
- [6] S. Andriamonje *et al.* (CAST Collaboration), JCAP **04** 010 (2007).
- [7] E. Arik *et al.* (CAST Collaboration), JCAP **02** 008 (2009).
- [8] S. Andriamonje *et al.* (CAST Collaboration), JCAP **12** 002 (2009).
- [9] S. Andriamonje *et al.* (CAST Collaboration), JCAP **03** 032 (2010).

Prospects of Search for Solar Axions with Mass over 1 eV and Hidden Sector Photons

R. Ohta^{1,6}, M. Minowa^{1,5}, Y. Inoue^{2,5}, Y. Akimoto³, T. Mizumoto¹, A. Yamamoto^{4,5}

¹Department of Physics, School of Science, the University of Tokyo

²International Center for Elementary Particle Physics, the University of Tokyo

³Graduate School of Medicine and Faculty of Medicine, the University of Tokyo

⁴High Energy Accelerator Research Organization (KEK), 1-1 Oho, Tsukuba, Ibaraki 305-0801, Japan

⁵Research Center for the Early Universe (RESCEU), School of Science, the University of Tokyo

⁶Research Fellow of the Japan Society for the Promotion of Science

^{1,2,3,4} 7-3-1 Hongo, Bunkyo-ku, Tokyo 113-0033, Japan

DOI: http://dx.doi.org/10.3204/DESY-PROC-2009-05/ryosuke_ohta

We present prospects of two experiments using the Tokyo Axion Helioscope. One is a search for solar axions. In the past measurements, axion masses from 0 to 0.27 eV and from 0.84 to 1.00 eV have been scanned and no positive evidence was seen. We are now actively preparing a new phase of the experiment aiming at axion masses above 1 eV. The other is a search for hidden sector photons from the Sun. We have been designing and testing some additional equipments, which have to be installed on the helioscope to search for hidden photons with mass of over 10^{-3} eV.

1 Introduction

The Sun could copiously emit weakly interacting particles, that could eventually be detected inside a sensitive detector at the Earth.

The axion is one of such particles. The existence of axions is implied by solutions to the strong CP problem [1]. Axions are expected to be produced in the solar core through their coupling to photons. This process is called Primakoff process. The outgoing axion has average energy of about 4 keV [2]. Sikivie proposed an ingenious experiment to detect such axions [3]. A detection schematic for solar axions is shown in Fig. 1. The detection device called axion helioscope is a system of a strong magnet and an X-ray detector, where the solar axions are transformed into X-ray photons through the inverse Primakoff process in the magnetic field. Conversion is coherently enhanced even for massive axions by filling the conversion region with light gas. If the axion mass m_a is at around a few eV, detection

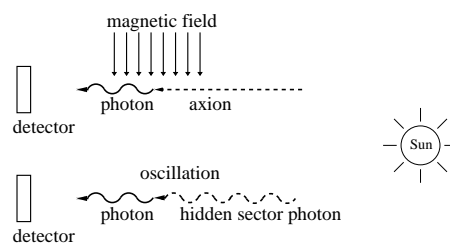


Figure 1: Detection schematics of solar axions and hidden photons from the Sun.

of the solar axion becomes feasible.

Hidden sector photons are another kind of weakly interacting particles. The existence of hidden photons is predicted by several extensions of Standard Model. If light hidden photons exist, they could be produced through kinetic mixing with solar photons [4, 5]. Therefore it is natural to consider the Sun as a source of low energy hidden photons. A schematic for the detection of hidden photons from the Sun is also shown in Fig. 1. Unlike the case of the axion, no magnetic field is required to transform photons into hidden photons.

In this paper we report the current status of two experiments. One is the search for solar axions and the other is the search for hidden photons from the Sun.

2 Tokyo Axion Helioscope

The schematic figure of the axion helioscope is illustrated in Fig. 2. It consists of a superconducting magnet, X-ray detectors, a gas container, and an altazimuth mounting. The magnet [6] consists of two 2.3-m long race-track shaped superconducting coils running parallel with a 20-mm wide gap between them. The transverse magnetic field in the gap is 4 T. The magnetic field can be maintained without an external power supply with a help of a persistent current switch. The magnet temperature is kept lower than 6 K by two Gifford-McMahon refrigerators. The container to hold dispersion-matching gas is inserted in the aperture of the magnet. It is made of four 2.3-m long stainless-steel square pipes and 5N high purity aluminium sheets wrapping around them to achieve high uniformity of temperature. The measured thermal conductance between both ends was 1×10^{-2} W/K at 6 K under 4 T. The one end of the gas container is suspended by three Kevlar cords. The other end at the opposite side is flanged to the magnet. This end is terminated with an X-ray window which is transparent above 2 keV and can hold gas up to 0.3 MPa. The gas introducing pipelines are also at this side and have an automated gas controlling system which enables us to scan wide range of axion mass. The generated X-rays are viewed by sixteen PIN photodiodes. Details on the X-ray detector are given in Ref. [7, 8]. Except for the gas controlling system, they are constructed in a vacuum vessel which is mounted on an altazimuth mount to track the Sun. It can track the Sun about a half of a day. During the other half of a day, background spectrum is measured.

Phase 1 of the solar observation was performed in December 1997 without the gas container [9]. Phase 2 was performed from July to September 2000 with the gas container and low density helium gas [10]. Phase 3 was performed from December 2007 to April 2008 with higher density helium gas than that of Phase 2 [11]. Since those measurements result in no positive signals of axion, upper limits on the axion-photon coupling constant $g_{a\gamma\gamma}$ were set to be $g_{a\gamma\gamma} < 6.0 - 10.4 \times 10^{-10} \text{ GeV}^{-1}$ for $m_a < 0.27 \text{ eV}$ and $g_{a\gamma\gamma} < 5.6 - 13.4 \times 10^{-10} \text{ GeV}^{-1}$ for $0.84 < m_a < 1.00 \text{ eV}$. We are now preparing the search for solar axions with mass above 1 eV introducing higher density helium gas than that of last phase. Figure 3 shows the expected upper limit of next measurement. Our previous limits and the some other bounds are also plotted in the same figure. The SOLAX [12], COSME [13], DAMA [14] and CDMS [15] are solar axions experiments which exploit the coherent conversion on the crystalline plains in germanium and a NaI detector. The experiment by Lazarus et al. [16] and CAST [17, 18, 19] are the same kind of experiments as ours. The limits $g_{a\gamma\gamma} < 7 \times 10^{-10} \text{ GeV}^{-1}$ is the solar limit inferred from the solar neutrino flux consideration [20]. Preferred axion models [21, 22, 23] are also shown by the shaded area in the Fig. 3.

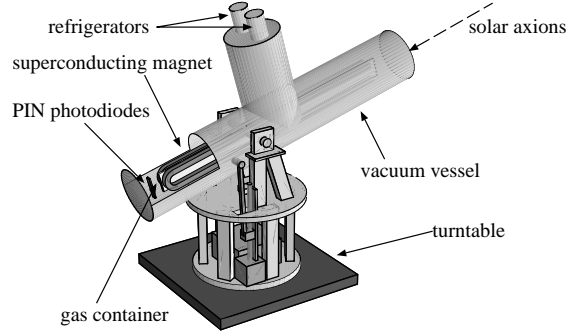


Figure 2: The schematic view of the axion helioscope.

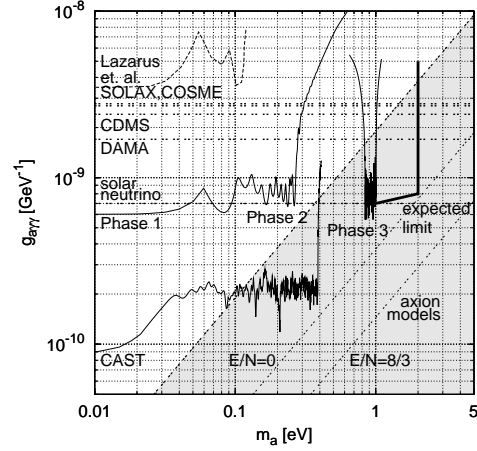


Figure 3: Exclusion limit on $g_{a\gamma\gamma}$ versus m_a at 95% confidence level.

3 Search for hidden photon

To search for hidden photons from the Sun, we plan to add an additional apparatus on the cylinder of the helioscope. A schematic design of the apparatus is illustrated in Fig. 4. It mainly consists of a vacuum vessel as a conversion region, a parabolic mirror, and a photomultiplier (PMT). In one side of the vessel, the parabolic mirror is attached to collect photons produced from the hidden photon - photon oscillation and the focal point of the mirror is set at the other side of the vessel. The mirror has a diameter of 50 cm, and a focal length of 1 m. On the focal point, the PMT is attached to detect collected photons. In addition, we plan to cool the PMT to reduce the dark count rate. As a preliminary experiment, we have cooled R329-02, a product of Hamamatsu photonics, and measured its dark count rate. The measured rate at -30 °C was about 10 Hz. This rate is several times lower than the dark count rate at room temperature. For the actual experiment, we plan to use a more suitable one than R329-02.

If we suppose the dark count rate is 10 Hz, pressure in the vessel is much less than 10 Pa, the length of conversion region is 1 m, the diameter of the mirror is 0.5 m, reflectivity of

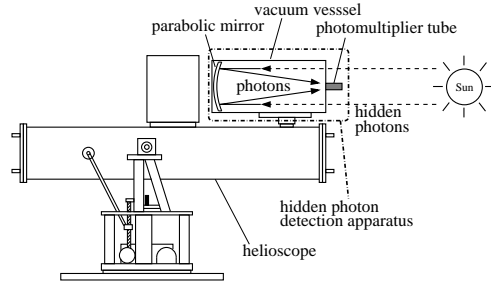


Figure 4: The schematic view of the apparatus to search for hidden photon from the Sun.

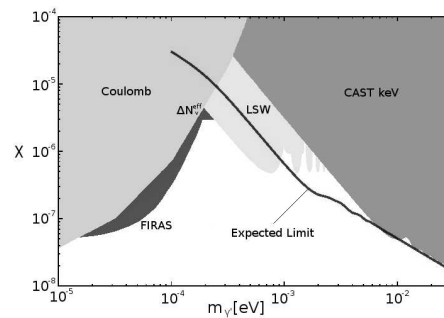


Figure 5: Exclusion limit on mixing strength between photon and hidden photon χ versus hidden photon mass $m_{\gamma'}$. The solid line shows our expected limit.

the mirror is 90 %, and measuring time is 10^6 s, we expect an exclusion region above the solid line shown in Fig. 5. The limits from other experiments and observations: Coulomb’s law tests [24, 25], “light shining through walls” experiments [26, 27], CAST [4] and exclusion from CMB observation [28, 29] are also shown in Fig. 5.

Acknowledgments

The authors thank the former director general of KEK, Professor H. Sugawara, for his support in the beginning of the helioscope experiment. This research was partially supported by the Japanese Ministry of Education, Science, Sports and Culture, Grant-in-Aid for COE Research and Grant-in-Aid for Scientific Research (B), and also by the Matsuo Foundation.

References

- [1] R. D. Peccei and Helen R. Quinn. *Phys. Rev. Lett.*, 38:1440–1443, 1977.
- [2] Georg G. Raffelt. arXiv:hep-ph/0504152. 2005.
- [3] P. Sikivie. *Phys. Rev. Lett.*, 51:1415, 1983.
- [4] Javier Redondo. *JCAP*, 0807:008, 2008.
- [5] Sergei N. Gninenko and Javier Redondo. *Phys. Lett.*, B664:180–184, 2008.
- [6] Y Sato et al. *Proc. of the 15th International Conference on Magnet Technology (MT-15) ed Liangzhen L, Guoliao S and Luguang Y (Beijing: Science Press)*, pages 262–265, 1998.
- [7] T. Namba, Y. Inoue, S. Moriyama, and M. Minowa. *Nucl. Instrum. Meth.*, A489:224–229, 2002.
- [8] Y. Akimoto, Y. Inoue, and M. Minowa. *Nucl. Instrum. Meth.*, A557:684–687, 2006.
- [9] Shigetaka Moriyama et al. *Phys. Lett.*, B434:147, 1998.
- [10] Yoshizumi Inoue et al. *Phys. Lett.*, B536:18–23, 2002.
- [11] Y. Inoue et al. *Phys. Lett.*, B668:93–97, 2008.
- [12] A. O. Gattone et al. *Nucl. Phys. Proc. Suppl.*, 70:59–63, 1999.
- [13] R. Bernabei et al. *Phys. Lett.*, B515:6–12, 2001.
- [14] A. Morales et al. *Astropart. Phys.*, 16:325–332, 2002.
- [15] Z. Ahmed et al. *Phys. Rev. Lett.*, 103:141802, 2009.
- [16] D. M. Lazarus et al. *Phys. Rev. Lett.*, 69:2333–2336, 1992.
- [17] K. Zioutas et al. *Phys. Rev. Lett.*, 94:121301, 2005.
- [18] S. Andriamonje et al. *JCAP*, 0704:010, 2007.
- [19] E. Arik et al. *JCAP*, 0902:008, 2009.
- [20] Paolo Gondolo and Georg Raffelt. *Phys. Rev.*, D79:107301, 2009.
- [21] David B. Kaplan. *Nucl. Phys.*, B260:215, 1985.
- [22] Mark Srednicki. *Nucl. Phys.*, B260:689, 1985.
- [23] S. L. Cheng, C. Q. Geng, and W. T. Ni. *Phys. Rev.*, D52:3132–3135, 1995.
- [24] E. R. Williams, J. E. Faller, and H. A. Hill. *Phys. Rev. Lett.*, 26:721–724, 1971.
- [25] D. F. Bartlett and S. Loegl. *Phys. Rev. Lett.*, 61:2285–2287, 1988.
- [26] M. Ahlers, H. Gies, J. Jaeckel, J. Redondo, and A. Ringwald. *Phys. Rev.*, D77:095001, 2008.
- [27] A. Afanasev et al. *Phys. Lett.*, B679:317–320, 2009.
- [28] Joerg Jaeckel, Javier Redondo, and Andreas Ringwald. *Phys. Rev. Lett.*, 101:131801, 2008.
- [29] Javier Redondo. arXiv:hep-ph/0805.3112. 2008.

GammeV: results and future plans at Fermilab

William Wester*

Fermilab, MS222, Batavia IL, USA

presented on behalf of the GammeV Collaboration

DOI: http://dx.doi.org/10.3204/DESY-PROC-2009-05/wester_william

GammeV is an axion-like particle photon regeneration experiment that employs the light shining through a wall technique. We obtain limits on the coupling of a photon to an axion-like particle that extend previous limits for both scalar and pseudoscalar particles in the milli-eV mass range. We have reconfigured our apparatus to search for chameleon particles. We describe the current results and future plans for similar activities at Fermilab.

1 Introduction

Weakly interacting sub-eV particles (WISPs) may exist as physics beyond the Standard Model and help explain fundamental questions such as what is the nature of dark matter or even shed insight into the underlying nature of dark energy. WISPs are a general class of new particles that include axions, axion-like particles, hidden sector photons, milli-charged particles, chameleons etc. In 2006, the PVLAS experiment reported [1] and then no longer observed [2] anomalous polarization effects of light traversing a magnetic field that could be interpreted as being mediated by an axion-like particle in the milli-eV mass range with a unexpectedly strong coupling to photons. New efforts world-wide [3] have started to investigate the possible existence of WISPs as much of the possible parameter space has been unexplored and experiments searching for these possible new particles can be mounted at modest cost.

2 Axion-like particle search

For axion-like particles, a previous laser experiment conducted in the early 1990's by a collaboration Brookhaven, Fermilab, Rochester, and Trieste (BFRT) used a "light shining through a wall" (LSW) [4] technique to set limits on sub-eV axion-like particles [5]. However, their utilization of existing 4.4m long magnets happened to result in a minimum with no sensitivity for an axion-like particle in the mass range suggested by the anomalous PVLAS result (the sine terms in Eq. 1 went to zero). The GammeV experiment [6] at Fermilab was designed to cover this missing region of insensitivity to directly test the axion-like particle interpretation of the anomalous result.

The GammeV apparatus is shown schematically in Fig. 1(a) and is used in a LSW configuration where, in the presence of an external magnetic field, a laser photon might oscillate into an axion-like particle that can traverse a "wall" and then have a small probability to regenerate

*This work is supported by the U.S. Department of Energy under Contract No. DE-AC02-07CH11359

back into a detectable photon. The formula for the probability of this regeneration process is given by the following:

$$P_{regen} = \frac{16B_1^2 B_2^2 \omega^4}{M^4 m_\phi^8} \sin^2\left(\frac{m_\phi^2 L_1}{4\omega}\right) \cdot \sin^2\left(\frac{m_\phi^2 L_2}{4\omega}\right) \quad (1)$$

where ω is the photon energy, M is a high mass scale inverse to the coupling to photons $g_{a\gamma\gamma}$, m_ϕ is the mass of the axion-like particle, and B_1 , L_1 , B_2 and L_2 are the magnetic field strengths and lengths in the photon conversion and regeneration regions, respectively.

The GammeV experiment utilizes two novel aspects in order to have increased sensitivity over the region of interest. The plunger is constructed so that it can place the “wall” either in the middle ($L_1 = L_2$) of the magnet or toward one end of the magnet ($L_1 \neq L_2$). Thus, the regions of insensitivity will be shifted in the two configurations. The second aspect is to utilize time correlated single photon counting techniques in order to have high efficiency for signal and very low noise. In this technique, the time of each 10 ns wide laser pulse (pulsed at 20 Hz) is recorded and correlated to the time of PMT pulses (also about 10 ns wide) which include dark pulses at approximately 100 Hz. The chance of a random PMT pulse being in time with a laser pulse is very small compared with the expected rate of in-time signal events if the PVLAS anomalous signal was due to an axion-like particle with large coupling to photons.

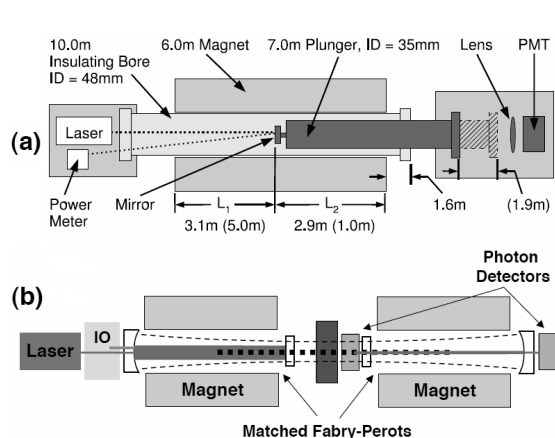


Figure 1: (a) Schematic diagram of the GammeV experimental apparatus showing a Nd:YAG laser frequency doubled to send 532 nm pulses down the warm bore of a Tevatron dipole magnet. The “wall” is mounted on a sliding vacuum tube, the plunger. (b) Schematic diagram of an enhanced LSW experiment using resonant regeneration with matched optical cavities.

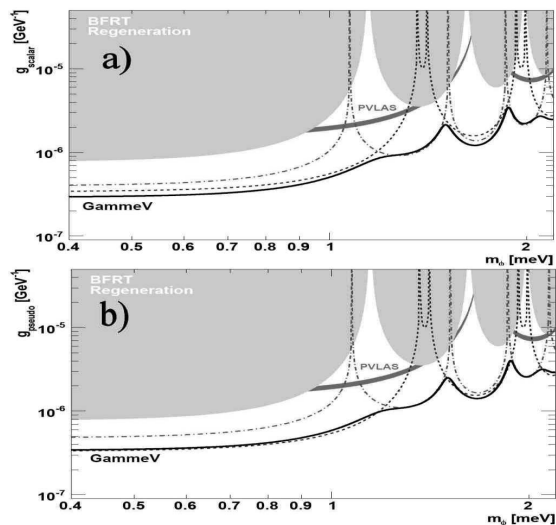


Figure 2: Published 3σ exclusion region of mass versus photon coupling obtained by GammeV for (a) scalar and (b) pseudoscalar axion-like particles. The PVLAS anomalous region of interest is shown along with the separate limits (dashed) for the wall in the center and the wall near one end.

No signal above background is observed. Figures 2(a),(b) show the resulting 3σ limits for the coupling of scalar and pseudoscalar axion-like particles to photons in milli-eV region.

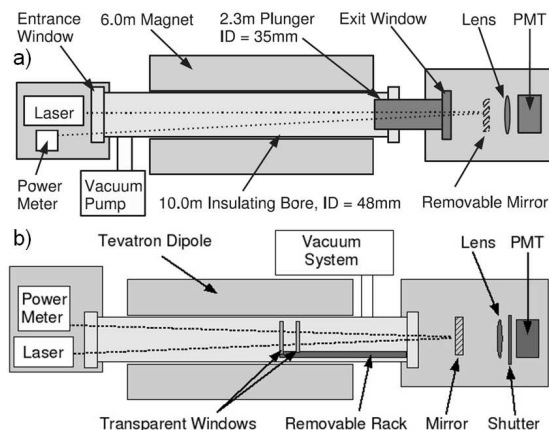


Figure 3: Schematic of the particle in a jar configuration for (a) GammeV and (b) the on-going GammeV-CHASE experiments.

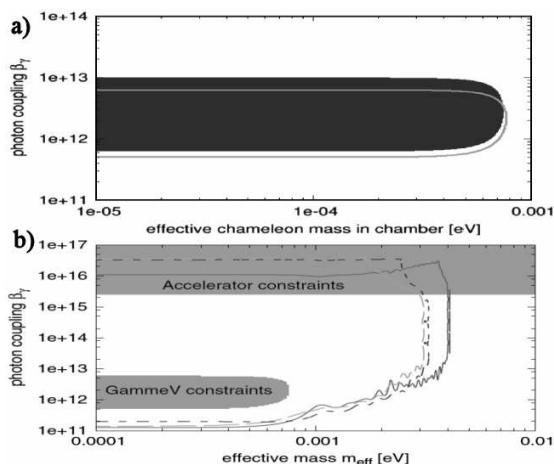


Figure 4: Exclusion region of the coupling normalized to the Planck mass to photons versus the effective chameleon mass (a) as published for the GammeV along with (b) prospects for GammeV-CHASE.

Figure 1(b) shows an enhanced LSW experiment that employs phased locked optical cavities on both the generation and regeneration side of the wall [8]. The ‘**G**ammeV **r**econstituted and **i**nstrumented with **m**agnets for **r**esonantly **e**nhanced **p**hoton **r**egeneration” (GRIM REPR [9]) project is in an R&D phase to develop the phase locking scheme between the cavities and to explore the achievable finesse, \mathcal{F} , of the long baseline cavities. The sensitivity to the $g_{a\gamma\gamma}$ coupling constant in this configuration scales as the product of the two \mathcal{F} ’s and linearly with the magnetic field length. With at least 12 Tevatron magnets in length and $\mathcal{F} \sim 10^5$, a sensitivity of $g_{a\gamma\gamma} < \sim 10^{-11}$ would be achievable. R&D is expected to continue for the next couple of years while Fermilab also explores a laser interferometer experiment that might be sensitive to “holographic noise” [10] - a possible jitter in space-time due to Planck scale effects.

3 Chameleon search

Chameleons are WISPs that usually take the form of a scalar particle coupled to the stress energy tensor in a potential such that their properties depend on the matter density of their environment. The GammeV apparatus was rearranged as shown in Fig. 3(a). In this configuration, a laser is shown through the chamber such that photons might oscillate into chameleons which reflect off of the exit vacuum windows or vacuum walls essentially building up a gas of such particles within the vacuum region. The laser is turned off and the PMT is turned on to look for an exponential signal above background as chameleons reconvert back into photons resulting in a detectable afterglow.

GammeV searched for chameleons using the apparatus shown in Fig. 3(a) where separately 5-hr runs of horizontal and vertical polarized laser light were shown through the magnetic field. After possibly building a population of chameleons, a 1-hr data taken period followed after

turning off the laser and turning on the PMT. No afterglow was observed and an exclusion region in the chameleon coupling to photons vs effective chameleon mass was obtained under the assumption that the chameleon potential had a characteristic mass dependence on matter density $m_{eff} \propto \rho^\alpha$ with $\alpha > 0.8$. The limitations on stronger coupling to photons were set by the fact that such strong couplings would have resulted in the regenerated photons appearing and decaying away before the PMT could be turned on. Weak couplings were limited by the noise of the PMT. Large effective masses were constrained by the long magnetic field length. The region of validity for $\alpha > 0.8$ was conservatively set due to the estimate of the vacuum level near the mechanical roughing pump.

A new effort, **GammeV - CHASE** (chameleon afterglow search), is on-going and should result in data recorded in 2010. In this re-incarnation, shown in Fig. 3(b), the limitations of the original chameleon search will all be addressed. Data taking at reduced magnetic field will allow a probe for very strong chameleon couplings to photons. A lower noise PMT will help improve the sensitivity for weak couplings. A “dish rack” that holds optical windows such that the 6 m magnetic field region is divided into regions of approximately 4.7 m, 1.0 m, and 0.3 m, will probe higher effective masses. Finally, removing the mechanical pump and utilizing very low vacuum enabled by cryopumping will allow for sensitivity of an extended range of α such that potentials consistent with various chameleon dark energy models can be probed [11].

4 Conclusions

A new research program at Fermilab has obtained published results for axion-like particle and chameleon searches. Next generation experiments have started or are undergoing R&D. The possibility that WISPs or other phenomenon might be observable using relatively inexpensive experimental optical set-ups allows for searches of physics beyond the Standard Model. Who knows, such crazy experiments might just reveal a new weirdness of nature.

References

- [1] E. Zavattini *et al.* [PVLAS Collaboration], Phys. Rev. Lett. **96**, 110406 (2006) [arXiv:hep-ex/0507107].
- [2] E. Zavattini *et al.* [PVLAS Collaboration], arXiv:0706.3419 [hep-ex].
- [3] See contributions to these proceedings from the ALPS, BMV, LIPSS, and OSQAR experiments.
- [4] K. Van Bibber, N. R. Dagdeviren, S. E. Koonin, A. K. Kerman and H. N. Nelson, Phys. Rev. Lett. **59**, 759 (1987).
- [5] R. Cameron *et al.*, Phys. Rev. D **47**, 3707 (1993).
- [6] A.S. Chou *et al.* [GammeV Collaboration], Phys. Rev. Lett. **100**, 080402 (2008). Additional description may be found at: <http://gammev.fnal.gov>.
- [7] P. Sikivie, Phys. Rev. Lett. **51**, 1415 (1983) [Erratum-ibid. **52**, 695 (1984)]. P. Sikivie, Phys. Rev. D **32**, 2988 (1985) [Erratum-ibid. D **36**, 974 (1987)].
- [8] G. Mueller, P. Sikivie, D. B. Tanner and K. van Bibber, Phys. Rev. D **80**, 072004 (2009) [arXiv:0907.5387 [hep-ph]].
- [9] Apologies but one of our collaborators (KVB) came up with this.
- [10] C. J. Hogan, arXiv:0905.4803 [gr-qc]. See also: www.fnal.gov/directorate/program_planning/Nov2009PACPublic/holon_proposal-2009.pdf.
- [11] A. Upadhye, J. H. Steffen and A. Weltman, Phys. Rev. D **81**, 015013 (2010) [arXiv:0911.3906 [hep-ph]].

The LIPSS search for light neutral bosons

Andrei Afanasev¹, Oliver K. Baker², Kevin Beard³, George Biallas⁴, James Boyce⁴, Minarni Minarni⁵, Roopchan Ramdon¹, Michelle Shinn⁴, and Penny Slocum²

¹Department of Physics, Hampton University, Hampton, VA 23668

²Department of Physics, Yale University, P.O. Box 208120, New Haven, CT 06520

³Muons, Inc., 552 N. Batavia Avenue, Batavia, IL 60510

⁴FEL Division, Jefferson Laboratory, 12000 Jefferson Avenue, Newport News, VA 23606

⁵Department of Physics, Universitas Riau (UNRI), Pekanbaru, Riau 28293 Indonesia

DOI: <http://dx.doi.org/10.3204/DESY-PROC-2009-05/keith.baker>

An overview is presented of the LIPSS experimental search for very light neutral bosons using laser light from Jefferson Lab's Free Electron Laser. This facility provides very high power beams of photons over a large optical range, particularly at infrared wavelengths. Data has been collected in several experimental runs during the course of the past three years, most recently in the Fall of 2009.

1 Introduction

There continues to be broad interest in experimental searches for sub-electron volt mass, spin-zero, weakly interacting particles. Searches for non-Standard Model couplings between photons and hypothetical light neutral bosons (LNBS) have been reported by the BMV collaboration [1], the GammeV collaboration at Fermi National Accelerator Laboratory (FNAL) [2] and the OSQAR collaboration at the European Center for Nuclear Research (CERN) [3] and was carried out originally by the BFRT collaboration [4]. These were mainly motivated by the reports in [5] and [6]. The experimental programs that explore the parameter space of weakly interacting, light, spin-zero, bosons by and large all use the light shining through a wall (LSW) technique of photon regeneration [7]; laser photons are sent through a strong magnetic field where some of them can convert into low-mass, weakly interacting bosons. These bosons then pass through a wall that serves to block the incident laser light, and reconvert into photons in a second magnetic field in a similar manner.

The Light Pseudoscalar and Scalar Particle Search (LIPSS) collaboration continues its search for evidence of photons coupling to LNBS in measurements at Jefferson Lab's (JLab's) Free Electron Laser (FEL) facility [8]. Improvements, mostly to FEL optics in order to increase the FEL beam power at 935 nm wavelength, have been made. Additionally, improvements in beam diagnostics such as beam pointing stability and focusing have been achieved during the past year.

2 Experimental setup and data analysis

One of the reasons for using the FEL at JLab is its ability to deliver a high power laser beam in the infrared region. The JLab FEL is capable of delivering more than 14 kW of power at 1.6 micron wavelength. The LIPSS experiment is housed in Laser Lab 1 of the FEL facility. The simplified LIPSS experimental setup is shown in Figure 1. FEL light is sent through an optical transport system to Turning Mirror 1 (TM1) in Lab 1. The beam then passes through a set of adjustable telescopes that collimate its width to approximately six to eight mm in diameter. The beam exits the FEL transport system with essentially 100 per cent linear polarization that can be adjusted for orientation either perpendicular or parallel to the upstream magnetic field region for, respectively, scalar or pseudoscalar boson searches. A polarization rotator is used to achieve this. After TM2, the beam passes the generation magnet volume (GV) where FEL laser photons may couple to a virtual photon from the magnetic field creating a very light neutral boson. The FEL beam then is sent to a beam dump that also functions as a power meter. Any LNBS created will then transverse this optical barrier and enter a second magnetic field region, a regeneration magnet volume (RV) where some may reconvert to real photons. The reconverted photons, having identical properties as the original FEL laser photons, then will be detected by a CCD camera in a light tight box (LTB). Inside the LTB, the beam of photons proceed to TM4, then pass through a Newport- KPX082AR16 50.2 mm lens that serves to focus the beam to one pixel on the CCD array. The CCD camera system is a Princeton Instrument Spec-10: 400BR. This CCD camera system is placed on a translation stage (Newport translation stage model 461-X-M) for easy movement during data taking. The setup also includes a light emitting diode (LED) and a convex lens, used to provide a beam spot on the CCD; this provides a reference on the CCD array. The turning mirrors are RMI mirrors with coatings that are optimized for 935 nm wavelength light. All the mirrors that are in contact with the FEL light are water cooled to minimize power absorption and damage on the mirrors. Irises are used along the beam path for beam alignment. The LTB is a ZARGES aluminum case painted inside with DAP paint. Outside of the LTB, there is a paper box layered with aluminum foil. Inside the LTB, there is also a light tunnel from the AR coated window to the CCD. This tunnel is made from black hutch board to eliminate stray light inside the box. The edge of the LTB is sealed by a rubber liner. Together, this provides a LTB environment that is essentially free of any stray light in Lab 1.

The LIPSS experiment uses IR light because of the report in [5] and because of the special features of the Spec 10:400BR CCD camera, the focusing lens, and AR coated windows. The CCD camera's quantum efficiency (QE) peaks in the visible region of the electromagnetic spectrum, but has a sizeable QE in the near IR region. After optimization, the 900 nm coated high reflector (HR) and output coupler (OR) mirrors resulted in a FEL laser beam centered at 935 nm. The alignment of the FEL beam through the generation magnet is critical for LNB production and detection, in the case that it can take place. Therefore two CCTV cameras monitored TM2 and TM3. The output of the cameras are fed to analog inputs of Spiricon (TM) hardware and software where the beam centroid and spot size can be monitored and recorded. The reference centroid position was determined using FEL alignment mode beam prior to the delivery of high power continuous-wave FEL beam into lab 1 (due to laser safety procedures). During the measurement, the beam positions are automatically adjusted. Prior to the FEL beam delivery, a green laser beam is used to align the turning mirrors, curved mirrors and other optics. This green laser beam is aligned with the FEL alignment mode beam and considered aligned with FEL high power beam. The coincidence of the green laser beam and

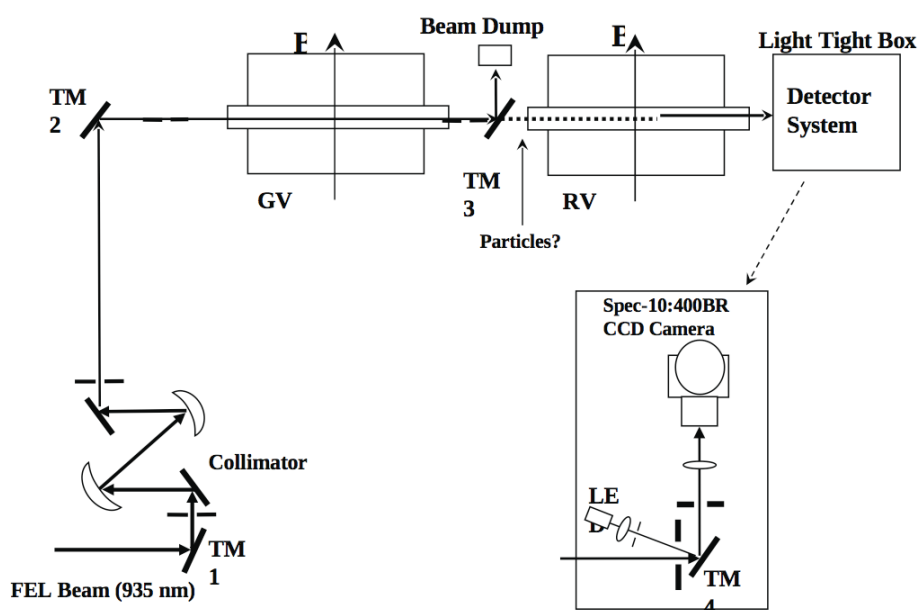


Figure 1: The LIPSS experimental setup.

the alignment mode beam is visually verified along the beam path starting at TM1. The fine adjustment is performed by monitoring the beam image on the CCD while adjusting the translation stage. The position of the one pixel green beam on the CCD is recorded as the center of the region of interest (ROI) in the CCD array. The beam from the LED is collimated first by a plano-convex lens. For easy alignment, the LED and the collimating lens is setup on one stage. A comparison was made between the focused green laser beam (532 nm) and a focused 935 nm light beam from a light source consisting of a Newport Tungsten Halogen Lamp and Oriel Mini Monochromator with spectral range from 500nm to 1.2mm. The light source was set between the two magnets and the light was sent through the vacuum pipe of the regeneration magnet and through the focusing lens without disturbing the beam alignment in the light tight box. There is only a one pixel difference between the center of the expanding 935 nm beam and the x and y positions of the focused pixel from the green laser.

The green laser beam (as well as the alignment mode FEL beam) is also used for testing the pointing stability of a laser beam. The change of the FEL beam position and shape on TM2 and TM3 can be monitored and recorded using spiricon (TM) software as explained above and the beam position is adjusted manually using picomotor controls. In order to ascertain the effect of this change on the ROI around the assigned one-pixel-area, a pointing stability test was performed. The simple test is implemented by moving TM2 horizontally. TM2 in 1 is mounted on a Parker-Daedal translation stage with a 2 inch travel precision micrometer. The green laser beam is focused to one pixel by the focusing lens in front of the CCD. The TM2 positions is varied while recording the counts in a 3x3 pixel area centered at the focused pixel. It was determined that 0.175 inch or 4.45 mm movement was needed in order for there to be a measureable effect comparing neighboring pixels with the in ROI (3 x 3 pixel area). This

experimental procedure was implemented for each run that provided results presented in [8].

To summarize, the LIPSS apparatus is performing well. FEL upgrades and installation of a variety of monitors for various parameters have improved the quality of the data. The FEL beam power was increased dramatically in 2009 compared with previous runs. The controls for beam stability on TM2 and TM3 were also improved. New experimental data have been taken as recently as Fall, 2009 and will be presented in a separate paper.

3 Acknowledgments

The authors thank the technical staff of the JLab FEL Division, especially F. Dylla, G. Neil, G. Williams, R. Walker, D. Douglas, S. Benson, K. Jordan, C. Hernandez-Garcia, and J. Gubeli, as well as M.C. Long of Hampton University for their excellent support of the experimental program. Several students and teachers, especially T. Robinson, contributed to this work during the summer months. Funding from the Office of Naval Research Award N00014-06-1-1168 is gratefully acknowledged.

References

- [1] C. Robilliard *et. al.*, Phys. Rev. Lett. **99**, 190403 (2007).
- [2] A.S. Chou *et. al.*, Phys. Rev. Lett. **100**, 080402 (2008); GammeV collaboration <http://gammev.fnal.gov>.
- [3] R. Ballou *et. al.*, CERN Report CERN-SPSC-2007-039 (2007); SPSC-M-762 (2007).
- [4] R. Cameron *et. al.*, Phys. Rev. D**47**, 3707 (1993).
- [5] E. Zavattini *et. al.*, Phys. Rev. Lett. **96**, 110406 (2006).
- [6] E. Zavattini *et. al.*, Phys. Rev. D**77**, 032006 (2008); http://axion-wimp.desy.de/index_eng.html (2007).
- [7] K.V. Bibber *et. al.*, Phys. Rev. Lett. **59**, 759 (1987).
- [8] LIPSS collaboration, Phys. Rev. Lett. **101**, 120401 (2008); Phys. Lett. **B679**, 317 (2009).

Status of the ALPS Experiment

Axel Lindner¹, for the ALPS Collaboration

¹DESY, Notkestraße 85, 22607 Hamburg, Germany

DOI: http://dx.doi.org/10.3204/DESY-PROC-2009-05/lindner_axel

The ALPS Collaboration runs a Light Shining through a Wall (LSW) experiment to search for photon oscillations into Weakly Interacting Sub-eV Particles (WISPs) often predicted by extensions of the Standard Model. The experiment is set up around a superconducting HERA dipole magnet at the site of DESY.

1 Status of ALPS

At the workshop in Durham an intermediate status of the experiment was presented (see [1]). In early autumn 2009 the set-up was completed and the final data run was concluded in December 2009. ALPS has placed limits on the probability of photon-WISP-photon conversions of a few $\times 10^{-25}$. These limits result in today's most stringent laboratory constraints on the existence of low mass axion-like particles, hidden photons and minicharged particles.

As the results are already published, the reader is referred to the publication[2] for further information.

References

- [1] A. Lindner [ALPS collaboration], *talk presented at the 5th Patras-Axion-WIMP-WISP Workshop, Durham, UK, 13-17 July 2009*, <http://axion-wimp2009.desy.de>.
- [2] K. Ehret *et al.*, Phys. Lett. B **689**, 149 (2010) [arXiv:1004.1313 [hep-ex]].

Search for Hidden Sector Photons in a Microwave Cavity Experiment

Rhys Povey¹, John Hartnett¹, Mike Tobar¹

¹Frequency Standards and Metrology Group, University of Western Australia, Perth, Australia

DOI: http://dx.doi.org/10.3204/DESY-PROC-2009-05/tobar_mike

In this proceeding we report the first results of a microwave cavity search for hidden sector photons. Using a pair of isolated resonant cavities we look for ‘light shining through a wall’ from photon - hidden sector photon oscillations. Our prototype experiment consists of two cylindrical, copper cavities stacked axially inside a single vacuum chamber. At a hidden sector photon mass of $39.58 \mu\text{eV}$ we place an upper limit on the kinetic mixing parameter χ at 7.8×10^{-6} . Whilst this result is inside already established limits our experiment has great scope for improvement.

1 Introduction

Many theories beyond the standard model predict an extra ‘hidden sector’ of particles which only very weakly interact with standard model matter [1, 2]. The hidden photon is thought to be massive, although very light in the sub-eV range, and able to kinetically mix with the standard photon thereby allowing oscillations between the photon and hidden sector photon [3]. Experimental searches for the hidden sector photon typically employ the ‘light shining through a wall’ (LSW) technique of indirect observation. As its name suggests this approach attempts to detect light passing through an impenetrable wall via a photon - hidden sector photon - photon oscillation. Until now this has only been carried out with lasers [4–13] but here we report the first LSW experiment using microwaves based on the proposal by Jaeckel and Ringwald [14].

2 Theory

To carry out microwave LSW we require two isolated cavities, an emitter cavity and detector cavity, at matched resonance frequencies. The emitter cavity is excited by a signal generator at its resonance frequency and a detection system attached to the detector cavity looks for a signal. The probability of transmission is given by [14]

$$\begin{aligned} P_{\text{trans}} &= \frac{P_{\text{det}}}{P_{\text{emit}}} = \chi^4 Q_{\text{emit}} Q_{\text{det}} \left(\frac{m_{\gamma'} c^2}{\hbar \omega_{\gamma'}} \right)^8 |\mathcal{G}|^2 \\ &= \chi^4 Q_{\text{emit}} Q_{\text{det}} \left(1 - \frac{k_{\gamma'}^2}{k_{\gamma}^2} \right)^4 |\mathcal{G}|^2 \end{aligned} \quad (1)$$

where \mathcal{G} is a dimensionless function encoding the geometric setup of the cavities,

$$\mathcal{G}\left(\frac{k_{\gamma'} }{k_\gamma}\right) = k_\gamma^2 \iiint_{V_{\text{emit}}} \iiint_{V_{\text{det}}} \frac{\exp(i k_{\gamma'} |\mathbf{x} - \mathbf{y}|)}{4\pi |\mathbf{x} - \mathbf{y}|} \mathbf{A}_{\text{emit}}(\mathbf{y}) \cdot \mathbf{A}_{\text{det}}(\mathbf{x}) d^3\mathbf{y} d^3\mathbf{x},$$

and P_{det} and P_{emit} are the power in and out of the respective cavities, χ is the kinetic mixing parameter, Q is the quality factor, $m_{\gamma'}$ is the hidden sector photon mass, ω_γ is the angular (and resonance) frequency of the photons, k_γ is the photon wavenumber, $k_{\gamma'}$ is the hidden sector photon wavenumber and \mathbf{A} is the normalized spatial part of the resonant electromagnetic gauge field inside the cavities. Calculations of this six dimensional integral had to be carried out numerically. As might be expected \mathcal{G} scales roughly to the reciprocal of separation distance between the two cavities. In our investigation of the probability of transmission and \mathcal{G} for axially stacked cylinders we found that increasingly higher order axial and radial modes were in most cases better but increasingly higher order azimuthal (whispering gallery) modes were worse. To maximize \mathcal{G} in the accessible X-band (8 – 12 GHz) frequency range for our experiment we chose to use the TE_{011} (fundamental transverse electric) cavity mode.

3 Experiment

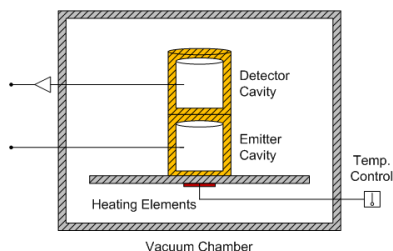


Figure 1: Schematic of the experimental setup.

The cavities were stacked axially on top of each other inside a vacuum chamber and temperature controlled to maintain the resonance frequency match. They were clamped down to provide good thermal contact. Isolation between the cavities was provided only by their individual cavity walls with no extra shielding being employed. As expected microwave leakage was a major problem in this simple setup. A diagram of the cavities in the vacuum chamber is shown in Figure 1.

To excite the emitter cavity a signal generator is used at its resonance frequency. To measure the resulting signal in the detector cavity the microwave circuit shown in Figure 2 is used. The output of the detector cavity passes through a low noise amplifier and is then mixed against a second signal generator set a few MHz off the cavity resonance frequency. This provides a signal at the offset frequency which is put through a low pass filter and preamplifier before being measured by a spectrum analyzer. A diagram of the full system is shown in Figure 2.

Operating the experiment, the detector cavity power output was measured to be 120.35 ± 1.50 dB below the power input of the emitter cavity. This relatively huge signal is most likely

Our experiment uses two cylindrical, copper cavities with an internal radius of approximately 2 cm and internal length of approximately 4 cm. A single loop probe was inserted in the middle of the side wall of each cavity and aligned and adjusted to maximize coupling to the TE_{011} resonance mode. Operating in the TE_{011} mode the cavities have quality factors of 9060 and 8370, resonance frequencies of 9.58806 GHz and 9.58794 GHz, and resonance bandwidths of 1.01 MHz and 1.17 MHz. The difference in resonance frequencies between the two cavities is 0.12 MHz, well within their resonance bandwidth of ~ 1 MHz.

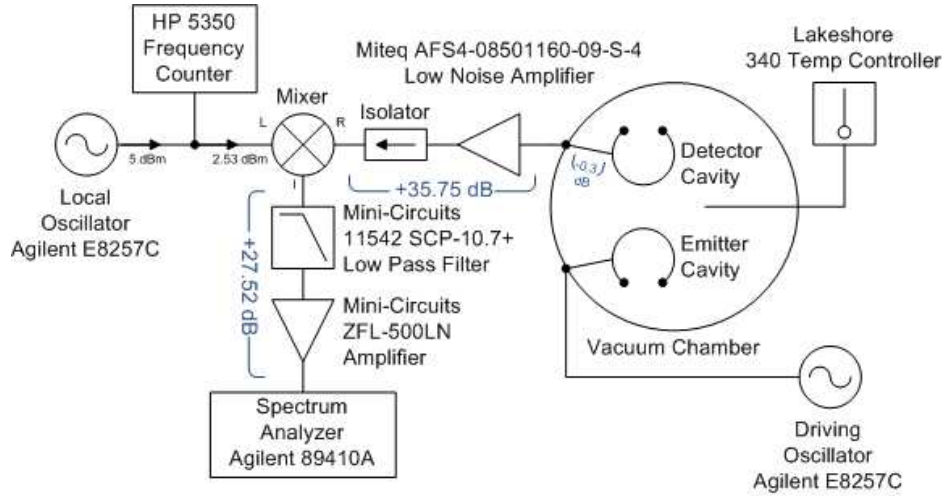


Figure 2: Diagram of the microwave circuit used in our cavity experiment.

due to microwave leakage inside the common vacuum chamber, probably predominately through the necessary pinhole in each cavity for vacuum pumping. Nevertheless by equation (1) we are able to place an upper limit on the kinetic mixing parameter χ from this experiment which is depicted in Figure 3.

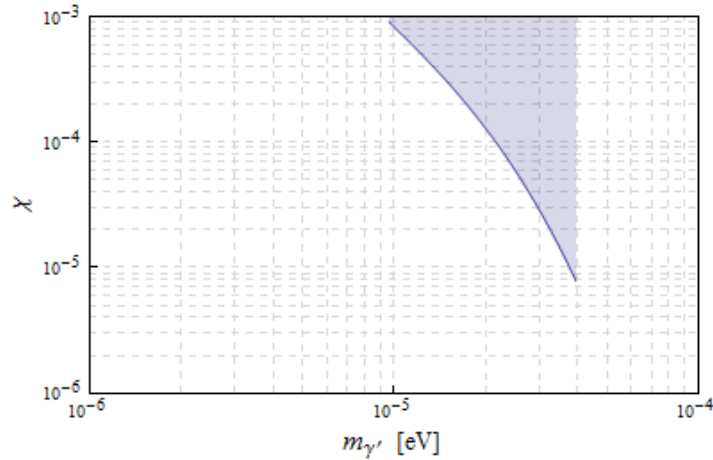


Figure 3: Hidden sector photon parameter space $(m_{\gamma'}, \chi)$ with the blue/gray shaded region excluded by this experiment. The peak occurs at 3.958×10^{-5} eV with $\chi = 7.8 \times 10^{-6}$.

4 Future work

Our results from this prototype experiment are not a betterment on previous hidden sector photon bounds [2, 15, 16], but do show promise for the future of microwave cavity LSW. Great improvements on this experiment can be made and a reduction in the χ limit by multiple orders of magnitude is possible. The two main areas for improvement are microwave leakage suppression and higher Q cavities. By separating our cavities into individual vacuum chambers we can greatly reduce the amount of leakage and hence be able to place a tighter limit on the mixing parameter. This extra separation comes at the cost of reducing \mathcal{G} but this should be outdone by a greater reduction in leakage. We can also use higher Q emitter and detector cavities to improve our sensitivity to χ . However if a moderate Q detector cavity is maintained whilst using a high Q emitter cavity we can avoid the challenge of frequency matching two narrow bandwidth resonant cavities.

References

- [1] S. A. Abel, M. D. Goodsell, J. Jaeckel, V. V. Khoze, and A. Ringwald, *JHEP* **07**, 124 (2008), arXiv:0803.1449.
- [2] M. Goodsell, J. Jaeckel, J. Redondo, and A. Ringwald, (2009), arXiv:0909.0515.
- [3] L. B. Okun, *Sov. Phys. JETP* **56**, 502 (1982).
- [4] R. Cameron *et al.*, *Phys. Rev. D* **47**, 3707 (1993).
- [5] G. Ruoso *et al.*, *Zeitschrift fr Physik C Particles and Fields* **56**, 505 (1992).
- [6] C. Robilliard *et al.*, *Physical Review Letters* **99**, 190403 (2007).
- [7] M. Ahlers, H. Gies, J. Jaeckel, J. Redondo, and A. Ringwald, *Physical Review D (Particles and Fields)* **76**, 115005 (2007).
- [8] A. S. Chou *et al.*, *Physical Review Letters* **100**, 080402 (2008).
- [9] M. Ahlers, H. Gies, J. Jaeckel, J. Redondo, and A. Ringwald, *Physical Review D (Particles and Fields)* **77**, 095001 (2008).
- [10] A. Afanasev *et al.*, *Physical Review Letters* **101**, 120401 (2008).
- [11] M. Fouché *et al.*, *Physical Review D (Particles and Fields)* **78**, 032013 (2008).
- [12] A. Afanasev *et al.*, *Physics Letters B* **679**, 317 (2009).
- [13] K. Ehret *et al.*, Resonant laser power build-up in ALPS - a “light-shining-through-walls” experiment, 2009, arXiv:0905.4159v1 [physics.ins-det].
- [14] J. Jaeckel and A. Ringwald, *Physics Letters B* **659**, 509 (2008).
- [15] E. R. Williams, J. E. Faller, and H. A. Hill, *Phys. Rev. Lett.* **26**, 721 (1971).
- [16] D. F. Bartlett and S. Lögl, *Phys. Rev. Lett.* **61**, 2285 (1988).

Search for 0.1 meV Axions and Hidden Photons Using Cu Resonant Cavities

P. L. Slocum, O. K. Baker, J. L. Hirshfield, Y. Jiang, G. Kazakevitch, S. Kazakov, M. A. LaPointe, A. Martin, S. Shchelkunov, A. Szymkowiak

Yale University

DOI: http://dx.doi.org/10.3204/DESY-PROC-2009-05/slocum_penny

Using a cylindrical Cu resonant cavity coupled to the pulsed 34.29 GHz magnicon at Yale, which provides several MW of RF power, we will search for the coupling ($g > 10^{-6}/\text{GeV}$) of two photons to a light neutral boson in the presence of a strong axial magnetic field. Using the same apparatus, we will also look for mixing between photons and hidden sector photons ($\chi > 10^{-7}$). A second cylindrical Cu cavity will allow reconversion to a 34.29 GHz photon. This approach is analogous to the “light shining through a wall” technique that has been implemented at shorter wavelengths. We discuss the design of the experiment as well as the expected sensitivity of the apparatus.

1 Introduction

The search for new physics beyond the standard model of elementary particles has been fueled partly by the model’s inability to address certain questions. For example it does not accommodate dark matter or dark energy, nor does it include a theoretical basis for the existence of gravity. It contains many parameters, such as the quark coupling constants, that have been measured empirically but whose magnitudes do not currently have theoretical explanations.

Extensions to the standard model have been proposed, several of which include a new light neutral boson (LNB) or axion-like particle (e.g., [1]). Other suggestions motivated by string theory [2, 3] predict a new “hidden sector” of particles that rarely interact with standard model particles. Of particular interest in these formulations is the region below 1 eV for hidden sector photons (HSPs) [3].

In this work we describe a “light shining through walls” experiment (see [4, 5, 6] and references contained therein) to search for LNBs and HSPs with masses near 34 GHz (0.1 meV). The experiment will be driven by the high-power 34 GHz microwave source at Yale (“magnicon”) [7, 8], pulsed at 10 Hz with a 1 μs width and a peak power of several MW. Using two resonant cavities [3, 9] positioned inside a 7 T magnet, we will look for interactions between 34 GHz photons and the new particles.

2 Magnet and Cryostat

The superconducting magnet is a 7 T Oxford unit with a room temperature vertical bore of width 89 mm. The magnet was designed for NMR work and as such has a field that is uniform to

1 % within 1 cm of the coil’s center. This uniformity is better than adequate for our experiment.

A separate cryostat has been custom built for this work by Cryo Industries, Inc. It consists of a He gas-cooled tube that fits vertically into the bore of the magnet. The coldest part of the tube will be placed into the center of the magnetic field and will be held at a temperature of approximately 10 K.

3 Resonant Cavities

There will be two resonant cavities made from OFHC copper in the experiment: a drive cavity and a signal cavity. The “drive” cavity will sit inside the bore of the magnet at the center of the field, but outside the separate cryostat. It will be critically coupled to the magnicon’s power. The “signal” cavity will also be inside the bore, adjacent to the drive cavity, but will be inside the cooled tube of the cryostat.

The signal and drive cavity dimensions and positions have been chosen to optimize the product of the two-cavity geometry factor [3] for hidden sector photons

$$G(k/\omega_0) = \omega_0^2 \int_{V'} \int_V d^3\mathbf{x} d^3\mathbf{y} \frac{\exp(ik|\mathbf{x} - \mathbf{y}|)}{4\pi|\mathbf{x} - \mathbf{y}|} A_{\omega_0}(\mathbf{y}) A'_{\omega_0}(\mathbf{x}),$$

squared, and the product of their two Q s. The result of the optimization is two side by side cylindrically shaped cavities, each operated in the TE011 mode. The Q of the drive cavity will be ~ 8000 , and the Q of the signal cavity will be several times higher due to the cooling.

The drive cavity will be tuned thermally with chilled water. The signal cavity will be tuned mechanically. One end of the signal cavity consists of a movable plunger as shown in Figure 1. The plunger and cavity are sealed hermetically by a flexible bellows with a 4 mm range of motion.

The height of the tuning plunger is controlled by moving a central rod. The top end of the rod will be mounted to a stepper motor (Physik Instrumente C-863) that will control the height of the plunger with submicron resolution and stability.

4 Receiver

The first component in the signal chain is a cryogenic amplifier with an integrated high electron mobility transistor (HEMT). The noise temperature of the HEMT amplifier at 34 GHz is approximately 22 K and its gain is 32 dB. Next the signal is mixed down to an intermediate frequency using a room-temperature Miteq AR2640LI8C.

After the mixer the signal is amplified by a series of room-temperature amplifiers preceded by a bandpass filter. The signal is filtered again before a diode detector. The DC output of the diode feeds into an Agilent 54855A oscilloscope for digitization before the PC-based data acquisition. Figure 2 shows a sketch of the initial components to be used in the receiver during the first phase of the experiment.

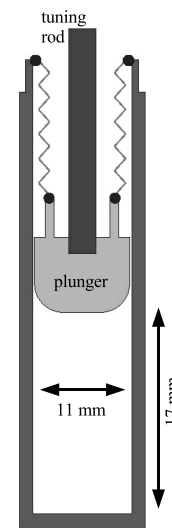


Figure 1: Sketch of the signal cavity with the plunger for tuning.

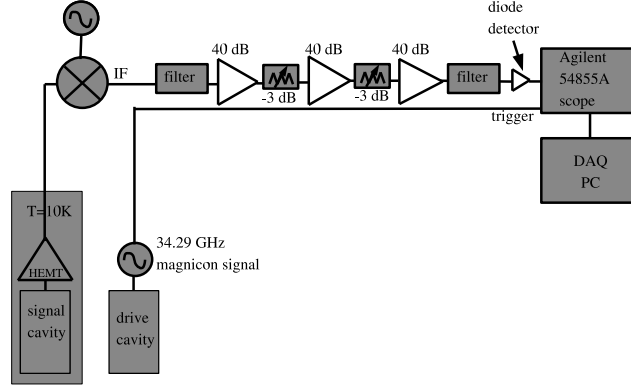


Figure 2: Subset of preliminary electronic components to be tested for use in the receiver.

5 Sensitivity

The sensitivity of the experiment to axion-like particles and hidden sector photons is defined in terms of a “ 5σ ” measurement, where

$$\sigma = \frac{N_s}{\sqrt{N_b}} \equiv 5.$$

N_s is the total number of signal photons and N_b is the total number of background photons. In the case of axion-like particles, the probability of detection P_{det} is [10, 11, 3]

$$P_{det} \approx \frac{B_{ext}^2 l^2}{4M^2} QQ' |G_a|^2, \quad (1)$$

where B is the magnetic field, l is the pathlength of the photon in B , M is the mass of the axion, and G_a is the geometry factor of the experiment for axions.

The number of background photons N_b is determined assuming a flat thermal noise spectrum $k_B T_N B$, where B is the measurement bandwidth. The noise temperature T_N for the system is driven by the noise figure of the first cryogenic amplifier, and will likely be on the order of 50–100 K. This translates to a noise power of $\sim 10^{-15}$ W, which is reduced to 10^{-20} W by gating with the duty cycle of the magnicon.

The number of signal photons N_s for hidden sector photons, or paraphotons, is given by [3]

$$P_{trans} \approx \chi^4 QQ' \frac{m_{\gamma'}^8}{\omega_0^8} |G|^2, \quad (2)$$

where χ is the sensitivity for photon-paraphoton mixing [3], $m_{\gamma'}$ is the mass of the hidden photon, and ω_0 is the energy of the incident photon. Using Eqs. 1 and 2 and assuming a geometry factor of order unity, Figure 3 shows the expected sensitivity of the apparatus to LNB and HSP particles for several experimental configurations.

SEARCH FOR 0.1 MEV AXIONS AND HIDDEN PHOTONS USING CU RESONANT CAVITIES

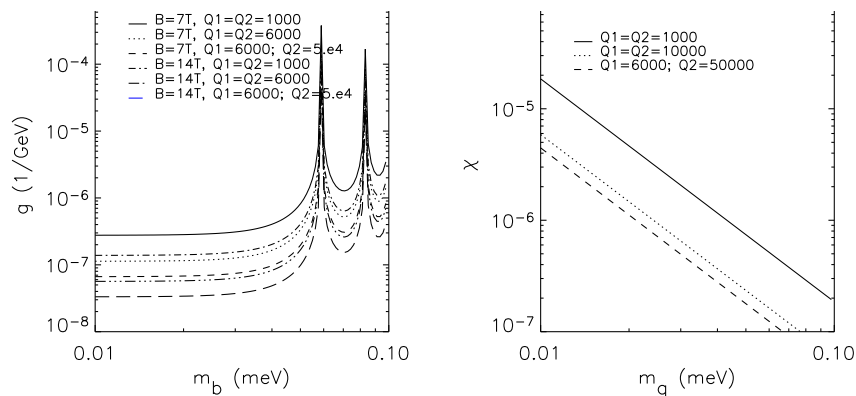


Figure 3: Plot of the expected results of this experiment for LNBs (left) and HSPs (right), assuming a range of values for the magnet field and cavity Q s.

6 Summary

The high power magnicon provides a unique opportunity to search for new particles with masses near 0.1 meV. The resonant cavity geometries have been optimized for efficiency and overall coverage. The initial receiver electronics have been selected to minimize noise power. With a cooled detector cavity and cryogenic amplifier, the sensitivity is expected to be on the order of $g > 10^{-6}/\text{GeV}$ for LNBs and $\chi > 10^{-7}$ for HSPs.

7 Acknowledgments

This work was supported by the Office of Naval Research and the Office of High Energy Physics at the Department of Energy.

8 Bibliography

References

- [1] R. D. Peccei and H. R. Quinn (1977). *Phys. Rev.* **D16** 1791 (1977).
- [2] M. Ahlers *et al.*, *Phys. Rev.* **D77** 095001 (2008).
- [3] J. Jaeckel and A. Ringwald, *Phys. Lett.* **B659** 509 (2008).
- [4] K. V. Bibber *et al.*, *Phys. Rev. Lett* **59** 759 (1987).
- [5] A. Afanasev *et al.*, *Phys. Lett* **B679** 317 (2009).
- [6] A. Afanasev *et al.*, *Phys. Rev. Lett* **101** 120401 (2008).
- [7] O. A. Nezhevenko, Gyrocons and magnicons: Microwave generators with circular deflection of the electron beam, *IEEE Trans. Plasma Sci.* **22** 756 (1994).
- [8] O. A. Nezhevenko, M. A. LaPointe, V. P. Yakovlev, and J. L. Hirshfield, “Commissioning of the 34-GHz, 45-MW Pulsed Magnicon”, *IEEE Trans. Plasma Sci.*, **32**, 994 (2004).
- [9] F. Caspers, J. Jaeckel, and A. Ringwald, arXiv:0908.0759v2.
- [10] R. Cameron *et al.*, *Phys. Rev.* **D47** 9 (1993).
- [11] E. Zavattini *et al.*, *Phys. Rev. Lett.* **96** 110406 (2006).

Status of the BMV experiment

Franck Bielsa¹, Rémy Battesti¹, Mathilde Fouché^{2,3}, Paul Berceau¹, Cécile Robilliard^{2,3}, Gilles Bailly^{2,3}, Sébastien Batut¹, Julien Mauchain¹, Marc Nardone¹, Oliver Portugall¹, Carlo Rizzo^{2,3}

¹Laboratoire National des Champs Magnétiques Intenses (UPR 3228, CNRS-INSA-UJF-UPS), F-31400 Toulouse Cedex, France.

²Université de Toulouse, UPS, Laboratoire Collisions Agrégats Réactivité, IRSAMC, F-31062 Toulouse, France.

³CNRS, UMR 5589, F-31062 Toulouse, France.

DOI: http://dx.doi.org/10.3204/DESY-PROC-2009-05/rizzo_carlo

In this contribution we present the status of the BMV experiment whose goal is to measure the vacuum magnetic birefringence.

1 Introduction

In this contribution we present the status of the BMV (Biréfringence Magnétique du Vide) experiment [1] whose goal is to measure the vacuum magnetic birefringence i.e. the birefringence induced in vacuum by the presence of an intense magnetic field. Linearly polarized light passing through a region where a magnetic field B perpendicular to the direction of propagation is present will acquire an ellipticity Ψ because of the vacuum magnetic birefringence. Ψ can be written as $\Psi = \frac{\pi}{\lambda} \Delta n B^2 L$, where λ is the light wavelength, Δn is the difference between the index of refraction of the light polarized parallel to the magnetic field and the index of refraction of the light polarized perpendicular to the magnetic field and L is the length of the magnetic field region. When B is given in Tesla Δn is expected to be about 4×10^{-24} . It is clear looking to the previous equation that the critical parameter for experiments looking for vacuum magnetic birefringence is $B^2 L$. Our choice, since the beginning in 2001, has been to reach a $B^2 L$ approaching 1000 T²m having a B as high as possible with an L as small as possible to set-up a table-top optical experiment which, we believe, has the best chances of success.

The value of Δn has been first calculated in the seventies [2] starting from the Heisenberg-Euler Lagrangian established in 1935 [3] to describe the photon-photon interactions in the framework of Quantum ElectroDynamics based on Dirac's model of the vacuum. At the lower orders in α , the fine structure constant, Δn can be written as

$$\Delta n = \frac{2}{15} \frac{\alpha^2 \hbar^3}{m_e^4 c^5} \left(1 + \frac{25}{4\pi} \alpha\right) \frac{B^2}{\mu_0} \quad (1)$$

where \hbar is the Planck constant over 2π , m_e is the electron mass, c the speed of light in vacuum, and μ_0 is the magnetic constant. The α^2 term is given in ref. [2]. The α^3 term has been first reported in ref. [4] and it corresponds to the lower order radiative correction to the main term. Its value is about 1.5% of the first order term.

Using the 2006 CODATA recommended values [5] for the fundamental constants, equation (1) gives $\Delta n = (4.031699 \pm 0.000005) \times 10^{-24} B(\text{T})^2$.

As we see, the error due to the knowledge of fundamental constants is negligible compared with the error coming from the fact that only first order QED radiative correction has been calculated. QED α^4 radiative correction should affect the fourth digit and the QED α^5 radiative correction the sixth digit. Thus measurement of Δn up to a precision of a few ppm remains a pure QED test.

It is known that an experiment designed to measure the vacuum magnetic birefringence can also give limits on the mass and the coupling constant of pseudoscalar particles that couples with two photons like axions or axionlike particles [6]. Using formulas given for example in ref. [6] on the ellipticity induced because of the existence of axionlike particles on polarized light propagating in the presence of a transverse magnetic field, one can infer the limits that can be given by an experiment like BMV [1]. If we suppose that the QED test has been successfully performed e.g. the Δn value given previously has been found experimentally with a precision of 10%, a coupling constant lower than about 5×10^7 GeV will be excluded for axionlike particles of a mass between 10^{-3} and 10^{-2} eV. A QED test of a precision of 1% i.e. at the level of the first radiative correction, will give a coupling constant limit of a few 10^8 GeV. Vacuum magnetic birefringence experiments are intrinsically different from astrophysics searches because they are terrestrial and all the experimental parameters are under control. Their discovery potential is therefore important. On the other hand, as far as we understand, their capacity to give interesting limits is reduced, and unless quoting unreasonable precisions in the QED test i.e. the measurement of Δn , astrophysical existing limits [7] are already better than the ones that can be obtained via the vacuum magnetic birefringence.

The BMV experiment is a collaboration between the Laboratoire Collision Agrégats Réactivité (LCAR) of Toulouse, France [8], the Laboratoire National Champs Magnétiques Intenses (LNCMI) of Toulouse and Grenoble, France [9], and the Laboratoire Matériaux Avancés (LMA) of Lyon [10], France. The apparatus is set up at the Toulouse site of the LNCMI, which is a laboratory specialized in pulsed magnetic fields.

To produce very high magnetic fields the only way is to have a strong current flowing into a coil. There are two main problems : heating and magnetic pressure. Pulsed fields have the advantage compared with continuous fields that coils do not have the time to heat and very high fields can be reached. On the other hand, magnetic pressure which is proportional to $\frac{B^2}{\mu_0}$ becomes very important and ultra strong conductors and special external reinforcement are needed. At the LNCMI of Toulouse, thanks to a 14 MJ bank of capacitors, pulsed fields of more than 80 T have been obtained using coils of solenoid type.

2 Present status

The BMV experiment is detailed in ref. [1]. We need a transverse magnetic field, since 2002 we have designed and tested a new geometry of coils, namely X-coils, which have reached more than 14 T over 0.25 m length corresponding to a 28 T²m. The coils are operated at liquid nitrogen temperature and the repetition rate is about 5 pulses per hour. In 2006 a clean room to host the experiment was realised. To increase the optical path of light in the magnetic field region we developed a Fabry-Perot cavity to which a laser is locked. We plan to use for such a cavity mirrors provided by LMA. Mirror losses are of the order of a few ppm and they always have to be kept in a dust free environment. A first version of the experiment mounted in

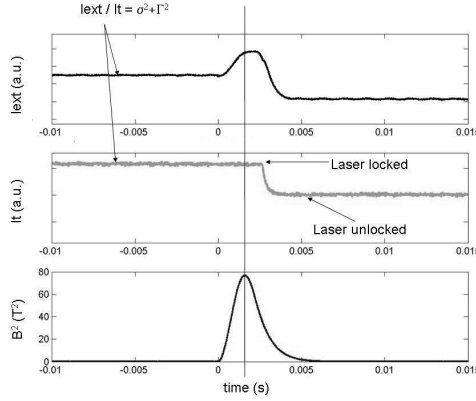


Figure 1: 1 atm Helium Cotton-Mouton effect : raw experimental data

our clean room consists of two X-coils with their cryostats surrounding the vacuum pipe and four vacuum chambers where polarizing prisms and cavity mirrors are located. Optics under vacuum is all placed on a 3.6 m table which satisfies our project requirement to have a table top experiment. As for data analysis, at the exit of the cavity we measure both the light intensity corresponding to light polarized like the light entering in the magnetic field region I_t and the light intensity corresponding to light polarized perpendicularly to the polarization of the light entering in the cavity I_{ext} . The ellipticity to be measured $\Psi(t)$ can be written as

$$\Psi(t) = \Gamma \sqrt{1 + \frac{I_{ext} - I_t(\sigma^2 + \Gamma^2)}{I_t \Gamma^2}} - \Gamma \quad (2)$$

where Γ is the ellipticity due to the cavity, and σ^2 is the polarizer extinction. When no magnetic field is present, and therefore $\psi(t) = 0$ one can obtain the value of Γ as a function of σ^2 , I_t and I_{ext} . Since in principle $\Psi(t) = kB^2(t)$, for each pulse we calculate the correlation between $\Psi(t)$ and $B^2(t)$, and finally a statistical analysis will give the mean value of k and its error.

We have recently taken data to measure the Cotton-Mouton effect of different gases [11], like air, molecular nitrogen and helium. The Fabry-Perot cavity used for such measurements is 2.2 meter long, corresponding to a free spectral range of 68 MHz. Once the laser is locked to the cavity we infer the cavity finesse by the measurement of the intensity decay time τ following a sudden stop of the light entering in the cavity. Typically τ is about 300 μs corresponding to a finesse of about 130 000, a cavity linewidth of about 520 Hz (FWHM), and a quality factor Q of about 5.4×10^{11} . Magnetic pulse duration is about 4 ms, which is comparable with the photon lifetime in the cavity. Actually, we have observed that ellipticity pulse is deformed by the cavity acting as a low pass filter of about 260 Hz cut-off frequency, as predicted in ref. [1]. In figure 1 we show the raw data corresponding to the Cotton-Mouton effect of Helium gas, which is the smallest that one can find in nature (except vacuum effect).

We have performed some measurements at different pressure between 0.1 to 1 atm. We have obtained a preliminary value for the Δn per Tesla of a 1 atm of Helium gas of $\Delta n = (2.1 \pm 0.4) \times 10^{-16}$ in agreement with the theoretical prediction $\Delta n = 2.4 \times 10^{-16}$ and the other

three experimental values published [12]. We have also performed measurements in vacuum that are compatible with zero within the errors. Thanks to the pulse duration our frequency working point is around 500 Hz, current sensitivity is about $10^{-7} 1/\sqrt{Hz}$, mostly limited by the photodiode noise equivalent power. We are upgrading the detection system. We are also working to decrease Γ and σ^2 which also limit the sensitivity.

3 Short term and long term perspectives

In the near future, we plan to measure helium Cotton-Mouton effect precisely with a sensitivity better than $\Delta n = 10^{-19}$ per Tesla per pulse, which also will give a precise calibration of our instrument. Vacuum measurements will follow. Using LMA mirrors (the expected cavity finesse is about 600 000) we plan to reach $\Delta n = 10^{-22}$ per Tesla and therefore to give new terrestrial limits on the oscillations of photons into massive particles in 2010.

Long terms perspectives depend on the possibility to have higher magnetic fields. We have designed a new pulsed coil, named XXL-Coil, which should reach a field higher than 25 T when a current higher than 27 000 A is injected. An XXL-Coil should provide more than 200 T²m. One XXL-Coil is under construction, and winding started in July 2009. Tests will follow as soon as possible. Eventually, three of them will be installed in the final set up. We hope in the next few years to finally reach our goal that is to measure the vacuum magnetic birefringence.

This work is supported by the *ANR-Programme non thématique* (ANR-BLAN06-3-139634), and by the *CNRS-Programme National Astroparticules*.

References

- [1] R. Battesti et al., Eur. Phys. J. D **46**, 323 (2008).
- [2] Z. Bialynicka-Birula and I. Bialynicki-Birula, Phys. Rev. D **2**, 2341 (1970).
- [3] W. Heisenberg and H. Euler, Z. Phys. **38**, 714 (1936).
- [4] V.I.Ritus, Sov. Phys. JETP, **42** 774 (1975).
- [5] Constants <http://physics.nist.gov/cuu/Constants/index.html>
- [6] R. Cameron et al., Phys. Rev. D **47**, (1993) 3707.
- [7] K.Zioutas et al. (CAST Collaboration), Phys. Rev. Lett. **94**, 121301 (2005).
- [8] <http://www.lcar.ups-tlse.fr/?lang=en>
- [9] <http://lncmi.cnrs.fr/>
- [10] <http://lma.in2p3.fr/Lmagb.htm>
- [11] C. Rizzo, A. Rizzo and D. M. Bishop, Int. Rev. Phys. Chem. **16**, 81 (1997).
- [12] R. Cameron et al., Phys. Lett. A **157**, 125 (1991); K. Muroo et al., J. Opt. Soc. Am. B **20**, 2249 (2003) ; M. Bregant et al., Chem. Phys. Lett. **471**, 322 (2009).

The status and prospects of the Q & A experiment with some applications

Hsien-Hao Mei¹, Wei-Tou Ni¹, and Sheng-Jui Chen², Sheau-shi Pan² (Q & A Collaboration)

¹Center for Gravitation and Cosmology, Department of Physics, National Tsing Hua University, Hsinchu, Taiwan 30013, Republic of China *mei@phys.nthu.edu.tw, wtni@phys.nthu.edu.tw*

²Center for Measurement Standards, Industrial Technology Research Institute, Hsinchu, Taiwan 30013 Republic of China

DOI: <http://dx.doi.org/10.3204/DESY-PROC-2009-05/mei.hsien-hao>

Motivated to measure the QED vacuum birefringence and to detect pseudoscalar-photon interaction, we started to build up the Q & A experiment (QED [Quantum Electrodynamics] and Axion experiment) in 1994. In this talk, we first review our 3.5 m Fabry-Perot interferometer together with our results of measuring Cotton-Mouton effects of gases. We are upgrading our interferometer to 7 m armlength with a new 1.8 m 2.3 T permanent magnet capable of rotation up to 13 cycles per second. We will use 532 nm Nd:YAG laser as light source with cavity finesse around 100,000, and aim at 10 nrad/Hz^{1/2} optical sensitivity. With all these achieved and the upgrading of vacuum, QED birefringence would be measured to 28% in about 50 days. Along the way, we should be able to improve on the dichroism detection significantly.

1 Introduction

In 1991, when Tsubono from University of Tokyo visited our Gravitation Laboratory in Tsing Hua University, we discussed the technical development of ultra-high sensitive interferometers for gravity-wave detection. During the last day before his departure, we pondered about how we could apply these developed techniques for fundamental physics and we discussed the possibility of doing the interferometric QED (Quantum Electrodynamics) tests. After analyzing the sensitivities, we believed that the QED birefringence would be measurable [1].

After the call for EOI's (Expression of Interest) of using the onsite SSC (Superconducting Super Collider) facilities in March, 1994 by DOE of USA, we submitted a joint EOI with a US team [2]. The topic of this EOI was chosen as one of the six topics for project definition study proposals. We then submitted such a proposal [3] in June and finished the study at the end of October, 1994 [4]. The project definition review was well-received. A five-year proposal [5] was submitted to the National Science Council of the Republic of China for the ROC part of the funding simultaneously. This proposal was approved in January, 1995 pending on the approval of the US proposal of the collaboration. Partial funding was allocated for the first year. However, due to lack of potential funding of the US counterpart, this program of collaboration was halted.

Nevertheless, in 1994, we started to build the experimental facility for the Q & A experiment (QED and Axion experiment) [6-8] acquiring two vacuum tanks of the laser-interferometric

gravity-wave detector type and working on the measurement of mirror birefringence [9]. Since 1991 we have worked on precision interferometry – laser stabilization schemes, laser metrology and Fabry-Perot interferometers. With these experiences, we started in 1994 to build a 3.5m/7m prototype interferometer for measuring vacuum birefringence and improving the sensitivity of axion search as part of our continuing effort in precision interferometry. In June, 1994 in the Marcel Grossmann Meeting at Stanford, we met the PVLAS people, exchanged a few ideas and encouraged each other. We learned that PVLAS also started in the same year adapting their earlier scheme proposed in 1979 [10].

In 2002, we finished the first phase of constructing the 3.5 m prototype interferometer and made some Cotton-Mouton coefficient and Verdet coefficient measurements [11]. Starting 2002, we have been in the second phase of Q & A experiment. The results of our second phase on dichroism and Cotton-Mouton effect (CME) measurement have been reported in [12] and [13]. In section 2 and section 3, we review our achieved optical sensitivity and summarize our gaseous CME measurement results. We are starting the 3rd phase of our Q & A experiment extending the 3.5 m interferometer to 7 m with upgrades. These together with the goal of this phase will be presented in section 4. Section 5 concludes with discussion and outlook.

2 Achieved optical sensitivity

The schematic of the present setup of our second phase is shown in Fig. 2 of reference [12] and Fig. 1 of reference [13]. These references gave details of the experimental setup. Fig. 1 shows a picture of the experimental apparatus. Our 3.5 m prototype interferometer is formed using a high-finesse Fabry-Perot interferometer together with a high-precision ellipsometer. The two high-reflectivity mirrors of the 3.5 m prototype interferometer are suspended separately from two X-pendulum-double pendulum suspensions mounted on two isolated tables fixed to the ground using bellows inside two vacuum chambers. The sub-systems are described in [14-16, 12]. Our results in this phase give $(-0.2 \pm 2.8) \times 10^{-13}$ rad/pass with 18,700 passes through a 2.3 T 0.6 m long magnet for vacuum dichroism measurement, and limit pseudo-scalar-photon interaction and millicharged fermions meaningfully [12].

3 Measurement of gaseous Cotton-Mouton effects

Upon passing through a medium with transverse magnetic field, linearly polarized light becomes elliptically polarized. Cotton and Mouton first investigated this in detail in 1905, and the phenomenon is known as Cotton-Mouton effect. We use our Q & A apparatus to measure the CMEs at wavelength 1064 nm in nitrogen, oxygen, carbon dioxide, argon, and krypton in a magnetic field $B = 2.3$ T at pressure $P = 0.5$ -300 Torr and temperature $T = 295$ -298 K. Our measured results are compiled in Table 1 [13]. For the Cotton-Mouton coefficient, we follow the convention of [17] and use the normalized Cotton-Mouton birefringence Δn_u at $P = 1$ atm and $B = 1$ T. Our results agree with the PVLAS results [18, 19] in the common cases (Kr, N₂, O₂) within 1.2σ . For Ar and CO₂ at 1064 nm, our results are new.

4 Upgrades

We are currently upgrading our interferometer from 3.5 m armlength to 7 m armlength in the 3rd phase. We have installed a new 1.8 m 2.3 T permanent magnet capable of rotation up to 13 cycles per second to enhance the physical effects. Figure 2 shows the configuration with our

new magnet. We are working with 532 nm Nd:YAG laser as light source with cavity finesse around 100,000, and aim at $10 \text{ nrad/Hz}^{1/2}$ optical sensitivity. *With all these achieved and the upgrading of vacuum, QED birefringence would be measured to 28 % in about 50 days.* Along the way, we should be able to improve on the dichroism detection significantly. To enhance the physical effects further, another 1.8 m magnet will be added in the future.



Figure 1: A picture of the experimental apparatus.



Figure 2: A picture of the new setup.

Gas	Normalized Cotton-Mouton birefringence Δn_u at $P = 1 \text{ atm}$ and $B = 1 \text{ T}$
N_2	$(-2.02 \pm 0.16^{\S} \pm 0.08^{\P}) \times 10^{-13}$
O_2	$(-1.79 \pm 0.34^{\S} \pm 0.08^{\P}) \times 10^{-12}$
CO_2	$(-4.22 \pm 0.27^{\S} \pm 0.16^{\P}) \times 10^{-13}$
Ar	$(4.31 \pm 0.34^{\S} \pm 0.17^{\P}) \times 10^{-15}$
Kr	$(8.28 \pm 1.26^{\S} \pm 0.32^{\P}) \times 10^{-15}$

\S : Statistical uncertainty

\P : Systematic uncertainty

Table 1: Measured Cotton-Mouton coefficients [13].

5 Discussion and outlook

We have heard a suite of motivations to search for (pseudo)scalar-photon interactions and to measure QED birefringence effect in this Patras 2009 workshop (See [20] and other articles in these proceedings; we refer the readers to various other experiments to the proceedings also). For QED birefringence, the next stage after detection is to measure the next-order effects which include hadron and potential new physical contribution [8]. This would be possible by extending the interferometer further with more rotatable permanent magnets. Many useful

techniques have been developed in the Gravitational Wave Detection Community. We have advocated using relevant techniques [1]. Recently, there is a proposal to use the VIRGO facility [21]. Further progress in this experimental field is expected in the near future.

We thank the National Science Council (NSC 96-2119-M-007-004, NSC 97-2112-M-007-002, NSC 97-2811-M-007-057, NSC 98-2112-M-007-009, and NSC 98-2811-M-007-033) for supporting the Q & A program.

References

- [1] W.-T. Ni *et al.*, *Mod. Phys. Lett.* **A6** 3671 (1991).
- [2] “Light Retardation in a High Magnetic Field and Search for Light Scalar/Pseudo-Scalar Particles Using Ultra-Sensitive Interferometry,” Joint EOI (Expression of Interest) submitted to the National Science Council of the Republic of China and the Department of Energy of the United States of America (April, 1994).
- [3] “Definition Studies for a proposal to Measure the Velocity of Light in a Magnetic Field”, proposal submitted to DOE of USA (June, 1994); “Experimental Search for Spin-Coupling Interactions and Light Scalar/Pseudo-Scalar Particles,” Prototype Study Proposal submitted to the National Science Council of the Republic of China (June, 1994).
- [4] U.S. Department of Energy, R-912, Light Retardation-Absorption and Axion (LIRA) Experiment – A Project Definition Study for On-Site Use of the Superconducting Super Collider Assets and Facilities, Final Report, Revision 1 (November 1994).
- [5] Test of Quantum Electrodynamical Birefringence and Search for Light Scalar/Pseudoscalar Particles, A Five-Year Proposal submitted to National Science Council (September, 1994).
- [6] W.-T. Ni *et al.*, in *Proceedings of the Sixth Marcel Grossmann Meeting on General Relativity*, Stanford, California, 1994 (World Scientific, Singapore, 1996).
- [7] W.-T. Ni, *Chin. J. Phys.* **34** 962 (1996).
- [8] W.-T. Ni, *Frontier Test of QED and Physics of the Vacuum*, ed. E. Zavattini, *et al.* (Sofia: Heron Press, 1998) p. 83;
- [9] H.-W. Cheng *et al.*, in *International Workshop on Gravitation and Cosmology*, December 14-17 (Tsing Hua Univ., Hsinchu, 1995), p.190.
- [10] E. Iacopini and E. Zavattini, *Phys. Lett.* **85B** 151 (1971).
- [11] J.-S. Wu, S.-J. Chen and W.-T. Ni, *Class. Quantum Grav.* **21** S1259 (2004).
- [12] S.-J. Chen, H.-H. Mei and W.-T. Ni (Q & A Collaboration), *Mod. Phys. Lett.* **A22** 2815 (2007) [arXiv:hep-ex/0611050].
- [13] H.-H. Mei *et al.*, *Chem. Phys. Lett.* **471** 216 (2009).
- [14] S.-J. Chen, S.-H. Mei and W.-T. Ni, Improving ellipticity detection sensitivity for the Q & A vacuum birefringence experiment, hep-ex/0308071 (2003).
- [15] S.-J. Chen, H.-H. Mei and W.-T. Ni, *J. of Phys.: Conf. Series* **32** 244 (2006)
- [16] H.-H. Mei, S.-J. Chen and W.-T. Ni, *J. of Phys.: Conf. Series* **32** 236 (2006).
- [17] C. Rizzo, A. Rizzo, D. M. Bishop, *Int. Rev. Phys. Chem.* **16** 81 (1997).
- [18] F. Brandi *et al.*, *J. Opt. Soc. Am.* **B15** 1278 (1998).
- [19] M. Bregant *et al.*, *Chem. Phys. Lett.* **392** 276 (2004).
- [20] W.-T. Ni, Constraints on pseudoscalar-photon interaction from CMB polarization observation, these proceedings.
- [21] G. Zavattini and E. Calloni, *Eur. Phys. J.* **C62** 459 (2009).

Interferometry in pulsed fields

Babette Döbrich¹ and Holger Gies^{1,2}

¹Theoretisch-Physikalisches Institut, Friedrich-Schiller-Universität Jena

²Helmholtz Institute Jena

Max-Wien-Platz 1, D-07743 Jena, Germany

DOI: <http://dx.doi.org/10.3204/DESY-PROC-2009-05/doesbrich.babette>

We discuss the particle-physics discovery potential of ground-based gravitational-wave interferometers. With the use of pulsed magnetic fields, current and future gravitational-wave interferometers could not only be utilized to observe phenomena of strong-field QED, but they could also be applied to sweep the parameter space of particles of the hidden sector.

1 Introduction

The presence of charged quantum vacuum fluctuations induces self-interactions of the electromagnetic field [1]. In particular, light passing through a strong external magnetic field is expected to travel at reduced velocity compared to the propagation through plain vacuum [2, 3].

As we argue in the following, the combination of ground-based gravitational-wave interferometers and strong pulsed magnetic fields forms an instrument which is sensitive enough to demonstrate nonlinearities in the propagation of light and thereby contribute to the research of strong-field QED [4]. At the same time, it facilitates a search for light particles beyond our current standard model of particle physics.

2 Alternative goals for gravitational-wave interferometers

In order to detect gravitational-waves by means of interferometry, two evacuated tubes of equal length L are installed orthogonally with respect to each other. The respective tubes have a mirror installed at their ends and thus form a cavity for a laser beam which is directed through both tubes by means of a beam splitter. An incoming gravitational-wave will induce a relative change $\Delta L(t)$ among the lengths of the two arms as a function of time. Alternatively, an *apparent* change of optical path length L can be caused by applying an external magnetic field $B(t)$ over a distance x in one of the interferometer arms, as the light traveling through the magnetic field region will propagate at reduced velocity. Using natural units $\hbar = c = 1$, this implies a so-called *strain* in the interferometer

$$h(t) = \frac{\Delta L}{L}(t) = \frac{x}{L}(1 - v(t)) , \quad (1)$$

as first suggested by [6], cf. also [7].

Since the sensitivity of the interferometer to the strain $h(t)$ is limited by diverse sources of noise, the temporal variation of $h(t)$ should be adapted to the region of highest sensitivity. Generically, gravitational-wave interferometers are most sensitive to variations at frequencies of about $\mathcal{O}(100\text{Hz})$. More precisely, the specific sensitivity of each interferometer can be read off its spectral noise density function $S_h(f)$, see e.g. [9]. In conclusion, for the detection of nonlinear light propagation with the help of gravitational-wave interferometers one needs magnetic fields varying at the millisecond scale.

In fact, such pulsed fields are provided by several magnetic field laboratories around the world. Focussing on the ongoing research at the Dresden High-Magnetic-Field-Laboratory (HDL) [8], we consider the specifications of a technically feasible Helmholtz-coil setup with a coil diameter of $x = 0.2\text{m}$. The need for a Helmholtz setup arises from the fact that no nonlinearities are induced for light traveling along the direction of the magnetic field lines. By contrast, for light traveling orthogonally to the magnetic field lines, the effect is maximized¹, depending on the beam polarization.

A feasible model for N subsequent field pulses is a damped sinusoidal oscillation:

$$B(t) = B_0 \sum_{i=0}^{N-1} \theta(t - t_i) \sin(2\pi\nu_B(t - t_i)) \exp(-\gamma(t - t_i)) , \quad (2)$$

with pulse frequency ν_B and a damping constant γ . For the following estimates, we assume $B_{\max} = 60\text{T}$ and $B_{\min} = -6\text{T}$ which fixes the amplitude $B_0 \approx 148\text{T}$ and relates the remaining parameters via $\gamma = 2\nu_B \ln |B_{\max}/B_{\min}|$.

A meaningful measure for the visibility of the strain $h(t)$ is the signal-to-noise-ratio (SNR) d . Its value is a measure for the likeliness that the strain is induced by the external magnetic field rather than due to random noise fluctuations. Applying a matched filter (or "Wiener filter") [9], the square of the SNR is given by

$$d^2 = 2 \int_0^\infty \frac{|\tilde{h}(f)|^2}{S_h(f)} df , \quad \tilde{h}(f) = \int_{-\infty}^\infty h(t) e^{-2\pi i f t} dt, \quad (3)$$

where $\tilde{h}(f)$ is the Fourier transform of the induced strain. A lever arm for the enhancement of this observable is provided by the fact that the setup for the field pulse is non-destructive and thus the pulse can be repeated after the magnet system has been re-cooled. Depending on the details of the setup, the re-cooling time of the magnet system is on the order of several minutes. To good accuracy, N subsequent pulses can enhance the SNR by a factor of \sqrt{N} :

$$d^2|_N \approx N d^2|_1. \quad (4)$$

3 Discovery potential at GEO600 and advanced LIGO

We start by computing the number of pulses required to achieve a total SNR of $\mathcal{O}(1)$ for the strain induced by nonlinear QED. To maximize the effect, the laser beam should be polarized in parallel to the external magnetic field lines. The velocity shift then reads [2, 3] $1 - v = 14B^2\alpha^2/(45m^4)$, where $\alpha \approx 1/137$ denotes the fine-structure constant and m the electron mass. Together with the parameterization of the field pulse, see Eq.(2), the velocity shift can

¹For this reason, also the drop-off in field strength perpendicular to the field lines which is generic for Helmholtz coils must be minimized.

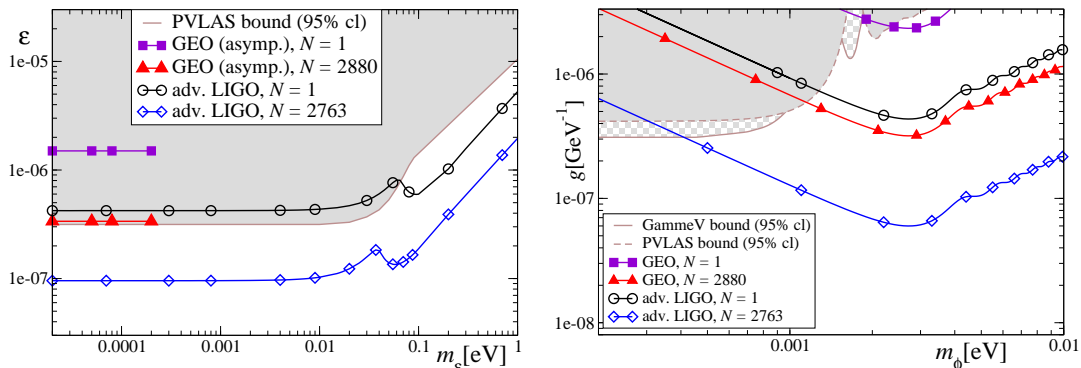


Figure 1: The figure on the left-hand side shows the discovery potential for spin- $\frac{1}{2}$ minicharged particles (MCP), while the figure on the right-hand side applies to axion-like particles (ALP). Already a single pulse measurement at advanced LIGO can improve the best current laboratory bounds [14, 16] in the respective coupling-mass planes.

be translated into the SNR through Eqs. (3) and (1), while the number of required pulses N enters through Eq. (4). We perform the calculation for the noise densities $S_h(f)$ of the advanced LIGO [10], which consists of interferometer arms of length $L = 4000\text{m}$, and GEO600 [11], where $L = 600\text{m}$. By a variation of the SNR with respect to the pulse frequency ν_B , we find that for the advanced LIGO $\nu_B \approx 47\text{Hz}$ yields the greatest strain, while for GEO600 $\nu_B \approx 273\text{Hz}$ is optimal. In terms of the number of required pulses, this would imply $N \approx 2763$ at advanced LIGO, demanding a continuous operation over a few days, which appears reasonable. (The operation time at GEO600, however, would be several years since $N \approx 2.3 \times 10^6$ pulses would be needed for an SNR of $\mathcal{O}(1)$ from the QED induced strain).

In analogy to the vacuum polarization induced by the electron fluctuations, also hypothetical particles with a weak coupling to photons can induce a velocity shift in the interferometer [5]. In the following, we therefore deduce the accessible parameter space with respect to coupling and mass for axion-like particles (ALPs) and minicharged particles (MCPs).

The velocity shift induced by fluctuating MCPs [13, 15] with fractional charge $Q = \epsilon e$ depends strongly on their mass m_ϵ . While for large masses, the scaling is analogous to the electromagnetic situation $(1 - v) \sim \epsilon^4 B^2 / m_\epsilon^4$, for low MCP masses the asymptotic limit reads $(1 - v) \sim -\epsilon^{8/3} B^{2/3} / \omega^{4/3}$, where the laser frequency $\omega = 1.2\text{eV}$ for the interferometers. We consider only MCP masses with a Compton wavelength smaller than the separation of the Helmholtz coils $\sim \mathcal{O}(1\text{cm})$, implying $m_\epsilon \gtrsim 2 \times 10^{-5}\text{eV}$. For smaller masses, the homogeneous-field assumption underlying the prediction for the velocity shift is no longer valid.

Uncharged scalar (S) and pseudo-scalar (P) ALPs couple to the \perp and the \parallel mode of the laser beam in the magnetic field, respectively. The corresponding velocity shifts read [12] $1 - v_{\parallel}^{\text{P}} = 1 - v_{\perp}^{\text{S}} = B^2 g^2 / [2m_\phi^2 (1 - \sin(2y)/2y)]$, where $y = xm_\phi^2 / (4\omega)$ with ALP mass m_ϕ and coupling g .

As displayed in Fig. 1, already a single-pulse measurement at advanced LIGO can improve the currently best laboratory bounds for MCPs [14, 16] and ALPs [14, 15] in the upper mass ranges (comparable to results for $\mathcal{O}(10^3)$ pulses at GEO600). Taking $N = 2763$ pulses at advanced LIGO, as needed for the QED effect, current laboratory bounds can be improved

almost in the entire mass range.

4 Conclusions

Pulsed magnetic fields such as provided by the Dresden High-Magnetic-Field-Laboratory can contribute to the research in the strong-field domain of QED for two reasons. Although they have generically a reduced field extent x in comparison to dipole magnets, they can provide for extremely high field strengths B . Since the velocity shifts induced by nonlinear QED, ALPs and the large mass regime of MCPs scale with xB^2 , the reduced field extent can well be compensated for, see also [17]. Secondly, their pulse frequency can be well matched to the region of highest sensitivity of gravitational-wave interferometers. For these reasons, combining strong pulsed magnetic fields with the interferometric techniques provided by modern gravitational-wave interferometers can give access to an unexplored parameter regime of strong field QED and at the same time allow to search for particles of a hidden sector.

Acknowledgments

B.D. would like to thank the organizers of the 5th Patras Workshop in Durham for the opportunity to contribute to the workshop on the one hand and even more profit from it on the other. The authors acknowledge support from the DFG under GRK1523, SFB/TR18, and Gi328/5-1.

References

- [1] W. Heisenberg and H. Euler, *Z. Phys.* **98** (1936) 714; V. Weisskopf, *Kong. Dans. Vid. Selsk. Math-fys. Medd.* **XIV**, 166 (1936); J. S. Schwinger, *Phys. Rev.* **82**, 664 (1951).
- [2] R. Baier and P. Breitenlohner, *Act. Phys. Austriaca* **25**, 212 (1967); *Nuov. Cim. B* **47** 117 (1967); S. L. Adler, *Annals Phys.* **67**, 599 (1971).
- [3] W. Dittrich and H. Gies, *Springer Tracts Mod. Phys.* **166**, 1 (2000).
- [4] B. Dobrich and H. Gies, *Europhys. Lett.* **87**, 21002 (2009) [arXiv:0904.0216 [hep-ph]].
- [5] H. Gies, arXiv:0812.0668, to appear in *Eur. Phys. J. D*, (2009); *J. Phys. A* **41**, 164039 (2008).
- [6] D. Boer and J. W. Van Holten, arXiv:hep-ph/0204207.
- [7] V. I. Denisov, I. V. Krivchenkov and N. V. Kravtsov, *Phys. Rev. D* **69**, 066008 (2004); G. Zavattini and E. Calloni, *Eur. Phys. J. C* **62**, 459 (2009) [arXiv:0812.0345 [physics.ins-det]].
- [8] T. Herrmannsdörfer, private communication; J. Wosnitza, *et al.*, in 2006 IEEE International Conference on Megagauss Magnetic Field Generation and Related Topics, G.F. Kiuttu, *et al.* (ed.) 197 (2008)
- [9] D. G. Blair, *The Detection Of Gravitational Waves*, Cambridge UP (1991); B. F. Schutz, in *Proc. Les Houches School on Astrophysical Sources of Gravitational Radiation*, Cambridge UP (1995).
- [10] D. Shoemaker, private communication; J. R. Smith [LIGO Scientific Collaboration], *Class. Quant. Grav.* **26**, 114013 (2009) [arXiv:0902.0381 [gr-qc]].
- [11] <http://www.geo600.uni-hannover.de/geocurves/>
- [12] L. Maiani, R. Petronzio and E. Zavattini, *Phys. Lett. B* **175**, 359 (1986); G. Raffelt and L. Stodolsky, *Phys. Rev. D* **37**, 1237 (1988).
- [13] H. Gies, J. Jaeckel and A. Ringwald, *Phys. Rev. Lett.* **97**, 140402 (2006).
- [14] E. Zavattini *et al.*, *Phys. Rev. Lett.* **96** (2006) 110406; *Phys. Rev. D* **77**, 032006 (2008).
- [15] M. Ahlers, H. Gies, J. Jaeckel and A. Ringwald, *Phys. Rev. D* **75**, 035011 (2007).
- [16] A. S. Chou *et al.*, *Phys. Rev. Lett.* **100**, 080402 (2008).
- [17] R. Battesti *et al.*, *Eur. Phys. J. D* **46**, 323 (2008).

ADMX's Continuing Search for Dark Matter Axions

Gray Rybka¹, on behalf of the ADMX Collaboration

¹ University of Washington

DOI: http://dx.doi.org/10.3204/DESY-PROC-2009-05/rybka_gray

Axions could solve the strong CP problem as well as be the source of dark matter. The ADMX experiment is currently searching for dark matter axions while testing SQUID amplifier technology to improve future searches. ADMX is currently sensitive to one broad class of axion-photon coupling models with masses near $3.5 \mu\text{eV}$. The next phase of ADMX will be sensitive to pessimistically coupled models over a much wider range of masses. Additionally, ADMX can be used to look for other light new-physics particles.

1 Axions and Dark Matter

Axions are light pseudoscalar particles that are a result of the Peccei-Quinn solution to the strong CP problem [1],[2],[3]. Axions could be produced in such quantities in the early universe to account for dark matter [4]. The interaction between axions and photons through the Primakoff effect [5] provides a means for detecting axions.

The requirements of both solving the strong CP problem and constituting a large fraction of dark matter favor a narrow range of possible axion masses and couplings [6],[4],[7]. The Axion Dark Matter Experiment (ADMX) is searching for dark matter axions over the first decade of the $1 \mu\text{eV}$ to 1meV favored mass region.

2 ADMX Design and Technology

ADMX is a axion cavity haloscope [8]; axions from the dark matter halo are stimulated to decay into photons by a strong magnetic field inside the experiment's microwave cavity. This excites electromagnetic modes inside the cavity which can be measured by an antenna. As the cavity is excited only when the total energy of the axion is equal to the cavity's resonant frequency, only a small range of axion masses may excite the cavity at any one time. Therefore the cavity's frequency must be tuned to allow a larger range of masses to be explored.

ADMX consists of a 22 liter cylindrical microwave cavity whose frequency is tuned by the position of two copper rods. The cavity sits inside a 7.6 Tesla magnet, and is kept at a temperature of 2 Kelvin by pumped liquid helium. An antenna in the top of the cavity leads to the amplifier electronics immediately above. Axion signals develop in the cavity, are amplified, and are carried out the top of the experiment, where they are mixed down and Fourier analyzed (Fig. 1). A more thorough description of the experiment can be found in [9].

The primary limiting factors to ADMX's axion photon coupling sensitivity are the system temperature and amplifier noise temperature. Previous incarnations of ADMX [10], were limited by the semiconductor amplifier noise, which had a minimum temperature of 2 K. The current

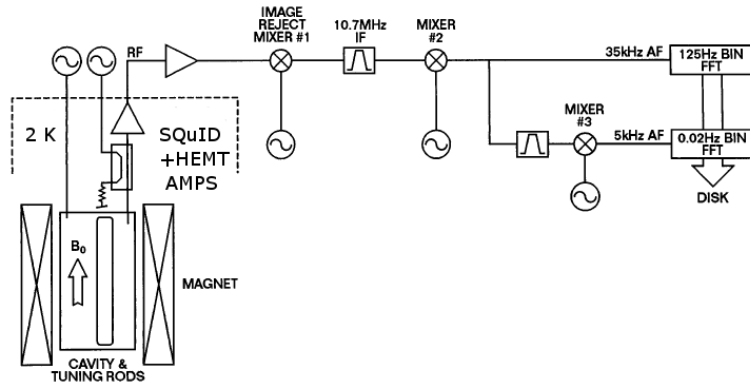


Figure 1: Schematic of ADMX receiver chain.

version of ADMX features a SQUID amplifier whose noise temperature can track physical temperature to as low as 100 mK [11]. The physical temperature of ADMX in this run, however, has not changed significantly from previous runs of the experiment, and so the axion-photon coupling sensitivity gain is slight; significant sensitivity gains will only come with improved cooling of the cavity. Given that SQUID amplifiers cannot function in magnetic fields, the main magnet's field must be canceled by a bucking coil, another addition to previous versions of ADMX. The primary technical challenge in this phase was to sufficiently cancel the field to insure proper SQUID functionality.

3 Preliminary Sensitivity and Phase 2

The 20 kHz wide raw power spectrum in the cavity is measured over 90 seconds, after which the rods are adjusted to change the cavity's resonant frequency. These spectra are corrected for the receiver transfer function and summed to give a power spectrum over a range of several MHz. Axion signals would appear in this power spectra as a narrow peak at a frequency corresponding to the axion mass with a width related to the velocity dispersion of dark matter axions near earth (Fig. 2).

If no signals are observed, an upper bound on axion-photon coupling over the covered mass range can be set. As of September 2009, the data taken by the 2009 run of ADMX is projected to be sensitive to axions models that couple stronger than the standard KSVZ ($e/n=0$) model as described in [12] for a standard virialized dark matter halo with local density of 0.45 GeV/cm^3 [13]. Sensitivity is greater for unvirialized dark matter models with a smaller velocity distribution or relative velocity to the solar system (Fig. 3).

With the successful demonstration of the SQUID amplifier and bucking coil system in the present version of ADMX, the next version of ADMX can be prepared. In "Phase 2" of ADMX, the cavity and amplifier will be cooled K to 100 mK by a dilution refrigeration system. This will increase the speed at which masses can be covered by a factor of 100, allowing the entire promising $1 \mu\text{eV}$ to $10 \mu\text{eV}$ mass range to be covered for reasonable axion-photon couplings with only one year of operation, even if axions are a subdominant fraction of dark matter. Construction of phase 2 will begin shortly after the completion of the present run.

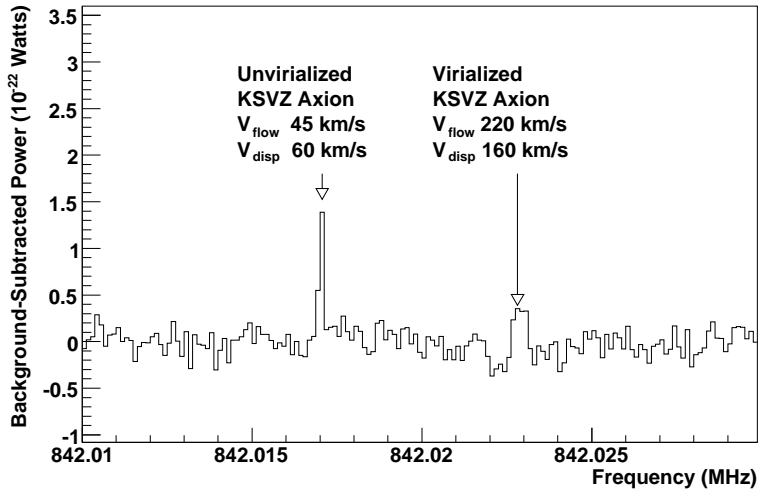


Figure 2: Two simulated axion signals imposed on a real power spectrum average.

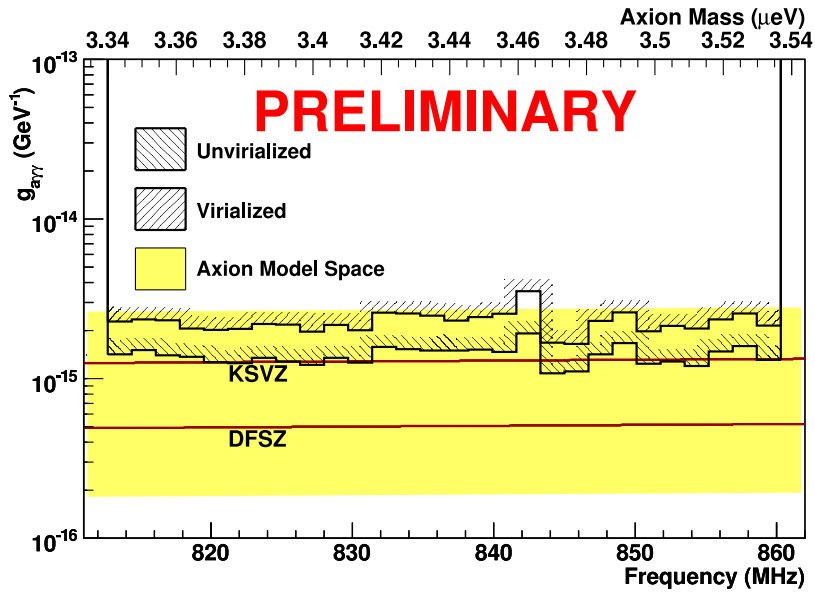


Figure 3: Preliminary ADMX sensitivity for the 2009 run.

4 Additional Searches

In addition to dark matter axions, ADMX has the potential to be sensitive to other light scalar and pseudoscalar particles. One example of these are chameleons, particles whose nonlinear self couplings lead to a density dependent mass and may be related to dark energy [14],[15], [16]. As low mass chameleons can be trapped inside the cavity, electromagnetic modes of the cavity can couple to chameleon modes. Once chameleon modes have been excited, their decay back into electromagnetic modes can be detected with the same system as is used to detect dark matter axions. With this method, ADMX should be highly sensitive to chameleon-photon coupling over a range of masses corresponding to the tuning range of the cavity. A chameleon search with ADMX is currently underway.

5 Conclusion

ADMX has demonstrated sensitivity to some promising axion dark matter models over a limited range of axion masses. Additionally, the current phase of ADMX has demonstrated the amplifier technology required to explore a range of potential dark matter axion masses and models. The upcoming Phase 2 of ADMX will utilize this technology combined with a lower temperature to have a good chance of seeing signs of axion dark matter if it exists. As well as being sensitive to dark matter axions, ADMX may also be sensitive to light new physics particles related to dark energy.

References

- [1] R. D. Peccei and Helen R. Quinn. *Phys. Rev. Lett.*, 38(25):1440–1443, Jun 1977.
- [2] Steven Weinberg. *Phys. Rev. Lett.*, 40(4):223–226, Jan 1978.
- [3] F. Wilczek. *Phys. Rev. Lett.*, 40(5):279–282, Jan 1978.
- [4] Michael Dine and Willy Fischler. *Physics Letters B*, 120(1-3):137 – 141, 1983.
- [5] H. Primakoff. *Phys. Rev.*, 81(5):899, Mar 1951.
- [6] L. F. Abbott and P. Sikivie. *Physics Letters B*, 120(1-3):133 – 136, 1983.
- [7] G. G. Raffelt. Astrophysical axion bounds. In *Axions*, volume 741 of *Lecture Notes in Physics*, pages 19–51. Springer Verlag, Dec 2008.
- [8] P. Sikivie. *Phys. Rev. Lett.*, 51(16):1415–1417, Oct 1983.
- [9] H. Peng, S. Asztalos, E. Daw, N. A. Golubev, C. Hagmann, D. Kinion, J. LaVeigne, D. M. Moltz, F. Nezrick, J. Powell, L. J. Rosenberg, P. Sikivie, W. Stoeffl, N. S. Sullivan, D. B. Tanner, M. S. Turner, and K. van Bibber. *Nucl. Instrum. Meth. A*, 444(3):569 – 583, 2000.
- [10] S. J. Asztalos, R. F. Bradley, L. Duffy, C. Hagmann, D. Kinion, D. M. Moltz, L. J. Rosenberg, P. Sikivie, W. Stoeffl, N. S. Sullivan, D. B. Tanner, K. van Bibber, and D. B. Yu. *Phys. Rev. D*, 69(1):011101, Jan 2004.
- [11] Michael Mück, Marc-Olivier André, John Clarke, Jost Gail, and Christoph Heiden. *Nuclear Physics B - Proceedings Supplements*, 72:145 – 151, 1999. Proceedings of the 5th IFT Workshop on Axions.
- [12] Jihn E. Kim. *Phys. Rev. D*, 58(5):055006, Jul 1998.
- [13] E. Gates, G. Gyuk, and M. Turner. *The Astrophysical Journal*, 449:L123 – L126, Aug 1995.
- [14] Justin Khoury and Amanda Weltman. *Phys. Rev. Lett.*, 93(17):171104, Oct 2004.
- [15] Justin Khoury and Amanda Weltman. *Phys. Rev. D*, 69(4):044026, Feb 2004.
- [16] A. S. Chou, W. Wester, A. Baumbaugh, H. R. Gustafson, Y. Irizarry-Valle, P. O. Mazur, J. H. Steffen, R. Tomlin, A. Upadhye, A. Weltman, X. Yang, and J. Yoo. *Phys. Rev. Lett.*, 102(3):030402, 2009.

Polarization measurements and their perspectives at the Low Energy Frontier

Giovanni Cantatore

University and INFN, Via Valerio 2, 34127 Trieste, Italy

DOI: http://dx.doi.org/10.3204/DESY-PROC-2009-05/cantatore_giovanni

Polarization measurements at low energy (1-2 eV) will soon probably be able to directly detect QED processes, such as photon-photon scattering. In principle, these techniques could also be used to probe particle production (Axion-Like Particles, Mini-Charged Particles, Chameleons, to mention a few) at the Low Energy Frontier. Reaching an interesting unexplored zone in the ALP parameter space is, however, currently beyond their power, even in very optimistic scenarios. Photon regeneration experiments, on the other hand, have the potential to extend the reach of laser experiments beyond what is possible with polarization detection schemes. Using the resonant regeneration idea one can exploit the coherence properties of the ALP and photon fields to enhance the ALP-photon conversion probability by a factor which can be as large as 10^{10} , or more, by using two frequency-locked Fabry-Perot optical resonators. The PVLAS-Phase II group in Trieste is attempting to build a table-top resonant regeneration pilot apparatus. At the moment, resonant regeneration appears as the sole purely laboratory-based method capable of investigating a region of the ALP parameter space now accessible, in part, only to astrophysical observations, such as those from the CAST magnetic helioscope for ALPs. In the optimistic, though not a priori excluded, case of a positive signal one would obtain a discovery of great scientific value.

1 Introduction

Precision measurements of the changes in the polarization state of a linearly polarized visible laser beam propagating through a magnetic field were introduced several years ago as a tool to investigate photon-photon scattering at low energies as described by QED [1]. In the course of the development of these techniques it became also clear [2] that the production of nearly massless particles, which we now call WISPs, for Weakly Interacting Sub-eV Particles, has a possible signature in terms of polarization. QCD axions [3] are a prime example of WISPs and remain the main goal of current WISP searches: their polarization signature is an induced birefringence, in the case of the production of a virtual axion, or an induced dichroism in the case of the production of a real particle. More recently, the possibility has emerged to exploit, at least in principle, polarization measurement to investigate other WISP particles such as Mini Charged (MCPs) and Chameleon particles [4]. The basic experimental technique can be thought of as a scattering off a "photon target", normally consisting of the virtual photons provided by a magnetic field, where one analyzes the polarization state of the scattered photons. The simplest way to detect polarization changes is to enclose the interaction region, where the

scattering takes place, between two crossed polarizers. This is called static detection and is severely limited by the extinction factor of the polarizers themselves. This number expresses the ratio of the intensity transmitted by a crossed polarizer versus the intensity incident on it. High quality polarizers may reach extinction factors of 10^{-8} , corresponding to an ellipticity of 10^{-4} , which is orders of magnitude larger than 10^{-11} , the typical ellipticity to be detected in QED experiments¹. To detect smaller ellipticities one must resort to the heterodyne technique, where the effect is made time-varying by acting on the magnetic field (either changing its intensity as in BFRT [5] or rotating it as in PVLAS [6]) and a carrier ellipticity is superimposed on it by means of an optical modulator. The heterodyne technique, combined with the amplification of the optical path provided by a Fabry-Perot resonant cavity, brings detectable ellipticities in the 10^{-9} range, the challenge now being gaining the two remaining orders of magnitude to access the QED regime.

2 Panorama of current polarization experiments

The current panorama of polarization experiments comprises the efforts in France, by the BMV group [7], at CERN, by the OSQAR collaboration [8], and in Taiwan, by Q&A [9]. These experiments have been active for several years and in the case of BMV are already in the preliminary data-taking phase. As an example of the new start-ups we will mention the PVLAS-Phase II [10] project which is pushing towards a reduction of the dimension of the apparatus down to true table-top level in order to better understand and control noise sources. All these experiments share common features: a low-energy (1-2 eV) linearly polarized laser beam probing a vacuum region where a transverse magnetic field is present, continuous light power with a maximum of 1 W, a time-varying physical effect, an optical path in the interaction region amplified by means of a resonant Fabry-Perot cavity. They also share, unfortunately, the same problem: a noise background limiting the sensitivity, which is defined as the minimum ellipticity angle which can be detected in a measurement lasting 1 s. The current common barrier is a sensitivity around 10^{-7} rad/ $\sqrt{\text{Hz}}$, meaning that to detect a 10^{-11} angle one would have to gather data continuously for 10^8 s.

Q&A uses 1 eV photons from a few mW power ND:YAG laser to probe a magnetic region where the time-varying field is provided by a rotating permanent 2.2 T dipole placed horizontally. Amplification of the optical path is given by a resonant Fabry-Perot cavity with the peculiarity of having its mirrors mounted on suspensions in order to attenuate seismic vibrations. Q&A tested relatively recently the performance of its apparatus by measuring the magnetic birefringence of a few gases.

The OSQAR collaboration intends to exploit the strength of two dipole LHC magnets by keeping the field static and applying the time variation to the polarization of the probing laser beam. The experiment is now in the optics development stage.

The BMV group is probably at this time the one nearest the goal of starting actual science runs. The main feature of BMV is relying on pairs of pulsed magnetic coils having a characteristic X shape. These coils provide magnetic pulses lasting a few ms with peak intensities of 12-14 T and give the time-variation needed for heterodyne detection. A high-finesse Fabry-Perot

¹We distinguish here between the birefringence Δn , which is the difference of the refractive indices relative to two orthogonal polarization states, and the ellipticity Ψ , which is the ratio of the semi-minor to the semi-major axes of the ellipse described by the light electric field. The relation between the two quantities is $\Psi = (\pi L/\lambda)\Delta n$, where L is the length of the interaction region and λ is the light wavelength.

resonator is employed to amplify the optical path, and to insulate its mirrors from contamination BMV houses its optical benches in a clean-room. The experiment has entered the final commissioning phase and they have recently reported the detection of a birefringence as low as $(-9.8 \pm 22.9) \cdot 10^{-17} \text{ T}^{-2}$, while the reference value corresponding to the QED photon-photon scattering is $\approx 4 \cdot 10^{-24} \text{ T}^{-2}$.

The main challenge for polarization experiments is lowering the noise background. The fact that all optical components exhibit an intrinsic birefringence and that changes in this birefringence are responsible for the least understood part of the background has ushered in the idea that reducing the size of the apparatus might help bringing also this noise under control. PVLAS-Phase II has built an optical ellipsometer sitting on a single optical bench, complete with a rotating 2.3 T permanent dipole magnet and a high finesse Fabry-Perot cavity ($F \approx 200000$). The goal is to achieve a sensitivity of at least $10^{-8} \text{ rad}/\sqrt{\text{Hz}}$, which would allow detecting the QED birefringence in a reasonable measurement time of 188 standard 8-hour workdays. Note that a further factor 10 improvement in sensitivity would bring this time down to 0.471 days. Such sensitivities, however, would not help polarization experiments significantly in the search for WISPs. Figure 1, for instance, shows a portion of the parameter space for Axion Like Particles (ALPs) where curves representing upper bounds are plotted for a few polarization experiments. As a reference, the "CAST barrier", representing the best currently available wide-band experimental limit ², and the "axion line"³, giving the locus of points compatible with a QCD axion, are also plotted.

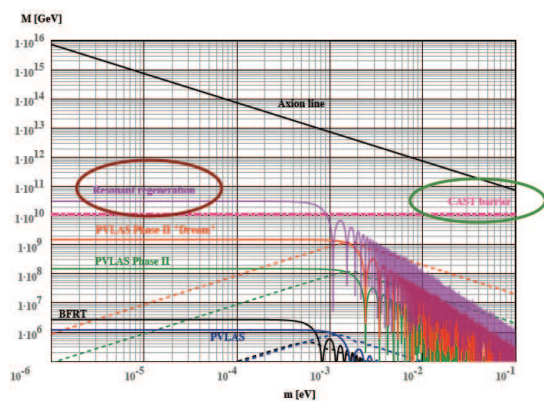


Figure 1: Comparison of upper bounds in the mass-inverse coupling plane for ALPs. "PVLAS" and "BFRT" label curves giving the bounds set by the PVLAS and BFRT, respectively. "PVLAS Phase II" and "PVLAS Phase II dream" label curves corresponding to the bounds reachable with the PVLAS-Phase II table-top apparatus with a sensitivity of $10^{-8} \text{ rad}/\sqrt{\text{Hz}}$ and $10^{-9} \text{ rad}/\sqrt{\text{Hz}}$, respectively. The curve labelled "Resonant regeneration" gives the bound reachable with a table-top resonant regeneration set-up (see text).

It is apparent from the plot that even in the best "dream" scenario, corresponding to the "PVLAS Phase II dream", where an extremely good sensitivity of $10^{-9} \text{ rad}/\sqrt{\text{Hz}}$ is assumed,

²The CAST limit is actually valid only up to masses around 1 eV, and is drawn here as a line for simplicity.

³The axion line should actually be a band to take into account the spread due to different models for the QCD axion.

polarization experiments cannot even approach the "CAST barrier", let alone the QCD axion line. In fact, the bounds for polarization experiments are plotted using the ellipticity angle that would be necessary to detect to reach the signature of QED photon-photon scattering. An ellipticity generated by axion-photon interactions would then be smaller than the QED effect and basically indistinguishable from it⁴. In conclusion, there is little hope of reaching the CAST barrier with polarization-type experiments unless a fantastic sensitivity is attained, and it can be safely stated that the primary mission of precision ellipsometers was and remains the detection of QED effects.

3 The future of laser experiments: resonant regeneration

The WISP concept encompasses different types of particles, however it is hardly disputable that the "Holy Grail" of WISP searches is still represented by ALPs and in particular by the QCD axion itself. The future of laser experiments, indeed the future of laboratory-type experiments in the field of axion detection, lies with the resonant regeneration concept.

Resonant regeneration was recently proposed [11] as the ultimate evolution of the light-shining-through-a-wall (LSW) scheme for producing and detecting axions in the laboratory. In resonant regeneration, both the magnet where particles are produced from photons and the magnet where the photons are regenerated from the particles are enclosed in resonant Fabry-Perot cavities of finesse F . This increases the overall probability of observing a regenerated photon by a factor proportional to F^2 . With the current techniques finesse can routinely reach 10^5 , meaning that the probability increases by 10^{10} .

The curve labelled "Resonant regeneration" in Figure 1 shows the bound which could be obtained by a table-top resonant regeneration experiment. Note how this bound is capable of breaking the "CAST barrier" with a purely laboratory-type experiment.

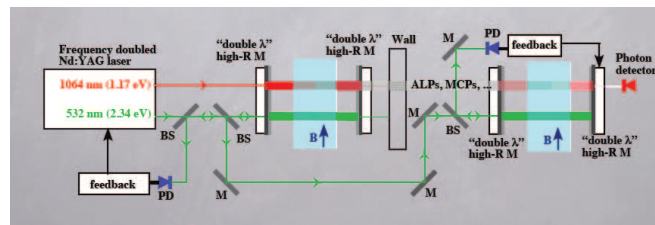


Figure 2: Proposed optical scheme to achieve the frequency-lock of two separate Fabry-Perot cavities. The scheme is based on a laser emitting two beams, one of which is obtained by frequency-doubling the first one, and on high-reflectivity mirrors having maximum reflectance at the two laser wavelengths (see text).

A few challenges must be met on the way to a successful resonant regeneration experiment. The first and most difficult one is meeting the requirement that the two Fabry-Perot must be frequency-locked and must also resonate on the same spatial mode. A possible scheme to meet this challenge, at least for the frequency-locking part, is sketched in Figure 2.

In this scheme, the laser is a ND:YAG solid state device emitting a primary beam in the infrared at 1064 nm and a secondary beam at 532 nm, obtained from the first by passing

⁴If a dichroism is also measured, however, there is the possibility of disentangling the two contributions.

through a non-linear duplicating crystal. These two beams are frequency-locked and coherent. The Fabry-Perot cavities are formed by high-reflectivity multi-layer dielectric mirrors coated for maximum reflectance at the two wavelengths of interest. One of the two beams is used to lock the laser frequency to the first cavity, which then becomes the reference, and then to lock the second cavity to the laser. The other beam, which is now naturally resonant with the cavities, is used for the actual photon regeneration measurement. Other challenges regard the need for a high power laser and for a low background detector capable of counting single-photons at 1-2 eV energies. 10 W lasers emitting continuously in the infra-red are commercially available, while going up to 100 W requires specialized expertise, using however existing technology. The detector challenge is actually a common problem for most WISP search experiments. A resonant regeneration experiment could certainly benefit from a detector such as the cooled APD being developed within the BaRBE project of INFN [12]. A better, but more difficult option, would probably be to use a Transition Edge Sensor (TES) for instance of the type developed by INFN Genova [13].

In conclusion, photon beams are the primary tools to explore the Low Energy Frontier, however of the two main types of experiments, polarization measurements and photon regeneration, only photon regeneration in its fully resonant version has the possibility of impacting significantly on WISP searches by breaking the "CAST barrier" and establishing the new experimental benchmark. Difficult challenges must be met on the road to a successful resonant regeneration experiments, however a handsome reward, in the form of a revolutionary scientific discovery, could be just around the corner.

References

- [1] E. Iacopini and E. Zavattini, Phys. Lett. B **85** 151 (1979).
- [2] L. Maiani, R. Petronzio and E. Zavattini, Phys. Lett. B **175** no.3 359-363 (1986); G. Raffelt and L. Stodolsky, Phys. Rev. D **37** 1237 (1988).
- [3] R.D. Peccei and H. Quinn, Phys. Rev. Lett. **38** 1440 (1977); R.D. Peccei and H. Quinn, Phys. Rev. D **16** 1791 (1977).
- [4] M. Ahlers *et al.*, Phys. Rev. D **77** 095001 (2008); P. Brax *et al.*, Phys. Rev. Lett. **99** 121103 (2007).
- [5] R. Cameron *et al.*, Phys. Rev. D **47** no.9 3707-3725 (1993).
- [6] D. Bakalov *et al.*, Quantum Semiclass. Opt. **10** 239 (1998).
- [7] R. Battesti *et al.*, Eur. Phys. J. D **46**, 323 (2008).
- [8] P. Pugnat *et al.*, CERN-SPSC-2006-035 (2006).
- [9] H.-H. Mei *et al.*, arXiv:0812.3328 (2008).
- [10] G. Cantatore *et al.*, arXiv:0809.4208 (2008).
- [11] P. Sikivie *et al.*, Phys. Rev. Lett. **98** no.17 4 (2007).
- [12] G. Cantatore *et al.*, Nucl. Instr. and Meth.in Phys. Res. A **617** 502-504 (2010)
- [13] D. Bagliani *et al.*, J. of Low Temp. Phys. **151** no.1 234-238 (2008).

Chapter 5

Direct Axion Signals

Searches for light Higgs/Axions at *BABAR*

Alessandro Gaz

University of Colorado, Boulder, Colorado 80309, USA

representing the *BABAR* Collaboration

DOI: http://dx.doi.org/10.3204/DESY-PROC-2009-05/gaz_alessandro

Searches for light Higgs bosons/axions have been performed by the *BABAR* Collaboration in their decays to the final states $\mu^+\mu^-$, $\tau^+\tau^-$ and *invisible*. The test of Lepton Universality from $\Upsilon(1S)$ decays allows also to set non trivial limits on the existence of exotic particles. No significant signal has been found and we get more stringent limits on the existence of those particles with respect to previously reported results.

1 Introduction

The Next to Minimal Super-Symmetric Standard Model (NMSSM) has been proposed in order to reduce the amount of fine tuning required in the MSSM. In such model a light CP-odd Higgs boson A^0 arises naturally and, if its mass is lower than $2m_b$, where m_b is the mass of the b quark, its existence is not constrained by the LEP experiments. The radiative decays of the Υ mesons ($\Upsilon(nS) \rightarrow \gamma A^0$) are a privileged place for searching for this particle [1]. Useful limits can be obtained at the current B -factories.

Moreover, the existence of an axion-like neutral light particle has been postulated to explain the positron excess seen by PAMELA [2]. According to [3], a particle A^0 with mass $m_K - m_\pi < m_{A^0} < \sim 800 \text{ MeV}/c^2$ dominantly decaying to charged leptons would explain the experimental data.

Experimental motivation for searching for a light particle decaying into muon pairs comes from the HyperCP experiment [4], which observed the decay $\Sigma^+ \rightarrow p\mu^+\mu^-$. The invariant masses of the $\mu\mu$ pair for the three signal events observed cluster around $214 \text{ MeV}/c^2$, suggesting the existence of an intermediate state decaying to charged leptons.

2 The *BABAR* detector and dataset

The *BABAR* detector is described in detail elsewhere [5]. The data used for these searches have been collected at the PEP-II asymmetric e^+e^- collider, located at the SLAC National Accelerator Laboratory. The relevant datasets are constituted by 30.2 fb^{-1} (14.5 fb^{-1}) taken at a center of mass energy corresponding to the mass of the $\Upsilon(3S)$ ($\Upsilon(2S)$) resonance. This corresponds to a sample of 122 (99) million $\Upsilon(3S)$ ($\Upsilon(2S)$) decays. The non resonant background has been studied by collecting data at center of mass energies away from the resonances.

3 Search for light Higgs bosons/axions

Higgs bosons/axions have been searched through the radiative decays of $\Upsilon(2,3S)$ mesons $\Upsilon(2,3S) \rightarrow \gamma A^0$ and A^0 decaying to the final states: *invisible*, $\tau^+\tau^-$, and $\mu^+\mu^-$.

3.1 $A^0 \rightarrow \textit{invisible}$

We study the radiative decays of the $\Upsilon(3S)$ sample; the experimental signature of an A^0 decaying to invisible is a monochromatic peak of the photon energy in the center of mass (CM) frame. The energy of the peak is given by:

$$E_\gamma = \frac{m_\Upsilon^2 - m_{A^0}^2}{2m_\Upsilon}$$

The dominant backgrounds for this analysis arise from processes like $e^+e^- \rightarrow \gamma\gamma$ and $e^+e^- \rightarrow e^+e^-\gamma$. The selection is optimized in two different regions of the photon spectrum: the High Energy Region $3.2 < E_\gamma < 5.5$ GeV, dominated by the two-photon background, and the Low Energy Region $2.2 < E_\gamma < 3.7$ GeV, dominated by radiative Bhabha events. The signal is searched for by performing a scan (in steps of 0.025-0.1 GeV) over the photon spectrum. We find no significant signal and the 90% Confidence Level (CL) upper limits we establish on the product branching fraction $BF(\Upsilon(3S) \rightarrow \gamma A^0) \times BF(A^0 \rightarrow \textit{invisible})$ (see Fig. 1) are in the range $(0.7 - 31) \times 10^{-6}$ [6].

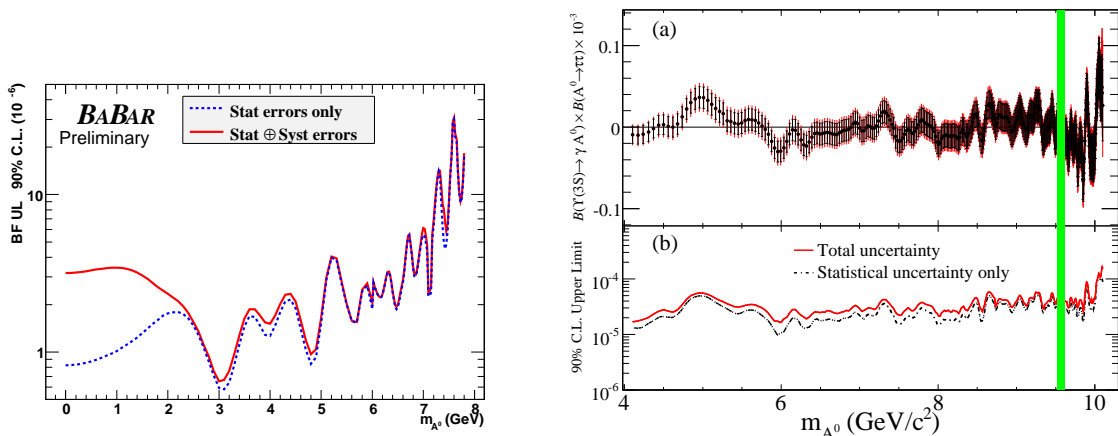


Figure 1: Left: results for the $A^0 \rightarrow \textit{invisible}$ analysis: the 90% CL upper limit on $BF(\Upsilon(3S) \rightarrow \gamma A^0) \times BF(A^0 \rightarrow \textit{invisible})$ is shown as a function of the photon energy. Right: results for the $A^0 \rightarrow \tau^+\tau^-$ analysis. Top: fitted product branching fraction $BF(\Upsilon(3S) \rightarrow \gamma A^0) \times BF(A^0 \rightarrow \tau^+\tau^-)$; bottom: 90% CL upper limits.

3.2 $A^0 \rightarrow \tau^+\tau^-$

The $\Upsilon(3S)$ sample is also used in the search for $\Upsilon(3S) \rightarrow \gamma A^0$, with $A^0 \rightarrow \tau^+\tau^-$. The τ leptons are requested to decay to either $e\nu\bar{\nu}$ or $\mu\nu\bar{\nu}$. Events with one energetic photon, two identified

leptons and missing energy consistent with the τ decays are selected. The selection is optimized in 5 different regions of the photon spectrum and the efficiency for signal events varies in the range 10 – 26%. Backgrounds arise from irreducible $e^+e^- \rightarrow \tau^+\tau^-$ events and higher order QED processes.

We look for a signal performing a scan on the photon energy spectrum ($0.2 < E_\gamma < 5.0$ GeV), fitting simultaneously the three final states (ee , $e\mu$, and $\mu\mu$). The region where $\chi_{bJ}(2P) \rightarrow \gamma\Upsilon(1S)$ is excluded from the scan. No significant signal is found and we set 90% CL upper limits (see Fig. 1) on the product branching fraction $BF(\Upsilon(3S) \rightarrow \gamma A^0) \times BF(A^0 \rightarrow \tau^+\tau^-)$ in the range $(1.5 - 16) \times 10^{-5}$ [7]. We also obtain an upper limit on the branching fraction of η_b decaying to τ pairs: $BF(\eta_b \rightarrow \tau^+\tau^-) < 8\%$.

3.3 $A^0 \rightarrow \mu^+\mu^-$

Both the $\Upsilon(2S)$ and $\Upsilon(3S)$ data samples are used in the search for $\Upsilon \rightarrow \gamma A^0$, $A^0 \rightarrow \mu^+\mu^-$. The final state is fully reconstructed by requesting one energetic photon and two charged tracks kinematically compatible with the decay of the Υ .

The signal is searched for by looking for a peak in the distribution of the *reduced mass* $m_R = \sqrt{m_{A^0}^2 - 4m_\mu^2}$. The dominant backgrounds arise from $e^+e^- \rightarrow \mu^+\mu^-\gamma$ events and by the Initial State Radiation production of the ρ , ϕ , $\psi(nS)$ and $\Upsilon(1S)$ mesons.

We perform a scan consisting of ~ 2000 points over the range $0.212 < m_{A^0} < 9.3$ GeV on the two datasets; the regions of the J/ψ and $\psi(2S)$ are excluded from the scan. We then extract the effective Yukawa coupling f_Υ of the bound $b\bar{b}$ state to the A^0 and combine the results (see Fig. 2). f_Υ is defined by:

$$\frac{BF(\Upsilon(nS) \rightarrow \gamma A^0)}{BF(\Upsilon(nS) \rightarrow \ell^+\ell^-)} = \frac{f_\Upsilon^2}{2\pi\alpha} \left(1 - \frac{m_{A^0}^2}{m_{\Upsilon(nS)}^2} \right),$$

where α is the fine structure constant. We find no significant signal [8]; we limit f_Υ to be at most 12% of the Standard Model coupling of the b quark to the Higgs boson. We also rule out the existence of a particle of 214 MeV mass suggested by the HyperCP results.

4 Test of Lepton Universality

In the Standard Model, the coupling of leptons with gauge bosons is independent of the lepton flavor. The existence of non-SM particles can be inferred from deviations from the predictions of the branching fractions of the $\Upsilon(1S)$ meson to lepton pairs.

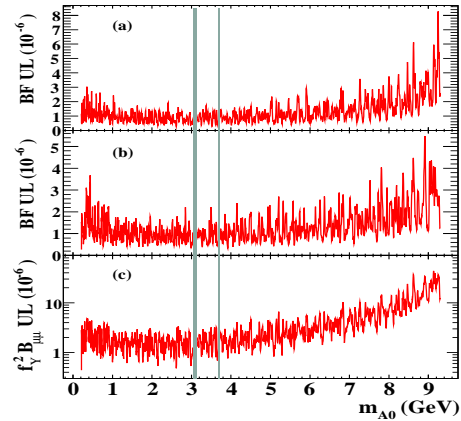


Figure 2: 90% CL upper limits on the product branching fractions of $\Upsilon \rightarrow \gamma A^0$, $A^0 \rightarrow \mu\mu$ for the $\Upsilon(2S)$ sample (top) and the $\Upsilon(3S)$ (middle). The bottom plot shows the combination of the above results in terms of the Yukawa coupling f_Υ .

The quantity:

$$R_{\tau\mu} = \frac{\Gamma_{\Upsilon(1S) \rightarrow \tau^+\tau^-}}{\Gamma_{\Upsilon(1S) \rightarrow \mu^+\mu^-}}$$

is predicted to be 1 in the Standard Model, neglecting very small corrections due to the mass difference between the two lepton species.

We study the events $\Upsilon(3S) \rightarrow \Upsilon(1S) \pi^+\pi^-$, $\Upsilon(1S) \rightarrow \mu^+\mu^-$, $\tau^+\tau^-$. The $\mu\mu$ sample is selected by fully reconstructing the event; the discriminant variables are the invariant mass of the muon pair $M(\mu^+\mu^-)$, and $\Delta M = M(\pi^+\pi^-\mu^+\mu^-) - M(\mu^+\mu^-)$. The $\tau\tau$ sample is selected requesting that the visible energy of the event is 5 GeV smaller than the collision energy, to account for the presence of the undetected neutrinos. The discriminating variable is the invariant mass of the recoiling $\pi^+\pi^-$ pair $M_{\pi^+\pi^-}$.

$R_{\tau\mu}$ is extracted from a simultaneous fit to the yields of the $\mu\mu$ and $\tau\tau$ samples. The result [9] is in agreement with the Standard Model expectations:

$$R_{\tau\mu} = 1.009 \pm 0.010 \pm 0.024,$$

where the first error is statistical and the second systematic.

5 Conclusions

The *BABAR* Collaboration performed searches for a light Higgs boson or an axion-like particle decaying to *invisible*, $\tau^+\tau^-$, and $\mu^+\mu^-$ final states in the radiative decays of $\Upsilon(nS)$ mesons. No significant signals have been found and sizable improvement over the previous upper limits set by the CLEO collaboration has been reached.

These measurements are still statistically limited; a very significant improvement in these searches could be obtained at one of the proposed *Super B-Factories*, particularly in the region around 10 GeV/ c^2 , where mixing with the η_b states can occur [10].

A significant improvement in the test of Lepton Universality has been obtained from which more stringent limits on the existence of exotic particles can be set.

References

- [1] R. Dermisek, J. F. Gunion, and B. McElrath, Phys. Rev. **D76** 051105 (2007).
- [2] O. Adriani et al., arXiv:0810.4995 [astro-ph]; arXiv:0810.4994 [astrp-ph].
- [3] Y. Nomura and J. Thaler, Phys. Rev. **D79** 075008 (2009).
- [4] HyperCP Collaboration: H. Park et al., Phys. Rev. Lett. **93** 021801 (2005).
- [5] *BABAR* Collaboration: B. Aubert et al., Nucl. Instrum. Methods Phys. Res., Sect A479, 1 (2002).
- [6] *BABAR* Collaboration: B. Aubert et al., arXiv:0808.0017 [hep-ex].
- [7] *BABAR* Collaboration: B. Aubert et al., arXiv:0906.2219 [hep-ex].
- [8] *BABAR* Collaboration: B. Aubert et al., Phys. Rev. Lett. **103** 081803 (2009).
- [9] G. Bonneaud, representing the *BABAR* Collaboration, Talk given at FPCP 2009, Lake Placid, NY, USA.
- [10] F. Domingo, U. Ellwanger, M.-A. Sanchis-Lozano, arXiv:0907.0348 [hep-ph].

Chapter 6

Indirect Astrophysical and Cosmological Searches for Axions and WISPs

Axion-like Particles and Circular Polarisation of Active Galactic Nuclei

A. Payez, J.R. Cudell, D. Hutsemékers

University of Liège, Allée du 6 Août 17, 4000 Liège, Belgium

DOI: http://dx.doi.org/10.3204/DESY-PROC-2009-05/payez_alexandre

The measurements of the linear polarisation of visible light from quasars give strong evidence for large-scale coherent orientations of their polarisation vectors in some regions of the sky. We show that these observations can be explained by the mixing of the photons with very light pseudoscalar (axion-like) particles in extragalactic magnetic fields during their propagation. We present a new treatment in terms of wave packets and discuss the circular polarisation.

1 Introduction

In this work [1], we are interested in the effect that axion-photon mixing can have on the polarisation of light coming from distant astronomical sources. In particular, the observations of redshift-dependent large-scale coherent orientations of AGN polarisation vectors can, at least qualitatively, even in very simple models, be reproduced as a result of such a mixing of incoming photons with extremely light axion-like particles in external magnetic fields. These observations, presented in the second edition of this conference [2], were based on good quality measurements of the linear polarisation for a sample of 355 measured quasars in visible light [3].

This has been discussed in terms of axion-photon mixing by several authors, in the case of plane waves [4] and a prediction from this mixing is an observable circular polarisation comparable to the linear one. Here, we present the case in which light is described by wave packets and show that the circular polarisation can be suppressed with respect to the plane wave case.

2 Axion-photon mixing using Gaussian wave packets

2.1 The idea behind this

The mixing of axion-like particles with photons is usually discussed mathematically in terms of infinite plane waves. Using that description, the Stokes parameters can be computed and predictions of the polarisation of light from the interaction can be given; the main properties of such a mixing being *dichroism* and *birefringence* (see [5] for a review of this case). While dichroism would be an interesting way to produce linear polarisation and, in particular, to explain the observations concerning quasars, birefringence—which is linked to the creation of circular polarisation—would give a very clear signature of the mixing. Indeed, in this formalism

of plane waves, except in extremely specific cases, the *circular polarisation* predicted *can be as large as the linear polarisation*¹.

The idea discussed here is to send wave packets into a region of uniform magnetic field and to compute the Stokes parameters. Before the magnetic field, the wave packets have the form:

$$E(x, t) = \int_{\omega_p}^{\infty} \frac{d\omega}{N} e^{-\frac{a^2}{4}(\omega-\omega_0)^2} e^{i\sqrt{\omega^2-\omega_p^2}(x-x_0)} e^{-i\omega(t-t_0)}, \quad (1)$$

where ω_p is the plasma frequency of the medium and a controls the initial width of the packet (in the limit $a \rightarrow +\infty$, this reduces to the plane wave case).

The main motivation for considering this formalism comes from the measurements of circular polarisation of some of the quasars considered in [3]. While axion-photon mixing would be an attractive explanation of the observations for linear polarisation, preliminary results show that circular polarisation of light from these AGN seems to be, in general, *much smaller* than the linear polarisation [6]. This means that if the creation of circular polarisation was really a smoking gun of ALP-photon mixing, no matter how refined the description, these observations would rule out the mixing mechanism and could only be used to constrain the existence of axion-like particles.

For these reasons, it can be interesting to work with wave packets, as new effects will be taken into account, including dispersion, separation of packets and coherence; effects that might be of importance for the Stokes parameters. Note that calculating the propagation of packets of the form (1) is numerically² tricky, as the computation of the Stokes parameters requires a spatial resolution of the order of the width of the wave packets after a propagation over huge distances in the magnetic field (we will usually consider one magnetic field zone of 10 Mpc [7] and initial wave packets of width $\lesssim 1\mu\text{m}$).

2.2 Results with wave packets

In the plane transverse to the direction of propagation, we choose a basis of two orthogonal linear polarisations, the same as the one used in the plane wave case, so that we will talk about polarisation parallel or perpendicular to the transverse external magnetic field \vec{B} . This being done, we next choose the electric fields $E_{\parallel}(x, t)$ and $E_{\perp}(x, t)$ both initially described by a function of the form (1). Then, we propagate these using the equations of motion for the electromagnetic field which take into account the interaction with pseudoscalar particles and find the expressions of the electric fields after a propagation, when axion-photon mixing is at work, inside a step-like magnetic field region.

We can then use the expressions of the Stokes parameters —which are observables built on intensities— that can, for example, be plotted as functions of x , the distance travelled inside the magnetic field, for a given propagation time, T . This is what is represented in Figure 1 which shows what the two packets look like (respectively $\mathcal{I}_{\parallel}(x, t = T)$ and $\mathcal{I}_{\perp}(x, t = T)$) but also the total intensity (which is just the sum of the two) and the unnormalised circular polarisation, $\mathcal{V}(x, t = T)$. This is for a beam with a central wavelength $\lambda_0 = 500$ nm, initially 100% linearly polarised, with its polarisation plane making a 45° angle initially with the magnetic

¹This is what one obtains if one does not assume very specific distributions of magnetic field orientations along the line of sight.

²We use Multiple-Precision Floating-point library with correct Rounding: www.mpfpr.org.

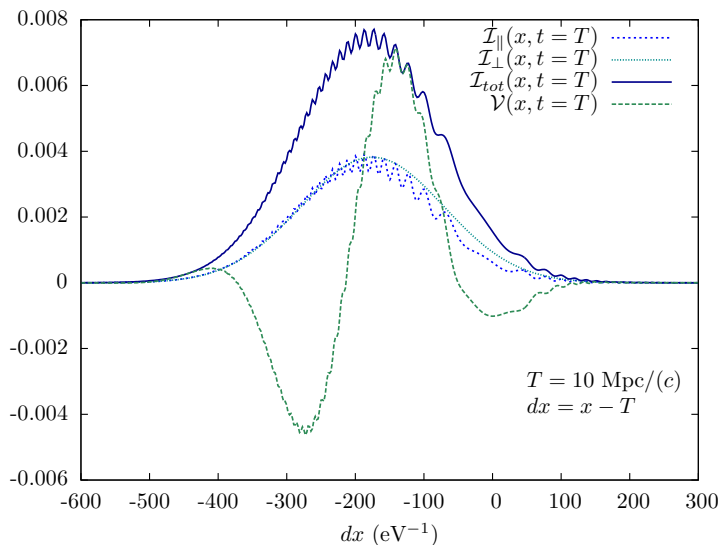


Figure 1: Wave packets: illustration after a propagation time T in an external magnetic field, in a strong mixing case —here, the axion mass is $m = 4.7 \cdot 10^{-14}$ eV, $\omega_p = 3.7 \cdot 10^{-14}$ eV and $g\mathcal{B} = 5.5 \cdot 10^{-29}$ eV. The initial width of the wave packet has been chosen $\simeq \lambda_0$.

field direction (i.e. $u(0) = \frac{U(0)}{I(0)} = 1$; $q(0) = v(0) = 0$)³; this angle being, in fact, the most favourable one for the creation of circular polarisation, due to birefringence. Note also that the abscissa is dx , the shift in position with respect to a frame moving at the speed of light c (namely, a maximum at $dx = 0$ corresponds to $|\vec{v}| = c$).

From the observational point of view, there is a macroscopic exposure time over which one should integrate these functions to obtain, finally, the value of the observable Stokes parameters, e.g.:

$$I(x) = \int_{\text{exposure time}} dt \mathcal{I}(x, t).$$

From these integrals, we obtain that the wave packet formalism leads to a circular polarisation, $v = \frac{V}{I}$, lowered with respect to plane wave case. Figure 2 illustrates the plane wave ($a \rightarrow \infty$) result: it shows the amount of circular polarisation gained due to axion-photon mixing with different values of the coupling $g\mathcal{B}$ (g being the axion-photon coupling constant). In that simpler case, it is known that $v = \frac{V}{I}$ oscillates between $-|u(0)|$ and $|u(0)|$, whereas in the wave packet case it is shown that there is a damping of these oscillations. It follows from this observation that v is no longer expected to be as large as the linear polarisation in general.

³ u and q are the two Stokes parameters required to describe fully the linear polarisation of a light beam, while v accounts for the circular polarisation.

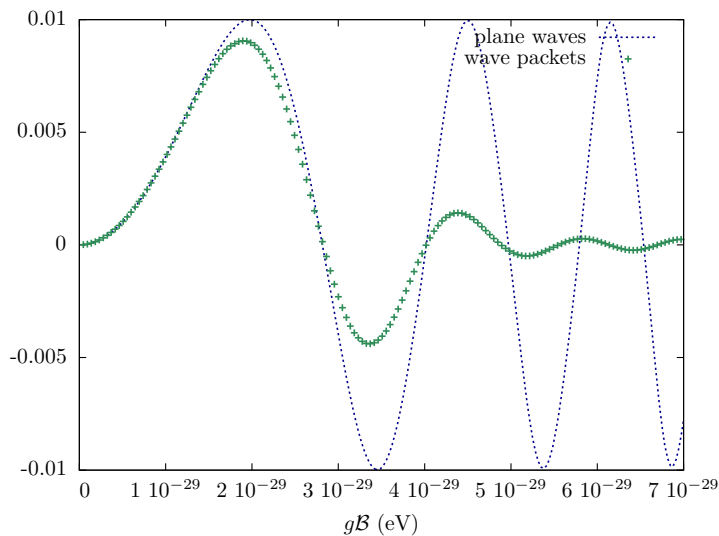


Figure 2: Circular polarisation for different values of the coupling in the case of initially partially linearly polarised light with $u(0) = 0.01$. λ_0 , ω_p —and a , for the wave packet— are the same as in Figure 1, other parameters are: $T = 10$ Mpc, $m = 4.3 \cdot 10^{-14}$ eV.

3 Conclusion

We have briefly presented axion-photon mixing with the use of wave packets. The main consequence of this treatment is the net decrease of circular polarisation with respect to what is predicted using plane waves. Hence, the lack of circular polarisation in the light from AGN does not rule out the ALP-photon mixing.

Acknowledgements

A. P. would like to thank the IISN for funding and to acknowledge constructive discussions on physical and numerical matters with Fredrik Sandin and Davide Mancusi.

References

- [1] A. Payez *et al.*, in preparation.
- [2] D. Hutsemékers, talk presented at the 2nd Joint ILIAS-CAST-CERN Axion Training Workshop, 2006
- [3] D. Hutsemékers, *A&A* **332** 410 (1998); D. Hutsemékers and H. Lamy, *A&A* **367** 381 (2001); D. Sluse *et al.*, *A&A* **433** 757 (2005); D. Hutsemékers *et al.*, *A&A* **441** 915 (2005).
- [4] See, for example, S. Das *et al.*, *JCAP* **0506** 002 (2005); D. Hutsemékers *et al.*, to appear in the Proceedings of the Astronomical Polarimetry 2008, July 6-11, 2008, Quebec (Canada), P. Bastien and N. Manset (Eds.), ASP Conf. Series [arXiv:0809.3088]; C. Burrage, A.C. Davis and D.J. Shaw, *Phys. Rev D* **79** 044028 (2009).
- [5] A. Payez, J.R. Cudell and D. Hutsemékers, *AIP Conf. Proc.* **1038** 211 (2008) [arXiv:0805.3946].
- [6] D. Hutsemékers *et al.*, in preparation.
- [7] J.P. Vallée, *Astron. J.* **99** 459 (1990).

Solar X-rays from Axions: Rest-Mass Dependent Signatures

Konstantin Zioutas¹, Mary Tsagri^{1,2}, Yannis Semertzidis³, Thomas Papaevangelou⁴, Antonios Gardikiotis¹, Theopisti Dafni^{5*} and Vassilis Anastassopoulos¹

¹University of Patras, Patras, Greece

²CERN, 1211 Geneve 23, Switzerland

³Brookhaven National Laboratory, Upton, NY, USA

⁴IRFU, Centre d' Études Nucleaires de Saclay, Gif-sur-Yvette, France

⁵Laboratorio de Física Nuclear y Astropartículas, Universidad de Zaragoza, Zaragoza, Spain

DOI: <http://dx.doi.org/10.3204/DESY-PROC-2009-05/zioutas.konstantin>

The spectral shape of solar X-rays is a power law. The more active the Sun is, the less steep the distribution. This behaviour can be explained by axion regeneration to X-rays occurring ~ 400 km deep into the photosphere. Their down-comptonization reproduces the measured spectral shape, pointing at axions with rest mass $m_a \sim 17$ meV/ c^2 , without contradicting astrophysical-laboratory limits. Directly measured soft X-ray spectra from the extremely quiet Sun during 2009 (SphinX mission), though hitherto overlooked, fit the axion scenario.

1 General considerations

A first, rough comparison between the visible Sun (~ 5800 K) and the well studied infant Universe [1] at a rather similar temperature (~ 3000 K) is interesting due to the striking contrast between the perfect blackbody distribution and the equivalent one from the Sun. If the predicted and measured tiniest fluctuations of the cosmic plasma of $\Delta T/T \sim 10^{-5}$ provide(d) fundamental new physics, one is even more tempted to conclude that the unpredictable and huge solar atmospheric fluctuations ($\Delta T/T \sim 10^3$), of otherwise unknown origin, might well be the imprints of hidden new physics beyond the standard (solar) model. One fundamental difference to be noted is the quasi-zero magnetic field in the cosmic plasma versus the unpredictably varying huge-sized solar magnetic fields in the Tesla scale. Is this already an indication for axions or the like? We follow this simplified but observationally driven question, arriving at atypical axion signatures in solar soft and hard X-rays. Remarkably, solar X-ray emission, above its steady component, follows spatio-temporally magnetic activity. Though, the (quiet) Sun X-rays are conservatively unexpected from a cold star as our Sun, and this is the solar coronal heating problem (since 1939), which otherwise remains '*one of the most perplexing and unsolved problems in astrophysics to date*' [1]. To put it differently, there is no lack of problems with solar X-ray emission. This and this kind of reasoning was behind the motivation of our approach of the solar axions or other particles with similar properties.

*E-mail address: Theopisti.Dafni@cern.ch

2 Solar magnetism as proxy for the CAST magnet

The CAST configuration is expected to transform one day solar axions to X-rays. Such processes can take place also elsewhere, e.g. at the Sun. Thus, the working principle of the short man-made axion helioscopes might be at work in large scales near the solar surface, thanks to the ubiquitous solar magnetism. These places can act then as natural axion-to-photon converters, which for some occasionally (spatiotemporally) occurring parameter ‘fine tuning’ might be much more efficient than any earth bound axion experiment. In fact, the rapid radial density change of the static Sun plus its wide dynamical excursions might well perform an accordingly wide plasma density scan that includes the axion resonance, i.e. the density which matches the axion rest mass ($\hbar\omega_{\text{pl}} \approx m_{\text{a}}c^2$). In addition, near the solar surface, this can give rise to a rather large coherence length ($>1-10$ km) due to the large photon mean free path length associated with the low density and low Z solar gas. Inside a specific solar layer, the resonance condition can indeed restore coherence over large distances, provided the axion rest mass is above ~ 10 meV/ c^2 . Both, a large oscillation length and a large transverse magnetic field component maximize the axion to photon conversion ($\propto B^2L^2$). And, it is this solar synergism which earth axion experiments try actually to restore, though with inherent practical limitations.

3 Solar axion(-like) signatures

No analog solar X-ray spectrum is even remotely similar to that expected from converted solar axions as they are outstreaming from the hot core [1]. Instead, all analog solar spectra, be it from the quiet Sun, be it from its (non-)flaring active regions, follow an actually ‘colorless’ power law shape, at least at first sight. But, is this expectation correct? To check this, we performed Monte Carlo simulation with the Geant4 code, which allows to follow the propagation of magnetically converted axions to X-rays below the solar surface. We argued in [1] how puzzling solar behaviour still fits the axion scenario, revising the so far widely mentioned picture [2], which predicts a bright X-ray spot, at the solar disc centre, from coherently converted pseudoscalars outstreaming from the solar core. But such a spot has not been detected as yet. We arrive, however, at different conclusions after comparing our simulation results with solar X-ray observations, which originate from the whole magnetic solar surface, pointing at the photosphere and/or the (lower) chromosphere as the actual axion-to-photon conversion layer. Thus, following the simulation of the propagation of X-rays in the outer layers of the Sun [1], the observed solar spectral shape can result from an axion conversion occurring in the upper solar sub-surface; the emerging X-rays undergo a down-comptonisation while propagating in a random walk towards the ‘visible’ solar surface, i.e. before escaping in free space isotropically. The concluded depth of the conversion was at about 350 km underneath the surface implying a rest mass of the axions or axion-like particles of ~ 17 meV/ c^2 . Note, in contrast, previous work [2] assumed the pseudoscalar conversion to occur above the solar surface, implying a rest mass (far) below $\sim 10^{-4}$ eV/ c^2 . Thus, there is no contradiction between these two otherwise complementary approaches, though their spectral shape and spatial origin of the X-rays from the Sun are completely different. In the past, the various solar X-ray activities have been overlooked as being axion in origin, because of their ‘wrong’ spectral shape and topology, while their strong brightness could not fit our quasi-prejudice that a signature from a dark matter particle candidate should be extremely faint.

Here we give a few more atypical solar axion signatures (for more details see section 6.2

in [1]). In fact, the ~ 10 MK hot solar corona above non-flaring active regions is a remarkably high temperature and of potential interest. It is worth mentioning that the corresponding quiet Sun corona temperature is ‘only’ 1-2 MK and that of the dramatic flares is about 10-20 MK, i.e. it is not much different, while neither the source nor acceleration mechanisms of the particles involved have been understood. Then, it is not unreasonable to assume that in all locations, i.e. quiet Sun, flaring and not-flaring active regions, a similar mechanism might be at work. Thus, also the otherwise unexpected soft X-ray emission from the quiet Sun can be driven by the same axion-regeneration mechanism, but occurring a little deeper into the solar subsurface. This explains, then, why the shape of the quiet Sun analog spectrum is similar, though much steeper and feebler due to more (in)elastic interactions [1]. Interestingly, helioseismology unravels subsurface differences between active and quiet regions: the stronger the surface magnetic field, the smaller the magnetic effects in the deeper layers, and vice versa [3]. Moreover, the magnetic effects in the deeper layers are the strongest in the quiet regions, consistent with the fact that these are basically regions with weakest magnetic fields at the surface.

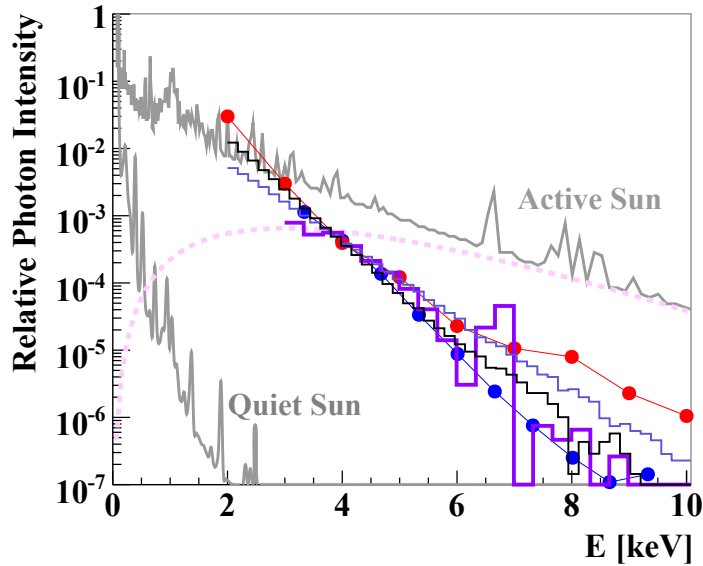


Figure 1: Solar X-ray spectra: Quiet and Active Sun (reconstructed)[1]. The other directly measured spectra (RESIK, RHESSI) refer to a flare (red)[4], non-flaring Sun (blue)[5] and pre-flaring periods (purple) after having subtracted the main X-ray flare component [6], whose distribution coincides with that of the ‘Active Sun’ above 3 keV (not shown). Two thin lines, black and blue, show the expected shape of reconverted outstreaming solar axions at a depth of 400 km and 350 km below the solar surface, respectively. The dashed line shows the initial X-ray spectrum from converted solar axions (for a recent directly measured quiet Sun X-ray spectrum, see [7]). *Note: the distributions are not to scale, emphasis is given to their shape.*

Figure 1 gives the analog spectra from the quiet and flaring Sun as well as from non-flaring active regions, including preflare periods. All spectra show actually a strikingly similar linear distribution in the log-lin plot, as expected from Geant4 simulation [1]. Especially, the recently

directly measured quiet Sun spectrum above 1 keV with the SphinX mission [7] confirms a perfect linear shape. The figure also gives the directly measured spectral shape of the emitted X-rays from the non-flaring Sun [5], a solar flare [4] and pre-flaring periods [6]. It is interesting to point out here that nothing requires a solar emission to be always from a high-temperature plasma, though it is usually offered as the simplest explanation [8], even more so if its energy source is unknown (e.g. the solar corona heating problem). Only their power law exponent is different from case to case (Fig. 1), with the quiet and flaring Sun being the two extreme cases, which is reasonable following the axion scenario [1]. Furthermore, it is widely accepted that flares are magnetic in origin, although their trigger remains elusive [10]. Interestingly, the peak of a flare X-ray intensity vs. B_{max} indicates a B^2 dependence [11]. In particular, the non-flaring active region AR7978 provided an excellent L_x vs. B^2 dependence, as it is expected from the Primakoff effect [9]; to have such a dependence for the soft X-rays, where the energy distribution from converted solar axions gets reduced (dashed line in Fig. 1), an energy degradation is required. The suggested multiple Compton scatterings allows this to happen [1].

4 Conclusion

The considered solar analog spectra fit an axion scenario starting a few 100 km below the solar surface, where outstreaming solar axions from the hot core, with a rest mass around $17 \text{ meV}/c^2$, can coherently convert to X-rays. The exact depth varies from case to case, depending on the actual solar conditions like density and magnetic field configuration, which, in addition, change dynamically continuously. The quiet/non-flaring solar X-ray brightness can be qualitatively (spectrum shape) and quantitatively (yield) reconstructed without the need to invent new physics beyond that of the standard QCD axions. However, to explain quantitatively also the active or even flaring Sun within the same scenario, one is forced to assume (much) stronger magnetic fields and/or larger conversion lengths due to an occasionally occurring ‘fine tuning’ between local density and axion(-like) rest mass; that this may happen occasionally is not far-fetched, since the more rare these ‘explosive’ solar events are, the more powerful they appear.

References

- [1] K. Zioutas, M. Tsagri, Y. Semertzidis, T. Papaevangelou, T. Dafni and V. Anastassopoulos, *New J. Phys.* **11** (2009) 105020 [arXiv:0903.1807 [astro-ph.SR]], and references therein.
- [2] E. D. Carlson and L. S. Tseng, *Phys. Lett. B* **365** 193 (1996).
- [3] C. H. Lin, S. Basu and L. Li, *Solar Physics* **257** 37 (2009), [arXiv:0809.1427v1 [astro-ph]].
- [4] J. Sylwester *et al.*, *Solar System Res.* **3479** (2005).
- [5] J.M. McTiernan, *ApJ*. **697** 94 (2009);
J. McTiernan and J. Klimchuk, sprg.ssl.berkeley.edu/~jim/hessi/agu2003_poster.ppt, AGU Meeting 2003.
- [6] M. Battaglia, L. Fletcher and A.O. Benz, *Astron. Astroph.* **498** 891 (2009) arXiv:0903.2754v1 [astro-ph.SR].
- [7] J. Sylwester, http://www.cbk.pan.wroc.pl/body/publikacje/2009/js_saariselka_sphinx.pdf;
http://www.cbk.pan.wroc.pl/body/publikacje/2009/SphinX_JS_Sorrento.pdf.
- [8] J. McTiernan, private communication, July 2009
- [9] K. Zioutas, K. Dennerl, M. Grande, D. H. H. Hoffmann, J. Huovelin, B. Lakic, S. Orlando, A. Ortiz, T. Papaevangelou, Y. Semertzidis, S. Tzamarias and O. Vilhu, *J. Phys. Conf. Ser.* **39** (2006) 103.
- [10] K. Zioutas, M. Tsagri, Y. Semertzidis and T. Papaevangelou, arXiv:0808.1545.
- [11] K. Zioutas, M. Tsagri, Y. Semertzidis, T. Papaevangelou, A. Nordt and V. Anastassopoulos, *Proc. Int. Conf. on Identification of Dark Matter (Rhodes)* (World Scientific) (2007) p 372 [astro-ph/0701627v6].

Cosmological axion bounds

Steen Hannestad¹, Jan Hamann¹, Alessandro Mirizzi², Georg G. Raffelt³, Yvonne Y. Y. Wong⁴

¹ Department of Physics and Astronomy, University of Aarhus, DK-8000 Aarhus C, Denmark

² Institut für theoretische Physik, Universität Hamburg, Luruper Chaussee 149, D-22761 Hamburg, Germany

³ Max-Planck-Institut für Physik (Werner-Heisenberg-Institut), Föhringer Ring 6, D-80805 München, Germany

⁴ Institut für Theoretische Physik E, RWTH Aachen University, D-52056 Aachen, Germany

DOI: <http://dx.doi.org/10.3204/DESY-PROC-2009-05/hannestad.steen>

We discuss current cosmological constraints on axions, as well as future sensitivities. Bounds on axion hot dark matter are discussed first, and subsequently we discuss both current and future sensitivity to models in which axions play the role as cold dark matter, but where the Peccei-Quinn symmetry is not restored during reheating.

The Peccei-Quinn (PQ) mechanism provides a simple explanation for the smallness of the QCD Θ parameter [1]. A consequence of this is the existence of axions, low mass pseudoscalars similar to pions, except that their mass and coupling strength are suppressed by a factor f_π/f_a , where $f_\pi \simeq 93$ MeV and f_a is the PQ scale. The axion mass is given by the relation

$$m_a = \frac{z^{1/2}}{1+z} \frac{f_\pi m_\pi}{f_a} = \frac{6 \text{ eV}}{f_a/10^6 \text{ GeV}}, \quad (1)$$

where $z \equiv m_u/m_d \sim 0.3 - 0.6$. Thus, there is a tight relation between m_a and f_a , known as the axion line. Axions couple to photons with a coupling $g_{a\gamma}$ of order $g_{a\gamma} \sim \frac{\alpha}{f_a}$ and are therefore in principle detectable even if f_a is much larger than the electroweak energy scale. A large number of direct detection experiments use this coupling to photons to search for axions, and are described in detail elsewhere in these proceedings.

Astrophysics also provides a stringent bound on the axion-photon coupling (see [2] for a thorough discussion). The most restrictive bound comes from constraints on the horizontal branch (HB) lifetime of globular cluster stars. If an additional source of energy loss from the core is present, the core Helium burning phase can be shortened to a point where the predicted number of HB stars in a globular cluster is in conflict with observations. The bound from this argument roughly corresponds to $g_{a\gamma} \lesssim 10^{-10} \text{ GeV}^{-1}$.

While this bound is formally very stringent, it is also model dependent, and it is possible to construct models with an axion photon coupling much smaller than the normally predicted α/f_a . However, in this case cosmology provides an important lower bound on f_a coming from the unavoidable coupling of axions to quarks. In this case, the main thermalisation mechanism is axion-pion conversion, $a\pi \leftrightarrow \pi\pi$. Provided that $f_a \lesssim \text{few} \times 10^7 \text{ GeV}$ axions couple sufficiently strongly to thermalise completely after the QCD phase transition at $T \sim 150$ MeV. If this is the case axions automatically provide a source of hot dark matter because they will have masses in the eV range.

Therefore, cosmological constraints on light neutrinos can be also be applied to axions in this range. The current upper bound on the axion mass is of order 0.5-1 eV [3, 4], corresponding to $f_a \gtrsim 10^7$ GeV. Fig. 1, taken from [4], shows the bound on m_a and $\sum m_\nu$ simultaneously.

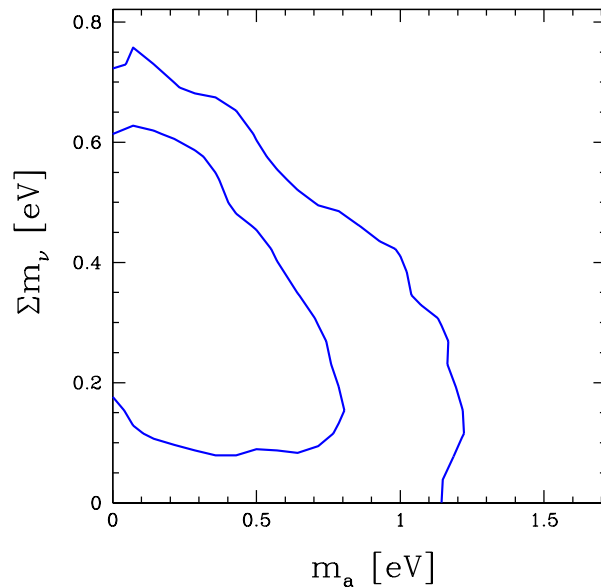


Figure 1: 68% and 95% contours in the $\sum m_\nu$ - m_a plane (taken from Ref. [4]).

If the PQ scale is much higher, axions never thermalise in the early universe, and their presence is caused solely by non-thermal production. During the QCD epoch of the early universe, a non-thermal mechanism produces axions as nonrelativistic coherent field oscillations that can play the role of cold dark matter [5]. In terms of the initial “misalignment angle” $\Theta_i = a_i/f_a$ relative to the CP-conserving minimum of the axion potential, the cosmic axion density is [6]

$$\omega_a = \Omega_a h^2 \simeq 0.195 \Theta_i^2 \left(\frac{f_a}{10^{12} \text{ GeV}} \right)^{1.184}. \quad (2)$$

If Θ_i^2 is of order unity, axions provide the dark matter of the universe if $f_a \sim 10^{12}$ GeV ($m_a \sim 10 \mu\text{eV}$).

One may also consider axions in another range beyond the classical cosmological window. In a scenario where the PQ symmetry is not restored during or after inflation, a single value $-\pi < \Theta_i < +\pi$ determines the axion density in our Hubble volume. It is possible that $\Theta_i \ll 1$, allowing for $f_a \gg 10^{12}$ GeV. This “anthropic axion window” is motivated because the PQ mechanism presumably is embedded in a greater framework. In particular, the PQ symmetry emerges naturally in many string scenarios, where f_a is naturally high (see also [7]).

An interesting signature of such a high f_a is the presence of primordial isocurvature fluctuations that can show up in future data. When axions acquire a mass during the QCD epoch, axion field fluctuations from the de Sitter expansion during inflation become dynamically relevant in the form of isocurvature fluctuations that are uncorrelated with the adiabatic fluctuations inherited by all other matter and radiation from the inflaton field. The isocurvature amplitude

depends on both f_a and H_I , the Hubble parameter during inflation, so observational limits on isocurvature fluctuations exclude certain regions in this parameter space [8, 9]. Since there is no trace of isocurvature fluctuations in existing data, perhaps a more interesting question is the remaining window for axions to show up in future data.

Now going into slightly more detail, when the PQ symmetry breaks at some large temperature $T \sim v_{\text{PQ}}$, the relevant Higgs field will settle in a minimum corresponding to $\Theta_i = a_i/f_a$, where $-\pi \leq \Theta_i \leq +\pi$. We assume that this happens before cosmic inflation, so throughout our observable universe we have the same initial condition except for fluctuations imprinted by inflation itself. The cosmic energy density in axions is given by Eq. (2) with Θ_i^2 replaced by $\langle \Theta^2 \rangle_i = \Theta_i^2 + \sigma_\Theta^2$, where $\sigma_\Theta^2 = H_I^2/(4\pi^2 f_a^2)$ is the inflation-induced variance, with H_I the Hubble parameter during inflation. All cosmologically viable models have $\Theta_i^2 \gg \sigma_\Theta^2$. Assuming that all of the cold dark matter consists of axions, according to current cosmological data $\omega_a = \omega_c = 0.109 \pm 0.004$. Assuming σ_Θ is small, one finds $\Theta_i = 0.748 \left(\frac{10^{12} \text{ GeV}}{f_a} \right)^{0.592}$ as a unique relationship between the initial misalignment angle and the axion decay constant.

As mentioned, axion-induced isocurvature fluctuations are uncorrelated with the adiabatic fluctuations inherited by other matter and radiation components from the inflaton, and the isocurvature fraction, α , of the total fluctuation power spectrum is given by [10]

$$\alpha \simeq 7.5 \times 10^{-3} \left(\frac{2.4 \times 10^{-9}}{A_S} \right) \left(\frac{0.109}{\omega_c} \right) \left(\frac{H_I}{10^7 \text{ GeV}} \right)^2 \left(\frac{10^{12} \text{ GeV}}{f_a} \right)^{0.816}, \quad (3)$$

where $A_S = \mathcal{P}(k = k_0)$ is the amplitude of the total primordial scalar power spectrum at the pivot scale $k_0 = 0.002 \text{ Mpc}^{-1}$.

[10] considered several different current and future data sets in order to constrain α : 1) Current data: WMAP plus auxiliary data sets. 2) Planck: Simulated TT , TE and EE spectra up to $\ell = 2000$ from the Planck satellite [11]. 3) CVL: Simulated, noiseless TT , TE and EE spectra up to $\ell = 2000$. Roughly equivalent to the projected CMBPol experiment [12].

Data set 1 gives $\alpha < 0.09$ at 95% confidence, consistent with the findings of Komatsu et al. [9]. For the future experiments and if no isocurvature signal shows up, we forecast 95%-credible upper limits of $\alpha < 0.042$ for Planck and $\alpha < 0.017$ for CVL.

The constraints and sensitivity forecasts on the isocurvature fraction α can be translated into axion parameters using equation (3). It can be written in the form

$$H_I = 3.5 \times 10^7 \text{ GeV} \left(\frac{\alpha}{0.09} \right)^{1/2} \left(\frac{\omega_c}{0.109} \right)^{1/2} \left(\frac{f_a}{10^{12} \text{ GeV}} \right)^{0.408}, \quad (4)$$

where the present upper bound on α has been used as a benchmark. Assuming axions are the dark matter, this constraint is shown in Fig. 2 with a line marked $\alpha = 0.09$. In this plot, taken from [10], we also show the relationship between f_a and Θ_i as dashed lines. Future sensitivities to α from Planck and CVL are shown labelled with the appropriate α values.

In conclusion, axions have a number of potentially very important consequences for cosmology, depending entirely on the value of the PQ symmetry breaking scale.

For low values of the breaking scale, axions are thermalised in the early universe and can act as a hot dark matter component. Such scenarios can be constrained by current observations of large scale structure, and while these constraints are formally much less stringent than astrophysical bounds using the axion-photon coupling, they are also less model dependent.

At intermediate scales, $f_a \sim 10^{12} \text{ GeV}$, axions may naturally act as a CDM candidate.

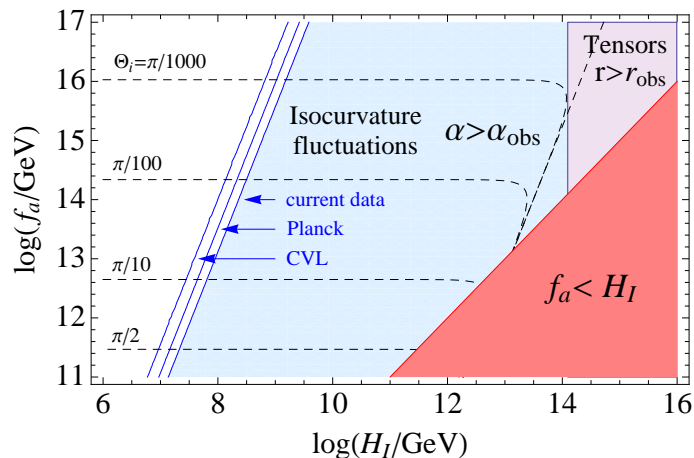


Figure 2: Exclusion and sensitivity regions in the plane of H_I (Hubble rate during inflation) and f_a (axion decay constant), assuming axions are all of the dark matter. The isocurvature exclusion region based on current data is shown in light blue. The sensitivity forecasts for Planck and CVL are also indicated. The dashed lines indicate the required Θ_i for a given f_a to obtain the full amount of axion dark matter. We also show the region of excessive tensor modes and the region $f_a < H_I$ where our late-inflation scenario is not applicable.

At the other end of the scale, a very high value of the PQ scale may also provide axion cold dark matter, but in this case there may be additional observational signatures in the form of axion isocurvature fluctuations. Such an isocurvature component could plausibly be observed by future CMB experiments, and would provide a very interesting new window on both axion physics and early universe cosmology.

References

- [1] R. D. Peccei, Lect. Notes Phys. **741** (2008) 3; J. E. Kim and G. Carosi, Rev. Mod. Phys., to be published (arXiv:0807.3125)
- [2] G. G. Raffelt, Lect. Notes Phys. **741**, 51 (2008).
- [3] S. Hannestad, A. Mirizzi and G. Raffelt, JCAP **0507** (2005) 002; A. Melchiorri, O. Mena and A. Slosar, Phys. Rev. D **76** (2007) 041303.
- [4] S. Hannestad, A. Mirizzi, G. G. Raffelt and Y. Y. Y. Wong, JCAP **0804** (2008) 019.
- [5] P. Sikivie, Lect. Notes Phys. **741** (2008) 19.
- [6] K. J. Bae, J. H. Huh and J. E. Kim, JCAP **0809** (2008) 005.
- [7] So-Young Pi, Phys. Rev. Lett. **52** (1984) 1725; A. D. Linde, Phys. Lett. B **201** (1988) 437; M. Tegmark, A. Aguirre, M. Rees and F. Wilczek, Phys. Rev. D **73** (2006) 023505.
- [8] D. H. Lyth, Phys. Lett. B **236** (1990) 408; M. Beltrán, J. García-Bellido and J. Lesgourgues, Phys. Rev. D **75** (2007) 103507; M. P. Hertzberg, M. Tegmark and F. Wilczek, Phys. Rev. D **78** (2008) 083507; L. Visinelli and P. Gondolo, Phys. Rev. D **80**, 035024 (2009).
- [9] E. Komatsu *et al.* [WMAP Collaboration], Astrophys. J. Suppl. **180** (2009) 330.
- [10] J. Hamann, S. Hannestad, G. G. Raffelt and Y. Y. Y. Wong, JCAP **0906**, 022 (2009).
- [11] M. Bersanelli *et al.*, eds., [Planck Science Team], arXiv:astro-ph/0604069.
- [12] D. Baumann *et al.* [CMBPol Study Team Collaboration], AIP Conf. Proc. **1141**, 10 (2009).

Chapter 7

Tentative Signals for WISPs

Searching for Axion-like Particles with Active Galactic Nuclei

Clare Burrage¹, Anne-Christine Davis², Douglas J. Shaw³

¹Theory Group, Deutsches Elektronen-Synchrotron DESY, 22607 Hamburg, Germany

²Department of Applied Mathematics and Theoretical Physics, Centre for Mathematical Sciences, Cambridge CB3 0WA, United Kingdom

³Queen Mary University of London, Astronomy Unit, School of Mathematical Sciences, Mile End Road, London E1 4NS, United Kingdom

DOI: http://dx.doi.org/10.3204/DESY-PROC-2009-05/burrage_clare

Strong mixing between photons and axion-like particles in the magnetic fields of clusters of galaxies induces a scatter in the observed luminosities of compact sources in the cluster. This is used to construct a new test for axion-like particles; applied to observations of active galactic nuclei it is strongly suggestive of the existence of a light axion-like particle.

1 Introduction

An Axion-Like Particle (ALP) is any scalar or pseudo-scalar field which couples to the kinetic terms of the photon. The pseudo scalar coupling to photons is identical to that of the axion; $\mathcal{L} \supset \frac{\phi}{4M} \epsilon_{\mu\nu\lambda\rho} F^{\mu\nu} F^{\lambda\rho}$, and a scalar field couples through the Lagrangian term; $\mathcal{L} \supset \frac{\phi}{4M} F_{\mu\nu} F^{\mu\nu}$. The presence of contact interactions between ALPs and photons means that ALPs affect the propagation of photons through a magnetic field. In such an environment a photon can oscillate into an ALP with probability [1]

$$P(z) = \sin^2 2\theta \sin^2 \left(\frac{\Delta(z)}{\cos 2\theta} \right). \quad (1)$$

Here z is the distance traveled, $\Delta(z) = m_{eff}^2 z / 4\omega$ and $\tan 2\theta = 2B\omega / Mm_{eff}^2$. $m_{eff}^2 = |m_\phi^2 - \omega_P^2|$, m_ϕ is the ALP mass, ω_P the plasma frequency of the medium, ω the photon frequency, B the magnetic field strength and M the strength of the photon-ALP coupling.

In these proceedings we describe a new test for ALPs which looks for the effects induced by strong ALP-photon mixing on the luminosity of astronomical objects observed through the magnetic fields of galaxy clusters. Our results apply to ALPs with masses $m_\phi \lesssim 10^{-12}$ eV. The constraints on the couplings of such ALPs are: 10^{11} GeV $\lesssim M$ for pseudo-scalars [2], and 10^{26} GeV $\lesssim M$ for scalars [3]. However a subclass of scalar ALPs known as *chameleonic* [4] ALPs avoid these constraints because their mass depends on the local density, their coupling is required to satisfy 10^9 GeV $\lesssim M$ [5].

2 Astronomy with ALPs

The magnetic fields of galaxy clusters fluctuate on many different scales. However, at the high frequencies we consider in what follows the simple cell magnetic field model can be shown to give the same results for ALP-photon mixing as modeling the variations in the magnetic field with a power spectrum. The cell model of the magnetic field assumes the field is made up of a large number of equally sized magnetic domains. The magnitude of the field strength is the same in each domain but the orientation of the field is randomly chosen.

When the probability of mixing between ALPs and photons is large the system of photons and ALPs can be evolved through a large number of randomly oriented magnetic domains analytically; this is known as the strong mixing limit. If L is the size of a magnetic domain, N the number of domains traversed and $P \equiv P(L)$ is the probability of photon to ALP conversion in one magnetic domain, we say that strong mixing occurs when $NP \gg 1$ and $N\Delta(L) \lesssim \pi/2$. In this limit the probability of mixing is large, and frequency independent. Strong mixing occurs in the magnetic fields of galaxy clusters for x-ray or gamma-ray photons if $M \lesssim 10^{11}$ GeV, assuming $m_\phi \lesssim \omega_P$.¹ Particles with such masses and couplings are allowed by current observations for pseudo-scalar fields and for chameleonic scalars.

As photon number is not conserved photon-ALP mixing will change the apparent luminosity of objects observed through the cluster. We define the attenuation factor to be the ratio of the flux of photons after passing through N domains to the initial flux of photons; $C = I_\gamma(N)/I_\gamma(0)$. Then in the strong mixing limit, assuming no initial flux of ALPs, the mean value for C is $C = 2/3$ [7], and its probability distribution is [8]

$$f_C(c; p_0) = \frac{1}{\sqrt{1-p_0^2}} \left[\tan^{-1} \left(\sqrt{a} \left(1 - \frac{2c_+}{1+p_0} \right)^{-1/2} \right) - \tan^{-1} \left(\sqrt{a} \left(1 - \frac{2c_-}{1-p_0} \right)^{1/2} \right) \right], \quad (2)$$

where $a = (1+p_0)/(1-p_0)$, $c_\pm = \min(c, (1 \pm p_0)/2)$ and p_0 is the initial polarization of the photons. This probability distribution has an unusual shape, and is very asymmetric about the mean. In the next Section we show that this can be exploited as a new test for ALPs.

3 Searching for ALPs with luminosity relations

To use the shape of the probability distribution (2) to look for ALPs we would need to know the high energy photon flux for a class of astronomical sources. We do not currently know of any ob-

¹The strength of the magnetic field is $B \approx 1 - 10 \mu\text{G}$, the size of a magnetic domain is $L \approx 1$ kpc and for a typical source inside the cluster we expect the light observed from that source to have traversed $N \approx 100 - 1000$ magnetic domains [6]. The plasma frequency in the intracluster medium is $\omega_P \approx 10^{-12}$ eV

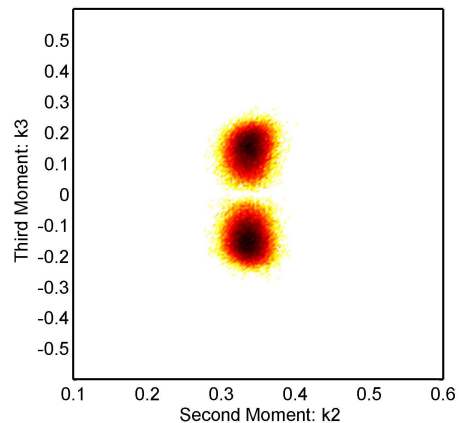


Figure 1: Simulated fingerprint for best fit Gaussian model

jects that are standard candles in x- or gamma-rays, however, for certain classes of object there exist *luminosity relations* which correlate the high frequency luminosity of an object with a feature of its low energy spectrum. At low frequencies light mixes weakly with ALPs and hence we assume that low energy observables are not affected by ALPs at leading order. Therefore luminosity relations can be used to normalize the high energy flux, so that the effects of ALPs are observable.

The relations typically take the form

$$\log_{10} Y_i = a + b \log_{10} X_i + S_i, \quad (3)$$

where Y_i is the high energy luminosity, and X_i is the low energy feature of the spectrum for the i -th object in the survey. S_i represent the scatter in individual measurements, it is standard in astronomy to assume they are normally distributed; $S_i = \sigma \delta_i$ where $\delta \sim N(0, 1)$. If the high frequency light mixes strongly with ALPs this will appear as an additional contribution to the scatter $S_i = \sigma \delta_i - \log_{10} C_i$, where the C_i are described by the probability distribution function (2).

For a given data set we use the likelihood ratio test to see if the data prefer strong ALP-photon mixing, or the null hypothesis of Gaussian noise.

We find the values of the parameters a , b and σ which maximize the likelihood of each hypothesis given the data, and then compare these two maximum likelihoods with the ratio $r(p_0) = 2 \log(\hat{L}_1(p_0)/\hat{L}_0)$, where $\hat{L}_1(p_0)$ is the maximum likelihood allowing for strong ALP-photon mixing and \hat{L}_0 is the maximum likelihood for models where the scatter is purely Gaussian. The two hypothesis have the same number of parameters and therefore $r(p_0)$ is equivalent to the Bayesian Information Criterion. Negative $r(p_0)$ is evidence against ALP strong mixing, and positive $r(p_0)$ is evidence for ALP strong mixing. $|r(p_0)| > 6$ is considered strong evidence, $|r(p_0)| > 10$ is considered very strong evidence.

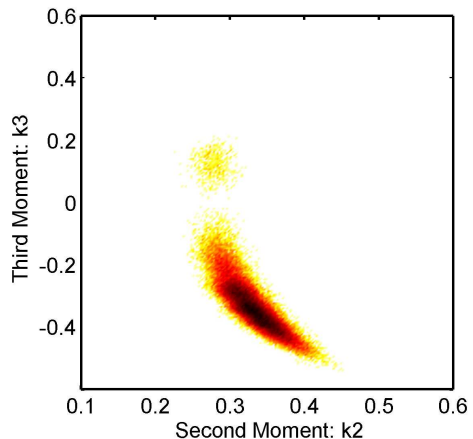


Figure 2: Simulated fingerprint for best fit ALP strong mixing model

4 Results from active galactic nuclei

To apply the test developed in the previous section we require a class of compact objects within galaxy clusters that emit x-ray or gamma-ray light and for which luminosity relations exist correlating the high energy luminosity with a feature of the low-energy spectrum. Active galactic nuclei (AGN) satisfy these requirements. For AGN a luminosity relation has been established between the 2 keV x-ray luminosity and the 5 eV optical luminosity. We have observations of 77 AGN from the COMBO-17 and ROSAT surveys [9] and 126 objects from the SDSS survey [10].

Applying the likelihood ratio test described in the previous section to these results we find $r(p_0 \lesssim 0.5) \approx 25$, where the expectation from AGN physics is that $p_0 < 0.1$ [11].

As a qualitative check of this result we plot *fingerprints* of the data. To do this we construct 10^5 new data sets, of the same size as the original, by bootstrap re-sampling (with replacement) of the original data set. For each data set we calculate the statistical moments of the

distribution $k_m(s_i) = [(1/N_p) \sum_i s_i^m]^{1/m}$ where $s_i = \log_{10} Y_i - (a + b \log_{10} X_i)$. These moments parametrize the shape of the probability distribution. Fingerprints of the data are then histogram plots of k_i vs. k_j for the resampled data sets. Figures 1 and 2 show example fingerprints for simulated data respectively without and with the effects of strong ALP-photon mixing. Darker regions indicate a higher density of points. Figure 3 shows the same plot for the data obtained from observations of AGN.

Comparing Figures 2 and 3 there is a clear qualitative similarity between the shapes of the predicted and observed distributions. This similarity persists when higher moments of the distribution are plotted.

The astrophysics underlying the luminosity relation for AGN is not known, and we cannot rule out that a combination of standard physical processes in the AGN conspires to mimic the effects of ALP-photon mixing. It can be shown, however, that the scatter in the luminosity relation is not redshift dependent, therefore the observed scatter is not due to evolution effects or an incorrect choice of cosmological model.

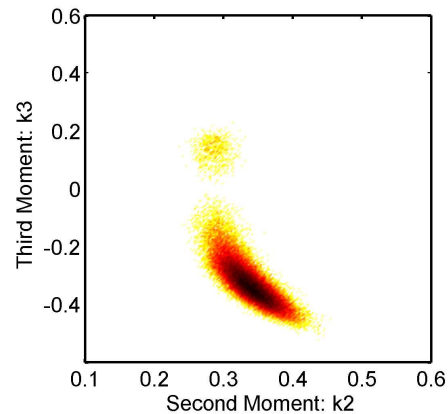


Figure 3: Fingerprint from AGN data

Acknowledgments

CB acknowledges support from the German Science Foundation (DFG) under Collaborative Research Centre (SFB) 676. ACD and DJS acknowledge STFC.

References

- [1] Georg Raffelt and Leo Stodolsky. Mixing of the Photon with Low Mass Particles. *Phys. Rev.*, D37:1237, 1988.
- [2] C. Amsler et al. Review of particle physics. *Phys. Lett.*, B667:1, 2008.
- [3] C. M. Will. Theory and experiment in gravitational physics. Cambridge, UK: Univ. Pr. (1993) 380 p.
- [4] Justin Khoury and Amanda Weltman. Chameleon Cosmology. *Phys. Rev.*, D69:044026, 2004.
- [5] Clare Burrage, Anne-Christine Davis, and Douglas J. Shaw. Detecting Chameleons: The Astronomical Polarization Produced by Chameleon-like Scalar Fields. *Phys. Rev.*, D79:044028, 2009.
- [6] C. L. Carilli and G. B. Taylor. Cluster Magnetic Fields. *Ann. Rev. Astron. Astrophys.*, 40:319–348, 2002.
- [7] Csaba Csaki, Nemanja Kaloper, and John Terning. Dimming supernovae without cosmic acceleration. *Phys. Rev. Lett.*, 88:161302, 2002.
- [8] Clare Burrage, Anne-Christine Davis, and Douglas J. Shaw. Active Galactic Nuclei Shed Light on Axion-like- Particles. *Phys. Rev. Lett.*, 102:201101, 2009.
- [9] Aaron T. Steffen et al. The X-ray-to-Optical Properties of Optically-Selected Active Galaxies Over Wide Luminosity and Redshift Ranges. *Astron. J.*, 131:2826–2842, 2006.
- [10] Iskra Strateva, Niel Brandt, Donald Schneider, Daniel Vanden Berk, and Cristian Vignali. Soft X-ray and Ultraviolet Emission Relations in Optically Selected AGN Samples. *Astron. J.*, 130:387–405, 2005.
- [11] S. Chandrasekhar. *Radiative transfer*. 1950.

Laboratory Tests of Chameleon Models

Philippe Brax¹, Carsten van de Bruck², Anne-Christine Davis³ and Douglas Shaw⁴

¹ Institut de Physique Théorique, CEA, IPhT, CNRS, URA 2306, F-91191Gif/Yvette Cedex, France

² Department of Applied Mathematics, University of Sheffield Hounsfield Road, Sheffield S3 7RH, United Kingdom

³ Department of Applied Mathematics and Theoretical Physics, Centre for Mathematical Sciences, Cambridge CB3 0WA, United Kingdom

⁴ Queen Mary University of London, Astronomy Unit, Mile End Road, London E1 4NS, United Kingdom

DOI: http://dx.doi.org/10.3204/DESY-PROC-2009-05/brax_philippe

We present a cursory overview of chameleon models of dark energy and their laboratory tests with an emphasis on optical and Casimir experiments. Optical experiments measuring the ellipticity of an initially polarised laser beam are sensitive to the coupling of chameleons to photons. The next generation of Casimir experiments may be able to unravel the nature of the scalar force mediated by the chameleon between parallel plates.

1 Chameleon Models

The observation of the acceleration of the universe has received no definite explanation yet. In fact, there is no convincing explanation for the smallness of the cosmological constant first introduced by Einstein to justify the existence of a spherical and static universe. It would be very natural to assume that there is an underlying mechanism, maybe a symmetry principle, which requires the cancelation of the cosmological constant. If this were the case, then the existence of a new matter component in the universe could be the explanation to its acceleration. The simplest form for this new type of dark energy is certainly a scalar field. Scalar fields are well-known candidates for the early acceleration phase of the universe. It might be that they also generate the late time acceleration. Typically, runaway models with an inverse power law

$$V = \frac{\Lambda^{4+n}}{\phi^n} \quad (1)$$

are interesting candidates as they lead to the acceleration of the universe when the field leaves an attractor solution as $\phi \approx m_{\text{Pl}}$. The existence of the attractor guarantees the independence of the late time acceleration from initial conditions. Once the scale Λ is appropriately tuned, these models also address the coincidence problem between matter, radiation and dark energy. Unfortunately if the scalar field couples to ordinary matter, its very small mass $m_\phi \approx H_0$ of the order of the Hubble rate now implies that a new fifth force should have been detected. Strong bounds on the coupling

$$\sqrt{8\pi G_N \alpha} = \frac{d \ln m_{\text{atom}}}{d\phi}$$

given by the Cassini experiments $\alpha^2 \leq 10^{-5}$ prevent the existence of such a coupling. In the absence of a mechanism which allows to decouple dark energy from matter, it seems that dark energy models would be ruled out.

In fact this is not the case thanks to the chameleon mechanism[1] which allows the scalar field to couple strongly to matter in a sparse environment while being almost decoupled in a dense setting. Let us consider a scalar-tensor theory with a Lagrangian

$$S = \int d^4x \sqrt{-g} \left(\frac{1}{16\pi G_N} R - \frac{1}{2} (\partial\phi)^2 - V(\phi) + \mathcal{L}_m(\psi_m, A^2(\phi)g_{\mu\nu}) \right)$$

The coupling function $A(\phi)$ is responsible for the coupling of the scalar field to matter. Choosing as an example

$$A(\phi) = \exp \frac{\phi}{M}$$

the coupling to matter given by

$$\alpha = \frac{m_{\text{Pl}}}{M}$$

can be large if $M \leq m_{\text{Pl}}$. Fortunately, the effective potential felt by the scalar field is not the bare runaway one introduced in the Lagrangian but

$$V_{\text{eff}}(\phi) = V(\phi) + \rho_m A(\phi)$$

which depends on the energy density of matter surrounding the scalar field. When this energy density is large, the scalar field is trapped at an effective minimum of the potential where the mass m_ϕ is environment dependent and can be very large in very dense regions. This is for instance the case in the atmosphere where the original Galileo experiment was carried out. In this case, the range $\lambda_\phi = m_\phi^{-1}$ of the fifth force mediated by the scalar field is smaller than the shortest detection range of gravitational interactions, i.e. much less than one millimeter. Unfortunately this mechanism is not efficient enough to hide scalar fields away in sparse environments such as the solar system where a strong interaction would lead to large deviations in the planetary motions. This is not the case thanks to a subtle and non-linear effect coined the thin shell effect. When Newton's potential for a body such as the sun is large enough, the scalar field is effectively trapped inside the body. The absence of any radiated scalar field outside the body implies that the generated scalar force is highly suppressed, hence no deviation in the motion of planets. Dark energy models where this property is present have been called chameleon models[2].

2 Laboratory Tests

Like all models invoked to solve cosmological problems, a precise understanding of the nature of chameleon particles would only be achieved by direct detection in laboratory experiments. The elusiveness of dark energy particles in gravitational experiments has led us to investigate their properties in precision experiments where tiny deviations from the standard model could be detected. Two different types of settings can be envisaged: Casimir and optical experiments[3, 4]. Let us consider the former first. The Casimir effect is one of the triumphs of quantum field theory inasmuch as true quantum fluctuations have observable macroscopic consequences. Indeed consider two parallel plates of conducting material facing each other at very short distance.

LABORATORY TESTS OF CHAMELEON MODELS

The quantum fluctuations of the electromagnetic field induce a power law force between the plates which is attractive and decays like the fourth power of the distance. Remarkably, this effect has been experimentally observed. Now chameleons would certainly generate an extra force between the plates. The force is also of the inverse power law type and is effective in the range $m_c^{-1} \leq d \leq m_b^{-1}$ where m_c is the large chameleon mass in the plates and m_b is the smaller chameleon mass in the vacuum between the plates. At short distances the force is nearly constant while it decays exponentially at large distance. The expression of the force is simply

$$\frac{F_\phi}{A} \sim \Lambda^4 (\Lambda d)^{-\frac{2n}{n+2}}$$

where A is the surface of the plates, hence amounting to a pressure. The scale Λ is the dark energy energy scale $\Lambda \sim 10^{-3}\text{eV}$ which corresponds to a small scale

$$\Lambda^{-1} \sim 82\mu\text{m}$$

The algebraic decay of the chameleon pressure is less steep than the algebraic decay of the Casimir force

$$\frac{F_\phi}{F_{\text{cas}}} \sim \frac{240}{\pi^2} (\Lambda d)^{\frac{2(n+4)}{n+2}}$$

implying that a detection of the chameleon can only be obtained for scales larger than Λ^{-1} . In fact, considering possible deviations from the Casimir force, a chameleon would lead to a difference of a few percent for $d = 10\mu\text{m}$ and would be around a hundred percent for $d = 30\mu\text{m}$. This is an exciting possibility as these distances may be probed in the next generation of Casimir experiments.

Optical experiments would probe a different sector of chameleon theories. So far, we have described chameleon theories as resulting from the effective properties of scalar-tensor theories conformally coupled to matter. In this particular setting, chameleons do not couple directly to photons. A coupling to photons can be introduced

$$\mathcal{L}_{\text{optics}} = \frac{e^{\phi/M}}{g^2} F_{\mu\nu} F^{\mu\nu}$$

which breaks conformal invariance. We have chosen the coupling scale M to be the same as the coupling scale to matter. In principle, these two couplings could be different. The coupling to photons has an important consequence in the presence of an external magnetic field. The chameleon can oscillate into a photon with a probability depending on the coupling strength. This is the Primakov effect and its inverse. This property can lead to observable effects in cavity experiments. When a polarised laser beam enters a cavity where a magnetic field is present, the laser polarisation orthogonal to the magnetic field oscillates into chameleons and vice versa. The lagging effect of the orthogonal polarisation compared the parallel one due to the oscillation into the massive chameleon traveling at a speed smaller than the speed of light implies that the laser light develops a non-vanishing ellipticity.

The mass of the chameleon in the cavity depends on the residual gas density and the magnetic field

$$\rho = \rho_m + \frac{B^2}{2}$$

implying that the coherence length of the laser beam in the cavity becomes magnetic field dependent

$$z_{\text{coh}} = \frac{2\omega}{m^2}$$

where ω is the frequency of the laser light. The mixing angle between the photons and the chameleons is given by

$$\theta = \frac{B\omega}{Mm^2}$$

At the position z in the cavity, the wave function of the orthogonal polarisation is given by

$$\psi(z) = N \left(1 - \frac{1}{N} \sum_{n=0}^{N-1} a_n(z) \right) \cos(\omega z + \frac{1}{N} \sum_{n=0}^{N-1} \delta_n(z))$$

corresponding to N passes of the photons before they leave the cavity through one of the mirrors. The attenuation and the phase shift are given by

$$a_n(z) = 2\theta^2 \sin^2 \frac{m^2(z+nL)}{4\omega}, \quad \delta_n(z) = \frac{m^2\theta^2}{2\omega}(z+nL) - \theta^2 \sin \frac{m^2(z+nL)}{2\omega}$$

When the cavity length $L = Pz_{\text{coh}}$ is commensurate with the coherence length, the attenuation and the phase shift simplify

$$a_T = \theta^2, \quad \delta_T = \pi \frac{N}{P} \theta^2$$

An important consequence of this result is that the ellipticity of the laser beam after going through the cavity is much larger than the rotation of the polarisation

$$\frac{\text{ellipticity}}{\text{rotation}} = \frac{\pi N}{P}$$

Of course, in real experiments the cavity is larger than the interaction length d with the magnetic field. Moreover the chameleon does not reflect instantaneously off the mirrors. This introduces a phase shift $\Delta_d = \frac{m_\phi^2 d}{\omega}$ for the decoherence due to the non-interacting zone and $\Delta_r = \frac{\pi n}{n+2}$ for the reflection. Taking these effects into account, one can give lower bounds on the coupling scale M depending on the expected sensitivities of future experiments. For instance, with a sensitivity of 10^{-14} radians per pass, one would expect a detection of the ellipticity when the coupling is $M \leq 10^8$ GeV.

In conclusion, chameleon fields which are motivated by dark energy and its gravitational properties could be within reach in next generation of Casimir and optical experiments.

References

- [1] Justin Khoury, Amanda Weltman, Phys.Rev. D69 (2004) 044026.
- [2] Philippe Brax, Carsten van de Bruck, Anne-Christine Davis, Justin Khoury, Amanda Weltman, Phys.Rev.D70:123518,2004.
- [3] Philippe Brax, Carsten van de Bruck, Anne-Christine Davis, David F. Mota, Douglas Shaw, Phys.Rev.D76:124034, 2007.
- [4] P. Brax, C. van de Bruck, A. C. Davis, D. F. Mota, D. J. Shaw, Phys.Rev.D76:085010, 2007.

A Hidden Microwave Background ?

- signatures of photon-WISP oscillations in the CMB -

Javier Redondo

Max-Planck-Institut, Föhringer Ring 6, D-80805 München, Germany

DOI: http://dx.doi.org/10.3204/DESY-PROC-2009-05/redondo-javier_2

The existence and cosmological signatures of a relic background of very weakly interacting sub-eV particles (WISPs), produced by photon-WISP oscillations is reviewed.

1 Introduction

A variety of very weakly interacting sub-eV particles (WISPs) appearing in a hidden sector of nature, i.e. a sector of particles carrying no standard model charges, can mix with photons. This is the case of the standard graviton, and also of hypothetical particles such as axions, axion-like-particles (ALPs) [1] or hidden photons (γ') [2]. In the last case, the mixing can be provided by a non-diagonal kinetic term, a so-called kinetic mixing that after a field redefinition appears as $\gamma - \gamma'$ mass mixing [3]. In all the previous cases, mixing cannot occur at tree level (these WISPs have spin different from 1). However, the existence of WISP couplings to *two* photons can produce an effective mixing term in a background magnetic field.

The WISP-photon mixing gives a non-diagonal contribution to the mass matrix which no longer allows photons to be propagation eigenstates. This leads to the phenomenon of photon oscillations and photon disappearance, analogously to the neutrino case. The $\gamma \leftrightarrow$ WISP conversion probability as a function of propagation length L in a medium of index of refraction n is given by

$$P(\gamma \rightarrow \phi) = \frac{4\delta^2}{(m_\phi^2 - m_\gamma^2)^2 + 4\delta^2} \sin^2 \left(\frac{((m_\phi^2 - m_\gamma^2)^2 + 4\delta^2)^{1/2} L}{4\omega} \right) = \sin^2 2\theta \sin^2 \left(\frac{\pi L}{L_{\text{osc}}} \right) \quad (1)$$

where m_ϕ is the WISP mass and $m_\gamma^2 \simeq -2\omega^2(n-1)$ is an effective photon mass with ω the photon frequency.

The mixing term δ depends on the particular WISP. For gravitons we have $\delta = \sqrt{32\pi} B\omega/M_{\text{Pl}}$ where B is the component of the external magnetic field perpendicular to the photon propagation direction and the Planck mass is $M_{\text{Pl}} = 1.22 \times 10^{19}$ GeV. Axions and ALPs have $\delta = gB\omega$, with g the two photon coupling (widely discussed in this workshop) and *they only mix with one photon polarization*. For hidden photons we have $\delta_{\gamma'} = \chi m_{\gamma'}^2$ with χ the kinetic mixing parameter. String motivated models give plausible values of χ in the $10^{-16} \sim 10^{-3}$ range [4].

Note that in vacuum, $\gamma \leftrightarrow$ WISP oscillations can be very suppressed if the WISP mass is much larger than δ . However, inspection of Eq. (1) reveals that, even in this case, the amplitude of oscillations can be made maximal (1, indeed) in a medium which gives a photon effective mass that matches the WISP mass ($m_\gamma = m_\phi$) producing a resonant effect.

A typical experiment looking for $\gamma \leftrightarrow$ WISP oscillations could be: 1) Take a very intense and well understood light source, 2) make it propagate the longest possible distance through 3) a medium whose index of refraction is fairly homogeneous and tunable and 4) try to detect a distortion in the light after propagation. 5) If no distortion is observed, tune another index of refraction (which makes resonant another WISP mass) and try again.

The cosmic microwave background provides an excellent source for such an experiment. First, it is a very well measured and understood source: the black-body nature of its spectrum is well accounted in terms of QED and standard thermodynamics in the Λ CDM cosmological model, and was measured to a precision of 10^{-4} by the FIRAS on the COBE satellite [5]. More precise measurements are also under consideration [6, 7]. Second, the CMB photons travelled through the very homogeneous primordial plasma. For most of the time, its index of refraction was smaller than one, which is a paramount requirement since otherwise m_γ^2 would be negative and a resonance impossible. Moreover, as the universe slowly expanded, the plasma became increasingly sparse and the the index of refraction decreased accordingly. As we will see, the photon effective mass swept all possible WISP masses. We can therefore look for signatures of WISPs regardless of their mass. Finally, CMB photons travel the longest conceivable distance for an experiment, basically the size of the universe, enhancing enormously the conversion probabilities and thus the WISP signatures.

2 Photon mass in the early universe

In our studies we have used a simplified model, yet containing the main features, for the effective photon mass in the primordial plasma. The typically dominant part is a positive contribution from the free electrons through the plasma frequency ω_P , while a negative (frequency-dependent) part from electrons bound in H atoms plays a role in special cases

$$m_\gamma^2 = \omega_P^2(X_e) \times \left[1 - 0.0073 \left(\frac{\omega}{\text{eV}} \right)^2 \left(\frac{1 - X_e}{X_e} \right) \right], \quad (2)$$

where $\omega_P(X_e) \simeq 1.6 \times 10^{-14}(1+z)^{3/2}X_e^{1/2}$ eV is the average plasma frequency in the current Λ CDM model and $X_e(z)$ is the hydrogen ionization fraction as a function of redshift (taken from [8] for recombination and modelled around redshift $z \sim 7 - 10$ for reionization).

3 Transition probability in an expanding universe

The transition probability in Eq. (1) is only valid in an homogeneous medium. In the expanding universe we should account for the variation in time or redshift of the different physical quantities and the problem becomes substantially more complex. Moreover, if the resonance happens before recombination photon scattering can be important during the resonance and shall be included. The latter case was explored in a first paper focusing on the γ' case [9] while resonances after recombination were presented in [10]. The ALP case was developed in [11]. While every case is different, it turns out that the results are equivalent in the regime of small transition probability. In these proceedings we present another way of reaching the same result by using the perturbative solution of the dispersionless equations of motion of the γ -WISP system as presented in [1]. Using the equivalence between length, time and redshift infinitesimals

$dL \simeq dt = H^{-1}(1+z)^{-1}dz$ (H the expansion parameter) we can write

$$P(\gamma \rightarrow \phi) = \left| \int dt \frac{\delta(t)}{2\omega} \text{Exp} \left\{ 1 \int^t dt' \frac{m_\phi^2 - m_\gamma^2(t')}{2\omega} \right\} \right|^2 \simeq \pi \frac{\delta^2}{m_\phi^2 \omega H} \left| \frac{d \log m_\gamma^2}{d \log(1+z)} \right|_{z=z_r}^{-1} \quad (3)$$

where for evaluating the integral we have used a saddle point approximation so that all quantities are to be evaluated in the resonance point $m_\phi = m_\gamma(z_r)$.

Note that due to the H refraction term several resonances occur for small masses and large frequencies [10, 11]. There is however a dominant one for which the last expression makes full sense, but this depends on the specific WISP. Fixing the WISP mass and neglecting the log derivative which amounts an $O(1)$ factor we find that: 1) in the hidden photon case $P \propto (\omega H)^{-1}$ which always decreases with redshift so the *latest* resonance is the most relevant and 2) in the ALP or graviton case $P \propto B^2 \omega / H$ so the *earliest* resonance dominates¹.

4 Signatures of a hidden CMB

The early $\gamma \rightarrow$ WISP conversions can leave different footprints in the CMB depending on when the resonant conversion happens. The CMB is unprotected from spectral distortions below a temperature $T \sim \text{keV}$ and the $\gamma \rightarrow$ WISP conversions are frequency dependent so they generally distort the blackbody shape. A careful² χ^2 analysis of the FIRAS monopole results allowed us to set strong constraints on hidden photons and ALPs with masses smaller than ~ 0.2 meV. Beyond this mass, the $\gamma \rightarrow$ WISP resonance happens when photons can regain a thermal distribution by interacting with the primordial plasma. This of course makes the FIRAS bounds disappear. Nevertheless, the WISPs produced contribute to the dark matter of the universe and therefore affect structure formation. Their oscillation origin makes these WISPs to have a similar spectrum than photons, so they are in fact hot dark matter relics. As such, they behave in a completely similar fashion to the standard neutrinos by free-streaming out of the primordial over-densities and suppressing the power spectrum at small scales. Their effects can be included in the number of effective neutrino species

$$N_\nu^{\text{eff}}(x) = \frac{N_\nu}{1-x} + \frac{8}{7} \frac{x}{1-x} \left(\frac{11}{4} \right)^{4/3} \quad (4)$$

where $x = \rho_\phi / \rho_\gamma$ is the fraction of the original photon density converted into WISPs during the resonance and N_ν is the effective number of neutrinos before the resonance. Comparing the value of N_ν^{eff} recently inferred from WMAP5, other anisotropy probes, large scale structure surveys and supernova data with the standard value $N_\nu = 3.046$ gives $x < 0.2$ with 95% C.L. This limit translates into severe constraints for the $\gamma \rightarrow$ WISP mixing.

A summary of the bounds obtained in [9, 10, 11] is shown in Fig. 1. Note that for ALPs we can only constrain the product of the coupling times a sky averaged magnetic field during the resonance $g \langle B^2 \rangle^{1/2}$. These results are of little use currently but can eventually turn into a fabulous diagnosis tool in the case of the discovery of an ALP, in which case one could

¹Primordial magnetic fields usually increase with redshift faster than $(1+z)$, indeed in our studies we used the most conventional assumption that $B = B_0(1+z)^2$.

²Whenever the resonance happens before recombination we included the re-thermalization processes of the photon spectrum.

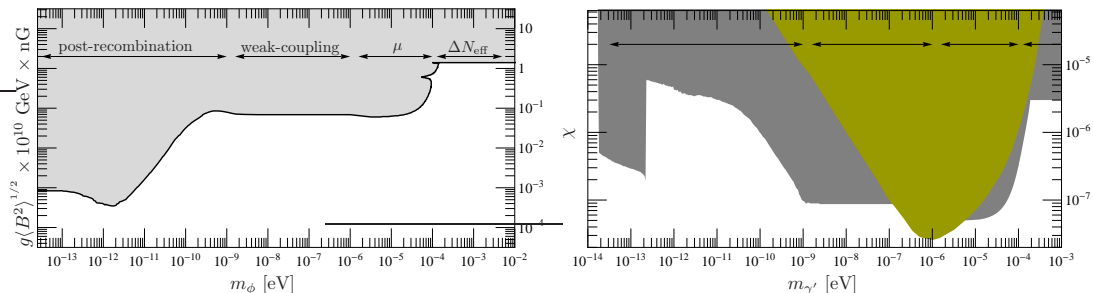


Figure 1: Constraints in the ALP (left) and hidden photon (right) parameter space from the signatures on the CMB left by a primordial $\gamma \rightarrow$ WISP resonant conversion. $\Delta N_{\nu}^{\text{eff}}$ is bounded by the WMAP5 power spectrum while for lower masses the bounds come from the FIRAS blackbody measurements. In the hidden photon case, the yellowish region is excluded by experimental searches of deviations of the Coulomb’s law [12].

constrain the existence of primordial magnetic fields (PMFs). Other possibility is that PMFs are discovered by other means in which case our bound will constrain the γ -ALP coupling. Bounds on g lie around the 10^{-10} GeV $^{-1}$ ballpark while those on PMFs are slightly above a nG. If the discovery of any of those is experimentally around the corner our bounds on the other can be very relevant. This seems to imply that the detection of both g and PMFs is very unlikely in the short term, specially for very small ALP masses. The graviton case can be read from the ALP graph when $m_\phi \rightarrow 0$. Since the coupling is known one obtains a bound on the primordial field intensity of 69 μ G. In the hidden photon case, our bounds complement and typically beat the previous bounds from modifications of the Coulomb’s law.

Acknowledgements

I would like to thank the organisers of this very interesting meeting and acknowledge support of the DFG cluster of excellence EXC 153 “Origin and Structure of the Universe”.

References

- [1] G. Raffelt and L. Stodolsky, *Phys. Rev.* **D37** (1988) 1237.
- [2] L. B. Okun, *Sov. Phys. JETP* **56** (1982) 502.
- [3] M. Ahlers, et al. *Phys. Rev.* **D76** (2007) 115005, [arXiv:0706.2836 \[hep-ph\]](#).
- [4] K. R. Dienes et al. *Nucl. Phys.* **B492** (1997) 104–118, [hep-ph/9610479](#); S. A. Abel et al. *Nucl. Phys.* **B685** (2004) 150–170, [arXiv:hep-th/0311051](#). , *Phys. Lett.* **B666** (2008) 66–70, [arXiv:hep-ph/0608248](#). and *JHEP* **07** (2008) 124, [arXiv:0803.1449 \[hep-ph\]](#); M. Goodsell, et al. *JHEP* **11** (2009) 027, [arXiv:0909.0515 \[hep-ph\]](#).
- [5] D. J. Fixsen et al., *Astrophys. J.* **473** (1996) 576, [arXiv:astro-ph/9605054](#).
- [6] D. J. Fixsen and J. C. Mather, *ApJ* **581** (2002) 817–822.
- [7] A. Kogut, [arXiv:astro-ph/9607100](#).
- [8] S. Seager, D. D. Sasselov, and D. Scott, [arXiv:astro-ph/9909275](#).
- [9] J. Jaeckel, J. Redondo, and A. Ringwald, *Phys. Rev. Lett.* **101** (2008) 131801, [arXiv:0804.4157 \[astro-ph\]](#).
- [10] A. Mirizzi, J. Redondo, and G. Sigl, *JCAP* **0903** (2009) 026, [arXiv:0901.0014 \[hep-ph\]](#).
- [11] A. Mirizzi, J. Redondo, and G. Sigl, *JCAP* **0908** (2009) 001, [arXiv:0905.4865 \[hep-ph\]](#).
- [12] D. F. Bartlett and S. Loegl, *Phys. Rev. Lett.* **61** (1988) 2285–2287.

Chapter 8

WISPs Theoretical Developments

Minicharges, Monopoles, and Magnetic Mixing

F. Brümmer

Institute for Particle Physics Phenomenology, Durham University, DH1 3LE, UK

DOI: http://dx.doi.org/10.3204/DESY-PROC-2009-05/bruemmer_felix

Minicharged particles (MCPs) arise naturally in extensions of the Standard Model with hidden sector gauge groups. Many such extensions also contain magnetic monopoles. For models containing both monopoles and MCPs, we clarify the role of the Dirac charge quantization condition in restricting the possible charges. We also show that monopoles of the hidden sector may manifest themselves as MCPs, by a generalization of the Witten effect, which we call *magnetic mixing*.

1 Introduction

Many extensions of the Standard Model contain additional U(1) gauge factors as part of a hidden sector. These may arise, for instance, directly from some string compactification, or from a non-abelian gauge factor spontaneously broken to U(1). For a single extra U(1), the most general low-energy Lagrangian for the abelian gauge fields is then

$$\begin{aligned} \mathcal{L} = & -\frac{1}{4} (F_{\mu\nu}F^{\mu\nu} + G_{\mu\nu}G^{\mu\nu} + 2\chi F_{\mu\nu}G^{\mu\nu}) \\ & - \frac{1}{32\pi^2} \left(\theta_F F_{\mu\nu}\tilde{F}^{\mu\nu} + \theta_G G_{\mu\nu}\tilde{G}^{\mu\nu} + 2\theta_{FG} F_{\mu\nu}\tilde{G}^{\mu\nu} \right). \end{aligned} \quad (1)$$

Here $F_{\mu\nu}$ is the field strength of electromagnetism, $G_{\mu\nu}$ is the field strength of the hidden sector U(1), $\tilde{F}_{\mu\nu}$ and $\tilde{G}_{\mu\nu}$ are the respective dual field strengths, and χ , θ_F , θ_G , θ_{FG} are constants.

The first line represents the ordinary kinetic Lagrangian, including a kinetic mixing term $2\chi F_{\mu\nu}G^{\mu\nu}$. If there are massive fields charged under both $F_{\mu\nu}$ and $G_{\mu\nu}$, kinetic mixing is generically induced radiatively [1]. Fields which were charged under $G_{\mu\nu}$ only will then pick up effective electromagnetic charges $\sim \chi$, and will show up as minicharged particles (MCPs).¹

The θ -terms in the second line are usually ignored in abelian theories. They do not affect the equations of motion and carry no topological charges. However, they do become important in the presence of magnetic monopoles: By the Witten effect [3], a $\theta_F F_{\mu\nu}\tilde{F}^{\mu\nu}$ term causes a monopole to pick up an electric charge $\sim \theta_F$. Similarly, as we will argue, a *magnetic mixing* term $\theta_{FG} F_{\mu\nu}\tilde{G}^{\mu\nu}$ will cause a hidden sector monopole to pick up a visible electric minicharge.

In the following we will consider models with both kinetic and magnetic mixing terms and with magnetic monopoles. We will show that the Dirac quantization condition for electric charges must be suitably modified in the presence of kinetic mixing, in order not to lead to a contradiction between charge quantization and the appearance of MCPs [4]. We will also demonstrate how magnetic mixing terms may give electric minicharges to hidden sector monopoles

¹For some concrete models in field theory and string theory, see e.g. [2].

[5]. Our considerations will in particular apply to the case where the hidden sector $U(1)$ is the remainder of a spontaneously broken non-abelian gauge group, in which magnetic monopoles appear naturally as 't Hooft–Polyakov monopoles [6].

2 Kinetic mixing and charge quantization

Let us start by ignoring the θ -terms for now and consider a model with a kinetic mixing term. For a $U(1) \times U(1)$ gauge theory with field strengths $F = dA$ and $G = dB$, the Lagrangian is

$$\mathcal{L} = -\frac{1}{4}F_{\mu\nu}F^{\mu\nu} - \frac{1}{4}G_{\mu\nu}G^{\mu\nu} - \frac{\chi}{2}F^{\mu\nu}G_{\mu\nu} - ej_{\mu}A^{\mu} - e'j'_{\mu}B^{\mu}.$$

Diagonalizing the gauge kinetic terms, by defining $C \equiv B + \chi A$ and $H \equiv dC = G + \chi F$ and eliminating B and G in favour of C and H , gives a coupling of the current j' to the gauge field A with charge $-\chi e'$. Identifying A with the photon of electromagnetism, hidden sector charged matter fields have picked up ordinary electric charges $\sim \chi$, thus becoming MCPs. If the MCPs are light, these induced charges must in fact be tiny to evade experimental bounds [7].

In the presence of magnetic monopoles, electric charges should be quantized [8]. This can most easily be seen as follows: Consider a static system consisting of an electron and a monopole. This system carries angular momentum, which semi-classically should be quantized [9]:

$$\mathbf{L} = \int d^3x \mathbf{x} \times (\mathbf{E} \times \mathbf{B}) = \frac{eg}{4\pi} \mathbf{n}.$$

Here e is the electron charge, g is the monopole charge, and \mathbf{n} is a unit vector pointing from one towards the other. Requiring $|\mathbf{L}|$ to be half-integral gives the Dirac quantization condition

$$eg \in 2\pi\mathbb{Z}. \quad (2)$$

It follows that the ratio of any two electric charges e_i and e_j should be rational, $e_i/e_j \in \mathbb{Q}$.

In models with a visible and a hidden sector $U(1)$, and with kinetic mixing between the two, this leads to a problem because the induced minicharges are proportional to χ , which is an arbitrary and generally irrational number. The problem is solved, however, if we only allow for monopoles which carry a suitable magnetic charge also under the hidden $U(1)$. For example, consider a model with an electron, an MCP, and a magnetic monopole with the following electric and magnetic charges:

Particle	q_{vis}	q_{hid}	g_{vis}	g_{hid}
electron	e	0	0	0
MCP	$-\chi e'$	e'	0	0
monopole	0	0	g	g'

The total angular momentum of the combined hidden and ordinary electromagnetic fields is, in a basis where the gauge-kinetic Lagrangian is diagonal,

$$\mathbf{L} = \int d^3x \mathbf{x} \times (\mathbf{E}_{\text{vis}} \times \mathbf{B}_{\text{vis}} + \mathbf{E}_{\text{hid}} \times \mathbf{B}_{\text{hid}}), \quad |\mathbf{L}| = \frac{q_{\text{vis}} g}{4\pi} + \frac{q_{\text{hid}} g'}{4\pi}.$$

It is quantized if the monopole charges are $(g, g') = (0, \frac{2\pi n}{e'})$ or $(g, g') = (\frac{2\pi m}{e}, \frac{2\pi \chi m}{e})$ or any linear combination of these, with $n, m \in \mathbb{Z}$. Only monopoles with these quantum numbers can

be consistently included in the model. This condition on monopole charges is in fact a special case of the Schwinger–Zwanziger dyon charge quantization condition [10] with multiple U(1)s.

In models with fundamental U(1)s, one may or may not choose to include magnetic monopoles. By contrast, in many models where one of the U(1)s is the remnant of a spontaneously broken non-abelian gauge group, magnetic monopoles necessarily appear as topologically non-trivial field configurations. As a simple example consider a model where the hidden sector gauge group is SU(2), spontaneously broken to U(1) by an adjoint scalar ϕ^a (the 't Hooft–Polyakov model [6]). The Lagrangian for the scalar and the hidden sector gauge field with field strength $G_{\mu\nu}^a$ is

$$\mathcal{L} = -\frac{1}{4}G_{\mu\nu}^a G^{\mu\nu a} - \frac{1}{2}(D_\mu\phi)^a(D^\mu\phi)^a + m^2\phi^a\phi^a - \lambda(\phi^a\phi^a)^2.$$

A field configuration which represents a monopole at the origin, $r = 0$, is given by $\langle\phi^a\rangle = r^a f(r)$ with $f(r)$ a certain function. It breaks SU(2) \rightarrow U(1) at large r . We can couple this model to a visible sector U(1) with field strength $F_{\mu\nu}$ by adding the terms

$$\Delta\mathcal{L} = -\frac{1}{4}F_{\mu\nu}F^{\mu\nu} - \frac{1}{2M}\phi^a G^{\mu\nu a} F_{\mu\nu}.$$

The last term represents kinetic mixing between the surviving hidden U(1) and the visible U(1). It is generated by integrating out heavy states which are charged under both the visible and the hidden sector gauge group. We have checked [4] in this setting that the 't Hooft–Polyakov monopole carries a monopole charge of precisely the allowed kind, as by the above discussion.

3 Magnetic mixing

In a model with a single U(1), a θ -term $\sim F^{\mu\nu}\tilde{F}_{\mu\nu}$ in the Lagrangian density gives electric charges to magnetic monopoles [3]. This can be seen as follows: Consider a magnetic monopole background with monopole charge g at $r = 0$, superimposed with some static gauge potential $(A^\mu) = (A^0, \mathbf{A})$. The θ -term can be written in terms of electric and magnetic fields as

$$-\frac{\theta}{32\pi^2}F^{\mu\nu}\tilde{F}_{\mu\nu} = \frac{\theta}{8\pi^2}\mathbf{E}\cdot\mathbf{B} = \frac{\theta}{8\pi^2}(\nabla A^0)\cdot\left(\nabla\times\mathbf{A} + \frac{g}{4\pi}\frac{\mathbf{r}}{r^3}\right).$$

By integrating by parts, the Lagrangian contains a piece

$$L = \int d^3r \mathcal{L} \supset -\frac{\theta}{8\pi^2} \int d^3r A^0 \nabla\cdot\frac{g\mathbf{r}}{4\pi r^3} = -\frac{\theta g}{8\pi^2} \int d^3r A^0 \delta^3(\mathbf{r}).$$

This is a coupling of an electric point charge $-\theta g/(8\pi^2)$, located at $\mathbf{r} = 0$, to the electrostatic potential A^0 . In other words, the monopole has acquired an electric charge.

In a model with a visible U(1) and a hidden U(1), and a magnetic mixing term

$$\mathcal{L} \supset -\frac{\theta_{FG}}{32\pi^2}F_{\mu\nu}\tilde{G}^{\mu\nu}$$

such as in Eq. (1), an analogous calculation [5] shows that hidden magnetic monopoles acquire visible electric charges. This is potentially very interesting with regard to phenomenology: Magnetic monopoles of ordinary electromagnetism are expected to be much heavier than M_{GUT} and therefore undetectable. Hidden sector monopoles, on the other hand, could very well be

relatively light. If they carry electromagnetic charges from magnetic mixing, they could be detected in the same way as MCPs.

For instance, if the monopole is again a 't Hooft–Polyakov monopole of a spontaneously broken non-abelian gauge group in the hidden sector, its mass is semi-classically given by the breaking scale, divided by the gauge coupling. For models with an arbitrarily low breaking scale, the monopole could be arbitrarily light. Alternatively, if a high breaking scale is preferred for naturalness reasons, one might speculate that the hidden sector gauge group could be strongly coupled, such that the semi-classical approximation is invalid and monopoles could still be light. In fact, with the Seiberg–Witten model [11] there exists even a calculable example of a gauge theory with 't Hooft–Polyakov monopoles becoming arbitrarily light in some strong-coupling region of moduli space.

Despite the fact that there is no non-abelian analogue of kinetic or magnetic mixing terms, they may be generated radiatively [5] once a non-abelian gauge group is broken to $U(1)$ (which is precisely the situation in which 't Hooft–Polyakov monopoles appear). For inducing these terms, the model should contain matter fields charged under both the visible and the hidden sector. Magnetic mixing can only be induced if these fields possess CP-violating couplings, since a magnetic mixing term itself violates CP.

Acknowledgments

The author would like to thank J. Jaeckel and V. V. Khoze for collaboration in [4, 5], and the organizers of the *5th Patras Workshop* for a pleasant and interesting meeting.

References

- [1] B. Holdom, *Phys. Lett. B* **166**, 196 (1986).
- [2] K. R. Dienes, C. F. Kolda and J. March-Russell, *Nucl. Phys. B* **492**, 104 (1997);
D. Lüüst and S. Stieberger, *Fortsch. Phys.* **55**, 427 (2007);
S. A. Abel and B. W. Schofield, *Nucl. Phys. B* **685**, 150 (2004);
S. Abel and J. Santiago, *J. Phys. G* **30**, R83 (2004);
R. Blumenhagen, G. Honecker and T. Weigand, *JHEP* **0506**, 020 (2005);
B. Batell and T. Gherghetta, *Phys. Rev. D* **73**, 045016 (2006);
S. A. Abel, J. Jaeckel, V. V. Khoze and A. Ringwald, *Phys. Lett. B* **666**, 66 (2008);
S. A. Abel, M. D. Goodsell, J. Jaeckel, V. V. Khoze and A. Ringwald, *JHEP* **0807**, 124 (2008).
- [3] E. Witten, *Phys. Lett. B* **86** (1979) 283.
- [4] F. Brümmer and J. Jaeckel, *Phys. Lett. B* **675** (2009) 360.
- [5] F. Brümmer, J. Jaeckel and V. V. Khoze, *JHEP* **0906** (2009) 037.
- [6] G. 't Hooft, *Nucl. Phys. B* **79** (1974) 276;
A. M. Polyakov, *JETP Lett.* **20** (1974) 194 [*Pisma Zh. Eksp. Teor. Fiz.* **20** (1974) 430].
- [7] S. Davidson, S. Hannestad and G. Raffelt, *JHEP* **0005**, 003 (2000).
- [8] P. A. M. Dirac, *Proc. Roy. Soc. Lond. A* **133** (1931) 60.
- [9] H. A. Wilson, *Phys. Rev.* **75** (1949) 309;
M. N. Saha, *Indian J. Phys.* **10** (1936) 145.
- [10] J. S. Schwinger, *Phys. Rev.* **144** (1966) 1087; *Phys. Rev.* **173** (1968) 1536;
D. Zwanziger, *Phys. Rev.* **176** (1968) 1489.
- [11] N. Seiberg and E. Witten, *Nucl. Phys. B* **426**, 19 (1994) [Erratum-ibid. *B* **430**, 485 (1994)]; *Nucl. Phys. B* **431**, 484 (1994).

Light Hidden $U(1)$ s from String Theory

Mark Goodsell

DESY, Notkestraße 85, 22607 Hamburg, Germany

DOI: <http://dx.doi.org/10.3204/DESY-PROC-2009-05/goodsell.mark>

The possible masses and kinetic mixings of hidden $U(1)$ s in the LARGE volume scenario are discussed, including the generalisation of the compact manifold to a $K3$ fibration.

1 Introduction

Many of the talks at PATRAS 2009 (for example that of A. Linder) described laboratory experiments capable of detecting light hidden $U(1)$ s; others (e.g. J. Redondo) discussed astrophysical and cosmological searches. As reviewed by J. Conlon, string compactifications generically give additional hidden gauge sectors, in particular hidden $U(1)$ s. This contribution aims to review how hidden $U(1)$ s arise in LARGE volume string compactifications [1] and their likely masses and interactions with the visible sector particles [2].

The LARGE volume scenario involves IIB string theory compactified on a Calabi-Yau manifold having volume \mathcal{V} of the form

$$\mathcal{V} = \tau_b^{3/2} - h(\tau_i) \quad \text{or} \quad \mathcal{V} = \tau_b^{1/2} \tau_b - h(\tau_i),$$

where h is a function of τ_i , the Kähler moduli of “small” cycles; and τ_b is the modulus corresponding to a large cycle. The first case corresponds to a “swiss cheese” manifold; the second is the generalisation to a $K3$ fibration where now τ_b represents the $K3$ fibre modulus.

One small cycle contributes a non-perturbative superpotential and this leads to the stabilisation of the Kähler moduli at a non-supersymmetric minimum, provided that the complex structure moduli have first been stabilised by three-form fluxes and that there are more complex structure moduli than Kähler moduli. The volume is stabilised at a large value; as high as 5×10^{27} (in units of the string length) for TeV scale strings, 5×10^{13} for an intermediate string scale $M_s \sim 10^{10}$ GeV, or ~ 50 for GUT scale strings. The standard model is realised upon $D7$ -branes wrapping some of the small cycles.

In this scenario there are three classes of candidates for light $U(1)$ s. One such class are from (closed) Ramond-Ramond strings [3], counted by the number of complex structure moduli. These may kinetically mix [4] with the hypercharge, but they have no matter charged under them, and since the LARGE volume scenario involves compactification on a Kähler manifold they do not have any axionic couplings and are therefore massless. Therefore they can only be detected by production of their gauginos [5].

We shall instead focus upon the open string $U(1)$ s supported on branes, which may have masses and charged matter. For these $U(1)$ s wrapping a cycle τ_i the gauge coupling is given by $g_i^{-2} = \frac{\tau_i}{2\pi g_s}$. For branes wrapping small cycles these give gauge couplings of the same order as the hypercharge, but if the brane wraps the large cycle τ_b , then the gauge coupling will be

hyperweak with $g_b^{-2} \sim \frac{\mathcal{V}^{2/3}}{2\pi g_s}$. In the case of a $K3$ fibration this can be even smaller; if $\tau_{b'} \ll \tau_b$ then we can in principle approach $g_b^{-2} \sim \frac{\mathcal{V}}{2\pi g_s}$ (although we require $\tau_{b'} \gg \tau_i$).

2 Kinetic Mixing

If we assume that the additional $U(1)$ s are hidden (in contrast to the Z' scenario, see e.g. [6]), in that there is no light matter charged under both the visible and hidden sector fields, then we can only detect them via kinetic mixing with the hypercharge [4]. The holomorphic kinetic mixing χ_{ab}^h between two gauge groups a, b with holomorphic gauge couplings g_a^h, g_b^h , appears in the Lagrangian density

$$\mathcal{L} \supset \int d^2\theta \left\{ \frac{1}{4(g_a^h)^2} W_a W_a + \frac{1}{4(g_b^h)^2} W_b W_b - \frac{1}{2} \chi_{ab}^h W_a W_b \right\},$$

and in type IIB compactifications must have the form

$$\chi_{ab}^h = \chi_{ab}^{1\text{-loop}}(z^k, y_i) + \chi_{ab}^{\text{non-perturbative}}(z^k, e^{-\tau_j}, y_i),$$

where z^k, y_i are the complex structure and brane position moduli respectively; the perturbative contributions cannot depend upon the Kähler moduli, and thus cannot be volume suppressed. After rescaling to the physical basis via the Kaplunovsky-Louis type relation [7, 2]

$$\frac{\chi_{ab}}{g_a g_b} = \text{Re}(\chi_{ab}^h) + \frac{1}{8\pi^2} \text{tr} \left(Q_a Q_b \log Z \right) - \frac{1}{16\pi^2} \sum_r n_r Q_a Q_b(r) \kappa^2 K,$$

(where K is the Kähler potential and $Z = \partial_\alpha \partial_{\bar{\beta}} K$ is the Kähler metric of matter fields) we find, since we are assuming no light matter charged under both hidden and visible sectors

$$\chi_{ab} \sim \frac{g_a g_b}{16\pi^2}.$$

This estimate is plotted in figure 1 for the case of branes on a collapsed (small, MSSM-like) cycle and on a LARGE cycle, taking into account the range of possibilities in the general $K3$ fibration scenario and allowing for an order of magnitude variation in the above estimate.

There is also the possibility, should the kinetic mixing be cancelled, that it is generated by supersymmetry breaking effects; but in the LARGE volume scenario the values obtained are typically very small [2].

3 $U(1)$ Masses

Masses for $U(1)$ s supported upon branes can be generated either via the Stückelberg mechanism or by explicit breaking with a charged field obtaining a vacuum expectation value. The latter could be due to a hidden Higgs mechanism or fermion condensate. We shall not discuss fermion condensates, as they would require some strong gauge dynamics in the hidden sector and the scale generated depends very sensitively upon the amount of hidden matter in the theory, so there is no generic prediction.

In the LARGE volume scenario anomalous $U(1)$ s automatically obtain masses at the string scale, via the Stückelberg mechanism where the $U(1)$ is eaten by an axion. However, many

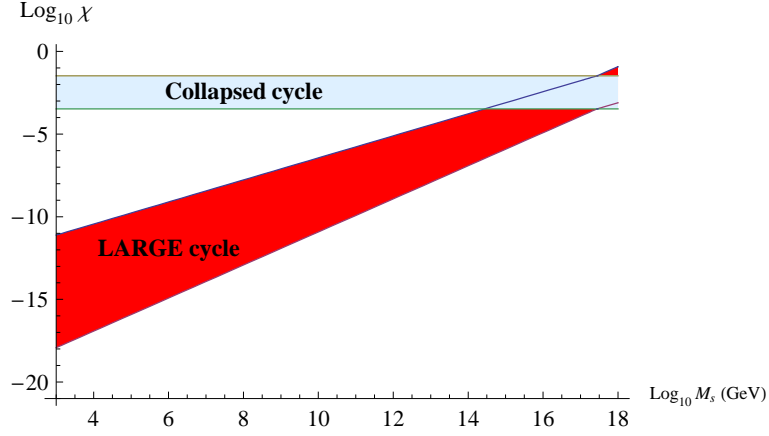


Figure 1: Kinetic mixing between the visible $U(1)$ and a $U(1)$ sitting on a collapsed cycle (upper, blue) or a hyperweak $U(1)$ on a LARGE cycle (lower, red) as a function of the string scale.

non-anomalous $U(1)$ s still obtain masses, but these generically contain some suppression by volume factors. There are two classes of axions that contribute; those counted by $h_-^{2,2}$ and those counted by $h_+^{1,1}$, respectively Hodge numbers odd and even under the orientifold. If we consider a simplified 2×2 mass matrix of $U(1)$ s where the first element corresponds to $U(1)$ s on small (or collapsed) cycles and the second to one wrapping the LARGE cycle (restricting here to the swiss cheese case), then for the two types of contribution we have

$$m_{\text{St}(1)}^2 = \frac{g_s}{2} M_s^2 \begin{pmatrix} \sim \mathcal{V}^{1/3} & \sim 1 \\ \sim 1 & \sim \mathcal{V}^{-1/3} \end{pmatrix}, \quad m_{\text{St}(2)}^2 = \frac{g_s}{2} M_s^2 \begin{pmatrix} \sim \mathcal{V}^{-1/3} & \sim \mathcal{V}^{-2/3} \\ \sim \mathcal{V}^{-2/3} & \sim \mathcal{V}^{-1} \end{pmatrix}.$$

Thus if the a brane wraps a cycle that is anti-invariant under the orientifold projection then the first term will dominate. However, in early constructions of the LARGE volume scenario $h_-^{2,2} = 0$. The second contribution arises only if the brane supports two-form fluxes. Thus a hyperweak gauge boson can acquire a mass $m_{\gamma'}$ as low as $\sim \text{meV}$ if the string scale is $\sim \text{TeV}$, for intermediate scale strings $m_{\gamma'} \sim \text{TeV}$ but for a higher string scale the Stückelberg masses are beyond the reach of current experiments.

Finally turning to a hidden Higgs mechanism with hidden Higgs pairs H_1, H_2 , the minimal potential is

$$V = m_1^2 |H_1|^2 + m_2^2 |H_2|^2 + m_3^2 (H_1 H_2 + c.c) + \frac{1}{2} (\xi_h + g_h |H_1|^2 - g_h |H_2|^2)^2,$$

where m_1, m_2, m_3 are soft masses and $\xi_h = g_Y \chi_{ab} \frac{1}{8} v^2 \cos 2\beta$ is a Fayet-Iliopoulos term generated by kinetic mixing with the hypercharge D -term, arising from the MSSM Higgs vev $v \simeq 246 \text{ GeV}$ and β the angle parametrising the relationship between up and down Higgs vevs. If we take the hidden sector gauge coupling to be of the same order as the hypercharge and the soft masses to be generated by “little gauge mediation” from the visible sector, then the Fayet-Iliopoulos term generates a hidden gauge boson mass of $\sim \text{GeV}$ [8]. However, if we take the hidden gauge group to be hyperweak, then due to the very small kinetic mixing, we can generate in principle small masses since $m_{\gamma'}^2 = 2g_h^2 (|H_1|^2 + |H_2|^2)$.

If the symmetry breaking is dominated by the Fayet-Iliopoulos term, then $m_{\gamma'} = 2g_h\xi$ and the m_i must necessarily be smaller than $g_h\xi$, so that the Higgs mass is $\sim g_h\xi \sim m_{\gamma'}$. Moreover, the above simple scenario leaves one Higgs field massless. This is a problem since the Higgs behaves like a minicharged particle, for which there are strict bounds if its mass is less than $\sim \text{MeV}$. This problem persists if we set $m_i > \xi$ so that the hidden $U(1)$ is broken by an MSSM-type Higgs effect, since there $\langle H_1 \rangle \sim \langle H_2 \rangle \sim m_i/g_h \rightarrow m_{\gamma'} \sim m_i$.

To obtain hidden photon masses smaller than $\sim \text{MeV}$, there is a natural mechanism involving an additional hidden $U(1)''$ symmetry with coupling $\tilde{g}_h \sim g_Y$ that obtains a mass $m_{\gamma''}$ via the Stückelberg mechanism. In this case, neglecting the Fayet-Iliopoulos term, the potential is modified to

$$\tilde{V} = m_x^2|H_1|^2 + m_x^2|H_2|^2 + m_3^2(H_1H_2 + c.c) + \frac{1}{2} \left[g_h^2 + \tilde{g}_h^2 \left(\frac{m_x^2}{m_x^2 + m_{\gamma''}^2} \right) \right] (|H_1|^2 - |H_2|^2)^2$$

where m_x is the mass of the modulus corresponding to the axion eaten by the $U(1)''$. We then obtain the relation

$$m_{\gamma'} \gtrsim \frac{1}{|W_0|} m_i \rightarrow m_{\gamma'} \gtrsim \frac{1}{|W_0|} \text{MeV},$$

where W_0 is a constant parametrising the vacuum expectation value of the superpotential of the underlying supergravity theory. By taking this to be large we can obtain a hierarchy between the hidden gauge boson and Higgs masses, but at the expense of some fine-tuning.

Acknowledgments

I would like to thank my collaborators on this subject: Karim Benakli, Joerg Jaeckel, Javier Redondo and Andreas Ringwald; and for useful conversations Michele Cicoli, Joe Conlon, Nick Halmagyi, Amir Kashani-Poor, Sameer Murthy and Waldemar Schulgin.

References

- [1] V. Balasubramanian, P. Berglund, J. P. Conlon and F. Quevedo, JHEP **0503** (2005) 007; C. P. Burgess, J. P. Conlon, L. Y. Hung, C. H. Kom, A. Maharana and F. Quevedo, JHEP **0807** (2008) 073; M. Cicoli, J. P. Conlon and F. Quevedo, JHEP **0810** (2008) 105; M. Cicoli, C. P. Burgess and F. Quevedo, JCAP **0903** (2009) 013; J. P. Conlon, A. Maharana and F. Quevedo, JHEP **0905** (2009) 109.
- [2] M. Goodsell, J. Jaeckel, J. Redondo and A. Ringwald, JHEP **0911** (2009) 027
- [3] H. Jockers and J. Louis, Nucl. Phys. B **705** (2005) 167; T. W. Grimm and A. Klemm, JHEP **0810** (2008) 077; T. W. Grimm, T. W. Ha, A. Klemm and D. Klevers, Nucl. Phys. B **816** (2009) 139; A. Arvanitaki, N. Craig, S. Dimopoulos, S. Dubovsky and J. March-Russell, arXiv:0909.5440.
- [4] J. Polchinski and L. Susskind, Phys. Rev. D **26** (1982) 3661; B. Holdom, Phys. Lett. B **166** (1986) 196; L. B. Okun, Sov. Phys. JETP **56** (1982) 502 [Zh. Eksp. Teor. Fiz. **83** (1982) 892]; F. del Aguila, G. D. Coughlan and M. Quiros, Nucl. Phys. B **307** (1988) 633 [Erratum-ibid. B **312** (1989) 751]; K. R. Dienes, C. F. Kolda and J. March-Russell, Nucl. Phys. B **492** (1997) 104; S. A. Abel and B. W. Schofield, Nucl. Phys. B **685** (2004) 150; S. A. Abel, J. Jaeckel, V. V. Khoze and A. Ringwald, Phys. Lett. B **666** (2008) 66; S. A. Abel, M. D. Goodsell, J. Jaeckel, V. V. Khoze and A. Ringwald, JHEP **0807** (2008) 124.
- [5] A. Ibarra, A. Ringwald and C. Weniger, JCAP **0901** (2009) 003.
- [6] P. Langacker, arXiv:0911.4294 [hep-ph].
- [7] V. Kaplunovsky and J. Louis, Nucl. Phys. B **422** (1994) 57; K. Benakli and M. D. Goodsell, arXiv:0909.0017.
- [8] N. Arkani-Hamed and N. Weiner, JHEP **0812** (2008) 104; E. J. Chun and J. C. Park, JCAP **0902** (2009) 026; C. Cheung, J. T. Ruderman, L. T. Wang and I. Yavin, Phys. Rev. D **80** (2009) 035008; D. E. Morrissey, D. Poland and K. M. Zurek, JHEP **0907** (2009) 050; Y. Cui, D. E. Morrissey, D. Poland and L. Randall, JHEP **0905** (2009) 076;

Chapter 9

Fifth Forces and Fundamental Symmetries

Tests of Lorentz symmetry

Ralf Lehnert

Instituto de Ciencias Nucleares, Universidad Nacional Autónoma de México
A. Postal 70-543, 04510 México D.F., Mexico

DOI: <http://dx.doi.org/10.3204/DESY-PROC-2009-05/lehnert.ralf>

A number of approaches to fundamental physics can lead to the violation of Lorentz and CPT symmetry. This talk discusses the low-energy phenomenology associated with such effects and reviews various sample experiments within this context.

Introduction.—The Standard Model (SM) and General Relativity (GR) provide an excellent phenomenological description of nature. However, from a theoretical viewpoint these two theories leave unanswered a variety of key conceptual questions. It is therefore believed that the SM and GR merge into a single unified theory at high energies that resolves these issues. One possibility for experimental research in this field is to increase the energy in experiments and hope to excite new degrees of freedom, which can give insight into such a unified theory.

A complementary experimental approach is characterized by tests at comparatively low or moderate energies, but with ultra-high precision. Various efforts along these lines, such as searches for axions, axion-like particles, weakly interacting massive particles, and weakly interacting sub-eV particles, have already been discussed at this meeting. This presentation is focused on another class of precision experiments, namely tests of Lorentz and CPT symmetry.

The special theory of relativity and its underlying Lorentz symmetry have been established over a century ago. Since that time, Lorentz symmetry has been subjected to numerous tests, but no credible experimental evidence for departures from Lorentz symmetry has been found. In fact, special relativity has matured into one of the most important cornerstones of physics. It provides not only the basis for present-day physics, but it is also the starting point for most theoretical approaches to new physics beyond the SM and GR.

In recent years, however, it has been realized that various of these approaches to new physics (although built on Lorentz invariance) can accommodate mild, minuscule deviations from this symmetry in the ground state [1]. Examples of candidate underlying models with the possibility of Lorentz violation are strings, loop quantum gravity, cosmologically varying scalars, non-commutative geometry, and multiverses [2]. A further motivation for Lorentz and CPT tests is provided by the fundamental character of these symmetries: they should be backed by experimental evidence of steadily increasing quality.

At energy regimes below the Planck scale, such departures from Lorentz and CPT symmetry can be described in great generality by the Standard-Model Extension (SME) [3]. The SME is an effective field theory that contains both the usual SM and GR. The remaining terms in the SME Lagrangian control the extent of Lorentz and CPT breakdown; they are constructed to involve all operators for Lorentz and CPT violation that are scalars under coordinate changes. This broad scope guarantees widest applicability: it eliminates the association to a particular underlying theory and ensures that practically all present and near-future experiments can be

analyzed with regards to their potential to measure Lorentz and CPT symmetry. Numerous investigations have been performed within the SME [4], which confirm its sound theoretical basis. The SME has become the standard framework for the identification and analysis of a wide variety of experimental studies [1, 5]. For instance, the SME predicts modifications in one-particle dispersion relations [6], which in turn could lead to vacuum Cherenkov radiation [7]. The absence of this effect at LEP leads to tight constraints on Lorentz violation in QED [8]. For other limits in electrodynamics, see, e.g., Refs. [9, 10].

The SME test framework.—A test framework that allows for departures from Lorentz and CPT symmetry is useful for the identification and analysis of suitable experiments. Establishing such a test model requires some preliminary thoughts. One issue is the multitude of approaches to underlying physics that can lead to Lorentz and CPT violation: there is presently no single realistic candidate fundamental theory whose low-energy limit can serve as the test framework. A related difficulty is the fact that for some theories beyond the SM and GR the low-energy limit is unknown or not unique. As a consequence, the test framework will be constructed by hand with the objective of relative independence of the details of the underlying physics.

The first step is to determine how Lorentz and CPT breakdown can be implemented into the test framework. One possibility that has proved to be the most general and useful is the inclusion of preferred directions modeled by background vectors and tensors while leaving the Lorentzian structure of spacetime unaffected. This idea is compatible with the fact that most candidate underlying models take Lorentz symmetry as a key basic ingredient. Once the model's dynamics is taken as Lorentz symmetric, symmetry breaking can essentially only arise along the lines of a Lorentz-violating ground state. Moreover, this implementation of deviations from Lorentz and CPT symmetry can maintain coordinate independence, a principle more fundamental than Lorentz symmetry. An immediate consequence is that different inertial coordinate systems are still connected via the usual Lorentz transformations. Violations of the symmetry become apparent only through the physical transformations: boosts and rotations of the experimental set-up; the background vectors and tensors are outside of experimental control and remain fixed under such physical transformations.

The springboard for the construction of the SME is the SM Lagrangian \mathcal{L}_{SM} and the Einstein–Hilbert Lagrangian \mathcal{L}_{EH} , which essentially contain the entire body of present-day physics. This guarantees that departures from Lorentz and CPT symmetry in all known physical systems can be described. The small Lorentz- and CPT-violating corrections $\delta\mathcal{L}_{\text{LIV}}$ are formed by contracting the background vectors and tensors with ordinary SM and gravitational fields to yield scalars under coordinate changes:

$$\mathcal{L}_{\text{SME}} = \mathcal{L}_{\text{SM}} + \mathcal{L}_{\text{EH}} + \delta\mathcal{L}_{\text{LIV}} . \quad (1)$$

Examples of terms present in the Minkowski-spacetime limit of $\delta\mathcal{L}_{\text{LIV}}$ are

$$\delta\mathcal{L}_{\text{LIV}} \supset b_\mu \bar{\psi} \gamma^\mu \gamma_5 \psi, (r_\mu \bar{\psi} \gamma^\mu \gamma_5 \psi)^2, (k_F)^{\alpha\beta\gamma\delta} F_{\alpha\beta} F_{\gamma\delta}, (k_{AF})^\alpha A^\beta \tilde{F}_{\alpha\beta}, \dots . \quad (2)$$

Here, ψ , A , and F are a conventional spinor field, a conventional gauge potential, and a conventional gauge field strength, respectively. The non-dynamical b_μ , r_μ , $(k_F)^{\alpha\beta\gamma\delta}$, and $(k_{AF})^\alpha$ are minute Lorentz-violating background vectors and tensors assumed to be generated by a candidate fundamental theory. Experimental tests seek to bound or measure these vectors and tensors. We finally mention that the minimal SME (mSME) is restricted by further physical requirements, such as translational invariance, the usual gauge symmetries, and power-counting renormalizability. For example, the mSME does not contain the r_μ term present in the above expression (2).

Lorentz violation via varying scalars.—In the construction of the SME, we have included the external non-dynamical background vectors and tensors that select preferred directions by hand without reference to underlying physics. A natural question to ask is whether such Lorentz-violating preferred directions can really be generated by candidate fundamental theories. We will briefly discuss one example illustrating that this is indeed the case: varying scalars.

Many theoretical approaches to underlying physics predict novel scalar fields. In fact, certain cosmological observations, such as the flatness and the accelerated expansion of the universe, can be explained by invoking new scalars. In such cosmological contexts, scalar fields can acquire nonzero expectation values with time dependencies driven by the evolution of the scale factor. As one example, we may consider $N = 4$ supergravity in four spacetime dimensions, which contains novel axion a and dilation b fields coupled via a function $f(a, b)$ to the electromagnetic field strength. In a simple cosmological model one can determine the evolution of a and b with the comoving time t . One of the couplings to electrodynamics then generates the effective Lagrangian term $f(t)F\tilde{F}$. In a local, experimental setting, such a term would indeed be perceived as a varying coupling—in this case, as a time-dependent θ angle.

A spacetime-dependent scalar, regardless of the mechanism that causes the variation, normally implies the breakdown of spacetime-translation invariance. But also Lorentz symmetry is typically violated in such situations because the gradient of the scalar selects a preferred direction. At the formal level, this fact is intuitively reasonable: the definition of the Lorentz-transformation generators contains the energy-momentum tensor, which is now no longer conserved. Thus, the usual time-independent boost and rotation generators no longer exist. To see this explicitly in our toy supergravity model, we can perform an integration by parts in the action:

$$f(t)F\tilde{F} \rightarrow -2(\partial^\alpha f)A^\beta\tilde{F}_{\alpha\beta} . \quad (3)$$

The cosmological background $f(t)$ is essentially outside of experimental control for the purposes of local measurements, so $\partial^\alpha f$ can be taken as non-dynamical. If we identify $-2(\partial^\alpha f)$ with $(k_{AF})^\alpha$ in Eq. (2), we explicitly see how this Lorentz- and CPT-violating Chern-Simons-type correction [9] can be generated by underlying physics.

Experimental tests.—Since Lorentz symmetry underpins many areas and concepts in physics, it can be tested in a multitude of physical systems. The tests with the best potential for highest sensitivity can be identified and analyzed with the SME. We briefly discuss three sample tests.

The first example concerns an astrophysical search for the Cherns-Simons-type term (3) mentioned earlier. A theoretical analysis of this term reveals that it causes birefringence. Even the smallest birefringence effects would accumulate for light that has traveled a sufficiently large distance. It is therefore unsurprising that the best experimental constraints on this particular type of Lorentz- and CPT-violation have been obtained from observations of cosmological sources. One predicted effect would be following. Suppose an astrophysical source is emitting flashes of light containing all polarizations. En route to Earth, such a pulse would separate because one of its two components travels faster than the other due to birefringence. A somewhat more sophisticated and sensitive approach is to observe a cosmological object known to emit a spectrum of mostly polarized light and measure the polarization of this light as a function of its wavelength at Earth. For birefringence due to a Chern-Simons-type interaction (3), this function should display a predicted characteristic. Such analyses have indeed been performed, and no such characteristic was found. This implies the bound $(k_{AF})^\alpha < 10^{-43}$ GeV [9, 10].

The second sample Lorentz test involves (anti)protons in Penning traps. The basic idea is as follows. The Lorentz-violating preferred background directions act in many respects just

like external fields. In conventional physics, such external fields can cause level shifts in bound systems like atoms (e.g., the Zeeman and Stark effects). Calculations within the SME reveal that Lorentz and CPT breakdown would cause similar level shifts for charges in Penning traps, for example. More precisely, the anomaly transitions would acquire opposite corrections for protons and their antiparticles. This fact can be employed to extract clean experimental limits on the b^μ coefficient (see expression (2)) for the proton with a sensitivity of about 10^{-24} GeV [11].

In the experimental investigations discussed above, gravitational effects could be neglected and the flat-spacetime limit of the SME was considered. However, tests involving gravity have recently been one focus of attention [12, 13]. In particular, antimatter, such as antihydrogen, offers the possibility of testing Lorentz and CPT symmetry in the SME's gravity sector. For instance, the acceleration of antihydrogen in the Earth's gravitational field could be investigated [13]. We also note that in gravitational contexts, various SME coefficients that are inaccessible in the flat-spacetime limit now become measurable [13].

Acknowledgments.—The author wishes to thank Jörg Jäckel for the invitation to this stimulating meeting. This work is supported by CONACyT under Grant No. 55310.

References

- [1] For recent reviews of various ideas in the subject see, e.g., V.A. Kostelecký, ed., *CPT and Lorentz Symmetry I-IV*, World Scientific, Singapore, 1999-2008; R. Bluhm, Lect. Notes Phys. **702**, 191 (2006) [hep-ph/0506054].
- [2] See, e.g., V.A. Kostelecký and S. Samuel, Phys. Rev. D **39**, 683 (1989); V.A. Kostelecký and R. Potting, Nucl. Phys. B **359**, 545 (1991); J. Alfaro, H.A. Morales-Técotl, and L.F. Urrutia, Phys. Rev. Lett. **84**, 2318 (2000); S.M. Carroll *et al.*, Phys. Rev. Lett. **87**, 141601 (2001); V.A. Kostelecký, R. Lehnert, and M.J. Perry, Phys. Rev. D **68**, 123511 (2003); O. Bertolami *et al.*, Phys. Rev. D **69**, 083513 (2004); J.D. Bjorken, Phys. Rev. D **67**, 043508 (2003); N. Arkani-Hamed *et al.*, JHEP **0701**, 036 (2007).
- [3] D. Colladay and V.A. Kostelecký, Phys. Rev. D **55**, 6760 (1997); Phys. Rev. D **58**, 116002 (1998); V.A. Kostelecký and R. Lehnert, Phys. Rev. D **63**, 065008 (2001); V.A. Kostelecký, Phys. Rev. D **69**, 105009 (2004); V.A. Kostelecký and M. Mewes, Phys. Rev. D **80**, 015020 (2009).
- [4] See, e.g., R. Jackiw and V.A. Kostelecký, Phys. Rev. Lett. **82**, 3572 (1999); V.A. Kostelecký *et al.*, Phys. Rev. D **65**, 056006 (2002); B. Altschul and V.A. Kostelecký, Phys. Lett. B **628**, 106 (2005); R. Lehnert, J. Math. Phys. **45**, 3399 (2004); Phys. Rev. D **74**, 125001 (2006); arXiv:0711.4851 [hep-th]; A.J. Hariton and R. Lehnert, Phys. Lett. A **367**, 11 (2007).
- [5] V.A. Kostelecký and N. Russell, arXiv:0801.0287 [hep-ph].
- [6] R. Lehnert, Phys. Rev. D **68**, 085003 (2003).
- [7] R. Lehnert and R. Potting, Phys. Rev. Lett. **93**, 110402 (2004); Phys. Rev. D **70**, 125010 (2004).
- [8] M.A. Hohensee *et al.*, Phys. Rev. Lett. **102**, 170402 (2009); Phys. Rev. D **80**, 036010 (2009).
- [9] S.M. Carroll, G.B. Field, and R. Jackiw, Phys. Rev. D **41**, 1231 (1990).
- [10] V.A. Kostelecký and M. Mewes, Phys. Rev. Lett. **99**, 011601 (2007); M. Mewes, Phys. Rev. D **78**, 096008 (2008).
- [11] R. Bluhm, V.A. Kostelecký, and N. Russell, Phys. Rev. D **57**, 3932 (1998).
- [12] Q.G. Bailey and V.A. Kostelecký, Phys. Rev. D **74**, 045001 (2006); H. Müller *et al.*, Phys. Rev. Lett. **100**, 031101 (2008); J.B.R. Battat, J.F. Chandler, and C.W. Stubbs, Phys. Rev. Lett. **99**, 241103 (2007); Q.G. Bailey, Phys. Rev. D **80**, 044004 (2009).
- [13] V.A. Kostelecký and J. Tasson, Phys. Rev. Lett. **102**, 010402 (2009).

Constraints on pseudoscalar-photon interaction from CMB polarization observation

Wei-Tou Ni^{1,2}

¹Center for Gravitation and Cosmology, Department of Physics, National Tsing Hua University, Hsinchu, Taiwan, 30013 ROC Email: weitou@gmail.com

²Purple Mountain Observatory, Chinese Academy of Sciences, Nanjing 210008, China

DOI: http://dx.doi.org/10.3204/DESY-PROC-2009-05/ni_wei-tou

Effective pseudoscalar-photon interactions would induce a rotation of linear polarization of electromagnetic wave propagating with cosmological distance in various cosmological models. Pseudoscalar-photon interactions are proportional to the gradient of the pseudoscalar field. From the phenomenological point of view, this gradient could be neutrino number asymmetry, any density current, or a constant vector. In these situations, Lorentz invariance or CPT may effectively be violated. CMB polarization observations are superb tests of these models and have the potential to discover new fundamental physics. In this paper, we review the constraints on pseudoscalar-photon interactions from CMB polarization observations.

1 Introduction

In 1973, we studied the relationship of Galilio Equivalence Principe (WEP I) and Einstein Equivalence Principe in a framework (the χ -g framework) of electromagnetism and charged particles, we found the following theory with (gravitational) interaction Lagrangian density

$$L_{\text{int}} = -\left(\frac{1}{16\pi}\right)(-g)^{1/2}\left[\frac{1}{2}g^{ik}g^{jl} - \frac{1}{2}g^{il}g^{kj} + \phi\varepsilon^{ijkl}\right]F_{ij}F_{kl} - A_k j^k (-g)^{1/2} - \Sigma_I \frac{ds_I}{dt} \delta(x - x_I), \quad (1)$$

as an example which obeys WEP I, but not EEP [1, 2, 3]. The nonmetric part of this theory is

$$L_{\text{int}}^{(NM)} = -\left(\frac{1}{16\pi}\right)(-g)^{1/2}\phi\varepsilon^{ijkl}F_{ij}F_{kl} = -\left(\frac{1}{4\pi}\right)(-g)^{1/2}\phi_{,i}\varepsilon^{ijkl}A_j A_{k,l} \pmod{\text{div}}, \quad (2)$$

where ‘mod div’ means that the two Lagrangian densities are related by partial integration in the action integral. The Maxwell equations [1, 3] are

$$F^i{}_{|k} + \varepsilon^{ikml}F_{km}\varphi_{,l} = -4\pi j^i, \quad (3)$$

where the derivation $|$ is with respect to the Christoffel connection. The Lorentz force law is the same as in metric theories of gravity or general relativity. Gauge invariance and charge conservation are guaranteed. The Maxwell equations are also conformally invariant.

The last term in equation (2) is reminiscent of Chern-Simons [4] term $e^{\alpha\beta\gamma}A_\alpha F_{\beta\gamma}$. There are two differences: (i) Chern-Simons term is in 3 dimensional space; (ii) Chern-Simons term is a total divergence.

A term similar to the one in equation (2) (axion-gluon interaction) occurs in QCD in an effort to solve the strong CP problem (Peccei and Quinn [5], Weinberg [6], Wilczek [7]). Carroll, Field and Jackiw [8] proposed a modification of electrodynamics with an additional $e^{ijkl}V_i A_j F_{kl}$ term with V_i a constant vector. This term is a special case of the term $e^{ijkl}\varphi F_{ij}F_{kl}$ (mod div) with $\varphi_{,i} = -\frac{1}{2}V_i$.

Various terms in the Lagrangians discussed in this section are listed in Table 1. Empirical tests of the pseudoscalar-photon interaction (2) from CMB polarization observation will be discussed in section 2. Section 3 will present an outlook.

Term	Dimension	Reference	Meaning
$e^{\alpha\beta\gamma}A_\alpha F_{\beta\gamma}$	3	Chern-Simons (1974[4])	Integrand for topological invariant
$e^{ijkl}\varphi F_{ij}F_{kl}$	4	Ni (1973[1], 1974[2],1977[3])	Pseudoscalar-photon coupling
$e^{ijkl}\varphi F^{QCD}_{ij}F^{QCD}_{kl}$	4	Peccei-Quinn (1977[5]) Weinberg (1978[6]) Wilczek (1978[7])	Pseudoscalar-gluon coupling
$e^{ijkl}V_i A_j F_{kl}$	4	Carroll-Field-Jackiw (1990[8])	External constant vector coupling

Table 1: Various terms in the Lagrangian and their meaning.

2 Constraints from CMB polarization observation

Pseudoscalar-photon interactions induce polarization rotation in electromagnetic propagation. From (3), for the right circularly polarized electromagnetic wave, the propagation from a point P_1 to another point P_2 adds a phase of $\alpha = \varphi(P_2) - \varphi(P_1)$ to the wave; for left circularly polarized light, the added phase will be opposite in sign [1]. Linearly polarized electromagnetic wave is a superposition of circularly polarized waves. Its polarization vector will then rotate by an angle α . When the propagation distance is over a large part of our observed universe, we call this phenomenon cosmic polarization rotation [9, 10].

Since the first successful polarization observation of the cosmological microwave background (CMB) in 2002 by DASI [11] (Degree Angular Scale Interferometer), there have been a number of observations [12-16] with better precision. These observations set limits on the electromagnetic polarization rotation due to effective pseudoscalar-photon interaction.

In the CMB polarization observations, there are variations and fluctuations. The variations and fluctuations due to scalar-modified propagation can be expressed as $\delta\varphi(2) - \delta\varphi(1)$, where 1 denotes a point at the last scattering surface in the decoupling epoch and 2 the observation point. $\delta\varphi(2)$ is the variation/fluctuation at the last scattering surface. $\delta\varphi(1)$ at the present observation point is fixed. Therefore the covariance of fluctuation $\langle [\delta\varphi(2) - \delta\varphi(1)]^2 \rangle$ gives

the covariance of $\delta\varphi^2(2)$ at the last scattering surface. Since our Universe is isotropic to $\sim 10^{-5}$, this covariance is $\sim (\xi \times 10^{-5})^2$ where the parameter ξ depends on various cosmological models [10, 17].

In 2002, the DASI microwave interferometer observed the polarization of the cosmic background [11]. E-mode polarization is detected with 4.9σ . The TE correlation of the temperature and E-mode polarization is detected at 95% confidence. This correlation is expected from the Raleigh scattering of radiation. However, with the (pseudo)scalar-photon interaction (2), the polarization anisotropy is shifted differently in different directions relative to the temperature anisotropy due to propagation; the correlation will then be downgraded. In 2003, from the first-year data (WMAP1), WMAP found that the polarization and temperature are correlated to more than 10σ [12]. This gives a constraint of about 10^{-1} for $\Delta\varphi$ [9, 18].

Further results [13-16] and analyses [15, 19-27] of CMB polarization observations came out after 2006. In Table 1, we update our previous compilations of [10, 17]. Although these results look different at 1σ level, they are all consistent with null detection and with one another at 2σ level. For the interpretation of cosmic polarization rotation in various cosmologic models, please see [10, 17].

The Faraday rotation due to a magnetic field is wavelength-dependent while the cosmic polarization rotation due to effective pseudoscalar-photon interaction is wavelength-independent. This property can be used to separate the two effects in more precise observations.

Reference	Constraint [mrad]	Source data
Ni [9, 18]	± 100	WMAP1 [12]
Feng, Li, Xia, Chen, and Zhang [19]	-105 ± 70	B03 [14]
Liu, Lee, Ng [20]	± 24	B03 [14]
Kostelecky and Mews [21]	209 ± 122	B03 [14]
Cabella, Natoli and Silk [22]	-43 ± 52	WMAP3 [13]
Xia, Li, Wang, and Zhang [23]	-108 ± 67	WMAP3 [13] & B03 [14]
Komatsu, <i>et al.</i> [15]	-30 ± 37	WMAP5 [15]
Xia, Li, Zhao, and Zhang [24]	-45 ± 33	WMAP5 [15] & B03 [14]
Kostelecky and Mews [25]	40 ± 94	WMAP5 [15]
Kahniashvili, Durrer, and Maravin	± 44	WMAP5 [15]
Wu, <i>et al.</i> [27]	$9.6 \pm 14.3 \pm 8.7$	QuaD [16]

Table 2: Constraints on cosmic polarization rotation from CMB (cosmic microwave background).

3 Discussion and Outlook

Better accuracy in CMB polarization observation is expected from PLANCK mission launched on May 14, 2009. Dedicated CMB polarization observers like B-Pol mission, CMBpol mission and LiteBIRD mission would improve the sensitivity further. These development would probe the fundamental issues of effective pseudoscalar-photon interactions discussed in this paper more deeply in the future.

We would like to thank the National Science Council (Grant Nos NSC97-2112-M-007-002 and NSC98-2112-M-007-009) and the National Natural Science Foundation (Grant Nos. 10778710 and 10875171) for supporting this work.

References

- [1] W.-T. Ni, A Nonmetric Theory of Gravity, preprint, Montana State University, Bozeman, Montana, USA (1973), <http://cgc.pmo.ac.cn>
- [2] W.-T. Ni, Bull. Am. Phys. Soc. **19** 655 (1974).
- [3] W.-T. Ni, Phys. Rev. Lett. **38** 301 (1977).
- [4] S.-S. Chern and J. Simons, Characteristic forms and geometric invariants *The Annals of Mathematics*, 2nd Ser. **99** 48 (1974).
- [5] R. D. Peccei and H. Quinn, Phys. Rev. Lett. **38** 1440 (1977).
- [6] S. Weinberg, Phys. Rev. Lett. **40** 233 (1978).
- [7] F. Wilczek, Phys. Rev. Lett. **40** 279 (1978).
- [8] S. M. Carroll, G. B. Field and R. Jackiw, Phys. Rev. **D41** 1231 (1990).
- [9] W.-T. Ni, Chin. Phys. Lett. **22** 33 (2005) [arXiv:gr-qc/0407113].
- [10] W.-T. Ni, Prog. Theor. Phys. Suppl. **172** 49 (2008) [arXiv:0712.4082] .
- [11] J. M. Kovac *et al.*, Nature **420** 722 (2002).
- [12] C. L. Bennett *et al.*, Astrophys. J. Suppl. **148** 1 (2003); and references therein.
- [13] D. N. Spergel *et al.*, Astrophys. J. Suppl. **170** 377 (2007); and references therein.
- [14] T. E. Montroy *et al.*, Astrophys. J. **647** 813 (2006); and references therein.
- [15] E. Komatsu *et al.*, Astrophys. J. Suppl. **180** 330 (2009) [arXiv:0803.0547].
- [16] C. Pryke *et al.*, Astrophys. J. **692** 1247 (2009).
- [17] W.-T. Ni, Int. J. Mod. Phys. **A18 & 19** 3493 (2009) [arXiv:0903.0756].
- [18] W.-T. Ni, Int. J. Mod. Phys. **D14** 901 (2005) [arXiv:gr-qc/0504116].
- [19] B. Feng *et al.*, Phys. Rev. Lett. **96** 221302 (2006).
- [20] G. C. Liu, S. Lee and K. W. Ng, Phys. Rev. Lett. **97** 161303 (2006); private communication.
- [21] A. Kostelecky and M. Mewes, Phys. Rev. Lett. **99** 011601 (2007).
- [22] P. Cabella, P. Natoli and J. Silk, Phys. Rev. **D76** 123014 (2007).
- [23] J.-Q. Xia *et al.*, Astron. Astrophys. **483** 715 (2008).
- [24] J.-Q. Xia *et al.*, Astrophys. J. **679** L61 (2008).
- [25] V. A. Kostelecky and M. Mewes, Astrophys. J. **689** L1 (2008).
- [26] T. Kahniashvili, R. Durrer and Y. Maravin, Phys. Rev. **D78** 123009 (2008).
- [27] E.-Y.-S. Wu *et al.*, Phys.Rev. Lett. **102** 161302 (2009).

Chapter 10

New Ideas

Photon Production From The Scattering of Axions Out of a Solenoidal Magnetic Field

Eduardo I. Guendelman¹, Idan Shilon¹, Giovanni Cantatore², Konstantin Zioutas³

¹Physics Department, Ben-Gurion University of the Negev, Beer-Sheva 84105, Israel

²Università and INFN Trieste, via valerio 2, 34127 Trieste, Italy

³University of Patras, Patras, Greece

DOI: <http://dx.doi.org/10.3204/DESY-PROC-2009-05/shilon.idan>

We calculate the total cross section for the production of photons from the scattering of axions by a strong inhomogeneous magnetic field in the form of a 2D delta function, a cylindrical step function and a 2D Gaussian distribution, which can be approximately produced by a solenoidal current. The theoretical result is used to estimate the axion-photon conversion probability which could be expected in a reasonable experimental situation. Finally, we have also considered scattering at a resonance $E_{axion} \sim m_{axion}$, which gives the most enhanced results.

In a series of recent publications by one of us [1], it was shown that an axion-photon system displays a continuous duality symmetry when an external magnetic field is present and when the axion mass is neglected. This allows one to analyze the behavior of axions and photons in external magnetic fields in terms of an axion-photon complex field. It is important to note here that the same duality symmetry exists also when considering massive photons, under the condition $m_\gamma = m_a$.

This new 2D formalism uses a duality symmetry between the axion field and the scattered component of the photon to define an axion-photon complex field as $\Psi = 1/\sqrt{2}(\phi + iA)$, where ϕ is the axion field and A is the photon component that takes part in the scattering process. We focus here on the case where an electromagnetic field with propagation along the x and y directions and a strong static magnetic field pointing in the z -direction are present. The magnetic field may have an arbitrary space dependence in x and y . For convenience let us neglect the axion mass so we can write the lagrangian in terms of the new canonical variables Ψ and its charge conjugate Ψ^*

$$\mathcal{L} = \partial_\mu \Psi^* \partial^\mu \Psi - \frac{i}{2} \beta (\Psi^* \partial_t \Psi - \Psi \partial_t \Psi^*) , \quad (1)$$

where $\beta(x, y) = gB(x, y)$ with $B(x, y)$ being the external magnetic field and where g is the photon-axion coupling constant. To apply these results to some specific system with a magnetic field, we write separately the time and space dependence of the axion-photon field as $\Psi(\vec{r}, t) = e^{-i\omega t} \psi(\vec{r})$.

As a first model, we consider a magnetic field of the form $B = \Phi \delta^2(x, y)$. This kind of a potential can not be realized in the lab but we will show that the results for this calculation have physical significance in the resonance case, where the scattering becomes isotropic.

Separating the time and space dependence of Ψ and considering the δ function potential gives the following equation of motion

$$[-\vec{\nabla}^2 + g\Phi E\delta^2(x, y)]\psi(\vec{r}) = E^2\psi(\vec{r}), \quad (2)$$

where E is the energy of the particle beam. Solving this equation while regulating the δ function by introducing the cut-off Λ yields the solution

$$\psi(\vec{r}) = e^{i\vec{k}\cdot\vec{r}} - G_k(r) \left[\frac{1}{g\Phi E} + \frac{\log(\Lambda/E)}{2\pi} + \frac{i}{2} \right]^{-1}, \quad (3)$$

where $G_k(r)$ is Green's function in two dimensions $G_k(r) = \frac{i}{4}H_0^{(1)}(kr) \xrightarrow{r \rightarrow \infty} \frac{1}{2\sqrt{2\pi kr}}e^{i(kr+\pi/4)}$.

The scattering amplitude $f(\theta)$ is found from the asymptotic behavior of the scattering wave function $\psi(\vec{r}) \rightarrow e^{i\vec{k}\cdot\vec{r}} + \frac{1}{\sqrt{r}}f(\theta)e^{i(kr+\pi/4)}$. Since there is no dependence on θ in $f(\theta)$ the scattering here is completely isotropic. Then, to first order in g we find that $\sigma_{tot}^\delta = \frac{g^2\Phi^2 E}{4}$. Thus, the probability is given by $P_\delta = \sigma_S/\sigma_G = \frac{g^2\Phi^2 E}{4D} = \frac{\pi^2 g^2 B^2 R^3 E}{8}$, where $\sigma_G = 2RL$ is the geometrical cross-section of the potential.

We wish to obtain eventually measurable quantities which can be incorporated in a laboratory experiment, thus we have to consider a more realistic function to describe the magnetic field generated by the solenoid. First, let us describe the inhomogeneous magnetic field by a Gaussian distribution around the solenoid's axis $\vec{B}(r) = B_0 e^{-\frac{r^2}{R^2}} \hat{z}$. Hence, the scattered wave function is

$$\psi(\vec{r}) = e^{i\vec{k}\cdot\vec{r}} + \frac{\sqrt{\pi}gB_0R^2\sqrt{E}}{2\sqrt{2}r} e^{-\frac{1}{4}(Rq)^2} e^{i(kr+\pi/4)}. \quad (4)$$

This gives for the scattering amplitude $f(\theta) = \sqrt{(\pi/8)}gB_0R^2E^{1/2}e^{-\frac{1}{4}(Rq)^2}$, where the explicit dependence of q (i.e the momentum transfer) on the angle is given by $q^2 = 2k^2(1 - \cos\theta) = 4k^2 \sin^2(\theta/2)$. Hence, The total 2D cross-section is given by

$$\int_0^{2\pi} |f(\theta)|^2 d\theta = \frac{\pi}{8}(gB_0)^2 R^4 E \int_0^{2\pi} e^{-\frac{1}{2}(Rq)^2} d\theta = \frac{\pi^2}{4}(gB_0)^2 R^4 E e^{-(Rk)^2} I_0((Rk)^2), \quad (5)$$

where $I_0(x) = J_0(ix)$ is the modified Bessel function. The argument of this function (i.e $(Rk)^2$) is very large ($1 \text{ eV} \times 1 \text{ cm} \approx 10^5$) so we can use the asymptotic form of the modified Bessel function which, by keeping only the first order term, gives the result $\sigma_{tot}^{Gauss} = \frac{\pi^{3/2}}{\sqrt{32}}g^2 B_0^2 R^3$, from which we find the conversion probability to be $P_{Gauss} = \frac{\pi^{3/2}}{8\sqrt{2}}g^2 B_0^2 R^2$.

Now we turn to consider the magnetic field generated by an ideal solenoidal current which is described by a step function realizing a uniform magnetic field pointing in the \hat{z} direction and constrained to a cylindrical region around the origin: $\vec{B}(\vec{r}) = B_0\hat{z}$ for $r < R$. Using the Fourier transformation of the step function we find that the scattering amplitude is now given by $f(\theta) = \sqrt{\frac{\pi}{2}}\frac{B_0 R g E^{1/2}}{q} J_1(qR)$, where the explicit dependence of q on θ was shown earlier here.

Before evaluating the integral for the total cross-section, let us write the total cross section for the square well case in terms of the delta function cross-section: $\sigma_{tot}^{well} = \sigma_{tot}^\delta \frac{2}{\pi} I(ER)$, where $I(ER) = \int_0^{2\pi} \left| \frac{J_1(qR)}{qR} \right|^2 d\theta$ is a dimensionless quantity which is a function of the multiplication

$E \cdot R$. Of course, the proportionality constant connects also the conversion probabilities for the δ function and square well cases. Denoting $ER = kR$ by η , the integral can be analytically solved with the solution $I(\eta) = \frac{\pi}{2} {}_2F_3(\{\frac{1}{2}, \frac{2}{3}\}; \{1, 2, 3\}; -4\eta^2)$, where ${}_2F_3$ is an hypergeometric function.

To analyze this solution we expand the hypergeometric function ${}_2F_3$ to a series. Then, for small η , $I(\eta)$ is converging toward the constant value $\pi/2$, thus giving the equality $\sigma_{tot}^{well} = \sigma_{tot}^\delta$. This result is expected since considering only small η values is equivalent to considering isotropic scattering because $\eta \ll 1$ means that $ER \ll 1$. Hence, the wavelength of Ψ is very large compared to the length scale of the potential. Therefore, this approximation corresponds to δ function limit of the step function, which, in turn, means that we consider isotropic scattering.

On the other end, we have the expansion for large η which shows that the integral approaches the limit $I \rightarrow \frac{8}{3\pi\eta} = \frac{8}{3\pi ER}$ very fast. This limit gives the result $P_{well} = \frac{1}{6}g^2B^2D^2 = \frac{2}{3}g^2B^2R^2$.

So far in this report, we have considered the axion field as a massless field in order to get the $U(1)$ symmetry between axions and photons. In fact, this symmetry holds up whenever the axion mass is equal to the (effective) photon mass inside a medium. Of course, in that case our conclusions will have to be modified. The term that has to be taken under consideration is an $1/\sqrt{(E^2 - m^2)^{1/2}}$ term which comes from the Green's function and will replace the current $1/\sqrt{E}$ in the scattering amplitude. Thus, in the $m_a \sim m_\gamma \neq 0$ case, the total two dimensional cross-section (for the δ function case) would have the following energy dependence: $\sigma_{tot} = \frac{\pi q^2 B^2 R^4 E^2}{4\sqrt{(E^2 - m^2)}}$, and we have a resonance when $E = m$. For an axion rest mass below ~ 1 eV, this can have practical consequences, for example, in laser generated axions when one can control the energy of the axion beam.

The limit of zero momentum means accounting only zero modes of the Fourier Transform, hence the 1D treatment of this process can not be justified since in the limit of zero momentum the scattering amplitude and the differential scattering cross-section become isotropic (i.e independent of the angle) and it is impossible to consider only one direction in the scattering.

To summarize, we have studied here the first examples of scattering which is not one dimensional and we have obtained enhanced probabilities. This effect is further increased in the case of resonant scattering that appears when $E = m$ and corresponds to isotropic scattering.

In the 1D case the conversion probability is $P_{1D} = g^2B^2l^2/4$, where l is the linear dimension associated with the extent of the magnetic field [4]. Hence, when trying to compare the conversion probability for the cylindrically symmetric geometry found by the method used in this work with the known 1D calculation it is not so obvious what is the correct length scale l that should be taken to calculate P_{1D} . The problem is that the notion of splitting does not make sense in 1D and that the scattering region is not an area but a line. Hence, the best way to discuss the relation between the two calculations will be to average the 1D probability over the scattering region for each case. In other words, we look at the 2D experiment as the weighted average of an infinite number of 1D experiments.

The general case is rather complicated since the scattering region may be infinite and the magnetic field may not be homogenous. However, a 1D analogue to the 2D experiment can be found and the weighted average can be done by choosing the magnetic flux as the averaging measure

$$P_{1D}^{avg.} = \frac{\int_{-\infty}^{\infty} \int_{-\infty}^{\infty} \frac{1}{4}g^2 |\int_{-\infty}^{\infty} B(x', y) dx'|^2 B(x, y) dx dy}{\int_{-\infty}^{\infty} \int_{-\infty}^{\infty} B(x, y) dx dy} . \quad (6)$$

For the step function case the scattering region is a cylinder with radius R . Hence, the

average of P_{1D} in this case is $P_{1D}^{well\ avg.} = \frac{2}{3}g^2 B_0^2 R^2$ a result which coincides with the 2D result.

When considering the Gaussian case the averaged 1D probability is $P_{1D}^{Gauss. avg.} = \frac{\pi}{\sqrt{3}} \frac{g^2 B_0^2 R^2}{4}$. The comparison of this result with the 2D result gives $P_{Gauss}/P_{1D}^{Gauss. avg.} = 1.085$ and thus the 2D result is bigger by 8.5%.

Despite Eq. (6) not all 2D experiments can have a 1D analogue. We have seen that when considering resonant scattering, the limit of zero momentum implies that the cross section is isotropic and there is no way to describe such a process with an analogous 1D calculation.

When considering scattering from a finite sized potential the enhancement of the conversion probability compared to the 1D case still gives probabilities in the same order of magnitude. This is due to the fact that the wavelength ($1/E$) of the Ψ wave function is much smaller than the length scale of the potential (R), which essentially results in a quasi-1D behavior of the system. When the wavelength will be smaller, or even comparable to the length scale of the potential we see that we get bigger enhancement since in this case the scattering becomes more and more isotropic and we essentially obtain δ function scattering.

The wavelength is determined by the momentum of the particles. For the massive case, the momentum approaches zero when the energy of the particles is of the order of the particle's mass. This situation, where the wavelength of the particles is much larger than any other length scale in the problem, is realized in the resonant scattering case. There we have shown explicitly that this limit gives an isotropic scattering for a finite potential and thus, conversion probabilities of the order of the δ function case.

Our results may also be applicable for solar scales as well. In the sun, magnetic flux tube can play the role of a solenoidal potential while the energy spectrum of photons is continuous. Thus, we expect to have both isotropic and anisotropic scattering. These magnetic flux tubes are enormous regions of constant magnetic flux with length scale of the order of about 10^2 km in diameter and 10^3 km in length. Hence, the conversion probability will be greatly enhanced.

Acknowledgments

The authors wish to thank J. Jaeckel and J. Redondo for useful correspondence and conversations. E.I. Guendelman thanks the university of Trieste and INFN for the kind hospitality and support during his visit to Trieste. I. Shilon thanks the organizers of the 5th Patras workshop, and in particular J. Jaeckel, for inviting and supporting participation in the workshop.

References

- [1] E.I. Guendelman, Mod. Phys. Lett. A **23** 191 (2008), arXiv: 0711.3685 [hep-th]; E.I. Guendelman, Phys. Lett. B **662** 227 (2008), arXiv: 0801.0503 [hep-th]; E.I. Guendelman, Phys. Lett. B **662** 445 (2008), arXiv: 0802.0311 [hep-th].
- [2] E. Arik, et al. (The CAST collaboration), JCAP 0902:008 (2009); arXiv: hep-ex/0810.4482.
- [3] K. van Bibber, P.M. McIntyre, D.E. Morris and G.G. Raffelt, Phys. Rev. D **39** 2089 (1989). See also: R. Rabadan, A. Ringwald, K. Sigurson, Phys. Rev. Lett. **96** 110407 (2006).
- [4] K. van Bibber, N.R. Dagdeviren, S.E. Koonin, A.K. Kerman and H.N. Nelson, Phys. Rev. Lett. **59** 759 (1987).

Photon \leftrightarrow Axion conversions in transversely inhomogeneous magnetic fields

Javier Redondo

Max-Planck-Institut, Föhringer Ring 6, D-80805 München, Germany

DOI: http://dx.doi.org/10.3204/DESY-PROC-2009-05/redondo_javier

We compute the photon-axion conversion probability in an external magnetic field with a strong transverse gradient in the eikonal approximation for plane waves. We find it typically smaller than a comparable uniform case. Some insights into the phenomenon of photon-axion splitting are given.

Recently, a possible enhancement of photon \leftrightarrow axion conversions in magnetic fields with strong gradients has been proposed [1, 2]. Such an enhancement is in the core of recent proposals to explain some aspects of the X-ray activity of the Sun: the longstanding corona problem and the triggering of solar flares [3, 4]. The core idea of these solutions is that axions created in the solar interior by the Primakoff effect, and therefore having energies corresponding to X-rays, could reconvert into photons in the outside layers of the Sun.

The standard mechanism for reconversion, inverse Primakoff, produces a too small deposition of energy to account for these effects. An alternative is the coherent conversion in the strong and long magnetic fields of the solar surface. An estimate of this effects using a 1-D formula for the reconversion probability is not very promising either, but recent claims suggest that this might be not adequate and a full 3-D calculation could lead to surprises [2, 4]. In particular, axion-photon conversion in strong magnetic field gradients has attracted some attention because could lead to an enhancement of the conversion probability due to the so-called “photon-axion splitting” [5]. If such an enhancement is realized, it could be very advantageous for laboratory experiments looking for axions, or axion-like-particles, to use quadrupole magnets instead of the usual dipoles. This possibility is already under consideration in the CAST helioscope and in the OSQAR “light-shining-through-walls” experiment [6].

In this contribution we present some simple calculations and physical insights on the phenomenon of photon-axion splitting. We find the 1-D estimation of the conversion probability to be reliable in the cases of interest. As a consequence, no enhancement is foreseeable in the solar environment and the use of quadrupoles presents no advantage over current dipoles.

1 Invitation: Mirages

A hot surface like a road in summer behaves as a mirror for objects and observers placed near to it. This phenomenon is called a “mirage” and has their origin on the curvature of light rays in the presence of a temperature gradient causing a gradient of the air’s refraction index.

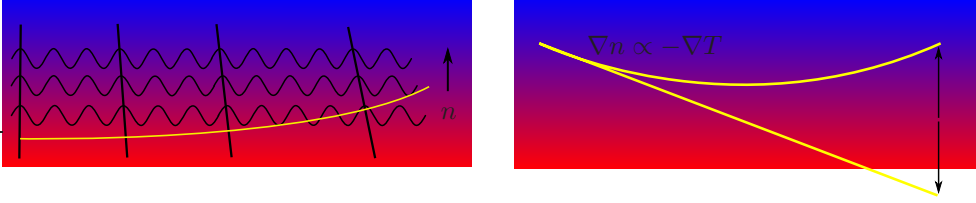


Figure 1: Qualitative evolution of a light wave propagating initially parallel to a hot surface, which forms a gradient of n . The index of refraction increases with altitude, so the wave-number k is increasingly larger with respect to the frequency ω , making the phase-fronts increasingly closer with altitude. As the phase-fronts become tilted, the light rays, which are perpendicular to them, bend upwards forming a inverted image.

2 The photon-axion system in a transverse gradient field

In a transverse external magnetic field (B), the component of the photon field along the external magnetic field (A) mixes with the axion (a) and the equations of motion can be written as [7]

$$\left[\square + \begin{pmatrix} m_a^2 & gB\omega \\ gB\omega & 0 \end{pmatrix} \right] \begin{pmatrix} A \\ a \end{pmatrix} = 0. \quad (1)$$

Let us take $m_a = 0$ for the purpose of illustration. In this case, the equations can be diagonalized by considering the linear superpositions $A_{\pm} = (A \pm a)/\sqrt{2}$ which therefore evolve according to

$$\square A_{\pm} = m_{\pm}^2 A_{\pm} \quad ; \quad \text{with} \quad m_{\pm}^2 = \pm gB\omega. \quad (2)$$

The A_{\pm} waves have indices of refraction with opposite sign given by $n_{\pm}^2 = 1 - m_{\pm}^2/\omega^2 = 1 \mp gB/\omega$ and therefore, in complete analogy with the mirage effect, the A_{\pm} rays will curve in *opposite* directions if there is a transverse gradient of the magnetic field. This leads to the so-called “photon-axion splitting” [5] with very speculative and spectacular consequences [8].

We can get a not very sophisticated first look at the photon \leftrightarrow axion conversion probability by looking at the evolution of A_{\pm} phase fronts. In Fig. 2 we can see a comparison of the homogeneous and constant gradient case. For this first look we neglect any diffraction effect and changes on the A_{\pm} amplitudes, we simply consider a 1-D problem for each value of x . The phase fronts of A_{\pm} separate a distance $(n_+^{-1} - n_-^{-1})\lambda_0 \simeq gB\lambda/\omega$ in a wavelength λ_0 . Equivalently, after a distance Z there is a phase difference of $\phi_+ - \phi_- \simeq -gBZ$ between the A_+ and A_- waves. This phase difference is constant in the x direction in the homogeneous case but increases linearly for a constant gradient.

The $\gamma \leftrightarrow a$ conversion probability per unit transverse length can be compared in both cases. In each case it can be written as $c\|e^{i\phi_+} - e^{i\phi_-}\|^2/4 = c\sin^2(gBZ/2)$ with $B = B_0$ for a constant field and $B = B_1x$ for the gradient case (c is a normalization unimportant for our purposes). The ratio of the two probabilities integrated over an interval $x \in (-X, X)$ is then

$$\frac{P|_{B=B_1x}}{P|_{B=B_0}} = \frac{\frac{1}{2}(1 - \text{sinc}(2gB_1XZ))}{\sin^2(gB_0Z/2)} \xrightarrow{gBZ \ll 1} \frac{1}{3} \left(\frac{B_1X}{B_0} \right)^2 \quad (3)$$

The last limit is relevant in usual practical applications, given the smallness of the values of the axion-photon coupling g allowed by stellar evolution arguments as well as the typical sizes and strengths of magnetic fields. Note that B_1X gives the maximum magnetic field in the x -interval we have used. Superconducting quadrupoles have their field gradients limited precisely

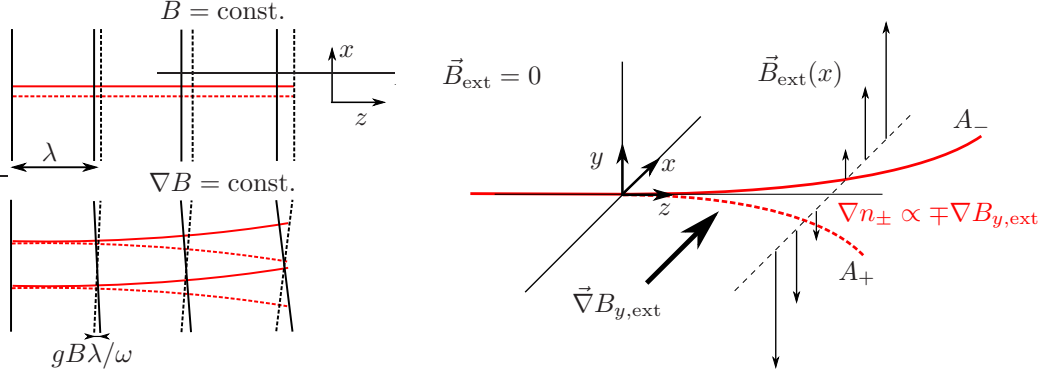


Figure 2: (LHS) Evolution of the $A_{\pm} = (A \pm a)/\sqrt{2}$ phase fronts (black dashed and solid, respectively) in the presence of a transversely homogeneous (up) and constant gradient (down) magnetic field. The corresponding rays are shown in red. (RHS) The gradient case shown in perspective.

by the critical field at the boundaries, so in comparing a quadrupole with a similar dipole one should use $B_1 X \sim B_0$. Quadrupoles are therefore less efficient than dipoles. This result is very easy to understand. By making the problem 1-D, only the strength of the magnetic field squared matters, which in average is of course smaller in a quadrupole than in a dipole.

3 Solution in the eikonal approximation

The most important 2-D features of the problem can be studied in the eikonal approximation. Starting with the ansatz $A_{\pm}(x, z, t) = \mathcal{A}_{\pm}(x, z)e^{-i\omega t}e^{i\omega S_{\pm}(x, z)}$ the equations of motion become

$$(\nabla S_{\pm})^2 - 1 \frac{1}{\omega} \frac{\nabla(\mathcal{A}_{\pm}^2 \nabla S_{\pm})}{\mathcal{A}_{\pm}^2} - \frac{1}{\omega^2} \frac{\nabla^2 \mathcal{A}_{\pm}}{\mathcal{A}_{\pm}^2} = 1 - \frac{m_{\pm}^2}{\omega^2} \equiv n_{\pm}^2(x) \quad (4)$$

The eikonal approximation amounts to neglect the second and third terms of the LHS, which are suppressed if diffraction effects occur in length scales much longer than the wavelength λ_0 . We will solve only the equation of A_+ since the solution of A_- is given by the former by changing the sign of the magnetic field. The eikonal equation $(\nabla S)^2 = n^2(x)$ can be solved by the method of characteristics, i.e. finding a one-parameter family of curves $\vec{r}_{x_0}(s) = (x(s), z(s))$ (we drop the trivial component y) that satisfy the Hamilton equations

$$\frac{d\vec{r}}{ds} = \vec{p} \quad ; \quad \frac{d\vec{p}}{ds} = \vec{\nabla} n^2 / 2 . \quad (5)$$

with initial conditions at the boundary of the magnetic field $\vec{r}(0) = (x_0, 0)$, $\vec{p}(0) = (0, n_0)$ with $n_0 = n(x_0)$. These are given by

$$\vec{r}(s, x_0) = (x_0 - \mathcal{B}s^2/4, sn_0) \quad (6)$$

where we have defined $\mathcal{B} = gB_1/\omega$, the quantity that controls the inverse of the radius of curvature of rays $R = 4\mathcal{B}^{-1}(1 + (\mathcal{B}s/2)^2)^{3/2}$, which turns out to be *huge* for typical parameters

$$\mathcal{B}^{-1} = \frac{\omega}{gB_1} \simeq 5 \times 10^{17} \text{m} \left(\frac{\omega}{\text{keV}} \right) \left(\frac{g}{10^{-10} \text{GeV}^{-1}} \right)^{-1} \left(\frac{B_1}{\text{T/cm}} \right)^{-1} \quad (7)$$

The angle of divergence of the A_{\pm} rays after a length z is $\theta_{\mathcal{B}} \simeq \mathcal{B}z$.

The eikonal function giving the evolution of the A_{\pm} phases is given by

$$S = \int_0^s \vec{\nabla} S \cdot d\vec{r}(s) = sn_0^2 + \frac{\mathcal{B}^2 s^3}{12} = zn(x) \left(\frac{2}{1 + \sqrt{1 - \xi^2}} \right)^{1/2} \left(\frac{2 + \sqrt{1 - \xi^2}}{3} \right), \quad (8)$$

where $\xi = \mathcal{B}z/(1 - \mathcal{B}x)$ is used. In Fig. 3 we show some rays and iso-contours of the eikonal function S . Defining $\Delta S(x, z, \mathcal{B}) = S(x, z, \mathcal{B}) - S(x, z, -\mathcal{B})$, the photon-axion conversion probability per unit transverse length in the eikonal approximation is

$$\frac{dP_{2D}/dx}{dP_{1D}/dx} = \frac{\sin^2 \omega \Delta S/2}{\sin^2 gBz/2} \xrightarrow{\mathcal{B}x < \mathcal{B}z \ll 1} \frac{\sin^2 (gB_1 x z/2 (1 + (\mathcal{B}z)^2/8))}{\sin^2 gBz/2}. \quad (9)$$

Where we have normalized again to the 1-D result for comparison. Note that this is a very small correction to our previous 1-D rough estimate if $\mathcal{B}z \ll 1$.

So far we have considered only infinite plane waves. If our photon or axion beam passes through a confined region of size X , it will suffer diffraction with a characteristic angle given by $\theta = 1.22\lambda_0/X$ which might be larger than the splitting angle if $\mathcal{B}z(\omega X) = gB_1 X z \ll 1$ (the typical case except maybe in very extreme conditions [8]). However, this certainly does not evade our conclusion when diffraction is negligible, which would occur for an helioscope using a quadrupole magnet. Indeed it is very likely that even beams with large diffraction don't show additional enhancements in the photon \leftrightarrow axion probability either. We have calculated the conversion probabilities for typical laser beam parameters used in light-shining-through-walls experiments and found no surprise at all. These results will be presented elsewhere [9]

Acknowledgements

I would like to thank the organizers of this very interesting meeting, and specially to the local committee, for having helped notably in creating a beautiful atmosphere and for taking care marvelously of all of us throughout the workshop.

References

- [1] E. I. Guendelman and I. Shilon, [arXiv:0808.2572](#) [hep-th].
- [2] E. I. Guendelman, I. Shilon, G. Cantatore, and K. Zioutas, [arXiv:0906.2537](#) [hep-ph].
- [3] K. Zioutas, M. Tsagri, Y. Semertzidis, and T. Papaevangelou, [arXiv:0808.1545](#) [astro-ph].
- [4] K. Zioutas, M. Tsagri, T. Papaevangelou, and T. Dafni, *New J. Phys.* **11** (2009) 105020, [arXiv:0903.1807](#) [astro-ph.SR].
- [5] E. I. Guendelman, *Phys. Lett.* **B662** (2008) 445, [arXiv:0802.0311](#) [hep-th].
- [6] See the contribution of A. Siemko in these proceedings.
- [7] G. Raffelt and L. Stodolsky, *Phys. Rev.* **D37** (1988) 1237.
- [8] D. Chelouche and E. I. Guendelman, *Astrophys. J.* **699** (2009) L5–L8, [arXiv:0810.3002](#) [astro-ph].
- [9] J. Jaeckel and J. Redondo, In preparation.

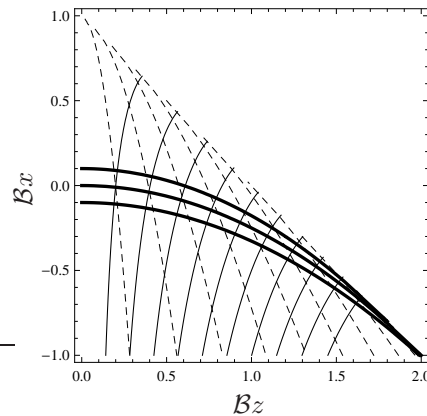


Figure 3: Rays (thick), phase fronts (thin) and iso-contours of optical path s (dashed) of the field $A_+ = (A+a)/\sqrt{2}$. A caustic is formed by the accumulation of rays in $\xi = 1$, ($\mathcal{B}z = 1 - \mathcal{B}x$), the wave cannot propagate in the upper region. The length scales are normalized to the characteristic length scale of the ray deflection \mathcal{B}^{-1} . The evolution of A_- is the mirror image with respect to the $x = 0$ line.

List of Authors

ADMX collaboration, 116
Afanasev, Andrei, 90
Ahlers, Markus, 3
Akimoto, Y., 82
ALPS collaboration, 94
Anastassopoulos, Vassilis, 137
Angloher, G., 11
ArDM collaboration, 31

BABAR collaboration, 127
Baer, Howard, 24
Bailly, Gilles, 104
Baker, Oliver K., 90, 100
Battesti, Rémy, 104
Batut, Sébastien, 104
Bauer, M., 11
Bavykina, I., 11
Beard, Kevin, 90
Belli, P., 35
Bento, A., 11
Berceau, Paul, 104
Bernabei, R., 35
Biallas, George, 90
Bielsa, Franck, 104
BMV collaboration, 104
Boyce, James, 90
Brümmer, Felix, 161
Brax, Philippe, 151
Brown, A., 11
Bruch, Tobias, 16
Bucci, C., 11
Burrage, Clare, 147

Cantatore, Giovanni, 73, 120, 181
Cappella, F., 35
CAST collaboration, 69, 73, 78
CDMS collaboration, 16
Cerulli, R., 35
Chen, Sheng-Jui, 108

Ciemniak, C., 11
Coppi, C., 11
Cudell, J. R., 133

d'Angelo, A., 35
Döbrich, Babette, 112
Dafni, Theopisti, 137
Dai, C. J., 35
DAMA/LIBRA collaboration, 35
Davis, Anne-Christine, 147, 151
Deuter, G., 11

Ferrer-Ribas, Esther, 69
Fouché, Mathilde, 104

GammeV collaboration, 86
Gardikiotis, Antonios, 137
Gaz, Alessandro, 127
Gies, Holger, 112
Goodsell, Mark, 165
Guendelman, Eduardo I., 181

Hamann, Jan, 141
Hannestad, Steen, 141
Hartnett, John, 96
Hauff, D., 11
He, H. L., 35
Henry, S., 11
Hirshfield, J. L., 100
Huff, P., 11
Hutsemékers, D., 133

Imber, J., 11
Inicicchitti, A., 35
Ingleby, S., 11
Inoue, Y., 82
Isaila, C., 11

Jakovčić, Krešimir, 78
Jiang, Y., 100

Jochum, J., 11

Karuza, Marin, 73
 Kazakevitch, G., 100
 Kazakov, S., 100
 Kiefer, M., 11
 Kim, SeungCheon, 43
 Kimmerle, M., 11
 KIMS collaboration, 43
 Kish, Alexander, 20
 Kraus, Hans, 11

Lanfranchi, J.-C., 11
 Lang, R. F., 11
 LaPointe, M. A., 100
 Lavalle, Julien, 59
 Lehnert, Ralf, 171
 Lin, Shin-Ted, 39
 Lindner, Axel, 94
 LIPSS collaboration, 90
 Lozza, Valentina, 73

Ma, X. H., 35
 Majorovits, B., 11
 Malek, M., 11
 Martin, A., 100
 Mauchain, Julien, 104
 McGowan, R., 11
 Mei, Hsien-Hao, 108
 Mikhailik, V. B., 11
 Minarni, Minarni, 90
 Minowa, M., 82
 Mirizzi, Alessandro, 141
 Mizumoto, T., 82
 Montecchia, F., 35
 Morselli, Aldo, 49

Nardone, Marc, 104
 Ni, Wei-Tou, 108, 175
 Nozzoli, F., 35

Ohta, Ryosuke, 82
 Otyugova, Polina, 31

Pantic, E., 11
 Papaevangelou, Thomas, 137
 Payez, Alexandre, 133
 Petricca, F., 11
 Pfister, S., 11

Portugall, Oliver, 104
 Potzel, W., 11
 Povey, Rhys, 96
 Pröbst, F., 11
 Prospero, D., 35

Q & A collaboration, 108

Raffelt, Georg, 141
 Ramdon, Roopchan, 90
 Redondo, Javier, 155, 185
 Rizzo, Carlo, 104
 Robilliard, Cécile, 104
 Roth, S., 11
 Rottler, K., 11
 Rybka, Gray, 116

Sailer, C., 11
 Schäffner, K., 11
 Schmalzer, J., 11
 Scholl, S., 11
 Schwanke, Ullrich, 55
 Seidel, W., 11
 Semertzidis, Yannis, 137
 Shaw, Douglas, 147, 151
 Shchelkunov, S., 100
 Sheau-shi, Pan, 108
 Sheng, X. D., 35
 Shilon, Idan, 181
 Shinn, Michelle, 90
 Slocum, Penny, 90, 100
 Stodolsky, L., 11
 Strandhagen, Ch., 11
 Strauss, R., 11
 Szymkowiak, A., 100

TEXONO collaboration, 39
 Tobar, Mike, 96
 Tolhurst, A. J. B., 11
 Tsagri, Mary, 137

van de Bruck, Carsten, 151
 von Feilitzsch, F., 11
 von Sivers, M., 11

Wang, R. G., 35
 Weniger, Christoph, 63
 Wester, William, 86
 Westphal, W.[†], 11

Wong, Yvonne Y., 141

Wong, Henry T., 39

XENON100 collaboration, 20

Yamamoto, A., 82

Ye, Z. P., 35

Zioutas, Konstantin, 137, 181

List of Participants

Ahlers, Markus, University of Oxford
Anastassopoulos, Vassilis, University of Patras/Greece
Araujo, Henrique, Imperial College London
Baker, Oliver, Yale University
Baer, Howard, Oklahoma University
Baudis, Laura, University of Zurich
Belli, Pierluigi, INFN - Roma Tor Vergata
Brax, Philippe, IPHT Saclay
Bruch, Tobias, University of Zurich
Bruemmer, Felix, IPPP, Durham University
Burrage, Clare, DESY
Caldwell, Jennifer, Univ of Arkansas at PineBluff
Cantatore, Giovanni, University and INFN Trieste - Italy
Chou, Aaron, Fermilab
Conlon, Joseph, Oxford University
Covi, Laura, DESY
Davenport, Martyn, CERN
Davis, Anne, Cambridge University
Dittus, Hansjorg, German Aerospace Centre
Doebrich, Babette, ITP Jena
Ehret, Klaus, DESY
Evans, Jonathan, South Carolina State University
Fairbairn, Malcolm, King's College London
Ferrer-Ribas, Esther, IRFU/CEA
Gaz, Alessandro, University of Colorado
Gil Pedro, Francisco, Oxford University
Goodsell, Mark, LPTHE, Paris
Hannah, Iain, University of Glasgow
Hannestad, Steen, Aarhus University
Jaeckel, Joerg, IPPP, Durham University
Jakovčić, Krešimir, Rudjer Boskovic Institute
Jenkins, Adrian, ICC
Kaboth, Asher, MIT
Karuza, Marin, INFN Trieste
Kharzeev, Dimitri, Brookhaven National Laboratories
Kim, SeungCheon, Seoul University
Kish, Alexander, University of Zurich
Kraus, Hans, University of Oxford
Kusmartsev, Fjodor, Loughborough University
Lavalle, Julien, University of Torino, Italy
Lehnert, Ralf, Universidad Nacional Autónoma de México
Lin, Shin-Ted, Institute of Physics Academia Sinica
Lindner, Axel, DESY
Lozza, Valentina, University of Trieste
Mei, Hsien-Hao, National Tsing Hua University
Minowa, Makoto, University of Tokyo, Physics Dept
Mokhtari, Zahra, Sharif University of Technology

Montanino, Daniele, University of Salento
Morselli, Aldo, INFN Roma Tor Vergata
Ni, Wei-Tou, Centre for Gravitation and Cosmology
Ohta, Ryosuke, University of Tokyo
Otyugova, Polina, University of Zurich
Payez, Alexandre, University of Liege
Read, Justin, University of Zurich
Redondo, Javier, DESY
Ringwald, Andreas, DESY
Rizzo, Carlo, Paul Sabatier University
Roszkowski, Leszek, The University of Sheffield
Rybka, Gray, University of Washington
Schwanke, Ullrich, Humboldt University Berlin
Shilon, Idan, Ben-Gurion University
Siemko, Andrzej, CERN
Slocum, Penny, Yale
Spooner, Neil, University of Sheffield
Tanner, David, University of Florida
Tobar, Michael, University of Western Australia
Todesco, Ezio, CERN
Weniger, Christoph, DESY
Wester, William , Fermilab
Williams, Peter, Daresbury Lab.
Zioutas, Konstantin, University of Patras/Greece